

1006
1006

Willis, 1974

COO-213E-13

FINAL REPORT

EXPLOSION-INDUCED GROUND MOTION, TIDAL AND TECTONIC FORCES AND THEIR RELATIONSHIP TO NATURAL SEISMICITY

Prepared for the

U.S. Atomic Energy Commission
Nevada Operations Office
Office of Effects Evaluation
Las Vegas, Nevada

under

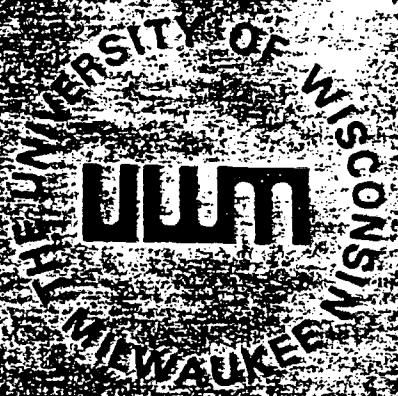
Contract No. AT(11-1)-2138
Administered by the
Chicago Operations Office

by
Dr. David E. Willis
Principal Investigator

Authors

D. E. Willis, R. W. Taylor, R. D. Torfin, P. J. Tatar,
K. L. Frevock, R. G. Poetzf, G. D. George, C. G. Bufe

DECEMBER 1974



DEPARTMENT OF GEOLOGICAL SCIENCES

NOTICE

THIS REPORT WAS PREPARED AS AN ACCOUNT OF WORK SPONSORED BY THE UNITED STATES GOVERNMENT. NEITHER THE UNITED STATES NOR THE UNITED STATES ATOMIC ENERGY COMMISSION, NOR ANY OF THEIR EMPLOYEES, NOR ANY OF THEIR CONTRACTORS, SUBCONTRACTORS, OR THEIR EMPLOYEES, MAKES ANY WARRANTY, EXPRESS OR IMPLIED, OR ASSUMES ANY LEGAL LIABILITY OR RESPONSIBILITY FOR THE ACCURACY, COMPLETENESS OR USEFULNESS OF ANY INFORMATION, APPARATUS, PRODUCT OR PROCESS DISCLOSED, OR REPRESENTS THAT ITS USE WOULD NOT INFRINGE PRIVATELY-OWNED RIGHTS.

Printed in the United States of America.

**AVAILABLE FROM THE
NATIONAL TECHNICAL INFORMATION SERVICE
U.S. DEPARTMENT OF COMMERCE
SPRINGFIELD, VIRGINIA 22151**

1006

COO-2138-13

FINAL REPORT

EXPLOSION-INDUCED GROUND MOTION, TIDAL AND TECTONIC
FORCES AND THEIR RELATIONSHIP TO NATURAL SEISMICITY

Prepared for

U.S. Atomic Energy Commission
Nevada Operations Office
Office of Effects Evaluation
Las Vegas, Nevada

under

Contract No. AT(11-1)-2138
Administered by the
Chicago Operations Office

by

University of Wisconsin-Milwaukee
Department of Geological Sciences
Milwaukee, Wisconsin

Dr. David E. Willis
Principal Investigator

Authors

D. E. Willis, R. W. Taylor, P. J. Tatar, R. D. Torfin
K. Revock, K. G. Poetzi, G. D. George, C. G. Bufe

December 1974

ABSTRACT

This report is an investigation, review and synthesis of the natural and man-made forces which influence the seismicity of the Nevada Test Site area and the adjoining regions. A comprehensive data file was compiled for earthquakes in the western United States. In excess of 33,000 earthquakes were used to analyze the seismicity of this region over the time period 1852 through 1973. Stereo projections which display earthquake epicenters as a function of geographic location and time were used to investigate trends of seismic activity. Perspective strain release surfaces for given time intervals were constructed to study cumulative strain release as a function of geographic location. Detailed seismicity studies were made for the following areas: a, the Nevada Test Site area; b, a region 50 to 1000 km from the Test Site centered on four shots of the megaton range; c, a portion of central California along the San Andreas fault system which had dense seismograph coverage; and d, for a small area adjacent to the Test Site where special broad-band high-gain seismographs were used to monitor the seismic activity during a five-week period centered around one of the megaton shots. The results of these studies showed that the underground nuclear testing program did not produce any detectable influence on the natural pattern of earthquake activity except in the immediate areas of the shots. Strainmeter data collected over a two-year period (1970-1971) in the Nevada Test Site area showed yearly strain differences of the order of 1×10^{-5} with strain ellipse axes showing maximum compression orientated to the northeast and maximum extension trending to the northwest. Strains of the order of 10^{-6} are believed necessary to cause earthquakes in prestressed regions which

contain existing fault zones. Theoretical earth tidal accelerations were cross-correlated with seismicity and with strainmeter data to determine the degree of correlation, if any. The only correlation found between seismicity and tidal accelerations or tidal strains was for microearthquakes which were restricted to a small area. The strainmeter data were found to correlate with all the periods contained in the theoretical earth tides and to correlate with yearly temperature variations. The effect of increasing seismograph station coverage on reported seismicity as a function of time was determined for a $4^{\circ} \times 4^{\circ}$ grid which includes the Nevada Test Site area. In the time period 1933 through 1942 the detection threshold across this area varied from an m_b magnitude of 4.0 in the southwest to 5.2 in the northeast. This detection threshold decreased with increased station coverage. During the time period 1963 through 1972 the threshold varied from 2.0 to 3.4, which is an average of about 2 magnitude units lower. The lower detection threshold did not influence significantly the cumulative strain release but it did result in a significant increase in the number of reported earthquakes.

ACKNOWLEDGMENTS

The authors would like to acknowledge the assistance given by the various organizations and personnel listed in Section 1 of this report with special acknowledgment to the U.S. Geological Survey, which provided earthquake data and assistance with analytical programs. Acknowledgment is also made for the computer programming assistance of A. F. Shakal and M. E. Willis. Special thanks is extended to Miss Mary Polzin who typed the manuscript and assisted in its preparation.

TABLE OF CONTENTS

Abstract.....	ii
Acknowledgments.....	iv
1.0 Introduction.....	1
2.0 Summary and Conclusions.....	5
3.0 Results and Discussion.....	13
3.1 Geologic and Tectonic Setting.....	13
California-Nevada Area.....	13
Geologic Description of the Nevada Test Site Area.....	19
3.2 History of Seismograph Deployment in Nevada and California.....	24
3.3 Effect of Seismograph Station Coverage on Reported Seismicity.....	31
3.4 Seismicity Investigations.....	41
3.4.1 California and Nevada Regions.....	41
Seismic Parameters and Their Relationship.....	41
Surface Wave, Body Wave, and Local Magnitudes.....	41
Perspective Plots.....	47
Visual Analysis - Perspective Plots.....	48
Cross-Correlation.....	75
Statistical Analysis.....	77
Visual Analysis - Stereo Projections.....	95
3.4.2 Nevada Test Site Seismicity.....	101
Earthquakes Detected by NTS Local Seismograph Networks.....	101
Stereo Projections of NTS Activity.....	110
3.5 Strain Measurements - Western U.S.....	112
General Theory.....	112
The Nature of Strain.....	112

Strain Measurement.....	113
Nevada Strainmeter Deployment.....	114
Short Period Strain Data.....	114
Scotty's Junction Strain.....	121
Sleeping Mountain Strain.....	134
Twin Springs Strain.....	137
Yucca Flats Temperature and Barometric Pressure.....	140
Secular Strain Data.....	149
Geodetic Strain.....	165
Residual Strain.....	170
3.6 Triggering of Earthquakes by Natural and Man-Made Forces.....	185
3.6.1 Earthquake Triggering by Underground Nuclear Detonations.....	185
Regional Seismic Activity: BOXCAR, BENHAM, JORUM, and HANDLEY.....	188
Method of Analysis.....	188
Accumulated Seismicity: Four 60-Day Periods.....	191
BOXCAR.....	193
BENHAM.....	195
JORUM.....	198
HANDLEY.....	201
Discussion of the Regional Seismic Activity.....	201
3.6.2 Triggering of Microearthquakes by Tidal Forces.....	203
Groom Mine Microearthquake Activity.....	203
3.6.3 Triggering of Earthquakes in the Central California Area.....	211
3.7 Magnitude Variations.....	238
References.....	261
Appendices A - D.....	A1 thru D7
Distribution List	

Figure	Page
3.1-1 Physiographic provinces of the California/ Nevada area.....	14
3.1-2 Map of postulated westward-moving continental block lying between landward extensions of the Mendocino and Murray fracture zones in the western United States.....	17
3.1-3 Rigid plate approximation to the present-day tectonics of the western United States.....	18
3.1-4 Geologic section of the crust and upper mantle, as interpreted from present evidence.....	20
3.1-5 Simplified tectonic map of south-central Nevada.....	23
3.2-1 Seismograph stations in the California/Nevada area.....	26
3.3-1 The minimum detection surface for the period from 1933-1942.....	34
3.3-2 The minimum detection surface for the period from 1943-1952.....	35
3.3-3 The minimum detection surface for the period from 1953-1962.....	36
3.3-4 The minimum detection surface for the period from 1963-1972.....	37
3.4-1 Relationship between body wave magnitude and local magnitude for earthquakes located in southern California and Nevada.....	42
3.4-2 Relationship (equations 2, 3 and 4) between surface wave magnitude, seismic wave energy (ergs), strain release ($\sqrt{\text{ergs}}$), and decibels.....	46
3.4-3 Yearly perspective plot of cumulative strain A-R release in California/Nevada area.....	49
3.4-4 10-year perspective plot of cumulative strain A-D release in California/Nevada area.....	69
3.4-5 Sample of the correlation coefficients obtained from the two-dimensional autocorrelation of the 1956 decibel values calculated from the strain release in the California/Nevada area.....	78

Figure		Page
3.4-6	Plot of the autocorrelation function of the 1956 cumulative strain release for SW-NE and NW-SE lags in the California/Nevada area.....	79
3.4-7	Plot of the autocorrelation function of the 1963 through 1972 cumulative strain release for SW-NE and NW-SE lags in the California/Nevada area.....	82
3.4-8	Plot of the autocorrelation function of the 1956 decibel values calculated from the cumulative strain release for SW-NE and NW-SE lags in the California/Nevada area.....	83
3.4-9	Plot of the autocorrelation function of the 1963 through 1972 decibel values calculated from the cumulative strain release for SW-NE and NW-SE lags in the California/Nevada area.....	84
3.4-10	Maximum correlation coefficients obtained from the two-dimensional cross-correlation of the 1956 decibel values with the decibel values for each year, 1950 through 1973, in the California/Nevada area.....	85
3.4-11	Sample of the correlation coefficients obtained from the two-dimensional cross-correlation of the 1956 decibel values with the 1953 decibel values calculated from the strain release in the California/Nevada area.....	87
3.4-12	Sample of the correlation coefficients obtained from the two-dimensional cross-correlation of the 1956 strain release with the 1953 strain release in the California/Nevada area.....	88
3.4-13	Maximum correlation coefficients obtained from the two-dimensional cross-correlation of the 1956 strain release with the strain release for each year, 1950 through 1973, in the California/Nevada area.....	90
3.4-14	Zero-lag correlation coefficients obtained from the two-dimensional cross-correlation of the 1956 strain release with the strain release for each year, 1950 through 1973, in the California/Nevada area.....	91

Figure	Page
3.4-15 Plot of yearly peak correlation coefficient locations for cross-correlation of the 1956 strain release with the strain release of each year, 1950 through 1973.....	92
3.4-16 Cumulative yearly strain release for the California/Nevada area from 1950 through 1973.....	93
3.4-17 Cumulative strain release for each 10-year period for the California/Nevada area from 1933 through 1972.....	94
3.4-18a Seismicity of Nevada from 1852 to 1962 using the catalog of Slemmons et al, 1965. The size of the + is proportional to magnitude, events of unknown magnitude are shown by an X. The figure is also the right view of the stereographic pair Figure 3.4-18a, Figure 3.4-18b.....	97
3.4-18b Left view of stereographic pair Figure 3.4-18a, 3.4-18b.....	98
3.4-19a Seismicity of Nevada from 1961 to 1973 using NEIS data. The size of the + is proportional to magnitude, events of unknown magnitude are shown by an X. The figure is also the right view of the stereographic pair Figure 3.4-19a, Figure 3.4-19b....	99
3.4-19b Left view of stereographic pair Figure 3.4-19a, Figure 3.4-19b.....	100
3.4-20 Weekly number of earthquakes: June 1969 through March 1973.....	102
3.4-21 Weekly accumulative seismicity: June 1969 through March 1973.....	103
3.4-22 Weekly accumulative seismicity after HANDLEY.....	104
3.4-23 Weekly strain release after HANDLEY.....	105
3.4-24 Weekly percent strain release accumulation 1970-1972.....	106
3.4-25 Weekly percent accumulative strain release after HANDLEY.....	107
34.-26 Body wave magnitudes - NTS shots.....	108

Figure	Page
3.5-1	Locations of the thirteen Nevada strainmeter stations listed in Table 3.5-2.....116
3.5-2	The cross-correlation function of Pinion Flats, California, north-south theoretical strain, cross-correlated with north-south theoretical earth tides calculated using Pinion Flats strainmeter coordinates.....118
3.5-3	Power spectral density plots of the autocorrelation function for autocorrelated north-south horizontal theoretical earth tides (top), calculated using Scotty's Junction, Nevada, station coordinates and autocorrelated Scotty's Junction (SCT) north-south horizontal strain component (bottom).....122
3.5-4	Plot of the cross-correlation function for Scotty's Junction, Nevada, (SCT) north-south horizontal strain component cross-correlated with the north-south theoretical earth tides, calculated using Scotty's Junction station coordinates.....124
3.5-5	Power spectral density plot of the cross-correlation function for Scotty's Junction, Nevada, (SCT) north-south horizontal strain component cross-correlated with north-south horizontal theoretical earth tides, calculated using Scotty's Junction station coordinates...127
3.5-6	Power spectral density plots of the autocorrelation function for autocorrelated northwest-southeast horizontal theoretical earth tides (top), calculated using Scotty's Junction, Nevada, station coordinates and autocorrelated Scotty's Junction (SCT) northwest-southeast horizontal strain component (bottom).....129
3.5-7	Power spectral density plot of the cross-correlation function for Scotty's Junction, Nevada, (SCT) northwest-southeast horizontal strain component cross-correlated with northwest-southeast horizontal theoretical earth tides, calculated using Scotty's Junction coordinates.....131
3.5-8	Power spectral density plots of the autocorrelation function for autocorrelated vertical theoretical earth tides (top), calculated using Scotty's Junction, Nevada, station coordinates and autocorrelated Scotty's Junction (SCT) vertical strain component (bottom).....133

Figure	Page
3.5-9 Power spectral density plot for Scotty's Junction, Nevada, (SCT) vertical strain component, cross-correlated with the vertical theoretical earth tides, calculated using Scotty's Junction station coordinates.....	135
3.5-10 Power spectral density plots of the autocorrelated function for autocorrelated northwest horizontal theoretical earth tides calculated using Sleeping Mountain, Nevada, coordinates (top) and autocorrelated Sleeping Mountain (SPM) northwest horizontal strain (bottom).....	136
3.5-11 Power spectral density plot of the cross-correlation function for the northwest horizontal strain component at Sleeping Mountain, Nevada, (SPM), cross-correlated with the northwest horizontal theoretical earth tides, calculated using Sleeping Mountain station coordinates...	138
3.5-12 Power spectral density plots of the autocorrelation function for the autocorrelation of the north-south horizontal theoretical earth tides (top), calculated using the Twin Springs, Nevada, station coordinates and the autocorrelation of the Twin Springs (TSP) north-south horizontal strain component (bottom).....	139
3.5-13 Power spectral density plot of the cross-correlation function for Twin Springs, Nevada, (TSP) north-south horizontal strain component, cross-correlated with the north-south horizontal theoretical earth tides, calculated using the Twin Springs station coordinates....	141
3.5-14 Power spectral density plots of the autocorrelation function for autocorrelated temperature (top) and barometric pressure (bottom) as recorded at the Yucca Flats, Nevada, weather station.....	142
3.5-15 Plot of the cross-correlation function for Yucca Flats, Nevada, temperature, cross-correlated with the vertical theoretical earth tides, calculated using the Yucca Flats weather station coordinates.....	144
3.5-16 Power spectral density plot of the cross-correlation function of Yucca Flats, Nevada, temperature, cross-correlated with vertical theoretical earth tides calculated using Yucca Flats weather station coordinates.....	145

Figure	Page
3.5-17	Power spectral density plots of the cross-correlation function for Scotty's Junction, Nevada, (SCT) north-south horizontal strain component, cross-correlated with Yucca Flats temperature (top) and barometric pressure (bottom).....148
3.5-18	Secular strain at the Scotty's Junction, Nevada, strainmeter site, from June 1970 to June 1971.....151
3.5-19	Secular strain at the Sleeping Mountain, Nevada, strainmeter site, from June 1970 to June 1971.....152
3.5-20	Secular strain at the Twin Springs, Nevada, strainmeter site, from June 1970 to June 1971.....153
3.5-21	Plot of Yucca Flats, Nevada, surface temperature averaged over 10-day intervals, from June 1970 to July 1971.....154
3.5-22	Secular strain change ellipses from short-base strainmeter data.....159
3.5-23	Stress patterns in Nevada.....161
3.5-24	Comparison of the observed strain field at Mina indicated by strain change ellipses, and composite focal mechanism solutions for local microearthquakes.....162
3.5-25	Comparison of the observed strain field at Mina indicated by strain change ellipses, and composite focal mechanism solutions for local microearthquakes.....163
3.5-26	Comparison of the observed strain field at Round Mountain indicated by strain change ellipses, and composite focal mechanism solutions for local microearthquakes.....164
3.5-27	Index map showing location of strain nets and level line for BENHAM explosion.....166
3.5-28	Caldera boundaries in Pahute Mesa area and strains related to the JORUM explosion.....168
3.5-29	Station displacements (arrows) calculated from a least squares adjustment of the observed changes in line length between March 1970 and April 1970 (includes HANDLEY event).....169

Figure	Page
3.5-30 Station displacements (arrows) calculated from a least squares adjustment of the observed changes in line length between April 1970 and May 1971, the year following the HANDLEY event.....	171
3.5-31 Comparison of BENHAM strain with pressure data from Olsen.....	175
3.5-32 Variation of strain step amplitude with distance.....	176
3.5-33 Records from short-base strainmeters located at Sleeping Mountain, Nevada, for the time period immediately surrounding the JORUM event.....	179
3.5-34 Records from short-base strainmeters located at Twin Springs, Nevada, for the time period immediately surrounding the JORUM event.....	180
3.5-35 Quasi-static strain vs. distance plot for MILROW and BENHAM nuclear events.....	182
3.6-1 Total number of earthquakes that occurred during each 24-hour period relative to the detonation times of BOXCAR, BENHAM, JORUM, and HANDLEY.....	192
3.6-2 Cumulative daily strain release for the area between 50 and 1000 km of BOXCAR, BENHAM, JORUM, and HANDLEY.....	194
3.6-3 Number of earthquakes that occurred during 24-hour periods relative to t_0 , the detonation time of BOXCAR, BENHAM, JORUM, and HANDLEY.....	196
3.6-4 Cumulative daily strain release for the area between 50 and 1000 km of the BOXCAR nuclear detonation.....	197
3.6-5 Cumulative daily strain release for the area between 50 and 1000 km of the BENHAM nuclear detonation.....	199
3.6-6 Cumulative daily strain release for the area between 50 and 1000 km of the JORUM nuclear detonation.....	200
3.6-7 Cumulative daily strain release for the area between 50 and 1000 km of the HANDLEY nuclear detonation.....	202
3.6-8 Plot of the cross-correlation function for Groom Mine, Nevada, microearthquakes hourly count, cross-correlated with vertical theoretical earth tides, calculated using the Groom Mine seismograph station coordinates.....	205

Figure	Page
3.6-9 Power spectral density plot of the cross-correlation function of Groom Mine, Nevada, (GM) microearthquake hourly count, cross-correlated with the vertical theoretical earth tides, calculated using Groom Mine seismograph station coordinates for the time period October 2, 1969 to October 5, 1969.....	207
3.6-10 Overlay plot of Groom Mine, Nevada, microearthquake hourly count (solid line) and the derivative of the vertical component of the theoretical earth tides (dashed line), calculated using the Groom Mine seismograph station coordinates.....	208
3.6-11 Plot of the cross-correlation function for Groom Mine, Nevada, microearthquakes hourly count, cross-correlated with the derivative of the vertical theoretical earth tides, calculated by using the Groom Mine seismograph station coordinates.....	209
3.6-12 Location of the San Andreas Fault System in central California, 35°N, 120°W, to 39°N, 123°W.....	211
3.6-13 Celestial events, hourly variations in gravity, and number of earthquakes in the San Andreas Fault System study area during day number 77, Mar. 18, 1969.....	214
3.6-14 Celestial events, hourly variations in gravity, and number of earthquakes in the San Andreas Fault System study area during day number 259, Sept. 16, 1969, the day of the nuclear event JORUM.....	215
3.6-15 Celestial events, hourly variations in gravity, and number of earthquakes in the San Andreas Fault System study area during day number 450, Mar. 26, 1970, the day of the nuclear event HANDLEY.....	216
3.6-16 Celestial events, nuclear events, strain release, and A-L number of earthquakes in the central California study area.....	218
3.6-17 Two year, 1969-70, average monthly seismicity and secular celestial events in the central California study area.....	234
3.6-18 Two year, 1969-70, total cumulative elastic strain energy release in the central California study area.....	235
3.6-19 Strain release power spectrum of the central California study area events within the interval from day number 213, Aug. 1, 1969, through day number 273, Sept. 30, 1969.....	237

Figure	Page
3.7-1 Estimated P_n velocity in the United States, based on data from deep seismic soundings, underground nuclear explosions, and earthquakes.....	241
3.7-2 Lateral variation of P wave differential attenuation at U.S. stations.....	243
3.7-3 Lateral variation of S wave differential attenuation at two U.S. stations.....	243
3.7-4 Rayleigh wave radiation pattern at $T = 20$ sec. observed from the BILBY nuclear explosion.....	246
3.7-5 Love wave radiation pattern at $T = 20$ sec. observed from the BILBY nuclear explosion.....	246
3.7-6 Contour map of average deviations from published M_g magnitudes of six NTS explosions (PILE DRIVER, GREELEY, BOXCAR, JORUM, HANDLEY) and two explosions on Amchitka Island (MILROW and CANNIKIN).....	249
3.7-7 Topographic map of North America.....	251
3.7-8 Tectonic map of North America.....	252
3.7-9 Comparison of epicentral distance average deviations from published M_g magnitudes of six NTS explosions (PILE DRIVER, GREELEY, BOXCAR, BENHAM, JORUM, HANDLEY) using 22 WWSSN and 22 CSN stations.....	254
3.7-10 Contour map of average deviations from published m_b magnitudes of six NTS explosions (PILE DRIVER, GREELEY, BOXCAR, BENHAM, JORUM, HANDLEY) and two explosions on Amchitka Island (MILROW and CANNIKIN).....	255
3.7-11 Comparison of average magnitude deviations from published m_b magnitudes of six NTS explosions (PILE DRIVER, GREELEY, BOXCAR, BENHAM, JORUM, HANDLEY) vs. epicentral distance using 24 WWSSN and 22 CSN stations.....	256
3.7-12 Relation of the epicenter of the south central Illinois earthquake of November 9, 1968, to faults of that region.....	258
3.7-13 Iso-magnitude contour map of surface wave magnitudes for the south central Illinois earthquake of November 9, 1968.....	259
3.7-14 Iso-magnitude contour map of body wave magnitudes for the south central Illinois earthquake of November 9, 1968.....	260

Table	Page
3.2-1 Operational periods for seismograph stations in California and Nevada.....	27
3.3-1 A comparison of the total number of reported events with the number of stations available for detection, for decade intervals from 1933 to 1973.....	32
3.3-2 The number of events in 10-year periods before and after removing the effects of increasing station coverage.....	38
3.3-3 Calculated strain release before and after removing the effect of increasing station coverage.....	39
3.4-1 Listing of large magnitude Nevada underground nuclear shots.....	74
3.5-1 Source and duration of earth strains.....	112
3.5-2 Nevada strainmeter installations.....	115
3.5-3 Diurnal and semi-diurnal earth tidal components and their associated periods.....	120
3.5-4 Short period cross-correlation coefficients for south-central Nevada strain components, Yucca Flats, Nevada, temperature and Groom Mine, Nevada, micro-seismic events, cross-correlated with theoretical earth tides and meteorological data.....	125
3.5-5 Long period cross-correlation coefficients for south-central Nevada strainmeter stations strain components cross-correlation with temperature.....	155
3.5-6 Yearly strain differences for strainmeter stations in south-central Nevada.....	158
3.5-7 Parameters for selected shots.....	173
3.5-8 HANDLEY strainmeter site and strain-step data.....	183
3.6-1 Correlation between seismicity and horizontal strain.....	210
3.6-2 Visual comparison between nuclear detonations, seismicity and strain release.....	231
3.6-3 Cross-correlation coefficients between seismicity, strain release and tidal accelerations.....	236

Table	Page
3.7-1 Percentage of energy radiated as seismic waves in various source rocks.....	239
3.7-2 Names and locations of seismograph stations.....	247
3.7-3 Source parameters for U.S. underground nuclear explosions.....	248

1.0 INTRODUCTION

The possible existence of either a geographical or a time dependent pattern in the natural occurrence of earthquakes and the possible influence of man-made activity on that pattern has been of considerable interest to seismologists, geologists, astronomers, and the layman for many years. Investigations of this nature are significant to the problems of earthquake prediction because they may reveal short-term seismic patterns, or may lead to a better understanding of long-term processes.

The detection of systematic temporal changes is difficult because of the relatively short period of time for which adequate earthquake data are available. The earliest reliable data on Nevada seismicity only extends back to 1852. Prior to the 1930's, only the larger earthquakes have been reported. Since the 1920's there has been a gradual increase in the number of seismograph stations put into operation. As a direct result there is an overall general increase of reported earthquake activity up to the present because of the larger number of seismograph stations in operation. Improvements in instrumentation and data analysis techniques have also contributed to the detection, location and the assignment of magnitudes for larger numbers of earthquakes, especially since the early 1960's.

Earthquake activity is episodic in nature. In 1973 there was a decrease in U.S. and world wide activity compared to 1972 and 1971, both in number and magnitude. These short-term variations are probably only perturbations on long-term cycles. Instrumental recordings have been obtained only since about 1900, but for giant earthquakes there

is a fairly complete record back to about 400 A.D. in Japan and China. The Chinese historical data indicates a four stage pattern in earthquake activity which repeats itself every 370 to 380 years. Increased major seismicity around the world has been correlated with the wanderings of the earth's magnetic poles, with changes in the rotation rate of the earth, with the intensity of solar activity (sun spots), and with the so-called Jupiter effect. The latter is a rare planetary line-up that occurs once every 179 years when all of the planets of the solar system are aligned on the same side of the sun. This will next take place in 1982. Solid earth tides caused by the gravitational attraction of the sun and moon have been correlated with the generation of earthquakes.

The detection of geographic or spatial patterns is difficult because of scattered instrumentation coverage and, to a limited extent, by the variations in instrumental response between seismograph stations. The latter effect has been reduced by the installation of standard-type equipment in the World Wide Standard Seismograph Network and the Canadian Network. These stations were installed in the early 1960's.

Man has been able to induce earthquakes by means of surface loading, detonation of large explosive shots underground, and by fluid injection. One of the earliest documented cases on the generation of earthquakes by surface loading was in connection with Hoover Dam. This massive dam contains 4,400,000 cubic yards of concrete and forms Lake Mead, which is some 115 miles long and reaches depths of 589 feet. It contains 10×10^{12} gallons of water and has a maximum water pressure at the dam's base of 45,000 pounds per square foot. The dam was completed in 1936 and shortly after it was filled a pattern of earthquake activity began which persisted

for many years. These earthquakes were probably caused by two factors - increased surface loading and an increase in the pore pressure in the underlying rock.

The injection of waste fluids at the Rocky Mountain Arsenal during 1962 to 1965 was followed by a pattern of earthquakes near the Denver area (Hollister and Weimer, 1968). In a series of controlled tests by the U.S. Geological Survey at the Rangely Oil Field in Colorado, scientists (Wallace, 1974) found that they could control at will the generation of earthquakes by the injection or withdrawal of fluids into the earth.

When large underground nuclear shots are detonated they are usually followed by a series of aftershocks - intense seismicity in the source region which correlates with the deterioration of the cavity formed by the detonation. When the cavity collapses (anywhere from a few minutes to several days) this aftershock activity will normally cease completely (Hamilton and others, 1969). In addition to these aftershocks, tectonic events (natural-appearing earthquakes) will sometimes be generated in the surrounding area at shallow depths (1 to 5 km). Most of these events will occur at distances less than 10 km from the shot. These tectonic events are probably related to the regional stress fields in the shallow crustal rocks and to the perturbation of that stress field caused by the explosion-generated elastic waves. Increased pore pressure in the rocks caused by the explosion could also change the strength of nearby rock and hence subject it to earlier failure due to the action of the regional stress field (Healy and others, 1970). It should be pointed out that both types of events, the aftershocks in the cavity region and the tectonic events, have always been considerably smaller in magnitude than the original shot.

Due to the Atomic Energy Commission's concern for any possible effects that the underground nuclear testing program might have on the tectonics and natural pattern of seismicity in the western United States, they initiated and sponsored a coordinated long term program of research conducted by numerous governmental agencies and universities. The purpose of this investigation was to conduct a review and synthesis of the geological and geophysical data relating to the natural seismicity in the western United States with emphasis on the Nevada Test Site area utilizing all the data available but with a special effort to correlate the data provided by the Atomic Energy Commission sponsored program.

The authors would like to list the personnel and organizations who have contributed data and/or assisted with these studies:

NOAA - (former) Earthquake Mechanism Laboratory - strainmeter studies
 D. Tocher, M. E. Blackford*, C. G. Bufe*

NOAA-ERL - seismicity studies
 R. Brazee, J. C. Stepp

University of California-Lawrence Livermore Laboratory - seismic studies
 H. Rodean and R. Rohrer

Colorado School of Mines - strainmeter studies
 M. Major, R. Butler and P. Romig

University of Nevada-Reno - seismicity and strain studies in northern and central Nevada. A. Ryall, S. D. Malone, and K. Priestly

California Division of Mines and Geology - seismicity studies
 D. Rogers

SANDIA Laboratory - seismicity studies
 D. M. Tendall

U.S.G.S. - Seismicity and Risk Analysis Branch (formerly NOAA/ESL - Special Projects Group, Las Vegas) - seismicity studies
 K. W. King, R. Navarro, and K. C. Bayer

U.S.G.S. - National Center for Earthquake Research - seismicity and strain studies
 C. G. Bufe, J. C. Savage, F. G. Fischer, and J. H. Healy

U.S.G.S. - National Earthquake Information Service - seismicity studies
 A. Tarr

* Now with U.S.G.S. - National Center for Earthquake Research

2.0 SUMMARY AND CONCLUSIONS

Most of the Nevada area lies within a system of mountain ranges and intervening valleys or basins that have a general north-south trend. These valleys and basins are bounded by block faulting. The latter are normal faults that were probably formed by the fragmentation and collapse of brittle rocks in the upper crust as the crust was undergoing extension.

There are two normal fault systems and two thrust fault systems that have been identified in the Nevada Test Site region. The older normal fault system which began about 26.5 million years (m.y.) ago had a general northeast trend while the younger normal fault system which began about 17.8 m.y. ago and continued to 7 m.y. ago had a general north trend. Intermixed with the normal faulting were two major thrust fault systems that occurred at an earlier geologic time period which caused several tens of miles displacement of rock formations from the west toward the east. There is also a major shear zone caused by a strike-slip fault system located along the southern boundary and to the west of the test site. There has been right-lateral movement of at least 25 miles along this zone, some of which has occurred within the last 17 m.y. During this same general time period that the normal fault systems were developed, seven volcanic centers (calderas) and five ash-flow tuff sheets occurred in and adjacent to the Nevada Test Site area (Ekren, 1968).

The pattern of natural earthquake activity in the study area is controlled by the tectonic or mountain building forces in the crust of the earth. The elastic deformation of the earth can be measured by geodetic instruments and strainmeters. The permanent deformations in

the crust caused by earthquakes can be detected and/or determined from measured fault displacements, strain or geodetic measurements and focal mechanism studies. A computation of strain change ellipses over a one-year time period using strainmeter data in the western U.S. disclosed a consistent pattern in the tectonic forces. The axes of maximum extension (or minimum compression) were found to trend northwestward while axes of maximum compression (or minimum extension) were found to trend to the northeast. Focal mechanism studies of recent earthquakes in the general region confirm this general pattern.

In connection with the strain change ellipses mentioned above, a detailed study was made of the strainmeter data for the three stations located in the general NTS area that were operated by NOAA and the Colorado School of Mines. The data were digitized to facilitate analytical analysis. Diurnal, semi-diurnal, and secular variations were determined. Cross-correlation of these records with meteorological and theoretical earth-tidal data disclosed that the strainmeters were sensitive to both earth tides and temperature. All periods contained in the theoretical earth tides were found in the recorded strain. Temperature and barometric pressure changes did not correlate with all of the peaks observed in the power spectrum of the strain data. The cross-correlation between barometric pressure and recorded strain had a low correlation coefficient. However, high correlation coefficients and small lag times were found between the earth tides and the strain data.

Geodetic strain studies by the U.S.G.S. were made of the area before and after the larger underground nuclear detonations to determine changes in the strain field caused by the shots. There has been a relaxation of the shot-imposed deformation following HANDLEY, the largest of the underground nuclear shots fired at NTS. The magnitude of this recovery is

greater than the original deformation and the area of the shot is considered to be stable. It is thought that the relaxation is from creep on those faults which were stressed by the shot.

Residual strains or tectonic stress changes measured on strainmeters for the larger shots at NTS were analyzed by several groups who concluded that any changes due to the shots were confined to distances of 100 km or less from the shots. "Quasi-static" strain steps were observed for the shots that correlate with the pressure decay in the shot cavity area. The magnitude of the permanent residual strains for many of these larger shots suggests that the shots were accompanied by significant fault movements in the source regions. For HANDLEY, the amount of fault movement required to explain the observed strain change would necessitate an earthquake with a magnitude 1.5 units or more smaller than the shot itself. To trigger an earthquake in the NTS area if there are no faults or prestress present, it has been estimated (Smith and others, 1969) that a strain of the order of 10^{-3} would be required. Smaller strains on the order of 10^{-6} might cause earthquakes in prestressed media, especially in areas that contain existing faults. Strains of this order are found only at short distances (≈ 15 km) from shots that have yields of about one megaton.

In order to study the seismicity of the California/Nevada area and especially the NTS area, a comprehensive earthquake file containing 28,986 western U.S. events was compiled for the time period 1900-1973. These data were obtained from the National Earthquake Information Service, the University of California-Berkeley, and the California Institute of Technology. Duplicate listings from these sources were removed from the file. The area covered extends from 25° to 50° North Latitude and 87° to

above 6.0 (JORUM and HANDLEY) did perturb the normal pattern of seismicity. Following HANDLEY there was an increase in activity that persisted for 20 to perhaps 30 weeks. During early 1973 there was an apparent slight increase in the normal pattern of earthquake activity for this area. This might be explained in part by the general decrease in activity of the testing program. An active testing program of large shots may cause a release of tectonic strain when normally the tectonic stresses would accumulate until released by natural earthquakes.

In order to examine in more detail any possible triggering of earthquake activity following nuclear tests, the regional seismic activity was determined for 30-day time periods before and 30-day time periods after four shots of the one megaton range that were detonated at NTS. The area included ranged from 50 to 1000 km from the shots. Accumulative daily strain release and total number of earthquakes during each 24 hour period were computed for all reported earthquakes that fell within these time periods and geographic coverage. No change in either the number of earthquakes or the strain release could be detected in the time period following these shots compared to the activity prior to the shots. The data base in this case was the composite file made up of the NEIS and Cal Tech-Berkeley listings.

As a further check on the above, a detailed study of the seismicity in central California along the San Andreas fault system was made for the years 1969 and 1970. This particular area was chosen since it had a dense network of high gain seismograph stations (83 to 109) deployed over a relatively small area. This allowed a network detection threshold of much lower magnitude earthquakes than would be possible with the

NEIS/Cal Tech-Berkeley data. For example, the Berkeley listings for the area contained a total of 122 earthquakes (most above magnitude 2.5) in 1970 while the U.S.G.S. net detected 2,319 earthquakes during the same time period, many of which had magnitudes of 1.5 or smaller. These data were examined for any correlations between earthquake activity and the testing program and for the possible triggering of earthquakes by solid earth tidal forces. Hourly and daily plots were made for the two year time period that displayed the variation in gravitational acceleration due to earth tides, occurrence of celestial events, number of earthquakes, earthquake strain release, and underground nuclear detonations. Two of the large NTS shots (JORUM and HANDLEY) were detonated during this time period. No correlation was found between the occurrence of earthquakes or their strain release and the testing program. In fact, the MILROW shot that was fired in the Aleutians was preceded by a large increase in strain release which one might fallaciously say triggered the shot. The earthquake data also showed a very low degree of correlation with the theoretical earth tides. Some increase in seismicity was found during the periods when the first time derivative of the theoretical vertical component of the tidal acceleration was near zero.

A tripartite network of three-component portable short-period seismograph stations that had broad-band high-gain capabilities was operated continuously for two weeks prior and three weeks after the JORUM shot at distances of 60 to 100 km from the source (Willis, 1970). These stations were located near active faults. No significant changes were observed in local microseismic activity to indicate that the shot caused any release in tectonic energy near these stations. However, when the microearthquakes

were cross-correlated with theoretical tidal strains and tidal acceleration a definite correlation was found. This appears to conflict with the data for central California. This apparent discrepancy can be explained by the fact that the microearthquakes were three or four orders of magnitude smaller than the smaller earthquakes recorded in the central California area and that they originated in a region of very small areal extent. The tidal forces, at least for the area and time period considered, did not contribute significantly to the triggering of larger magnitude earthquakes.

The effect of seismograph station coverage on reported seismicity was analyzed by determining detection threshold levels for an areal grid system that extended from 35° to 39° North Latitude and 115° to 119° West Longitude. This area includes the Nevada Test Site. The time period from 1933 through 1972 was divided into four 10-year periods. Average station coverage for each time period was determined. Assumed station noise levels were taken from published background noise surveys. During the time period 1933 through 1942 the detection threshold increased from an m_b of 4.0 in the southwest corner to an m_b of 5.2 in the northeast corner of the grid system. For each succeeding 10-year period the detection threshold decreased with the increasing seismograph station coverage. In the 1963 through 1972 time period the threshold varied from 2.0 to 3.4, which is an average decrease of about 2 m_b magnitude units. The cumulative strain release and number of earthquakes were computed for each 10-year period. The decreased detection threshold did not significantly influence the strain release for each time period but it did result in a larger total number of reported earthquakes.

3.0 RESULTS AND DISCUSSION

3.1 Geologic and Tectonic Setting

California-Nevada Area

Nevada, except for its southwestern corner, lies entirely within the Basin and Range province as defined by Thornbury (1965). This province is basically governed by block faulting which has created mountain ranges and intermontane basins trending in a north-south direction. California, unlike Nevada, is defined by Thornbury (1965) as a "state of strongly contrasting geomorphic regions because of the juxtaposition by faulting of numerous earth blocks having dissimilar rock types, structures and geologic histories." Evident in Thornbury's descriptions is the fact that faulting has been an important factor in the formation of California's and Nevada's present-day geology. The provinces defined in the California/Nevada area are outlined in Figure 3.1-1.

The relationship between faulting and plate boundaries in the California/Nevada area was examined in detail by a number of investigators in light of recent advances in plate tectonics theory. A notable feature of America's west coast is the absence of a trench and associated island arc commonly found along the Circum-Pacific Belt. Also noteworthy is the existence of the San Andreas system, an extensive set of faults paralleling the California coast. Atwater (1970) and Anderson (1971) investigated the history of the North American and Pacific plates, as it related to the formation of the San Andreas system.

In the mid-Cenozoic, an oceanic rise or spreading zone situated in the Pacific Ocean approached a trench or subduction zone which paralleled the west coast at that time. Oceanic crust between the rise and trench, the Farallon Plate, was consumed at the trench more rapidly than it was formed

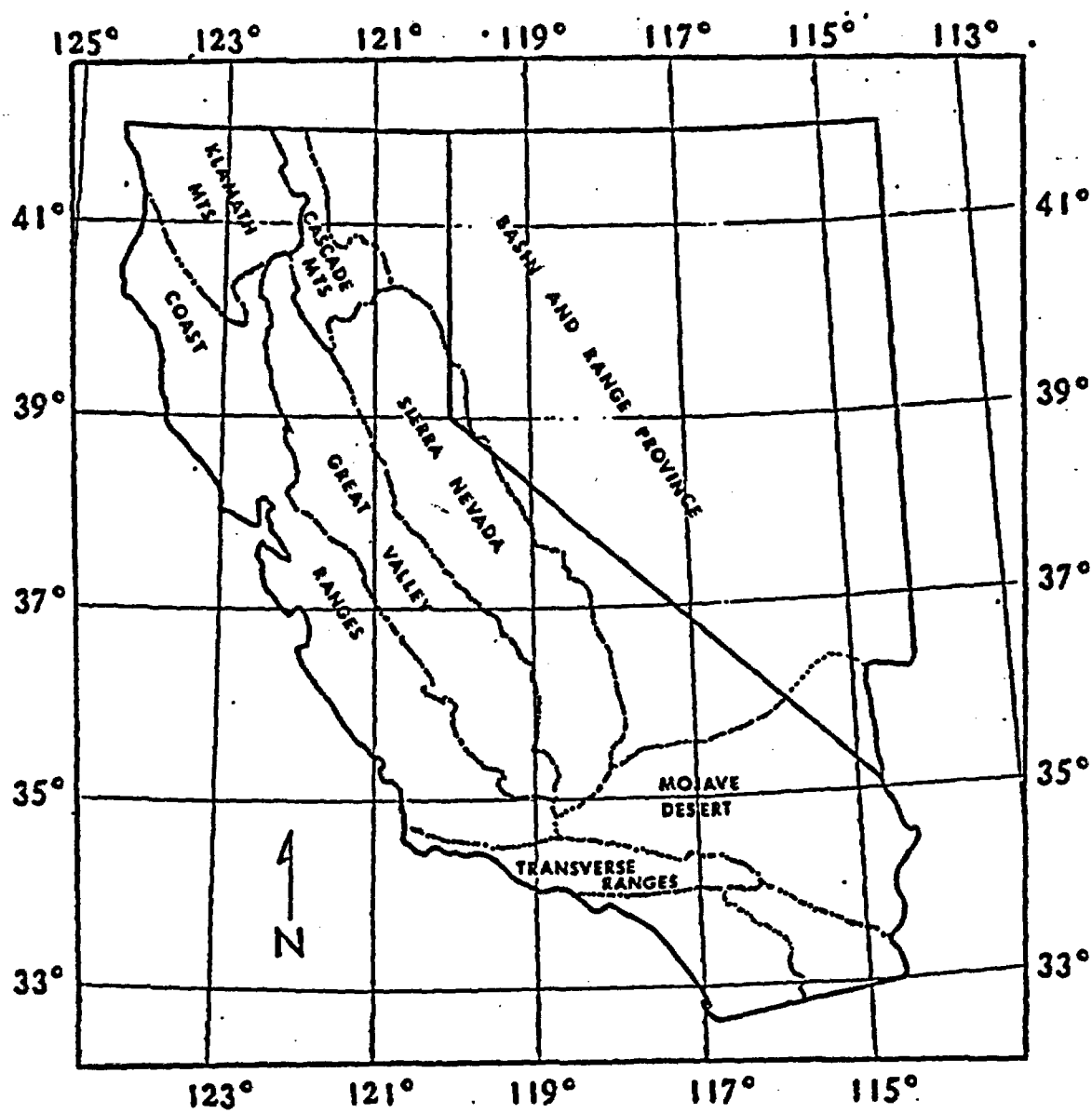


Figure 3.1-1. Physiographic provinces of the California/Nevada area. Modified from Thompson and Talwani, 1964, p. 1540.

at the rise. As a result of the differential consuming and spreading rates, the rise approached very near to the northern California coast about 29 m.y. ago. When the weak spreading center encountered the trench, it broke and abutted itself against the North American Plate. The relative movements between the abutting North American and Pacific Plates was expressed as right lateral strike-slip faults, i.e., the San Andreas system. Mutual destruction of the rise and trench started along the northern California coast between the Mendocino and Murray fracture zones approximately 29 m.y. ago and proceeded south to approximately the southern California/Mexico border within 6 to 10 m.y. Atwater and Molnar (1973) estimated the average movement between the Pacific and North American Plates was about 2 cm/yr from 38 to 10 m.y. ago, increasing in late Tertiary to about 4 cm/yr between 10 and 4.5 m.y. ago, and about 5.5 cm/yr from 4.5 m.y. ago to the present.

Thompson and Burke (1973) consider Nevada and California to lie in the wide broken zone existing between the Pacific and North American Plates. The relative movement of these plates results in strike-slip faulting in parts of California as evidenced by the San Andreas Fault system. In the Basin and Range Province, the relative plate movement creates a zone of spreading resulting in extension faulting. Cook (1969) and Suppe and others (1974) are basically in agreement with this concept and postulate the existence of a rigid plate in the western United States.

Cook (1962) postulated a mantle convection current, associated with the landward extension of the East Pacific Rise, which rose beneath the eastern part of the Basin and Range Province and moved eastward relative to the North American Plate. According to Cook (1969), the crustal drag caused by the convection current forced

a large continental-type block to move westward into the Pacific Ocean about 50-100 km. in the California region between the landward projections of the Mendocino and Murray fracture zones, which were probably major lines of weakness existing before the formation of the East Pacific Rise.

Areas of tension, translation and compression resulting from the postulated convection current and continental block movement are shown in Figure 3.1-2. Tension occurring in the Nevada area is responsible for the block faulting which created the mountain ranges and intermontane basins of the Basin and Range Provinces. Translation has occurred along right-lateral faults of the block's northern edge and left lateral faults of the block's southern edge. These right-lateral and left-lateral faults are the proposed continental extensions of the Mendocino and Murray fracture zones, respectively. Compression taking place at the leading edge of the westward-moving continental block may be manifested as intense Pliocene and Pleistocene deformation of California's Coast Ranges and as overthrusting along the southern margin of the block.

Suppe and others (1974) present a somewhat different picture of the plate boundaries in the western United States. Figure 3.1-3 is their rigid plate approximation to the present-day tectonics of the western United States. With respect to the North American Plate, the Western U.S. Plate rotates counterclockwise and has its pole of rotation in southern California. The present-day Western U.S. Plate is bounded by the Utah seismic zone, the Garlock Fault and perpendicular Owens Valley-Death Valley graben system, and the southern Nevada seismic zone. Several sub-plates are needed to explain the seismic zones of the California/Nevada area. Although the plate constructions of Cook and Suppe and others differ, they both could account for the present-day faulting and seismic zones observed in the California/Nevada area.

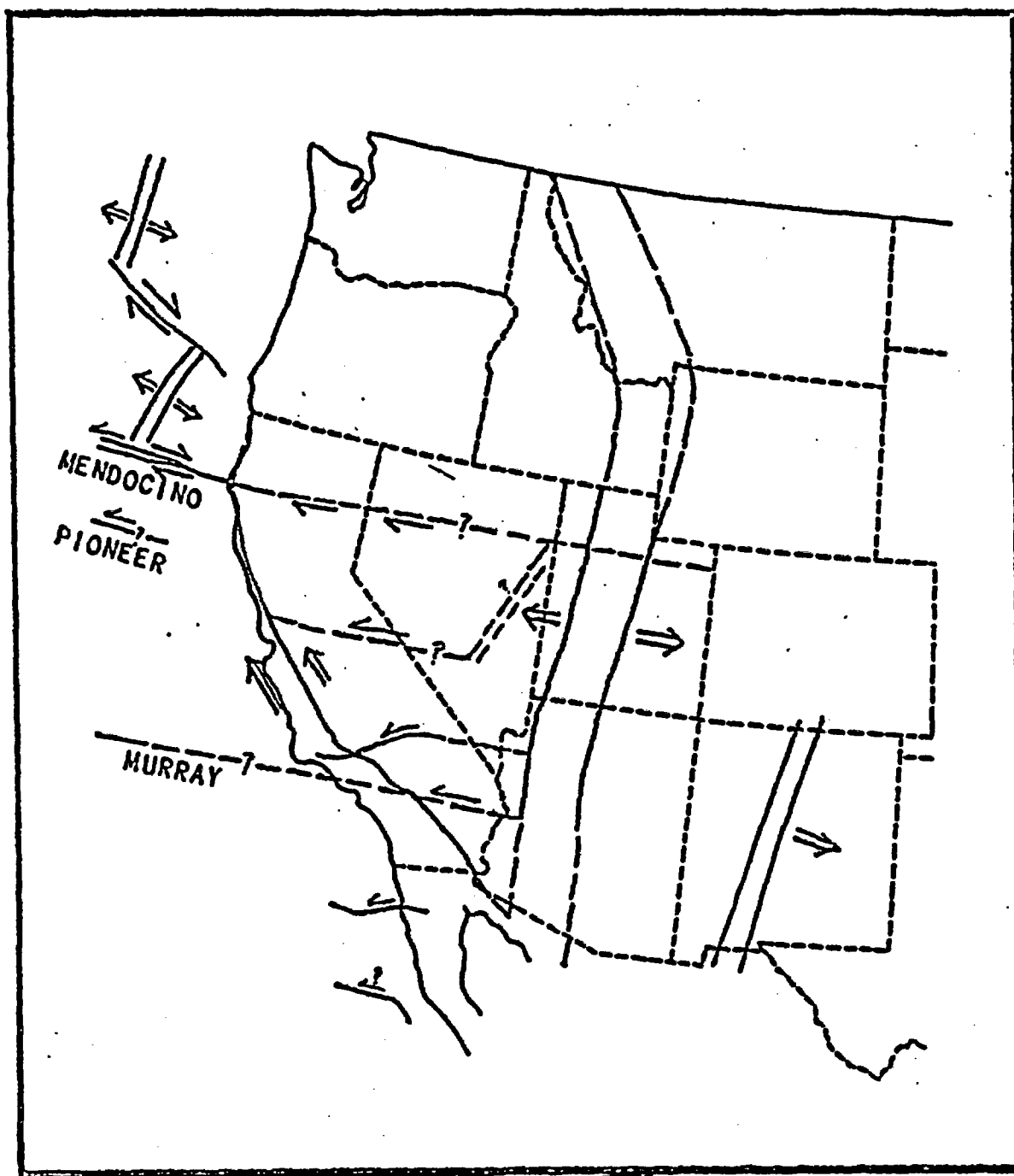


Figure 3.1-2. Map of postulated westward-moving continental block lying between landward extensions of the Mendocino and Murray fracture zones in the western United States. Modified from Cook, 1969, p. 491.

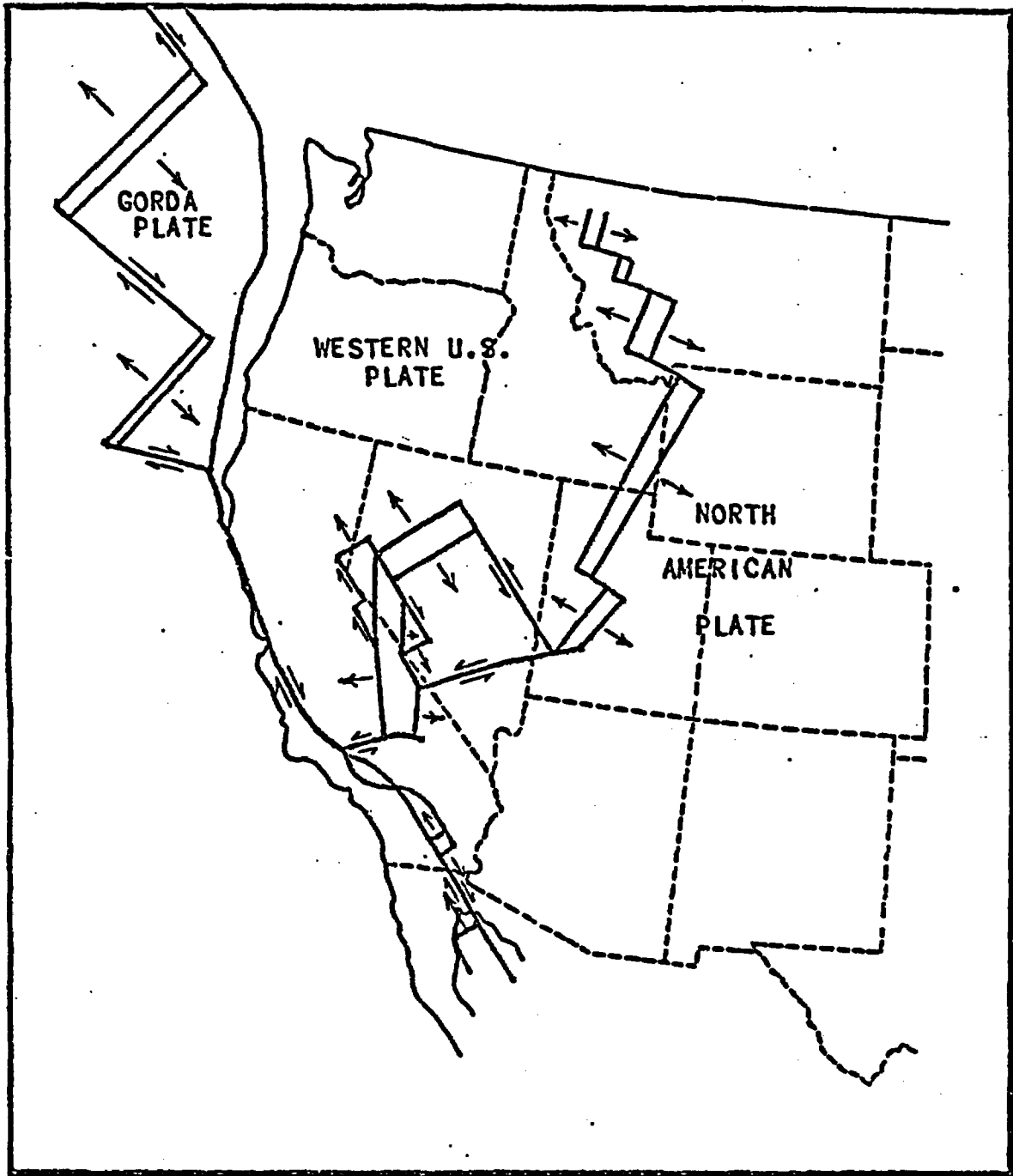


Figure 3.1-3. Rigid plate approximation to the present-day tectonics of the western United States. Modified from Suppe and others, 1974, figure 5.

Like the seismically active areas, the western U.S. exhibits an anomalous low velocity layer in the upper mantle. Press (1960) investigated the crust and upper mantle beneath parts of the Transverse Ranges, Mojave Desert, and Basin and Range Province. Basing his interpretation on seismic refraction, surface wave dispersion, and gravity data, he defined a gabbroic-ultramafic rock layer with a compressional wave velocity of 7.7 km/sec lying between the traditionally defined crustal material (granite rock with compression wave velocity of 6.1 km/sec) and upper mantle material (ultramafic rock with compressional wave velocity of 8.1 km/sec).

Thompson and Talwani (1964), using basically the same investigative techniques as Press (1960), studied the crust and upper mantle beneath parts of the California Coast Ranges, the Great Valley, the Sierra Nevada and the western Basin and Range Province. Figure 3.1-4 approximately satisfied the geophysical and geological data used. An anomalous upper mantle layer with a velocity and density approximately 3 percent less than normal underlies the whole area.

Geologic Description of the Nevada Test Site Area

The Nevada Test Site and surrounding area lies about fifty miles east of the average eastern boundary of the Cordilleran eugeosyncline and about one hundred miles west of the approximate eastern boundary of the miogeosyncline. The area also lies close to the Walker Lane-Las Vegas Valley shear zone, a transcurrent fault system in which Longwell (1960) concluded that there has been twenty-five miles of right-lateral strike-slip displacement. The area is structurally complex, corresponding to other areas in southern Nevada where intense crustal deformation has been the rule.

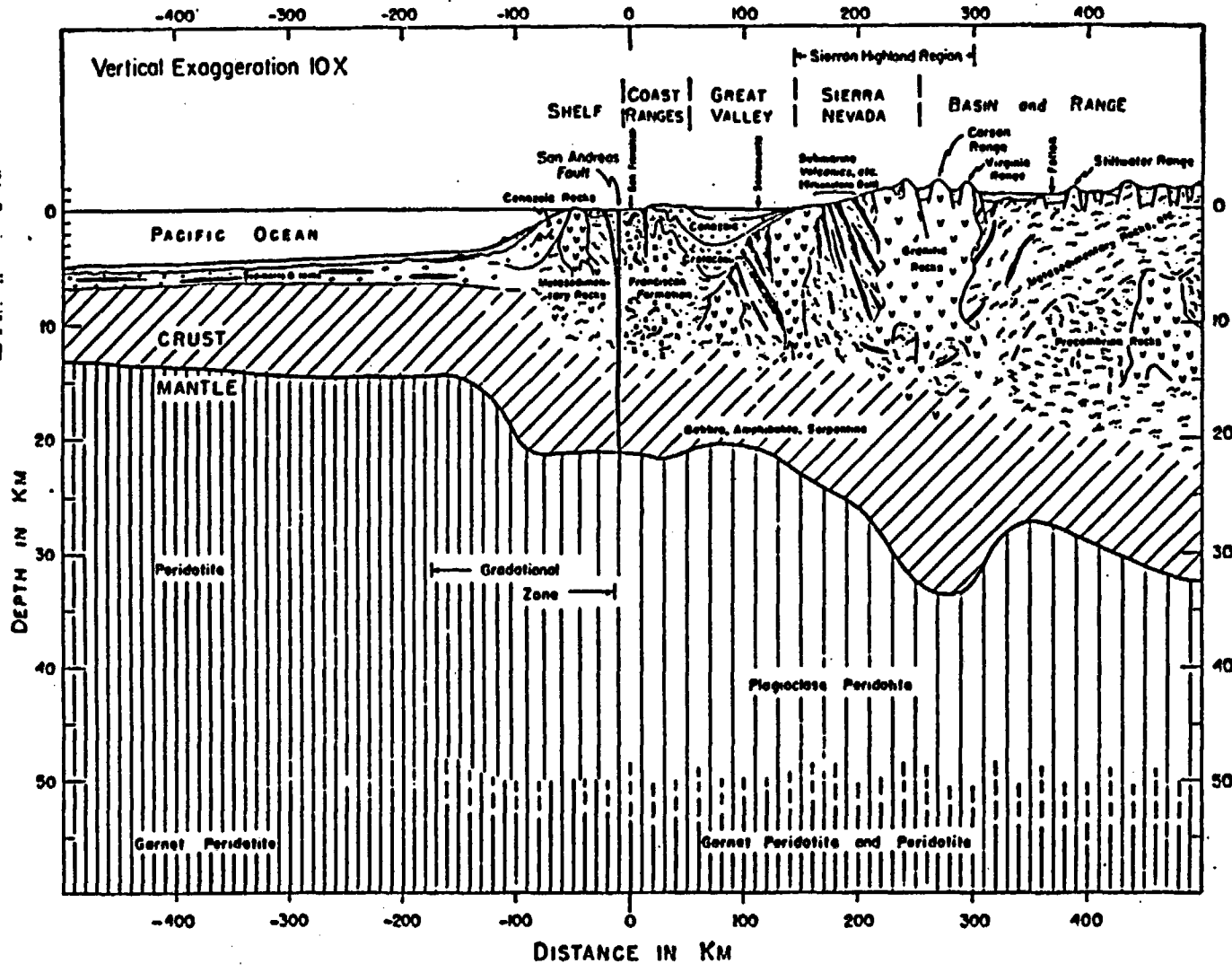


Figure 3.1-4. Geologic section of the crust and upper mantle, as interpreted from present evidence. The rock identities suggested in the upper mantle and lower crust are speculative. From Cook, 1964, p. 9.

Thrust faulting is concentrated in the vicinity of Yucca Flats, while normal faulting has affected almost every part of the Nevada Test Site area.

The exposed rocks include a wide variety of Upper Precambrian and Paleozoic sedimentary rocks, as well as Tertiary volcanics and Quaternary valley fill. The Upper Precambrian and Paleozoic sediments have an aggregate thickness of approximately 40,000 feet. These rocks account for 30 percent of all outcrops in the region. The Upper Precambrian and lowermost Cambrian are predominantly clastic with quartzite being the major lithology. The remaining Paleozoic is composed of nonclastics, of which more than 70 percent is carbonate. Other lithologies found in the Paleozoic include conglomerates, quartzites, and shales.

Rocks of the Mesozoic are limited to granitic intrusives in the Test Site area. The Tertiary rocks, which are dominantly volcanic in nature, have a thickness of more than 30,000 feet. The volcanic rocks consist mostly of rhyolite and tuff, but include many other igneous types. Locally, near the base, these rocks are often interbedded with conglomerates and layers of fresh water, marly limestones probably Miocene in age. Quaternary rocks comprise the majority of the landfill. These rocks consist of detritus derived from adjacent bedrock areas.

A generalized geologic history of the area includes: thrusting and folding during the early and middle Mesozoic time; granodiorite and quartz monzonite intrusion during late Mesozoic time; high angle normal faulting during late Mesozoic or early Tertiary time; and eruption and deposition of volcanic rocks during the Oligocene through Pliocene time. Normal faulting has continued to the present day. Smith and Kind (1972) have

published a microtectonic map of the area (Figure 3.1-5) which displays a local network of high angle normal faulting with the general trend of north-northwest.

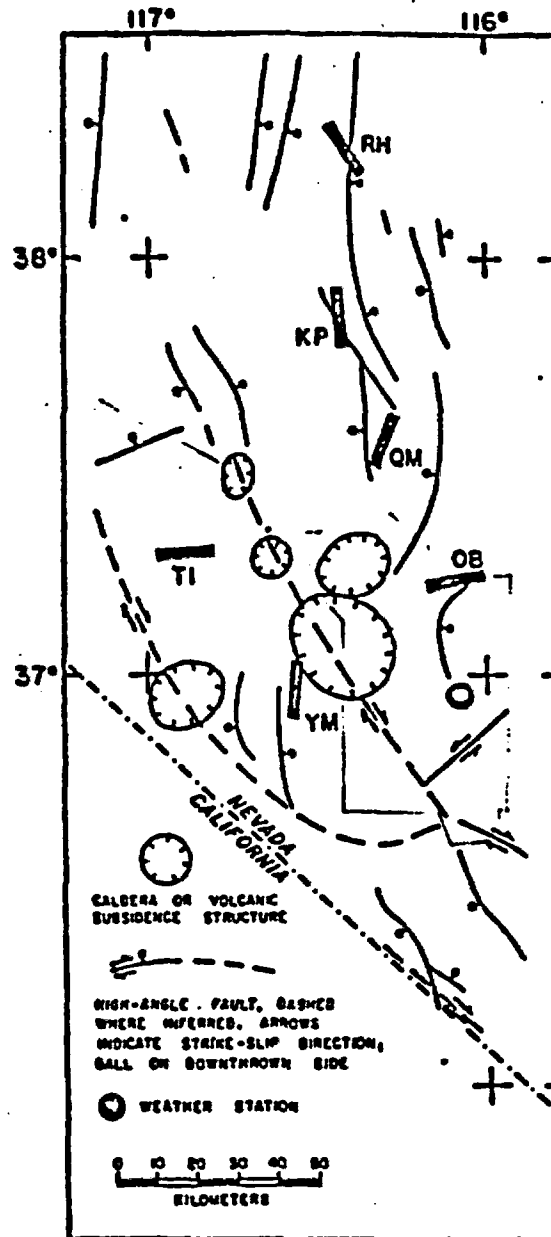


Figure 3.1-5. Simplified tectonic map of south-central Nevada. Heavy black bars are locations and orientations of strainmeters used in a study by Smith and Kind. Modified from Smith and Kind, 1972, page 4977.

3.2 History of Seismograph Deployment in Nevada and California

Any endeavor to study the seismicity of a region must by necessity begin with an accurate and continuous earthquake file. Epicenters, magnitudes, and origin times must be known for the earthquakes occurring within the area and time span to be studied. Only with a network of continuously operating, well-equipped seismograph stations can this be accomplished.

The foresight of such scientists as Holden, Ewing, Milne, and Grey have made it possible to study in detail the seismicity of the California/Nevada area. This area contains the first seismograph stations established in America (Lauderback, 1942). Besides being noteworthy for their early establishment, the seismograph stations at Mount Hamilton and Berkeley have operated continuously since their inception, with improvements in seismometry being made as improved instrumentation became available.

Holden's "California System" established in 1888, was probably the first attempt at a network of cooperative stations, all reporting to the Lick Observatory (Lauderback, 1942). In 1923, a network of seismograph stations was established in southern California with Pasadena as the central station. This network was jointly maintained by the Carnegie Institution and the California Institute of Technology, with complete responsibility given to the California Institute of Technology in 1936 (Gutenberg, 1955).

Two sources of earthquake listings covering the California/Nevada area are used in this study. The first is the California Institute of Technology-University of California-Berkeley Data Tape (Cal Tech-Berkeley Tape). This tape lists all events reported by both networks from 1910 through 1971. All magnitudes listed on the Cal Tech-Berkeley Tape are

local magnitudes (M_L). The second earthquake listing was obtained from the National Earthquake Information Service (formerly NOAA/NOS). Events from 1900 through 1960 are listed on NEIS' World Quakes-Historical tape, events from 1961 through 1971 are listed on NEIS' WSSS tapes, and events from 1972 through 1973 are listed on NEIS PDE cards. NEIS lists the body wave magnitude (m_b), surface wave magnitude (M_s), and local magnitude (M_L) for each event when they are available.

Seismograph stations in the California/Nevada area operated by the California Institute of Technology; University of California-Berkeley; University of Nevada-Reno; Lawrence Livermore Laboratories; USGS National Center for Earthquake Research, Yucca Flats, Nevada; Sandia Laboratories; and USGS S.R.A.B., Nevada, are shown in Figure 3.2-1. The station density in any particular area does not necessarily reflect the earthquake detection capability for that area. Due to cultural noise and microseismic storm activity occurring in parts of the California/Nevada area; certain stations must operate at relatively low gains. Thus, earthquake detection capability is determined by both the seismograph station density and the operating conditions at the stations. Woollard (1969) estimated that the North American seismograph stations in operation since the International Geophysical Year (1957-1958) are capable of detecting all magnitude 4.0 and greater earthquakes in almost all of North America. Hileman and others (1973) examined the southern California area in particular and estimate that the California Institute of Technology seismograph stations, a fairly close-spaced network operating in an area of cultural noise, are capable of detecting all magnitude 3.0 and greater events. Table 3.2-1 gives the operating dates for as many of the seismograph stations shown in Figure

TABLE 3.2-1

Operational Periods for Seismograph Stations in California and Nevada

STATION	NETWORK	OPERATING DATES
NRR	U. of Nevada-Reno	4-64 to present
ORV	"	10-69 to 7-71
JAS	"	10-69 to present
LVK	"	11-69 to present
HBM	"	3-70 to present
FPN	"	9-71 to present
SMN	"	1-72 to present
BEL	"	1-72 to present
KVN	"	1-72 to present
DFOD	"	1-72 to present
NRCP	"	1-72 to present
NRWP	"	1-72 to present
ARC	U. of California	1948 to present
FHC	"	9-68 to present
MLC	"	1956 to present
MIN	"	1938 to present
BRK	"	1962 to present
BKS	"	1887 to present
PCC	"	1965 to present
MHC	"	1887 to present
GCC	"	1965 to present
FRI	"	3-71 to present
SAO	"	1966 to present
LLA	"	1961 to present
PRS	"	1961 to present
PRI	"	1961 to present
BAR	Calif. Institute of Tech.	1-52 to present
BBC	"	6-51 to 9-57
CBR	"	7-72 to present
CPE	"	11-72 to present
CSP	"	11-70 to present
CLC	"	7-49 to present
CWC	"	10-65 to present
CRS	"	5-49 to 8-50
DLT	"	7-50 to 8-59
ECC	"	11-56 to 9-70
FTC	"	11-52 to 9-70
GLA	"	12-66 to present
HAI	"	9-29 to 10-65
HAY	"	9-56 to present
IKP	"	11-72 to present
IRC	"	11-71 to present
ISA	"	1-54 to present
KRC	"	10-52 to 12-65
LGC	"	7-71 to present
LJC	"	5-27 to 7-52
LSM	"	5-71 to present
MWC	"	4-28 to present

STATION	NETWORK	OPERATING DATES
PLM	Calif. Institute of Tech.	9-39 to present
PVR	"	3-56 to 11-62
PAS	"	3-27 to present
PEC	"	11-71 to present
PRR	"	3-50 to 9-51
PYR	"	11-70 to present
RVR	"	10-26 to present
SCI	"	7-67 to 10-68 & 11-71 to present
SJQ	"	7-71 to present
SNC	"	7-57 to 1-68
SPH	"	7-71 to present
SBC	"	5-27 to present
CIS	"	7-71 to present
SYP	"	6-67 to present
SWM	"	3-66 to 12-70
SCY	"	9-71 to present
TIN	"	7-72 to present
TCC	"	7-71 to present
TPC	"	5-72 to present
TWL	"	11-71 to present
VPD	"	7-71 to present
WDY	"	8-50 to 8-52
MNN (MNV)	LLL	12-67 to present
Landers	"	8-68 to present
Kanab	"	10-68 to present
EKO	"	9-69 to present
TNP	Sandia	9-61 to present
Darwin	"	9-61 to present
Leeds	"	4-63 to present
Nelson	"	10-63 to present
ELY	"	12-67 to 4-73
BMN	"	12-67 to present
ALA	U.S.G.S. (NOAA/ERL)	1966 to 1972
BTY	"	1964 to 1972
ETS	"	7-68 to 1972
EUR	"	1950 to present
LVN	"	1965 to 5-72
LSM	"	1968 to present
MCV	"	1969 to present
SMN	"	1970 to 1972
TSV	"	1970 to 1972

3.2-1 that could be determined. Additional stations not shown in either include 15 USGS stations of the NTS net (Pahute Mesa), most of which were in operation in 1968 through 1972, and the USGS stations of the central California net. The number of stations in the latter net has increased from 101 in 1969 to approximately 150 at present.

From the Cal Tech-Berkeley listing and the NEIS listings, a single earthquake listing for the western United States was compiled. This was accomplished by first removing duplicate events from the Cal Tech-Berkeley listing. Duplicate events were defined as those earthquakes which were reported by both networks and which occurred within 0.4° of latitude and longitude and 1.75 minutes of time of each other, except in the case of aftershock sequences. The NEIS listings were searched for all events occurring within the western United States as defined by 25° to 50° North Latitude and 87° to 135° West Longitude. The Cal Tech-Berkeley listing, with duplicates removed, was then merged with the western United States NEIS data. Chronological ordering and removing of duplicates were carried out simultaneously with the merging. Finally, all announced nuclear shots were removed or flagged so that they could be deleted from the depictions of natural seismicity. Springer and Kinnaman's (1971) listing of nuclear shots and the Atomic Energy Commission's Revised Nuclear Test Statistics (1973) were used to identify which of the events were nuclear shots. All sorting, removing of duplicates and merging was accomplished with the aid of the UNIVAC 1110 computer system operated by the University of Wisconsin. The final earthquake listing is titled Western-US Main-File/1900-1973 and is contained on magnetic tape held by the Department of Geological Sciences, University of Wisconsin-Milwaukee. Western-US Main-File/1900-1973 contains

28,986 events occurring within the area bounded by 25° to 50° north latitude and 87° to 135° west longitude for the years 1900 to 1973, inclusive.

3.3 Effect of Seismograph Station Coverage on Reported Seismicity

Investigations of seismic activity as a function of time within selected areas do not in general account for changes in the detection capability of the monitoring network from which the initial data are derived. It is, therefore, implicitly assumed that no significant changes in the detection network occurred during the study period and that all measured changes in seismic activity actually occurred. While this approach has proven useful, the possibility exists that measured changes in seismic activity have resulted not from any physical factors but rather from an increase in the detection ability of the involved network. Thus, a few seismic stations operating in a given area would be expected to detect a few earthquakes, while the existence of many seismic stations in the same area would lead to the detection of many earthquakes. It is this effect which has led to the observation (usually not serious) that seismic recording stations cause earthquakes.

For many areas of the earth, such as the oceans and remote parts of South America, the assumption of a relatively constant detection network is justified. For other areas of the earth, however, such an assumption is completely unjustified. This is particularly true of the Nevada area where the advent of a nuclear testing program led to the installation of numerous seismic stations designed to monitor the characteristics of the various explosions. These same stations would, of course, monitor natural seismic activity and would be expected to detect a number of seismic events which had previously gone undetected. This effect is clearly shown in Table 3.3-1, where the total number of events detected in decade intervals is compared to the best available estimate of

stations in the detecting network. While Table 3.3-1 demonstrates the qualitative effect of station coverage on number of reported events, it is not possible to base quantitative conclusions on the effect of additional stations, since the effect of an additional station depends upon the position and noise level of the added station and upon the number, locations and noise levels of the existing stations.

TABLE 3.3-1

A Comparison of the Total Number of Reported Events with the Number of Stations Available for Detection, for Decade Intervals from 1933 to 1973

Time Interval	Number of Stations in Regional Network	Number of Reported Earthquakes
1933-1942	9	467
1943-1952	13	904
1953-1962	26	1162
1963-1972	46	1056

A quantitative approach to the problem of station coverage is provided by the work of Booker (1964), who derived a set of equations governing the minimum magnitude event at a given location which could be detected by a given station. For a given set of M stations it is then possible to calculate the minimum magnitude for which there exists a probability P that a subset of $N \leq M$ stations will detect the event. By performing the calculations at each point of an areal grid it is possible to construct a minimum detection surface for any selected area. The resulting surface indicates the minimum magnitude event which would

be reliably detected by the existing network.

Using a modified FORTRAN program due to Booker (1964), the above calculations were performed on a 0.25° grid for a 4° x 4° area of Nevada. The area extended from 115°W Longitude to 119°W Longitude and from 35°N Latitude to 39°N Latitude. The assumed station noise levels, necessary in performing the calculations, were taken from Frantti (1965). The station locations and history were taken from the summary provided with this report.

The detection surface for the stations which existed during the period 1933-1942 is shown in Figure 3.3-1. It is evident from the figure that the detection ability of the stations existing at that time varied from an m_p of 4.0 in the southwest to an m_p of 5.2 in the northeast.

The criterion used in determining Figure 3.3-1 was that there existed an 80% probability that at least three stations of the existing network would locate the event. This criterion is probably somewhat higher than that which actually existed and, hence, events with magnitudes less than that indicated by Figure 3.3-1 were reported during the period 1933 to 1942. Using the same detection criterion the minimum magnitude surfaces for the periods 1943-1952, 1953-1962 and 1963-1972 are shown in Figures 3.3-2 through 3.3-4. It is evident from these figures that the minimum detectable event associated with any point of the sector changed very little during the period from 1933-1952. For the period from 1953-1962 the minimum event decreased significantly in the southwest region but remained relatively constant over the remainder of the sector. In the final period, 1963-1972, the minimum detectable

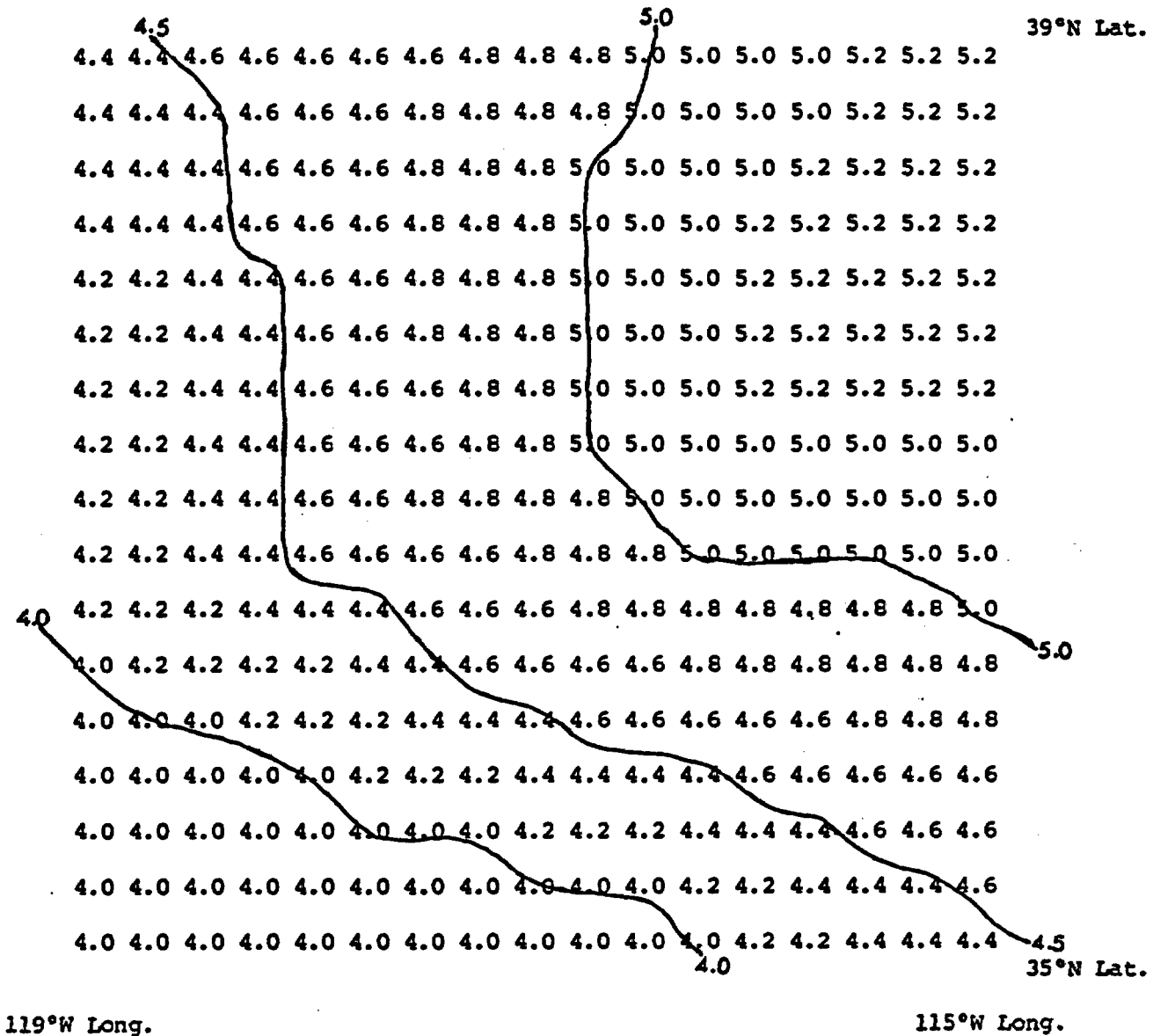


Figure 3.3-2. The minimum detection surface for the period from 1943-1952.

event decreased dramatically over the entire region. This final period reflects the influence of the various station networks installed to monitor the activities of the underground testing program.

In an attempt to eliminate the effects of station coverage, the measured activity in each decade period, as determined by the network existing at that time, was sorted on the basis of the calculated detection surface for the period 1933-1942. The results should provide a measure of the seismic activity which would have been observed in the 4° sector of Nevada if the station coverage had remained constant at the 1933-1942 level. The number of events seen in each period after filtering through the 1933-1942 detection surface are shown in Table 3.3-2. For purposes of comparison, the total number of events with reported magnitudes for each period are also shown in Table 3.3-2.

It is evident from Table 3.3-2 that the number of events in each period, after removing the effects of increased station coverage, remains relatively constant for the first three periods and then exhibits a marked decrease for the 1963-1972 period. This is in contrast to the total data which exhibits a steady increase during the first three periods and a minor decrease in the final period.

The strain release for the various periods, after removing the effects of increasing station coverage, and the strain release calculated from all events in the period are shown in Table 3.3-3. On the basis of this table it would appear that a continued decrease in strain release has occurred since the 1943-1952 period. This conclusion would not be obvious on the basis of the total data which contains the effects of increasing station coverage.

TABLE 3.3-2

The Number of Events in 10-Year Periods Before and After
Removing the Effects of Increasing Station Coverage

Period	No. of Events After Filtering Through the 1933-1942 Detection Surface	Total Number of Events with Reported Magnitudes
1933-1942	196*	467*
1943-1952	413	904
1953-1962	300	1162
1963-1972	112	1056

* The total number of events which were actually reported during this period differs significantly from the number which theoretically should have been detected. This difference does not necessarily reflect upon theory employed, but more likely upon the input parameters to the theory. It is possible that a station, which has not been accounted for in this report, existed during the 1933-1942 period somewhere in the Nevada area. It is also possible that all stations have been accounted for but that long term increases in seismic background noise have occurred. Thus, the recent measurement of noise levels which were assumed appropriate to the 1933-1942 period may have been too high.

TABLE 3.3-3

Calculated Strain Release Before and After
Removing the Effect of Increasing Station Coverage.

Period	Strain Release after Filtering Through the 1933-1942 Detection Surface	Strain Release Based on Total Number of Events with Reported Magnitudes
1933-1942	0.5×10^{11}	0.9×10^{11}
1943-1952	$1.0 \times 10^{11*}$	$2.0 \times 10^{11*}$
1953-1962	0.5×10^{11}	1.0×10^{11}
1963-1972	0.2×10^{11}	1.0×10^{11}

* This interval includes the 1952 Kern Co., California earthquake of magnitude 7.7.

Tables 3.3-2 and 3.3-3 demonstrate the importance of removing effects of changing station coverage from the data base prior to forming conclusions concerning changes in natural seismicity. The attempts at removing the effects of station coverage as reported here are preliminary and are not beyond criticism. Nevertheless, the method does yield data less biased by changing station coverage than the raw data base. When viewed in the light of a constant station coverage, the data does appear to indicate a decrease in the strain release associated with the period of underground testing.

3.4 Seismicity Investigations

3.4.1 California and Nevada Regions

Seismic Parameters and Their Relationship

Surface Wave, Body Wave, and Local Magnitudes

An important parameter that has to be considered when discussing the seismicity of a region is the magnitude of the individual earthquakes.

Three earthquake magnitude scales are in general use including the local magnitude (M_L), body wave magnitude (m_b) and surface wave magnitude (M_S).

As noted in Section 3.2, local magnitudes are listed on the Cal Tech-Berkeley data tape. When available, body wave magnitude (m_b), surface wave magnitude (M_S), and local magnitude (M_L) are listed on the NEIS data. The local and body wave magnitudes were converted to their equivalent surface wave magnitudes to establish a base from which the strain release could be calculated.

An investigation of the m_b vs. M_L relationship for earthquakes occurring in southern California and Nevada showed that the original Richter relationship does not fit the earthquake data for this area very well over the range 2.5 to 5.0 M_L as shown in Figure 3.4-1. Plotted in this Figure are the NEIS (USGS) m_b vs. Pasadena M_L for earthquakes in southern California and Nevada that are listed in the NEIS earthquake data file for 1961-1972. The second degree approximation obtained from a least squares fit

$$m_b \text{ (NEIS)} = 3.73 - .16 M_L + .08 M_L^2$$

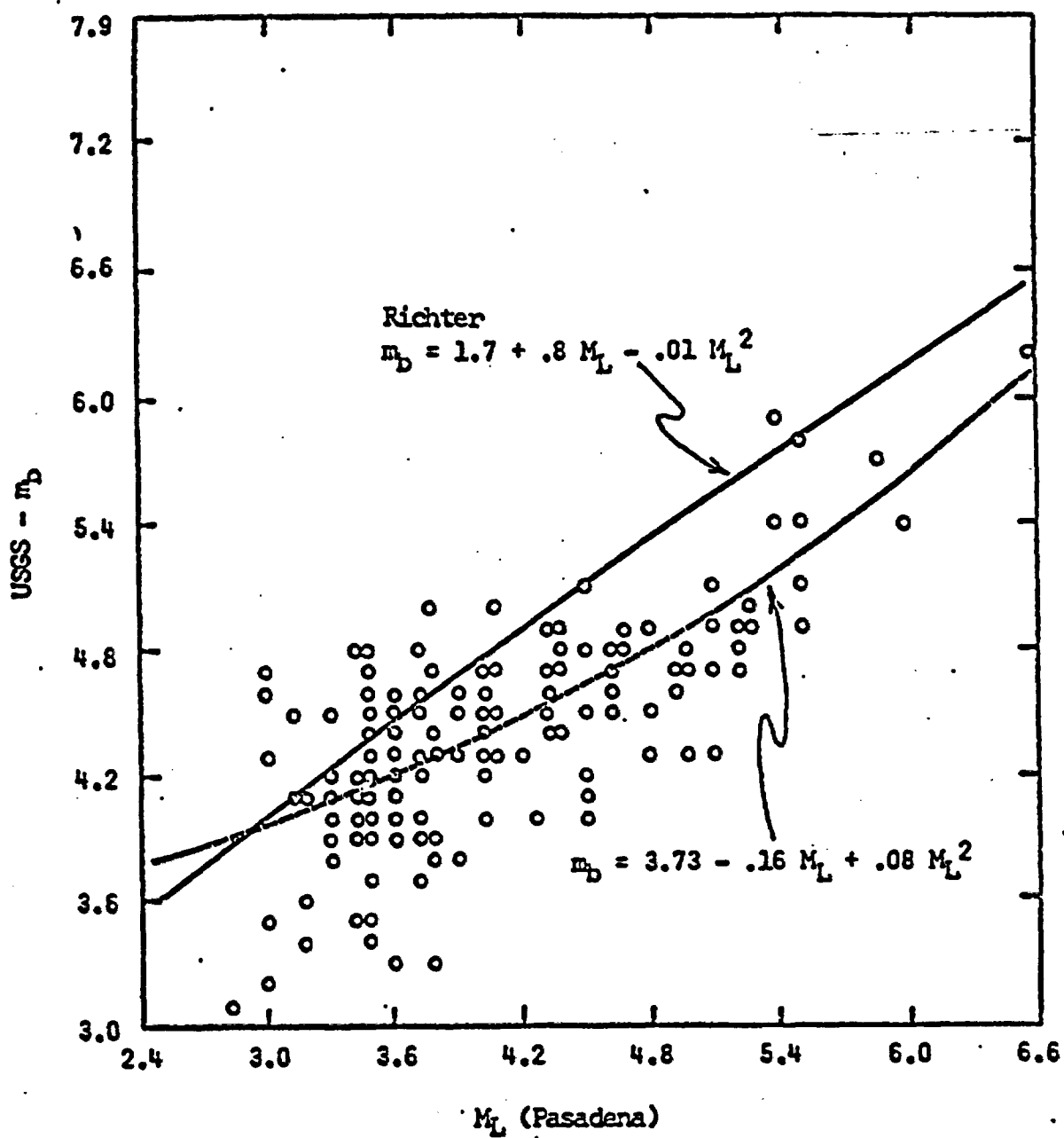


Figure 3.4-1. Relationship between body wave magnitude and local magnitude for earthquakes located in southern California and Nevada. Modified from George and others, 1974, figure 3.

represents the data more accurately and is used in this study⁻¹ to convert M_L to its equivalent m_b for M_L greater than 2.5. For M_L less than 2.5 the original Richter relationship

$$m_b = 1.7 + .8 M_L - .01 M_L^2$$

is used to convert M_L to its equivalent m_b . The conversion of m_b to M_S is

-1 The above relationship was established early during the course of this investigation and was used for computing strain release. Toward the end of this study when more data were available the entire earthquake file was searched for all California/Nevada earthquakes where m_b vs. M_L and m_b vs. M_S data were available for the same earthquake. 339 earthquakes were identified that had both m_b and M_L magnitudes ranging between 3.0 and 6.0. 51 earthquakes were found that had both m_b and M_S magnitudes ranging between 4.0 and 6.6. A least squares fit for these data gives the following relationships:

m_b vs. M_L - 1st, 2nd, 3rd order fits

$$m_b = 2.43 + .48 M_L$$

$$m_b = 4.40 - .48 M_L + .11 M_L^2$$

$$m_b = 5.24 - 1.07 M_L + .25 M_L^2 - .01 M_L^3$$

M_S vs. m_b - 1st and 2nd order fits

$$M_S = -1.91 + 1.33 m_b$$

$$M_S = 8.33 - 2.59 m_b + .37 m_b^2$$

The revised relationships were not used in any of the computations but are included here for the record. The difference between the two second order fits for m_b vs. M_L would correspond to less than 0.2 magnitude units over the range of 3.0 to 6.0. The revised m_b vs. M_S first order fit above gives an M_S equivalent magnitude that ranges from 0.5 to 1 units larger than would be obtained by using Richter's (1958) original relationship.

accomplished by use of the relationship

$$M_s = 1.59 m_b - 3.97 \quad (\text{Richter, 1958})$$

Seismic Wave Energy and Strain Release

Assuming that an earthquake is generated by the release of accumulated strain (ϵ) in a volume of rock (V) with an average elastic constant (μ), the energy (E) stored in the rock as elastic strain is

$$E = 1/2\mu\epsilon^2V \quad (\text{Benioff, 1951}) \quad (1)$$

If no loss of energy occurs during the conversion of stored energy to seismic wave energy, it follows that E is also the energy of the earthquake and ϵ is the strain rebound. Taking the square root of equation (1)

$$E^{1/2} = (1/2\mu V)^{1/2}\epsilon$$

According to Benioff (1951), it is generally impossible to determine μ and V for a given earthquake; for any given fault, however, they are assumed constant:

$$(1/2\mu V)^{1/2} = C$$

and therefore

$$E^{1/2} = C\epsilon$$

or the square root of the radiated energy is proportional to the strain rebound. Since the purpose of this study is to determine the pattern of migration of earthquake activity through time, it is valid to use strain release to compare earthquake activity in the same area at different times. We need only make the assumption that C for a given fault or area remains constant through the time interval studied.

The strain release ($E^{1/2}$) is computed by taking the square root of the seismic wave energy (E) as defined by

$$\log E = 12.25 + 1.44 M_S \quad (\text{Bath, 1968}) \quad (2)$$

or

$$E^{1/2} = 10(6.125 + 0.72 M_S) \quad (3)$$

where E is in ergs. The strain release ($E^{1/2}$) is not measurable strain in a physical sense and could be more definitively referred to as quasi-strain or quasi-strain release; however, in keeping with convention the term strain release will be used to refer to the quantity $E^{1/2}$. The cumulative strain release ($E_C^{1/2}$) can now be defined as the summation of the strain release computed for each individual earthquake within a unit area

$$E_C^{1/2} = \sum_{i=1}^n E_i^{1/2}$$

Decibel values used in presenting the perspective plots are calculated using the relationship

$$db = 20 \log \left[\sum_{i=1}^n \frac{E_i^{1/2}}{E_0^{1/2}} \right] \quad (4)$$

where $E_0^{1/2}$ is the strain release of a magnitude zero earthquake or 1.318×10^6 ergs^{1/2}.

The relationship (equations 2, 3 and 4) between surface wave magnitude, seismic wave energy (ergs), strain release ($\sqrt{\text{ergs}}$), and decibel values is illustrated in Figure 3.4-2. For example, a magnitude (M_S) 4.5 earthquake releases approximately 5.25×10^{18} ergs of seismic wave energy. This is

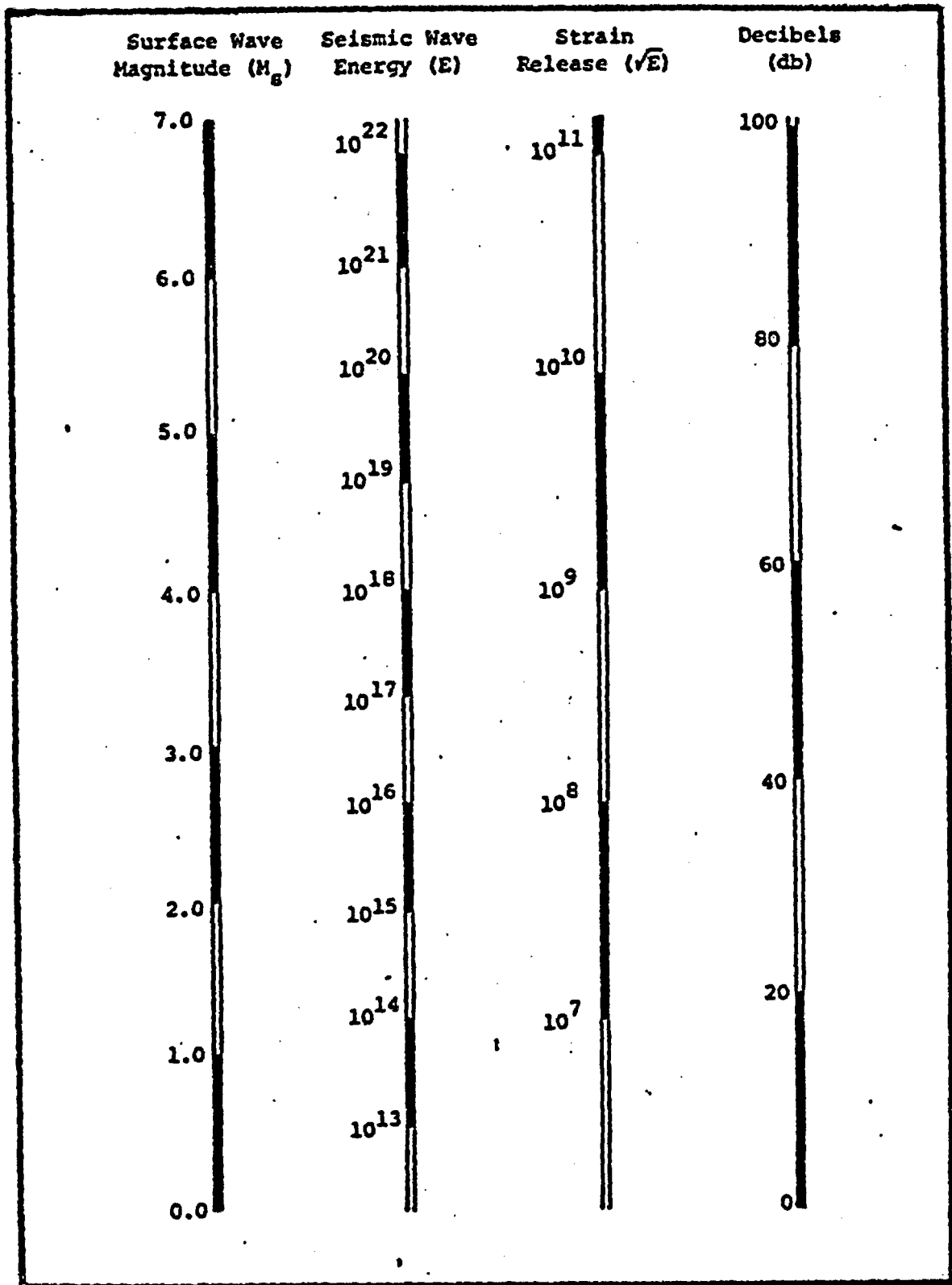


Figure 3.4-2. Relationship (equations 2, 3 and 4) between surface wave magnitude, seismic wave energy (ergs), strain release ($\sqrt{\text{ergs}}$), and decibels. For example, a magnitude (M_s) 4.0 earthquake is equivalent to 1.00×10^{18} ergs of seismic wave energy, 1.00×10^9 ergs $^{1/2}$ of strain release, and 57.7 decibels.

equivalent to 2.29×10^9 ergs^{1/2} of strain release or 72 decibels. It would take 5.2 magnitude (M_S) 4.0 earthquakes to release the same amount of seismic wave energy as the one 4.5 M_S earthquake. By using the decibel values rather than the strain release, a smoothing factor is introduced into the presented data. Note also that the M_S and db scales are proportional.

Perspective Plots

The program used to compute and plot strain release was developed by A. F. Shakal in 1972 to facilitate the visual display of the spatial and temporal data being studied under this investigation. Willis and others (1973) first used the program to visually display seismic activity in only the Nevada area as a function of time (1852 to 1973) and space. In this previous report, the improved seismograph station coverage became evident in the strain release data for the period 1931-35. The beginning of seismic activity associated with the filling of Lake Mead was clearly demonstrated in the 1936-40 time period. This seismic activity continued until about 1955. The earthquake activity in 1954 in the areas of Dixie Valley, Fairview Peak and Rainbow Mountain east of Fallon, Nevada, was indicated as very predominant peaks in the strain release. Minor changes in the program were made to facilitate the use of the larger data base of the California/Nevada area and to exclude nuclear shots and explosions from the cumulative strain release values. Basically, the program searches the data tape for the time window to be studied and computes the cumulative strain release for each $1/4^\circ$ by $1/4^\circ$ grid unit for the earthquakes within that time window. The cumulative strain release is then plotted in perspective using a digital X-Y plotter. The horizontal axes

represent latitude and longitude in $1/4^\circ$ increments. The vertical axis represents the cumulative strain release scaled in decibels. The input data deck contains input parameters which control the time window size, grid unit size, reference magnitude, plot size, lettering size, and the direction from which the perspective plot is drawn.

Visual Analysis - Perspective Plots

Seismic activity in the California/Nevada area for each year, 1956 through 1973, is shown in perspective plots looking toward the northwest (Figure 3.4-3, A-R). To keep the perspective plots as uncluttered as possible, no physical or cultural features were plotted. Instead, a transparent overlay (Plate A) is provided to help locate state boundaries and major cities.

Two zones of continuous high seismicity are evident in Figure 3.4-3, A-R. One extends along the entire coast of California; the other extends from the southern California coast to north-central Nevada. Ryall and others (1966) called this second zone the Ventura-Winnemucca zone and noted that although it followed a discontinuous line of historic fault breaks, it appeared not to be related to or defined by structures considered to be the dominant tectonic elements of the region. Woollard (1969) also defined two independent branches of seismicity in the California/Nevada area; one following the coast, and the other following the east flank of the Sierra Nevada batholith and merging with the coastal branch in northern Baja, California. Some northwest-southeast alignments can be seen in the Nevada area. The faults in this region trend north-south, on the average, so one could expect to see more north-south alignments. The northwest-southeast alignments suggest a possible pattern of activity of en echelon sections

Figure 3.4-3. Yearly perspective plot of cumulative strain release in California/Nevada area. Plot is based on magnitudes and intensities of earthquakes which occurred in the California/Nevada area.

A. 1956
B. 1957
C. 1958
D. 1959
E. 1960
F. 1961
G. 1962
H. 1963
I. 1964
J. 1965
K. 1966
L. 1967
M. 1968
N. 1969
O. 1970
P. 1971
Q. 1972
R. 1973

Figure 3.4-3A

1956

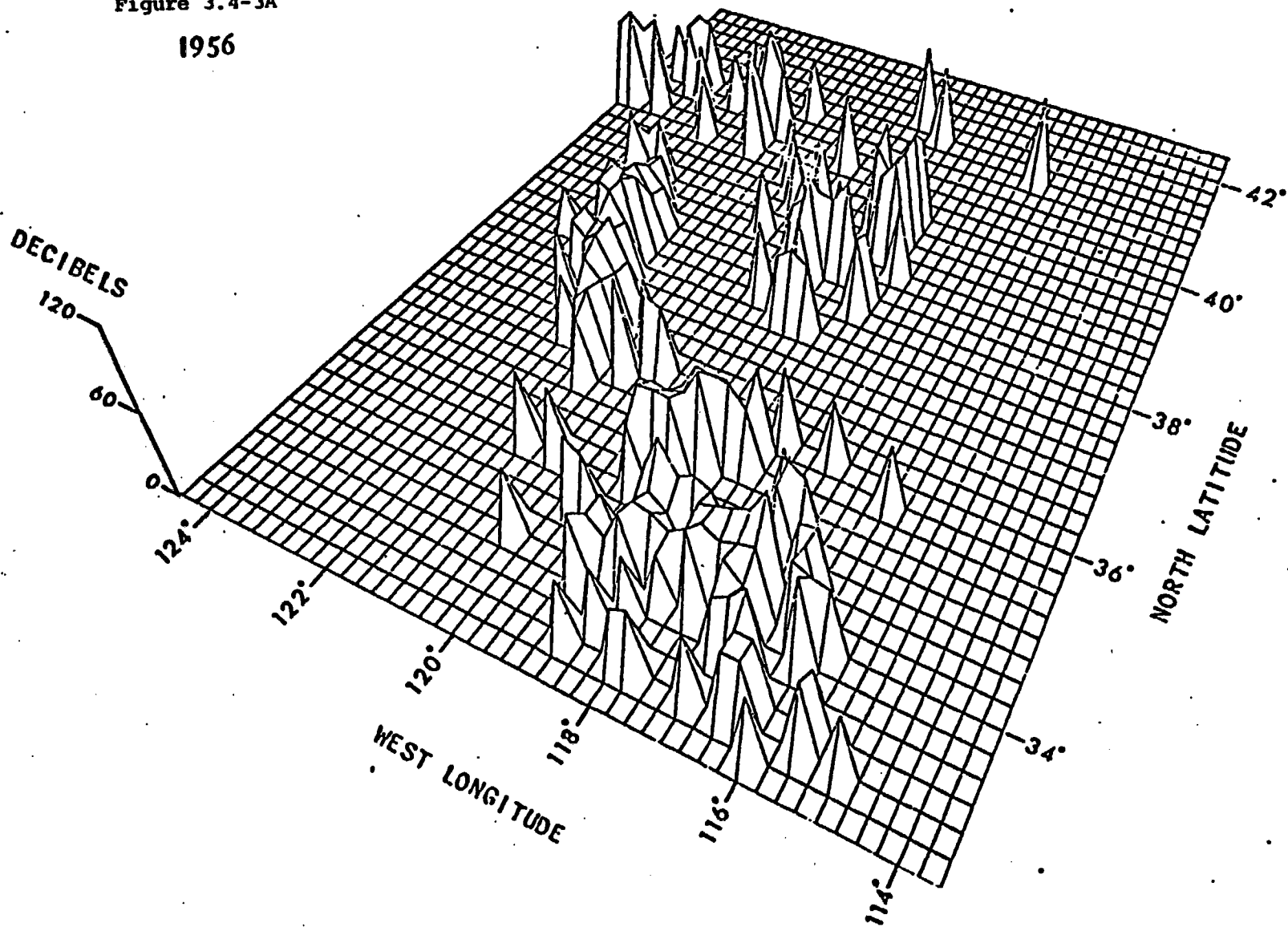


Figure 3.4-3B

1957

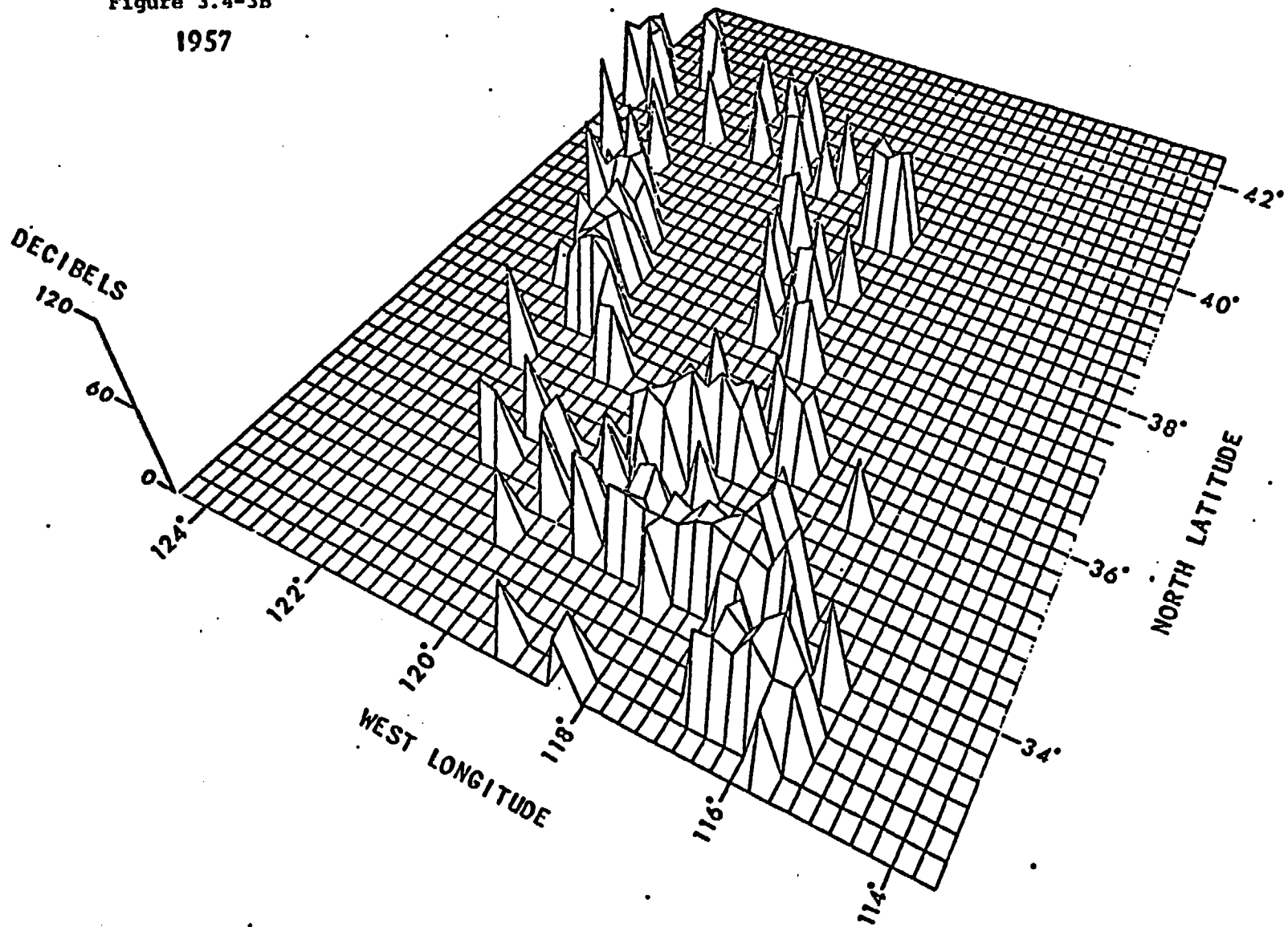


Figure 3.4-3C

1958

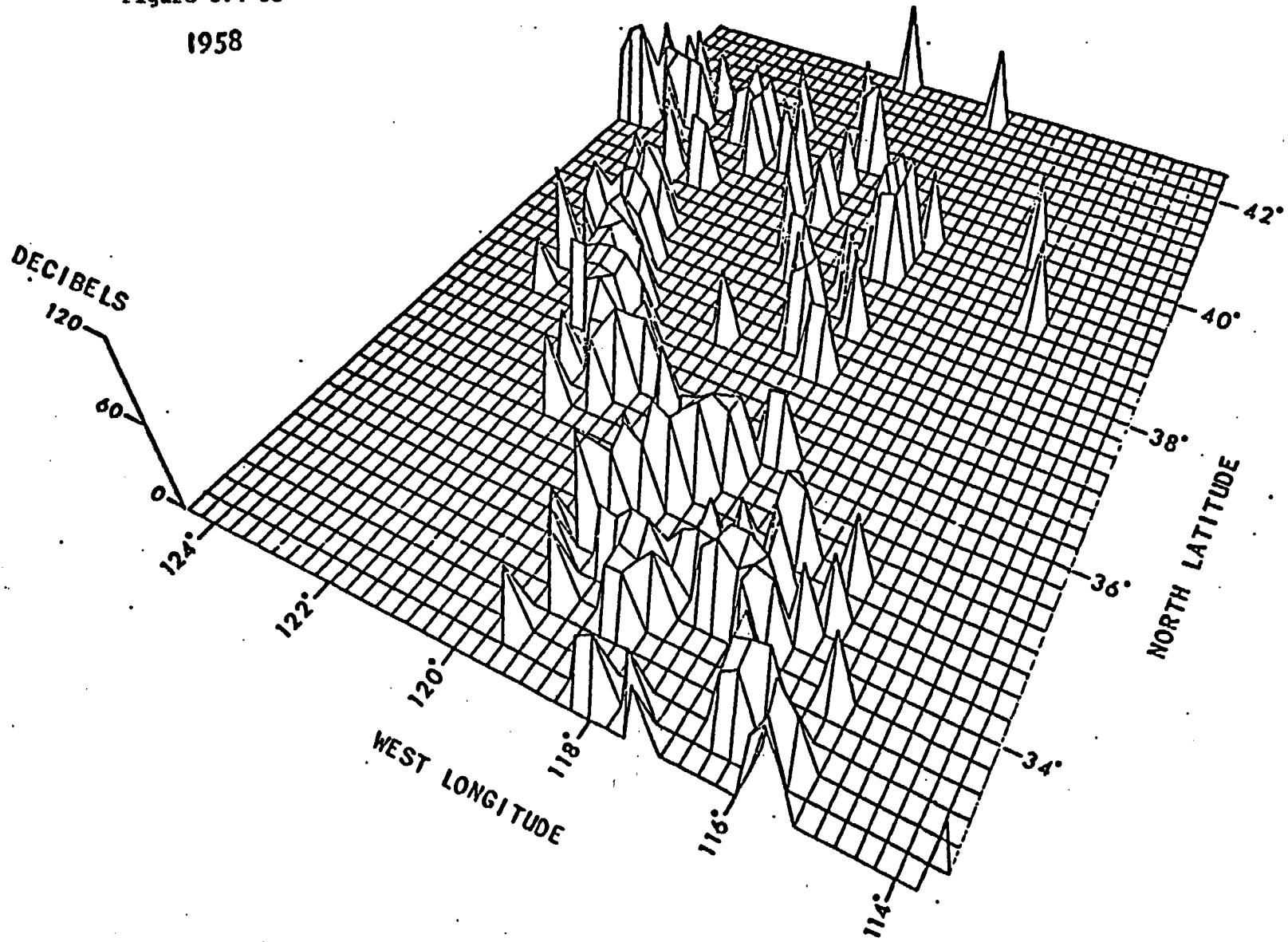


Figure 3.4-3D

1959

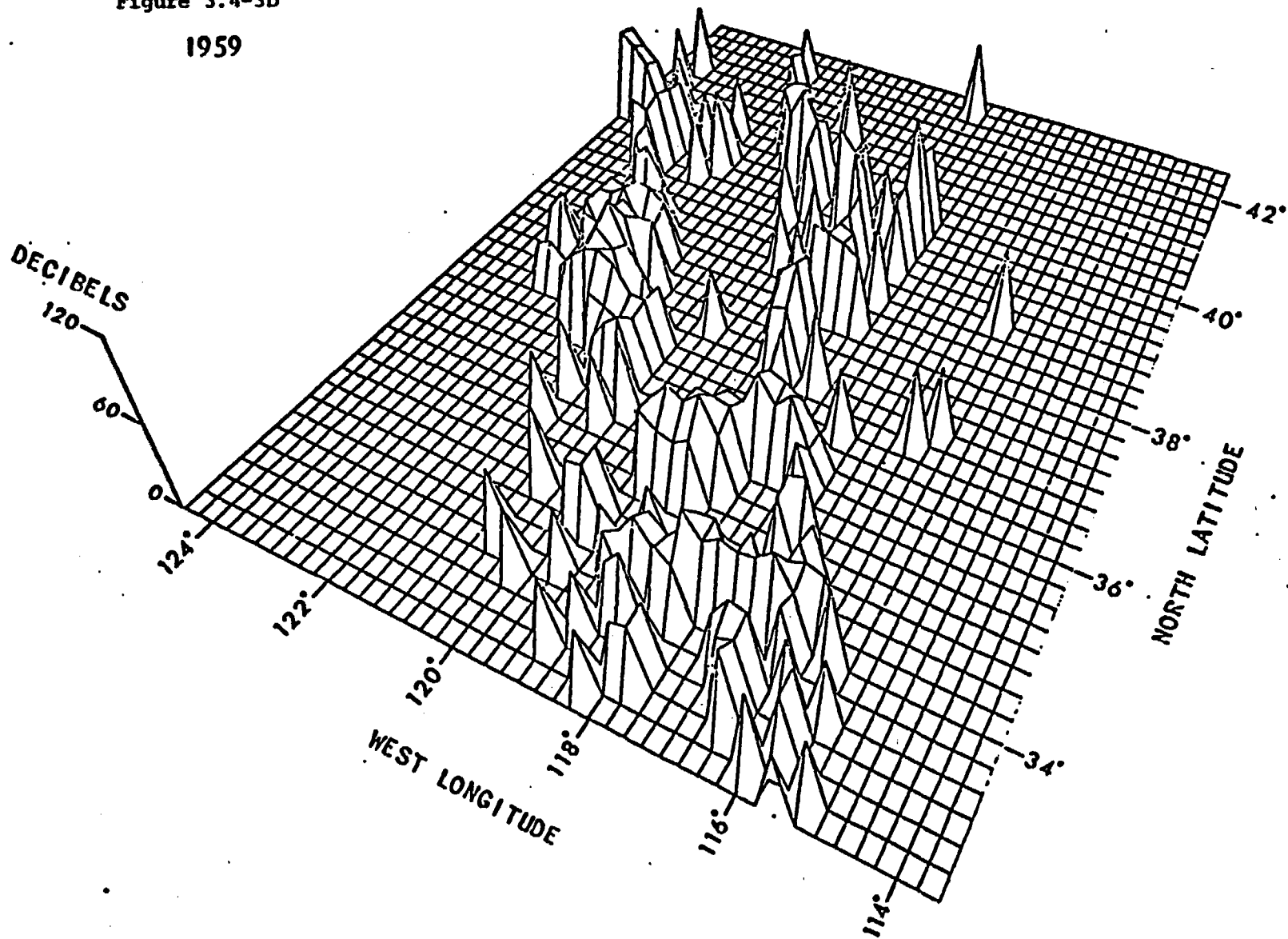


Figure 3.4-3E
1960

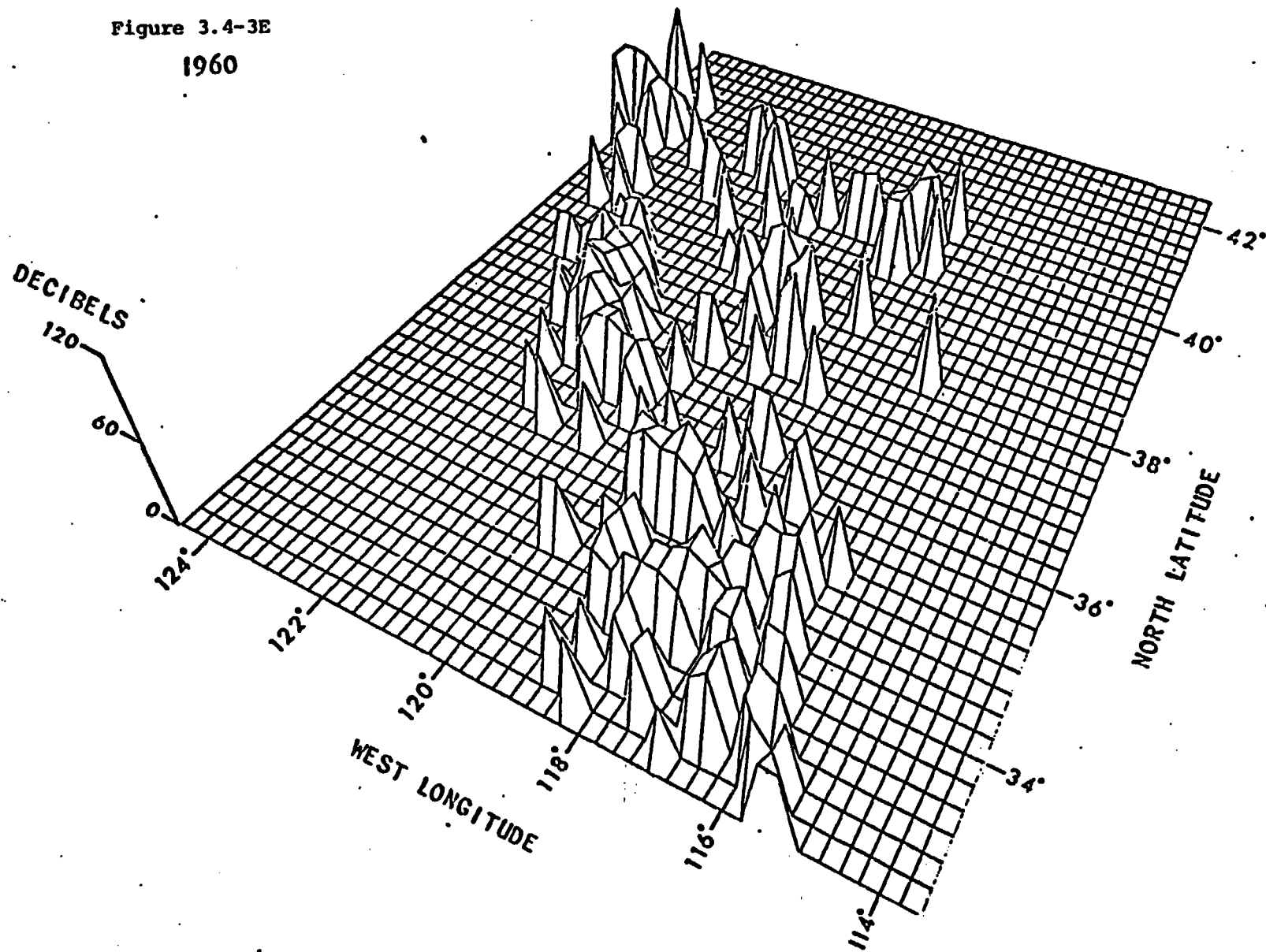


Figure 3.4-3F
1961

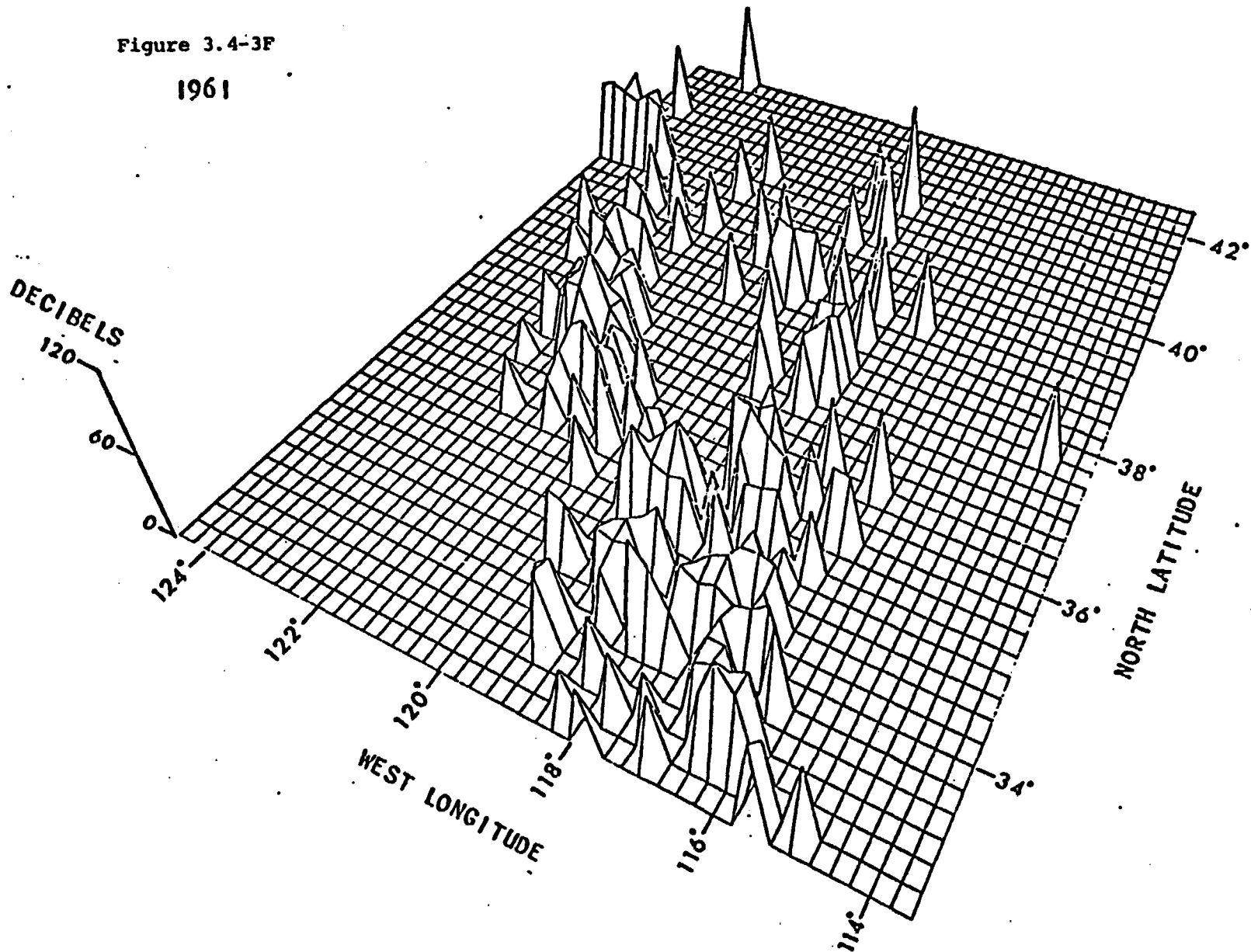


Figure 3.4-3G
1962

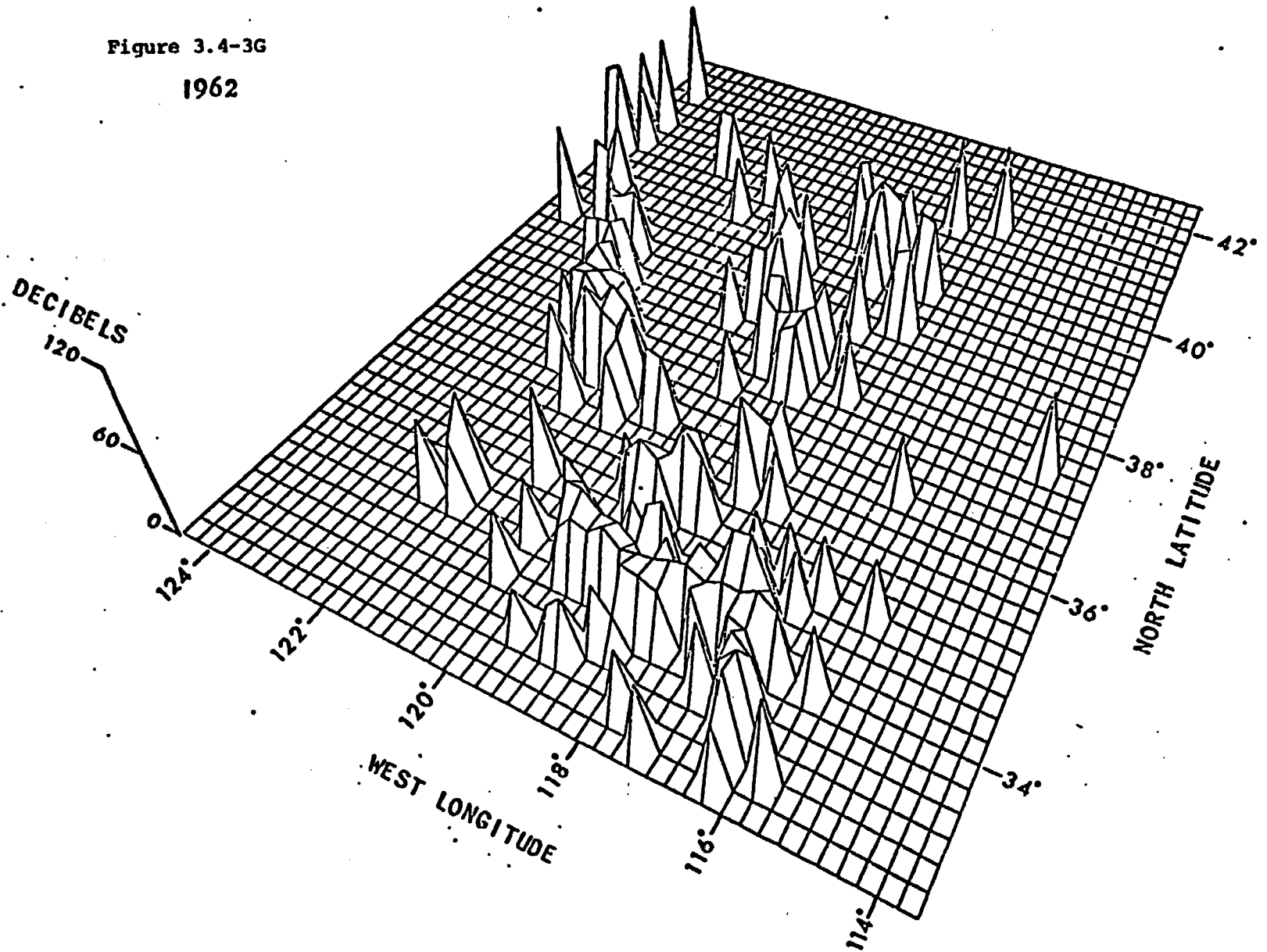


Figure 3.4-3H

1963

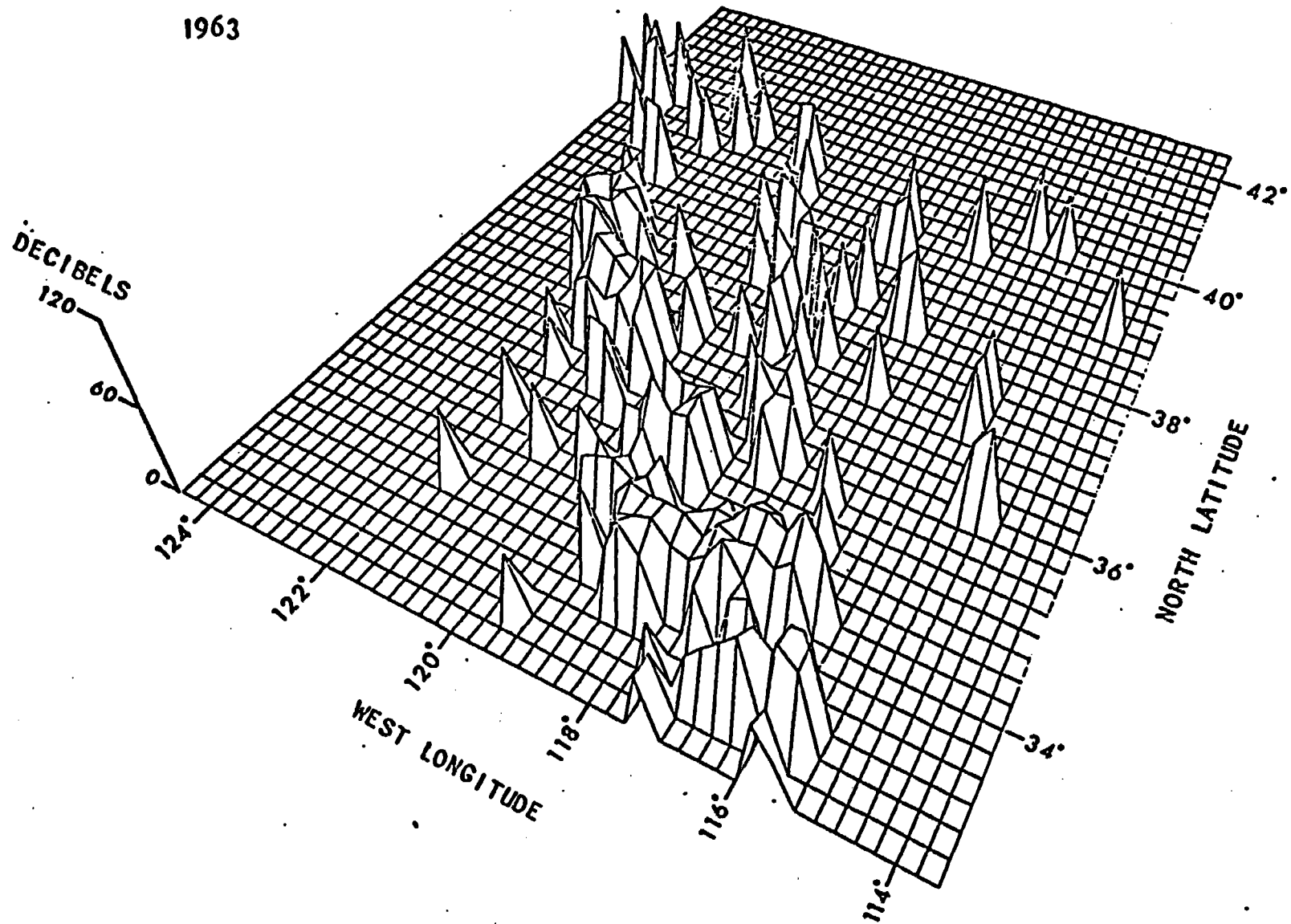


Figure 3.4-3I

1964

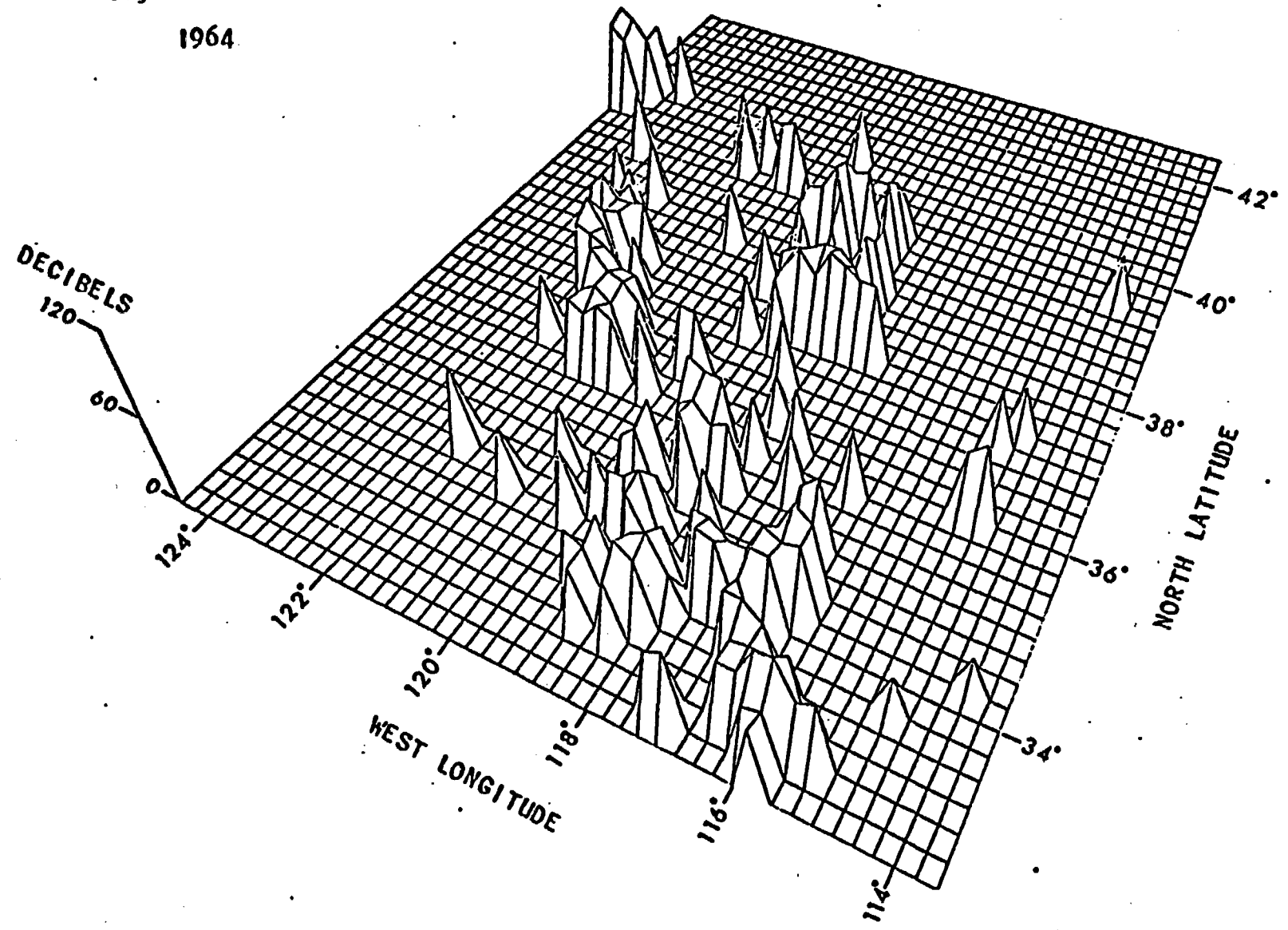


Figure 3.4-3J
1965

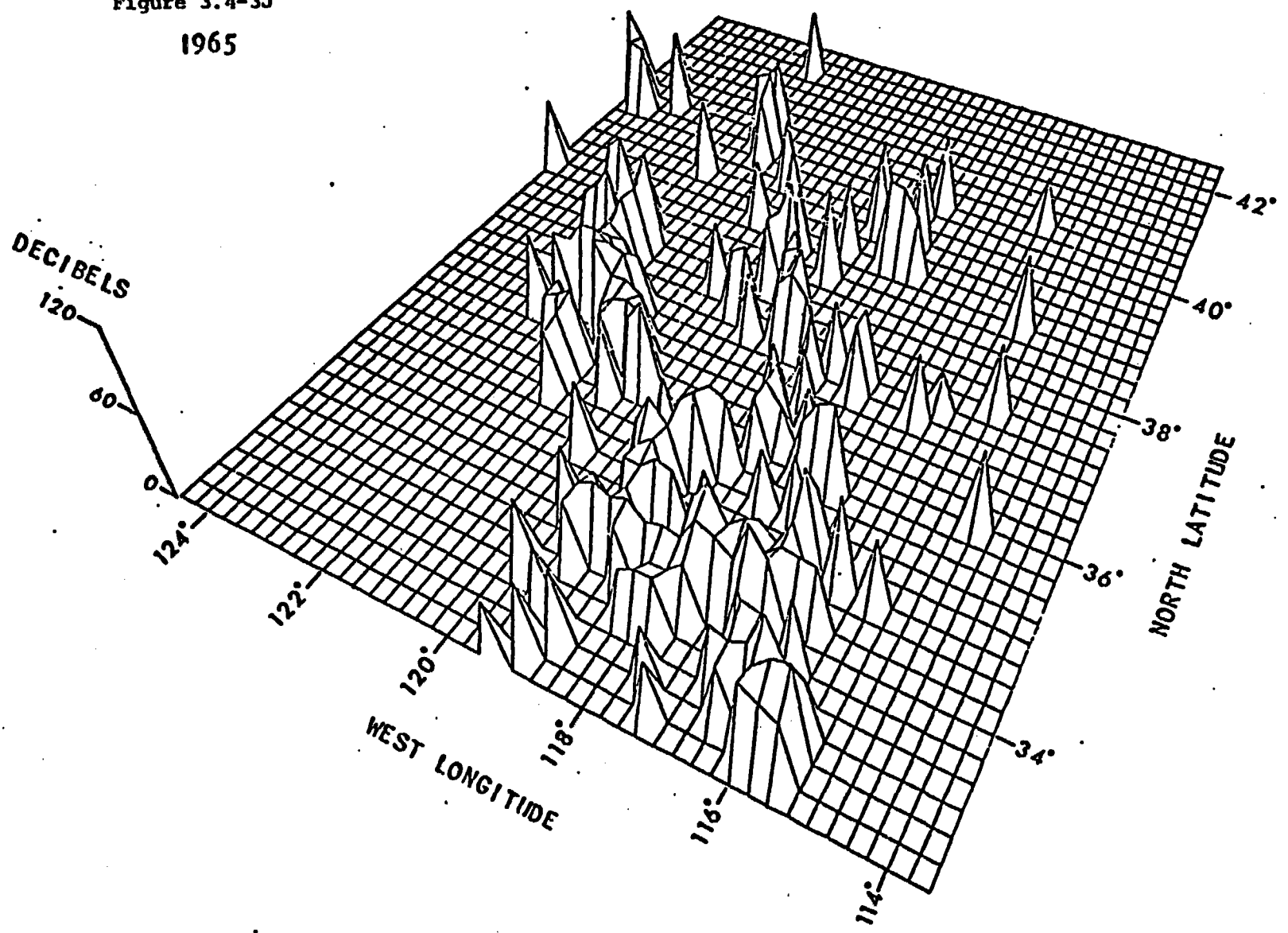


Figure 3.4-3K

1966

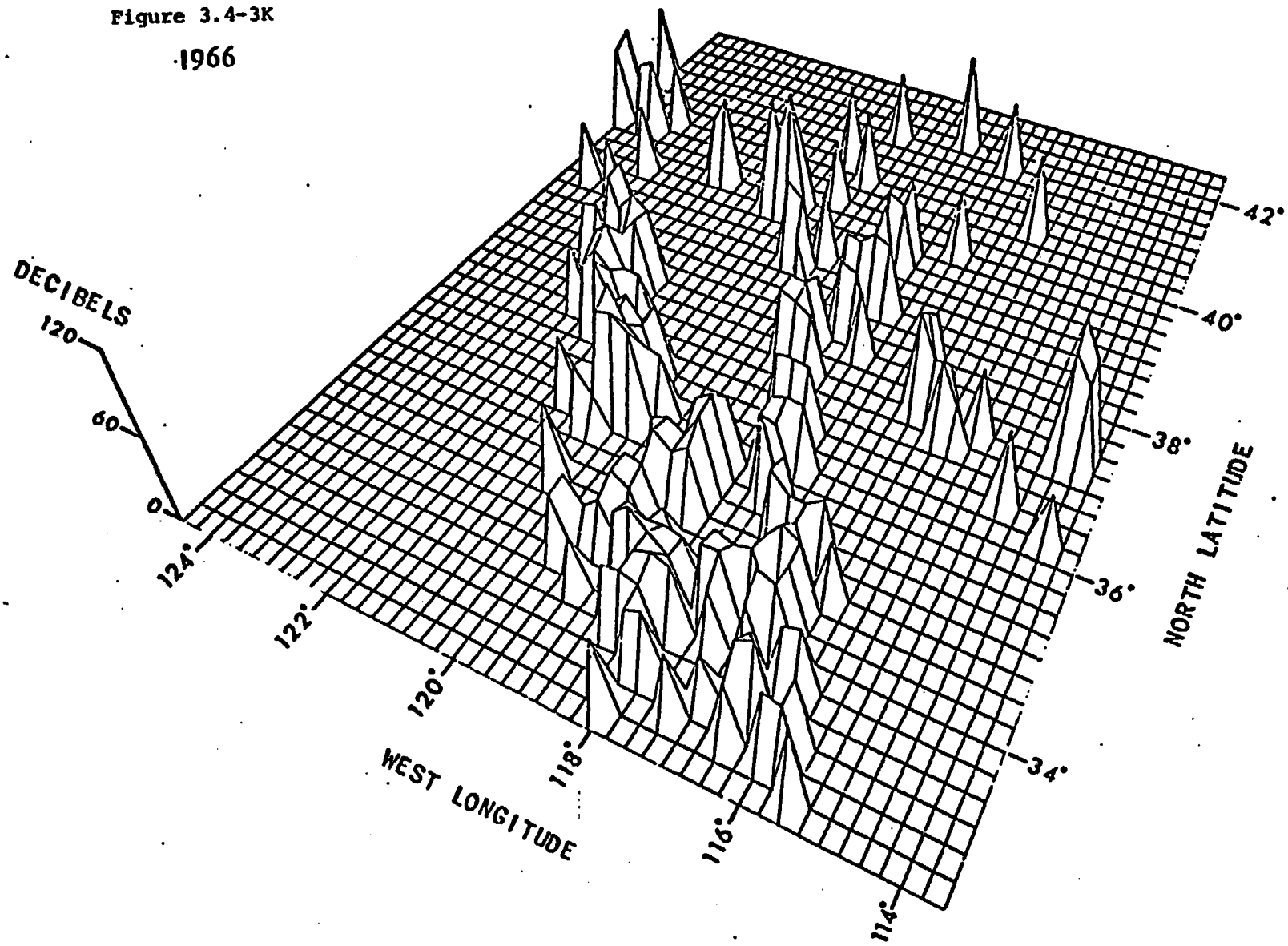


Figure 3.4-3L

1967

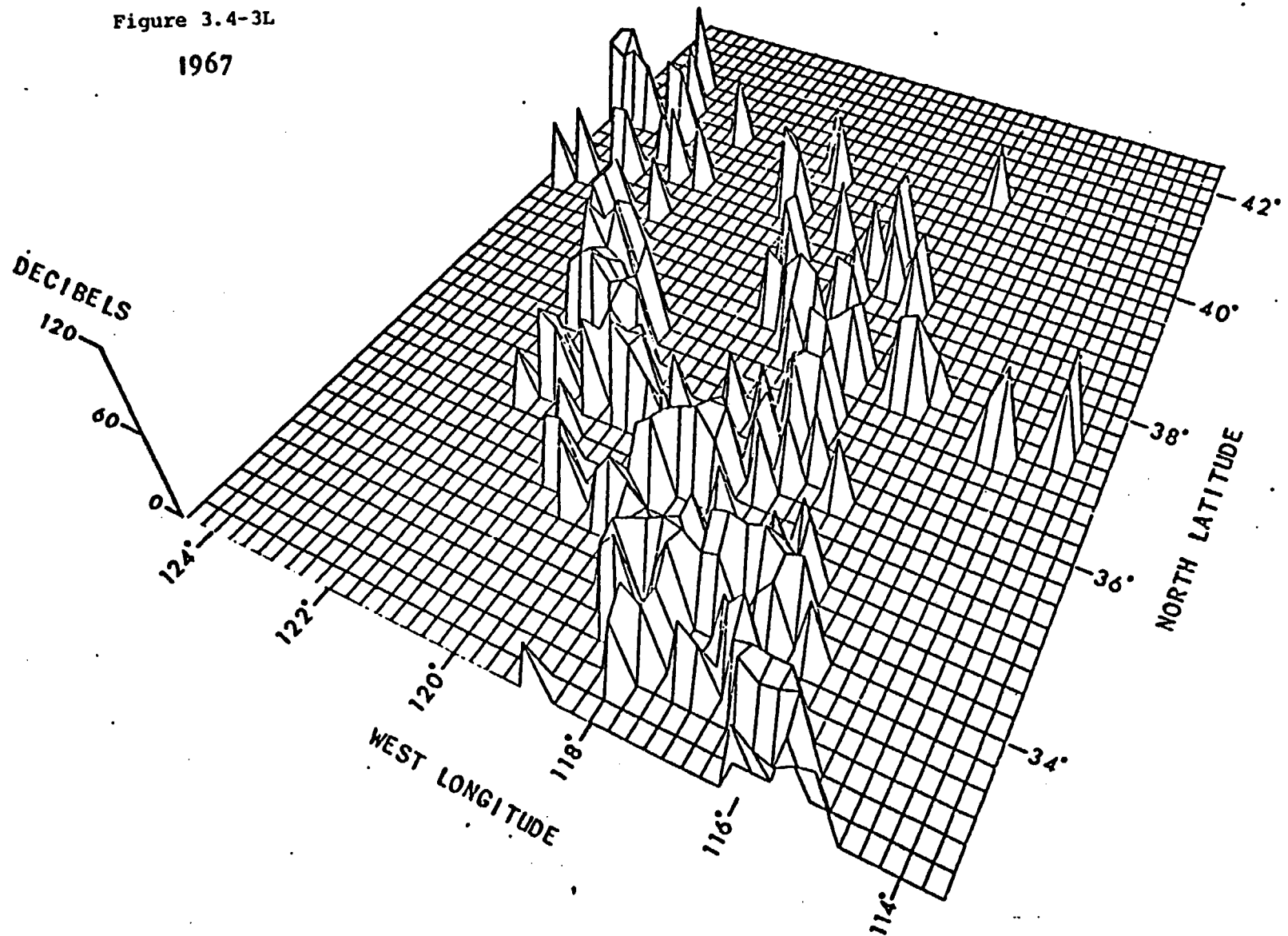


Figure 3.4-3M

1968

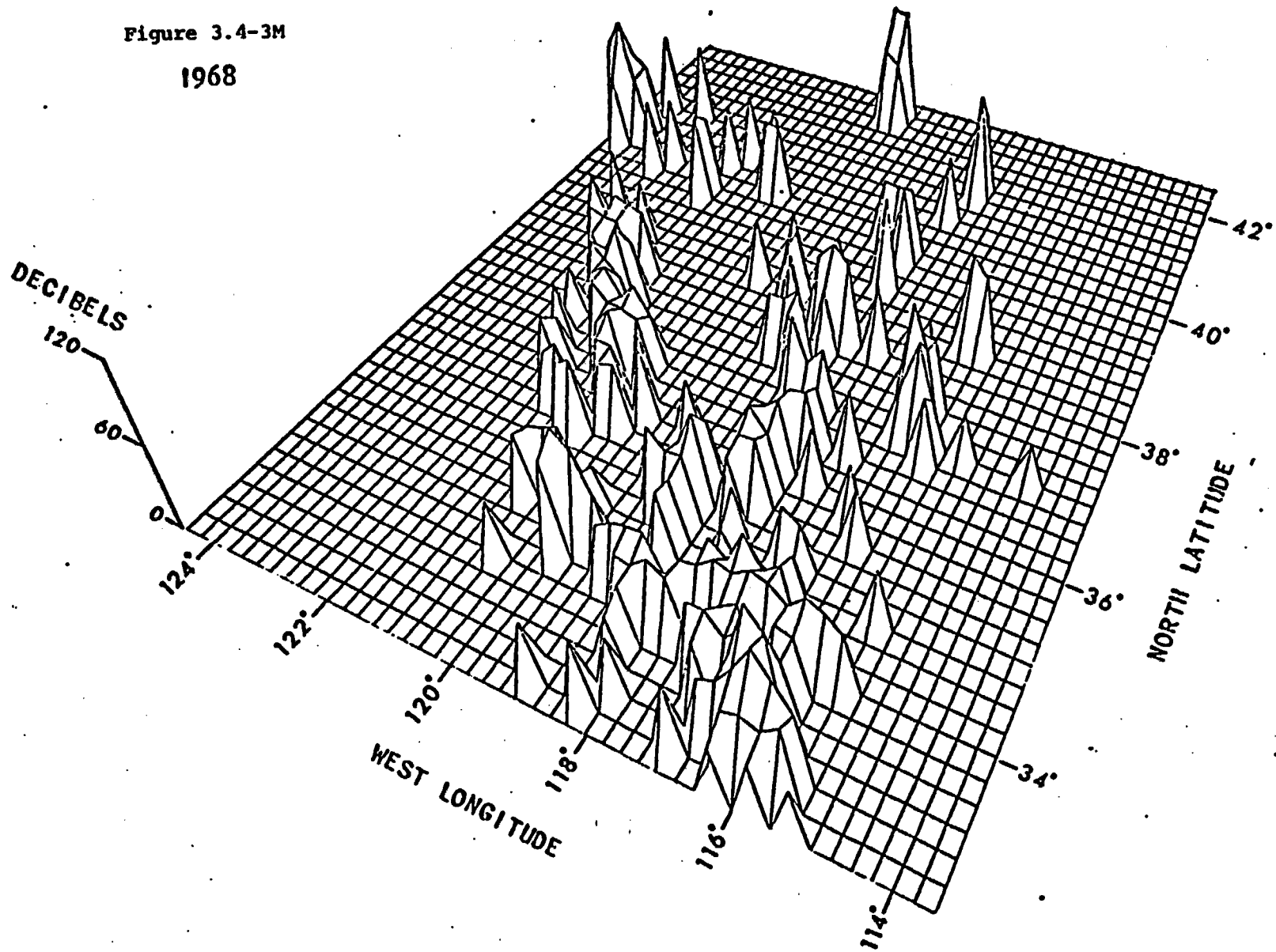


Figure 3.4-3N

1969

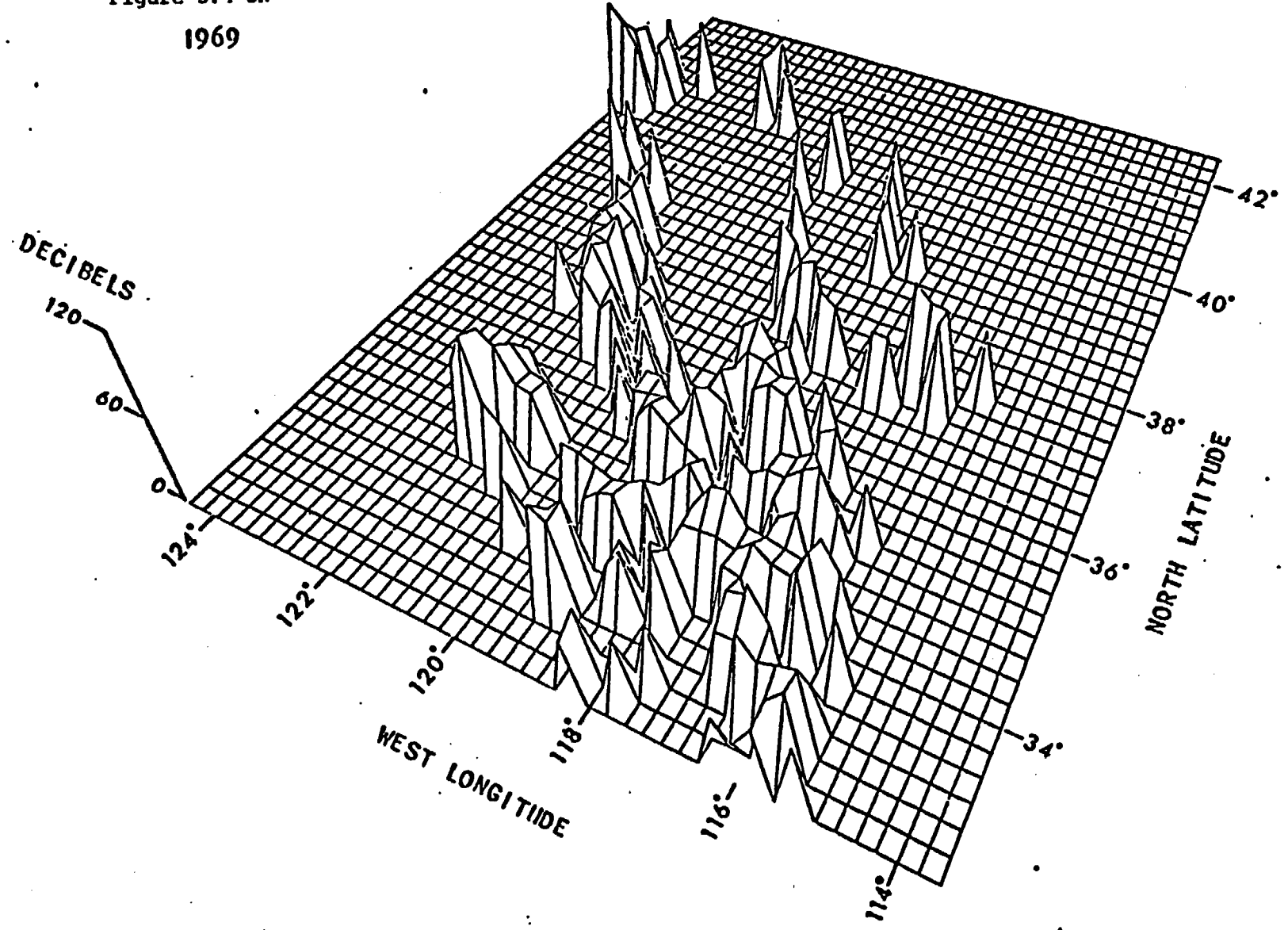


Figure 3.4-30

1970

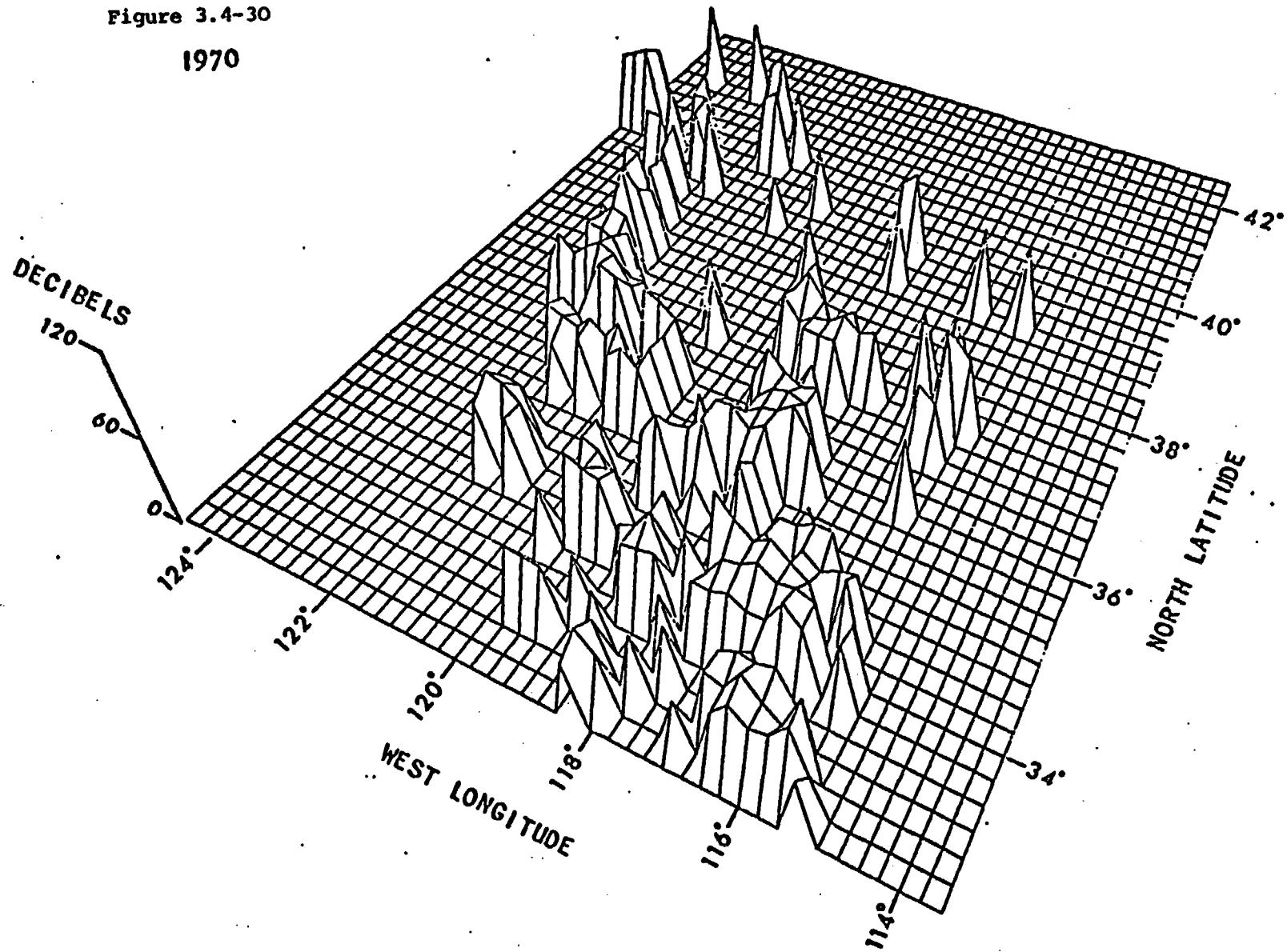


Figure 3.4-3P

1971

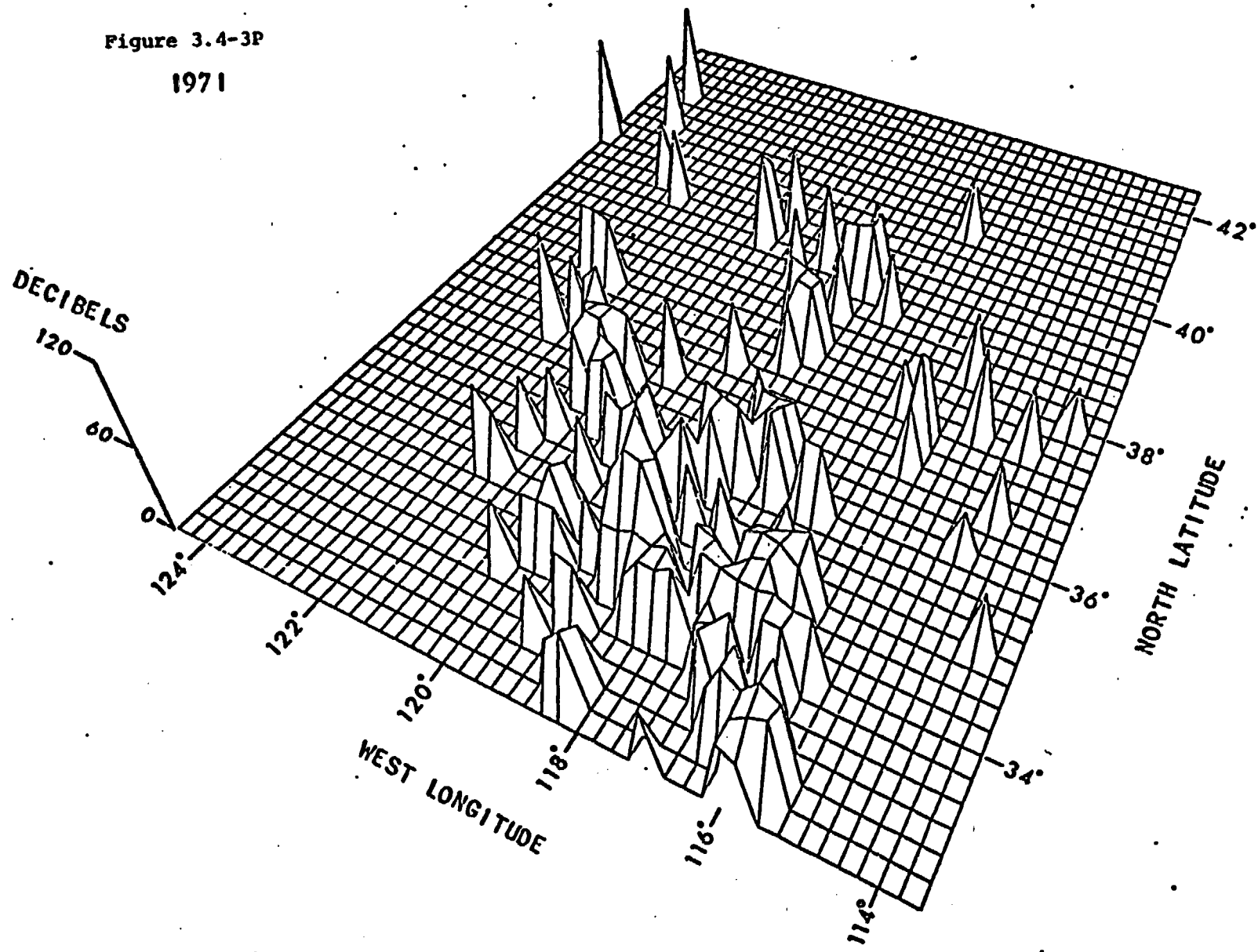


Figure 3.4-3Q
1972

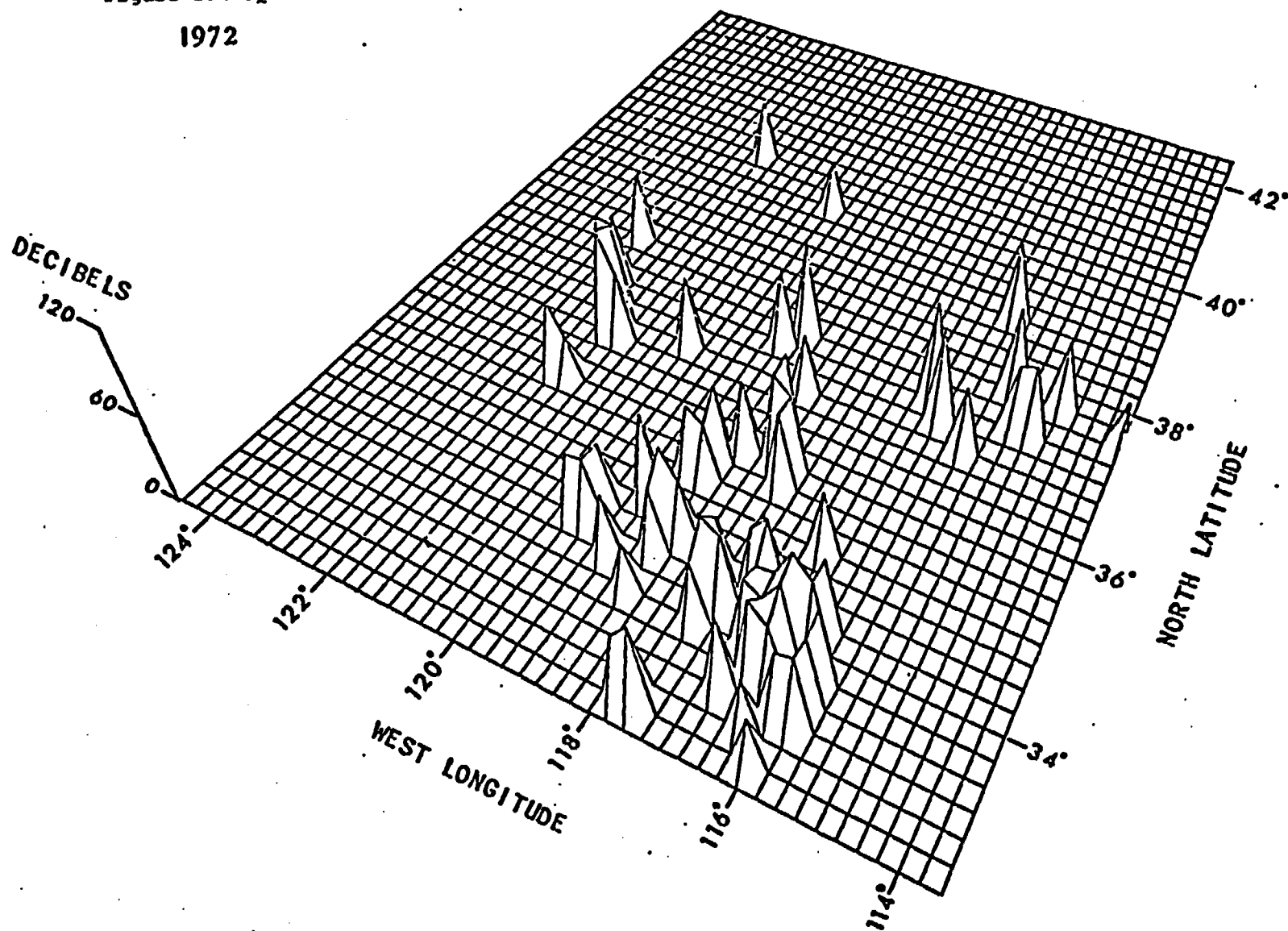
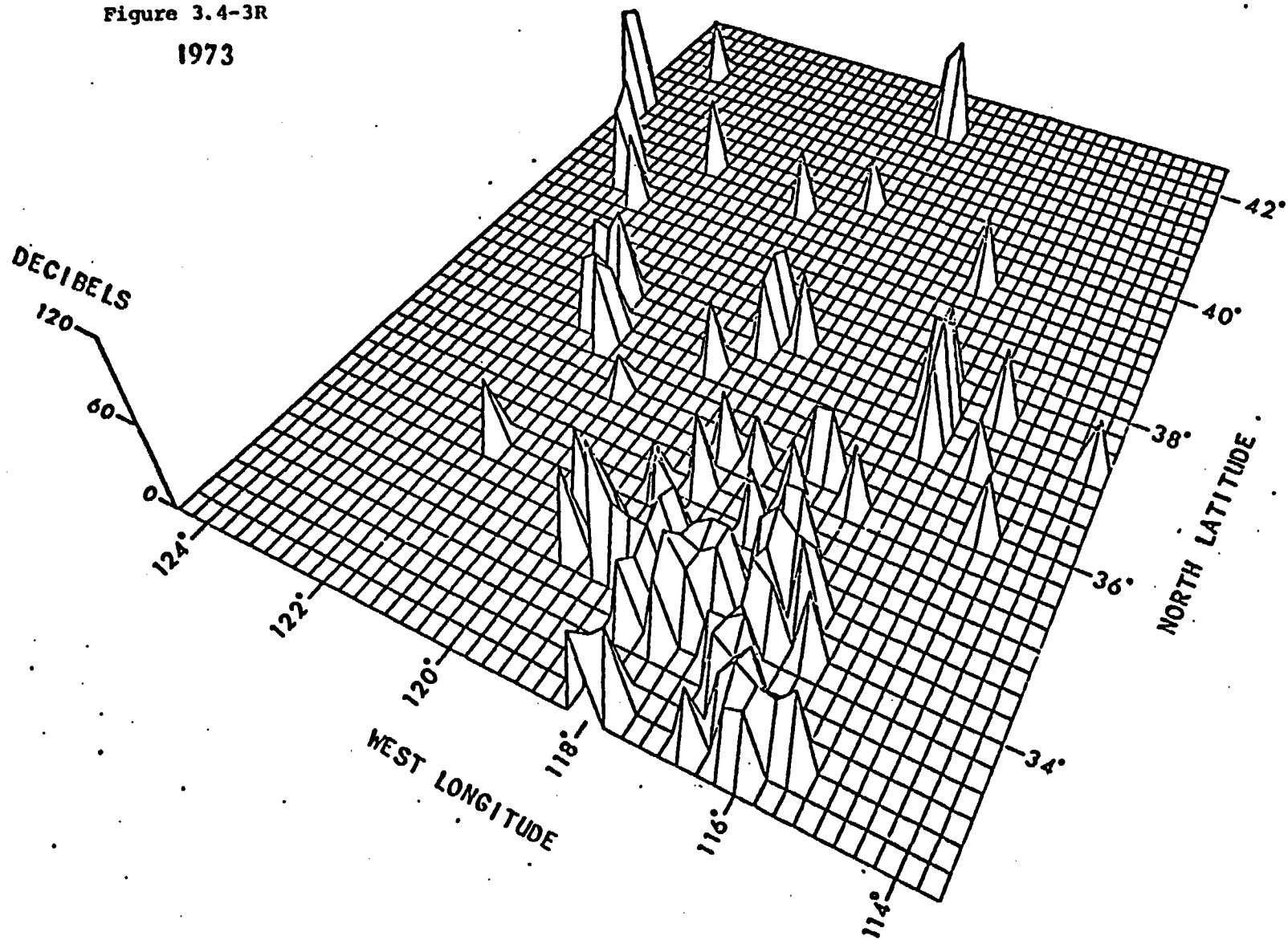


Figure 3.4-3R
1973



of north-south trending faults, which are stepped to the left. This pattern is similar to the opening of tension cracks that are visible on a much smaller scale along the San Andreas and Calaveras faults in zones that have experienced relatively high rates of recent fault creep. Thus a regional right lateral shear in a zone trending northwesterly could possibly explain these alignments. In contrast to the two more permanent zones of seismic activity mentioned above, transient seismic activity occurs over most of the California/Nevada area. Notable exceptions are the central and southern California offshore area, the northeastern corner of Nevada, extreme north-central and northeastern California, the extreme southeastern corner of California, and the northern half of the Great Valley. These aseismic zones are more clearly viewed in Figure 3.4-4A-D, where the seismic activity is displayed in 10-year intervals. The first four aseismic zones appear to lie outside the wide broken zone postulated by Thompson and Burke (1973) to exist between the North American and Pacific Plates. The fifth aseismic zone, the northern Great Valley, separates the coastal seismic zone and the Ventura-Winnemucca seismic zone in northern and central California. No migration of seismic activity is apparent in either the 1-year or 10-year perspective plots. The perspective plots of 1972 and 1973 appear to show an overall decrease in seismic activity. This is due in part to the fact that our data set does not include the Cal Tech-Berkeley data base after 1971. Elimination of the Cal Tech-Berkeley data base decreases the detection capability previously discussed for the California/Nevada area, since the detection capability of the NOAA network could be as low as 4.5 for parts of the California/Nevada area. Therefore, the change observed in the 1972 and 1973 perspective plots is questionable with regard to a real migration of or decrease in seismic activity.

Figure 3.4-4. 10-year perspective plot of cumulative strain release in California/Nevada area. Plot is based on magnitudes and intensities of earthquakes which occurred in the California/Nevada area.

- A. 1933-42
- B. 1943-52
- C. 1953-62
- D. 1963-72

Figure 3.4-4A
1933-1942

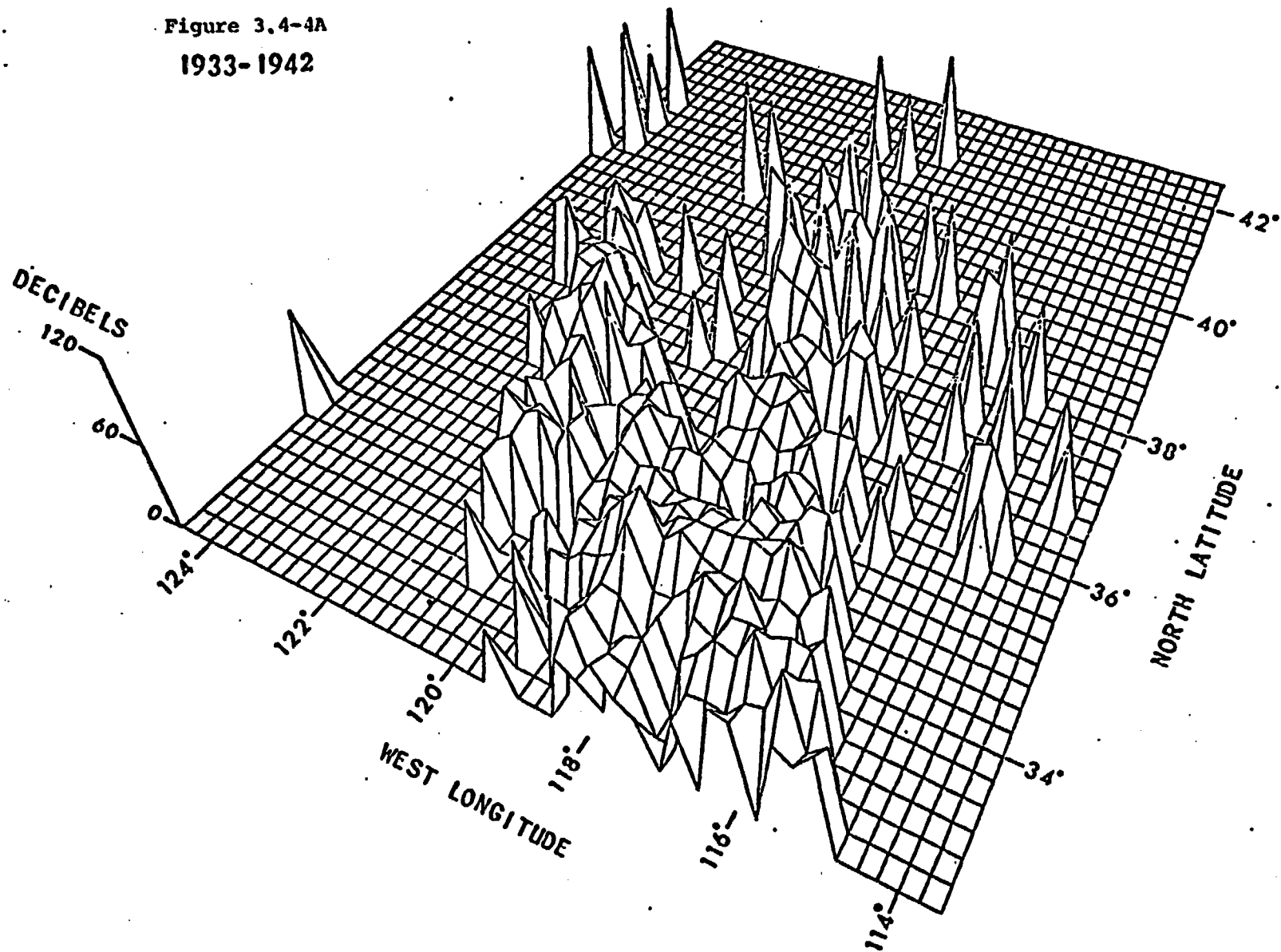


Figure 3.4-4B
1943-1952

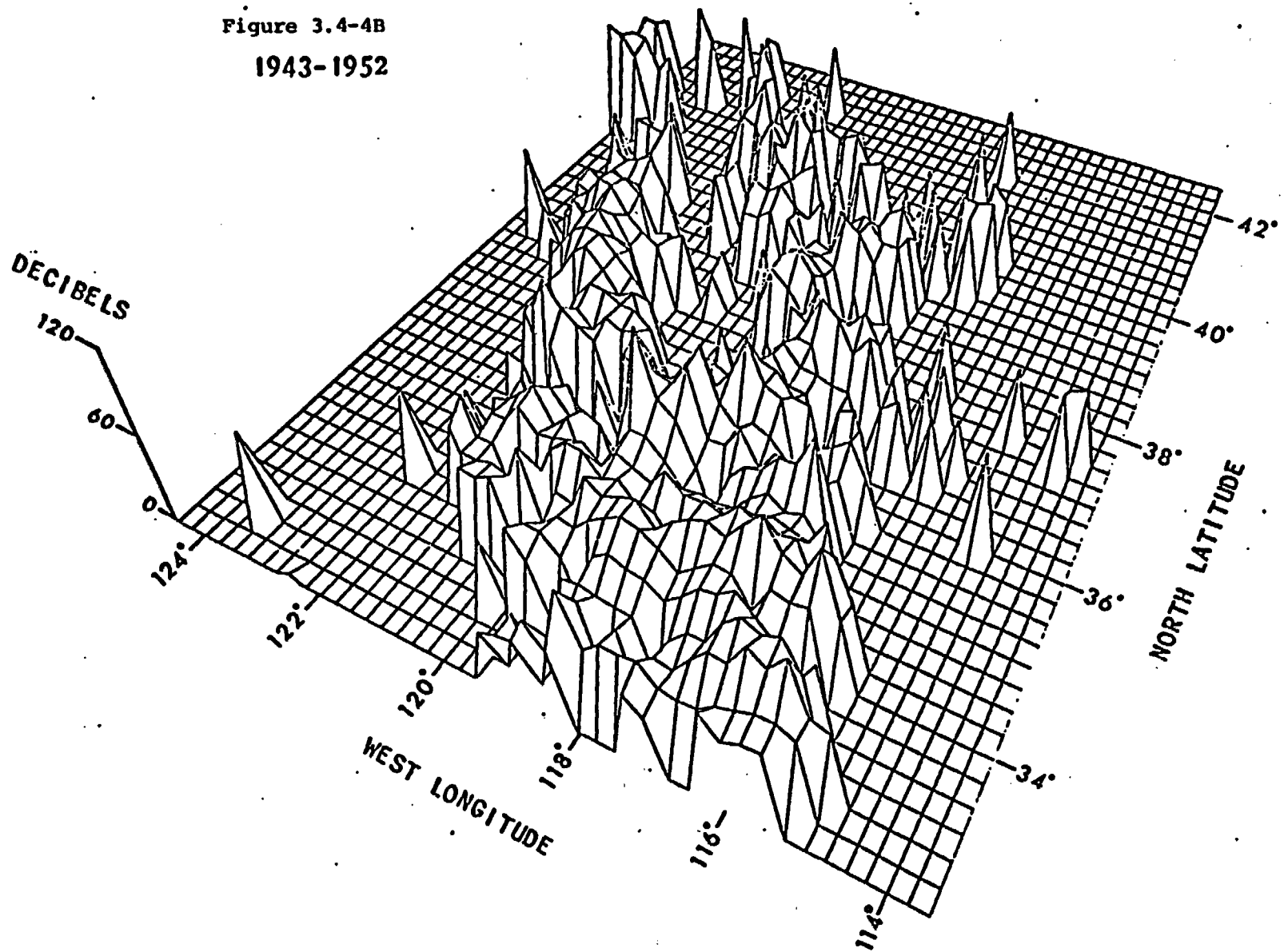


Figure 3.4-4C
1953-1962

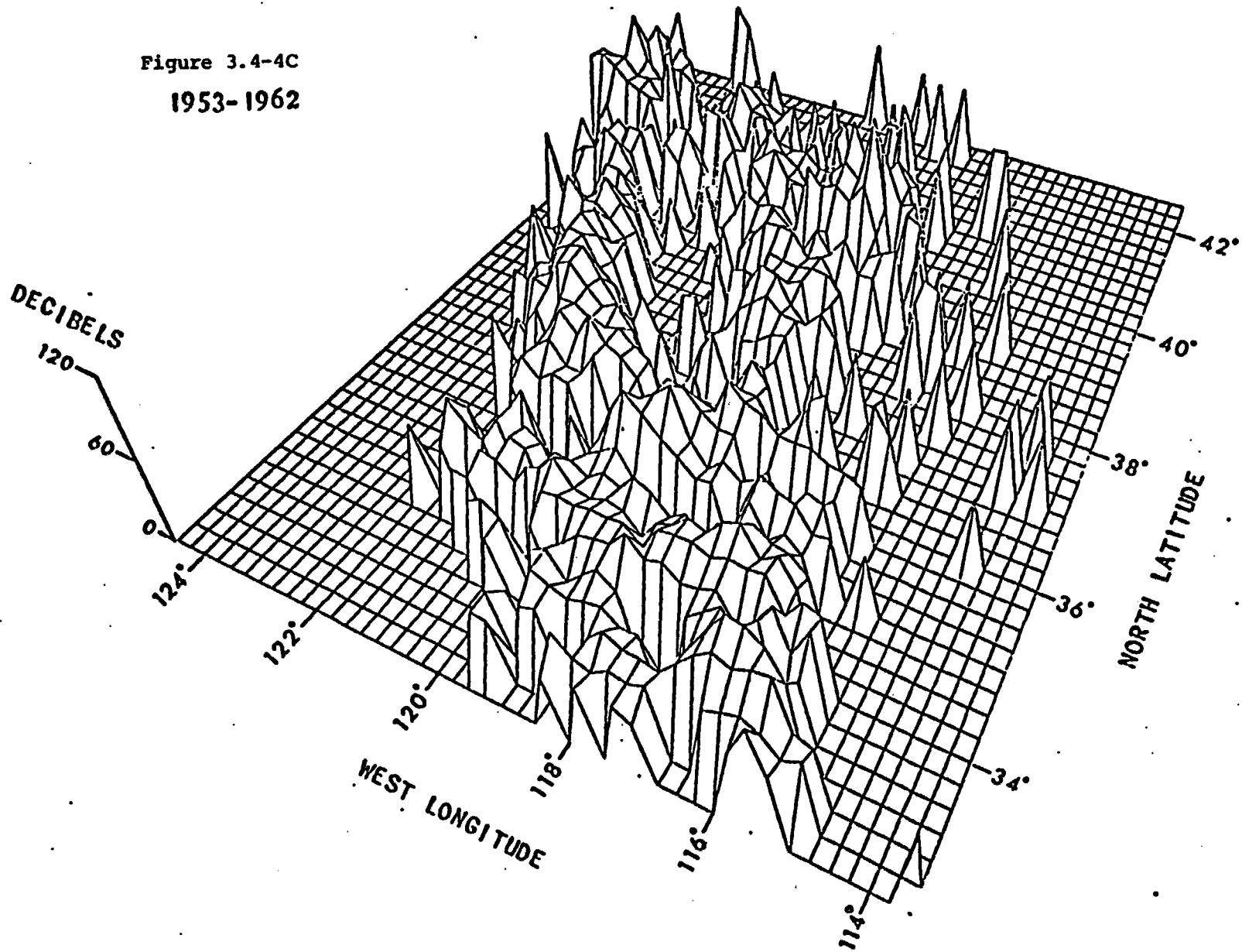
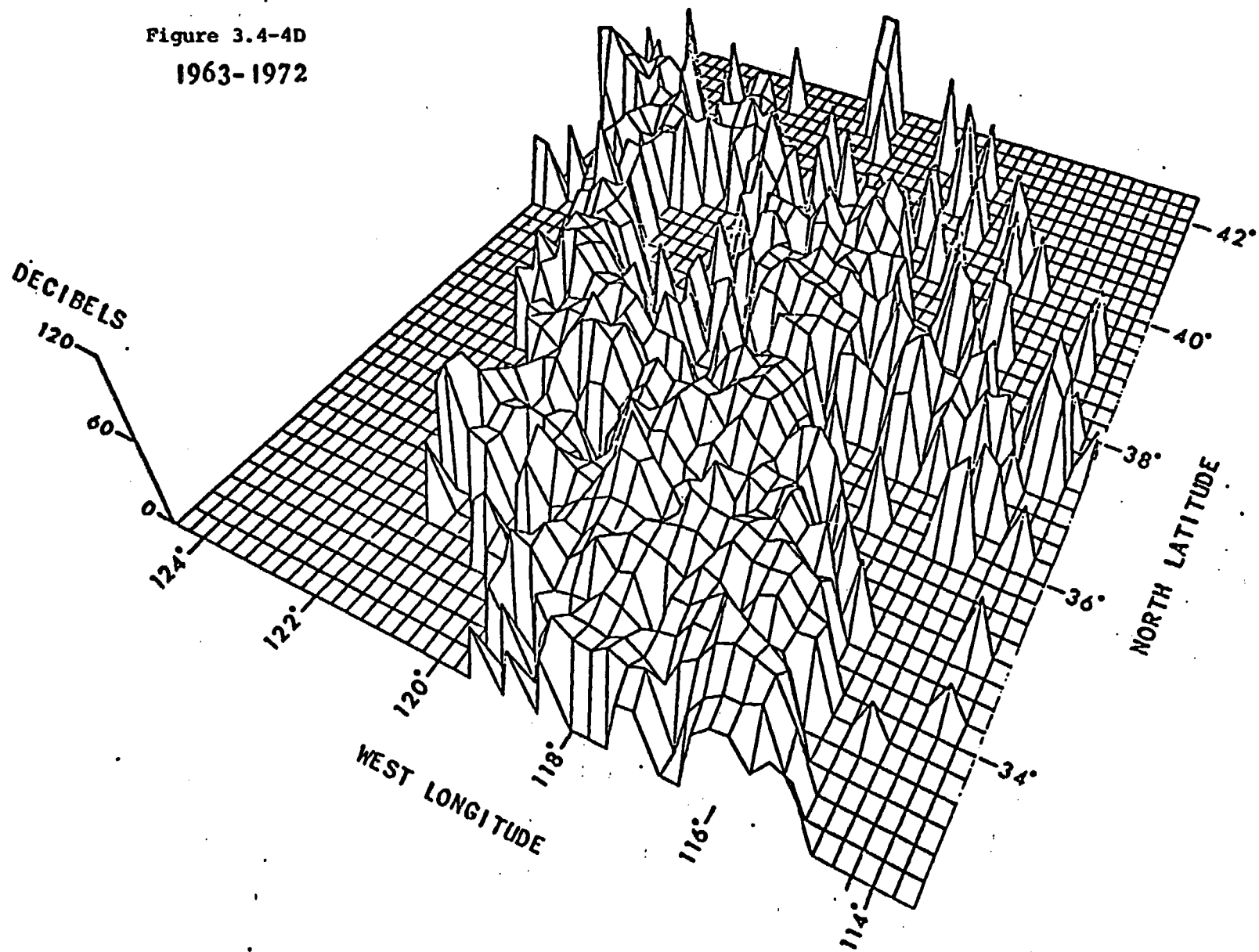


Figure 3.4-4D
1963-1972



The location of the major testing activity at NTS falls in the following areas: 37.0°-37.3°N and 116.0°-116.5°W. The FAULTLESS shot of January 1968 was located at 38.6°N, 116.2°W. If these areas are spotted on the plastic overlay (Plate 1B, and the overlay is superimposed on each perspective plot, the earthquake activity in these local areas can then be readily followed from year to year during the 1956-1973 time interval. It should be kept in mind that in 1957 only one underground nuclear shot was detonated at NTS, in 1958 four underground shots were fired, two of which had magnitudes above 4.0, and no shots were fired in 1959 or 1960.

The eight large shots of m_b magnitude larger than 6.0 are shown in Table 3.4-1.

TABLE 3.4-1

Listing of Large Magnitude Nevada Underground Nuclear Shots

				m_b	M_s	M_L
HALFBEAK	6/30/66	37.3°N	116.3°W	6.02	5.7	5.9
GREELEY	12/20/66	37.3°N	116.4°W	6.3	6.1	6.2
FAULTLESS	1/19/68	38.6°N	116.2°W	6.25	6.1	
BOXCAR	4/26/68	37.3°N	116.5°W	6.3	6.3	5.4
BENHAM	12/19/68	37.2°N	116.5°W	6.3	5.6	6.2
JORUM	9/16/69	37.3°N	116.5°W	6.2	5.1	6.3
HANDLEY	3/26/70	37.3°N	116.5°W	6.5	5.3	6.2
ALMENDRO	6/06/73	37.2°N	116.3°W	6.1		5.9

Cross-Correlation

It was previously noted that seismic activity is characterized by spatial and temporal dependencies. Previous investigations have tended to visually examine spatial representations of seismic activity over various time windows in an attempt to define spatial migration of temporal changes. While such efforts have yielded valuable data, they do fail to provide quantitative results or to account for the random components undoubtedly associated with seismic activity.

Two-dimensional spatial cross-correlation provides a method for the quantitative investigation of seismic activity. For the reader not familiar with correlation techniques, a brief introduction to the subject may be found in Appendix B. If measured activity during some base period t_i is denoted by $a_i(x,y)$, then it would appear reasonable to write

$$a_i(x,y) = s_i(x,y) + n_i(x,y)$$

where

$s_i(x,y)$ is the deterministic component of seismic activity

$n_i(x,y)$ is a random component of seismic activity which is assumed stationary.

The two-dimensional cross-correlation $\phi_{ij}(x,y)$ is then given by

$$\phi_{ij}(x,y) = \int_{-\infty}^{\infty} \int_{-\infty}^{\infty} a_i(\eta,\xi) a_j(x + \eta, y + \xi) d\eta d\xi$$

or

$$\begin{aligned} \phi_{ij}(x,y) &= \phi_{s_i s_j}(x,y) + \phi_{s_i n_j}(x,y) + \phi_{s_j n_i}(x,y) \\ &+ \phi_{n_i n_j}(x,y) \end{aligned}$$

If the original assumption concerning the random and stationary nature of $n(x,y)$ is valid, then

$$\phi_{ij}(x,y) = \phi_{s_i s_j}(x,y)$$

If simple migration of $s(x,y)$ is involved then the maximum value of $\phi_{s_1s_j}(x,y)$ will occur at a lag of Δx and Δy and equal $\phi_{s_1s_j}(x + \Delta x, y + \Delta y)$. Hence, migration of the seismic activity should result in migration of the peak correlation. The maximum value of $\phi(x,y) = f(j)$ measures the degree to which a consistent pattern of seismic activity is maintained in time.

The statistical method of cross-correlation is used in this study to compare the seismicity of the California/Nevada area on a one and ten year basis. Both the strain release and their equivalent decibel values used in the perspective presentations are cross-correlated. The seismicity of 1956 is cross-correlated with that of 1951 through 1955 and 1957 through 1973 on a yearly basis. Nineteen fifty-six was chosen as the base year because it has the most complete data set prior to the initiation of underground nuclear testing. The seismicity computed for the 10-year period 1933-1942 is cross-correlated with seismicity of the 3 following 10-year periods; 1943-1952, 1953-1962, and 1963-1972.

Cross-correlation of two discrete, two-dimensional data sets X and Y was calculated using the formula

$$\phi_{a,b} = \frac{\sum_{i=1}^m \sum_{j=1}^n ((X_{i-a,j-b} - \bar{X}) \times (Y_{i,j} - \bar{Y}))}{[(\sum_{i=1}^m \sum_{j=1}^n (X_{i,j} - \bar{X})^2) \times (\sum_{i=1}^m \sum_{j=1}^n (Y_{i,j} - \bar{Y})^2)]^{1/2}}$$

where

ϕ = cross-correlation coefficient

m = number of latitudinal grid units

n = number of longitudinal grid units

a = latitudinal lag for which ϕ is calculated, + is north, - is south

b = longitudinal lag for which ϕ is calculated, + is east, - is west

\bar{X} = mean of data set X

\bar{Y} = mean of data set Y

For example, $\phi_{2,4}$ is the coefficient of cross-correlation for data set X lagged over data set Y 2 grid units north and 4 grid units east. The two-dimensional cross-correlation produces a maximum value at the position of optimum correlation.

To minimize computer requirements, the cross-correlation was actually performed in the Fourier transform domain. The method and FORTRAN program are described in more detail in George (1974). Approximately 25 percent of the total lags were utilized. These are systematically centered about the zero lag position.

Statistical Analysis

Before examining the two-dimensional cross-correlation of seismic activity for 1- and 10-year intervals in the California/Nevada area, an examination of the two-dimensional autocorrelation of the seismic parameter, strain release, and its equivalent decibel values was performed. Plotted in Figure 3.4-5 is a sample of the correlation coefficients obtained from the autocorrelation of the 1956 decibel values. The correlation coefficients are computed for each $1/4^\circ$ of latitudinal and longitudinal lag and are contoured at an interval of 0.25 units. Zero lag position is located at the center of the plot. Two perpendicular cross sections (AA' and BB') of correlation coefficients are plotted in Figure 3.4-6. These cross sections are the autocorrelation functions of the 1956 cumulative strain release for SW-NE and NW-SE lags. Note in Figures

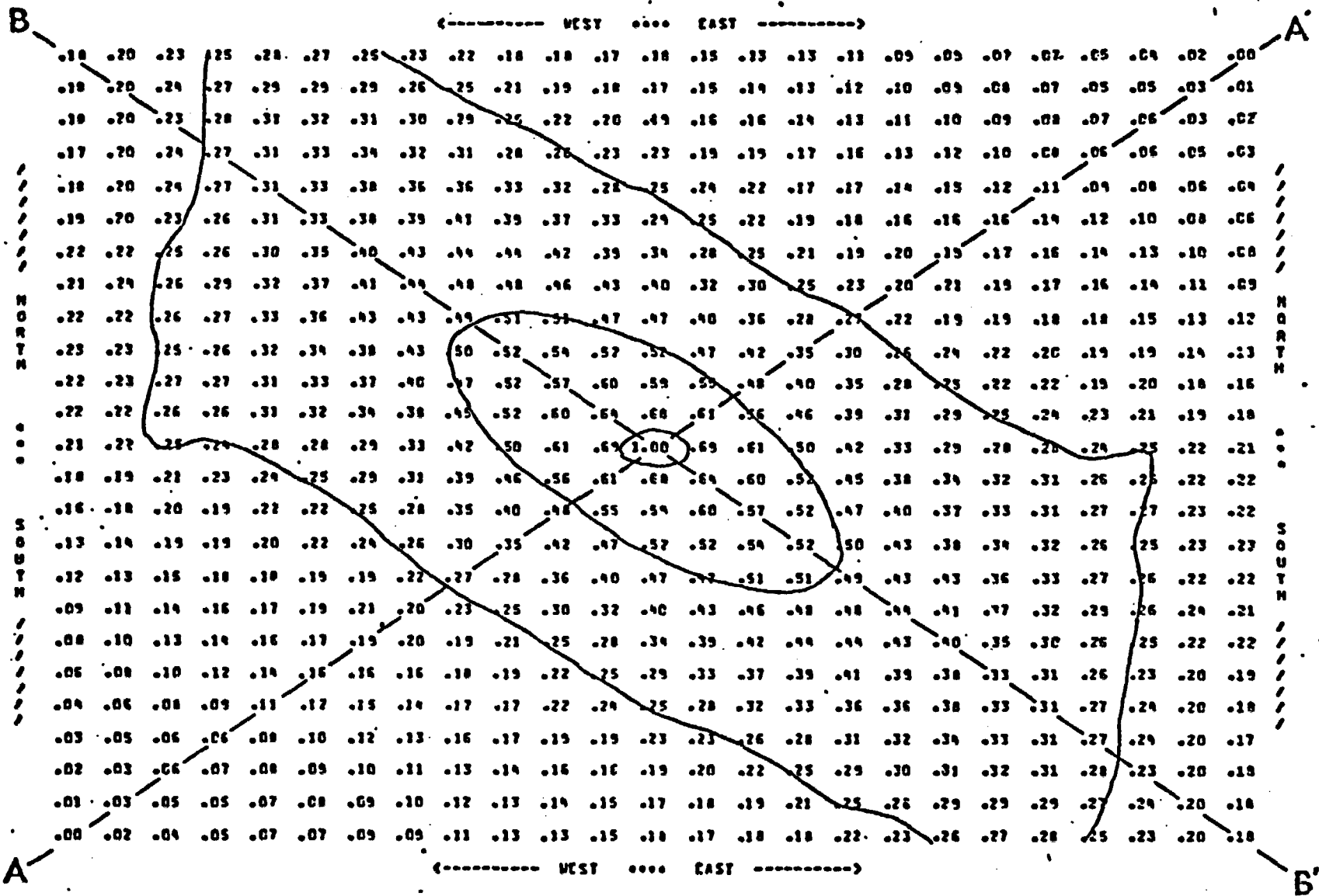


Figure 3.4-5. Sample of the correlation coefficients obtained from the two-dimensional autocorrelation of the 1956 decibel values calculated from the strain release in the California/Nevada area. Correlation coefficients are computed for each 1/4° of latitudinal and longitudinal lag. The zero lag position is at the center of the plot. The correlation coefficients are contoured at an interval of 0.25.

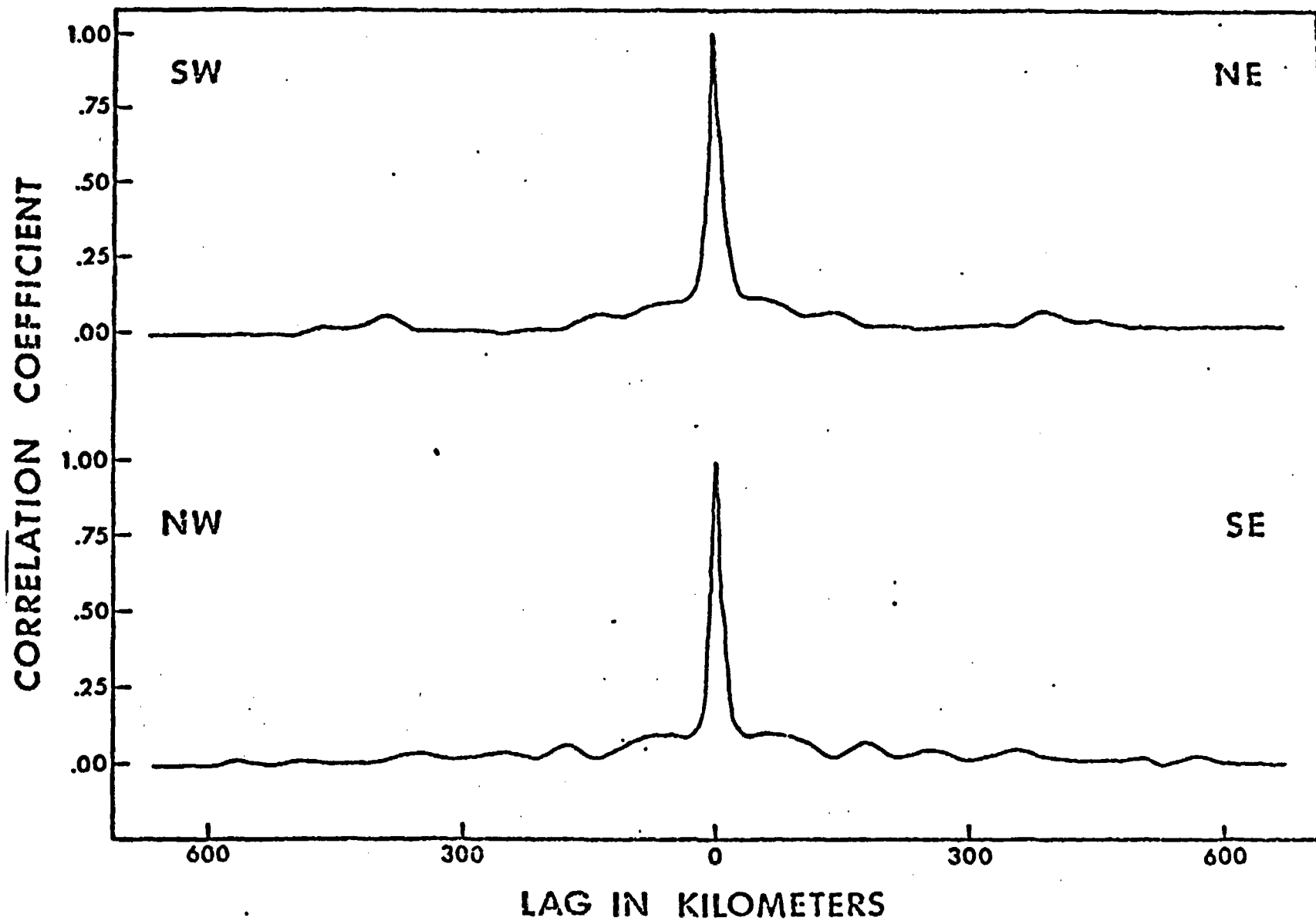


Figure 3.4-6. Plot of the autocorrelation function of the 1956 cumulative strain release for SW-NE and NW-SE lags in the California/Nevada area.

3.4-5 and 3.4-6 that the autocorrelation function is radially symmetric about the zero lag position. The sharp peak at zero lag, which falls off rapidly to correlation coefficients in the range 0.00 to 0.10, indicates that there is no spatial correlation to the spatial pattern of the cumulative strain release in the California/Nevada area during 1956. This autocorrelation function, in fact, approximates closely the autocorrelation function of random white noise. Similarly, the autocorrelation function of the cumulative strain release (Figure 3.4-7) for the 10-year period 1963-1972 also approximates very closely the autocorrelation function of random white noise, indicating no spatial correlation to the spatial pattern of the 10-year cumulative strain release. The lack of spatial correlation is probably due to the weighting of large earthquakes, an inherent property of the strain release parameter. Figures 3.4-8 and 3.4-9 are plots of the autocorrelation function of the cumulative strain release scaled in decibels for 1956 and the 10-year period 1963-1972, respectively. Noticeable in these figures is the gradual decrease in the correlation coefficient as compared to the rapid decrease in the correlation coefficients in Figures 3.4-6 and 3.4-7. Also noteworthy is the more gradual decrease of the correlation coefficients in the NW-SE direction than in the SW-NE direction. This is due to the N27°W elongation direction of the seismic belt observed in Figures 3.4-3 and 3.4-4. The elongation of the seismic belt is also indicated by the N31°W elongation direction of the correlation coefficient contours in Figure 3.4-5. The strike of the San Andreas fault varies between N40°W to N60°W.

Summing up briefly the results of the two-dimensional autocorrelation; a NW-SE extension of the spatial pattern is observed for the autocorrelation

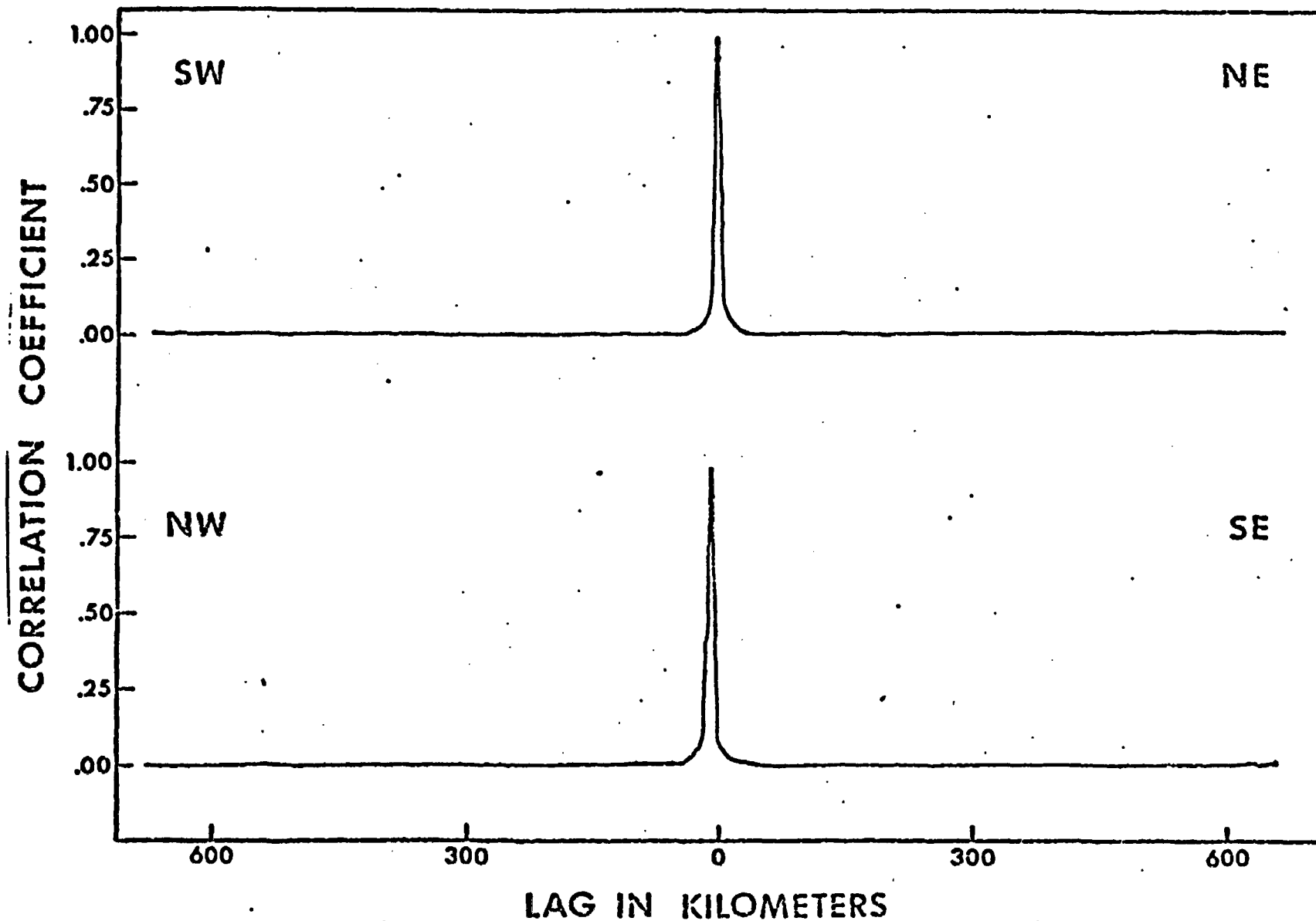


Figure 3.4-7. Plot of the autocorrelation function of the 1963 through 1972 cumulative strain release for SW-NE and NW-SE lags in the California/Nevada area.

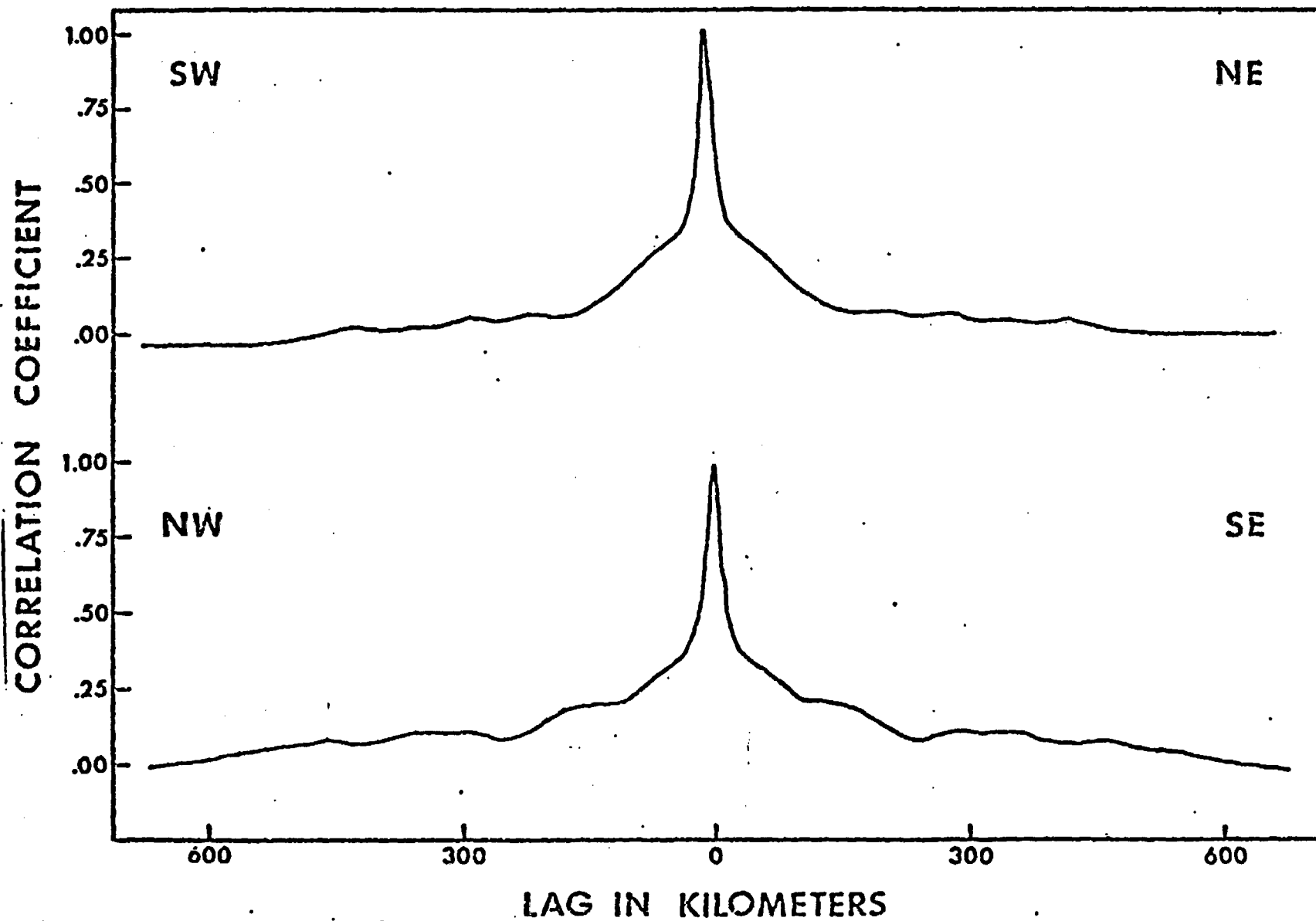


Figure 3.4-8. Plot of the autocorrelation function of the 1956 decibel values calculated from the cumulative strain release for SW-NE and NW-SE lags in the California/Nevada area.

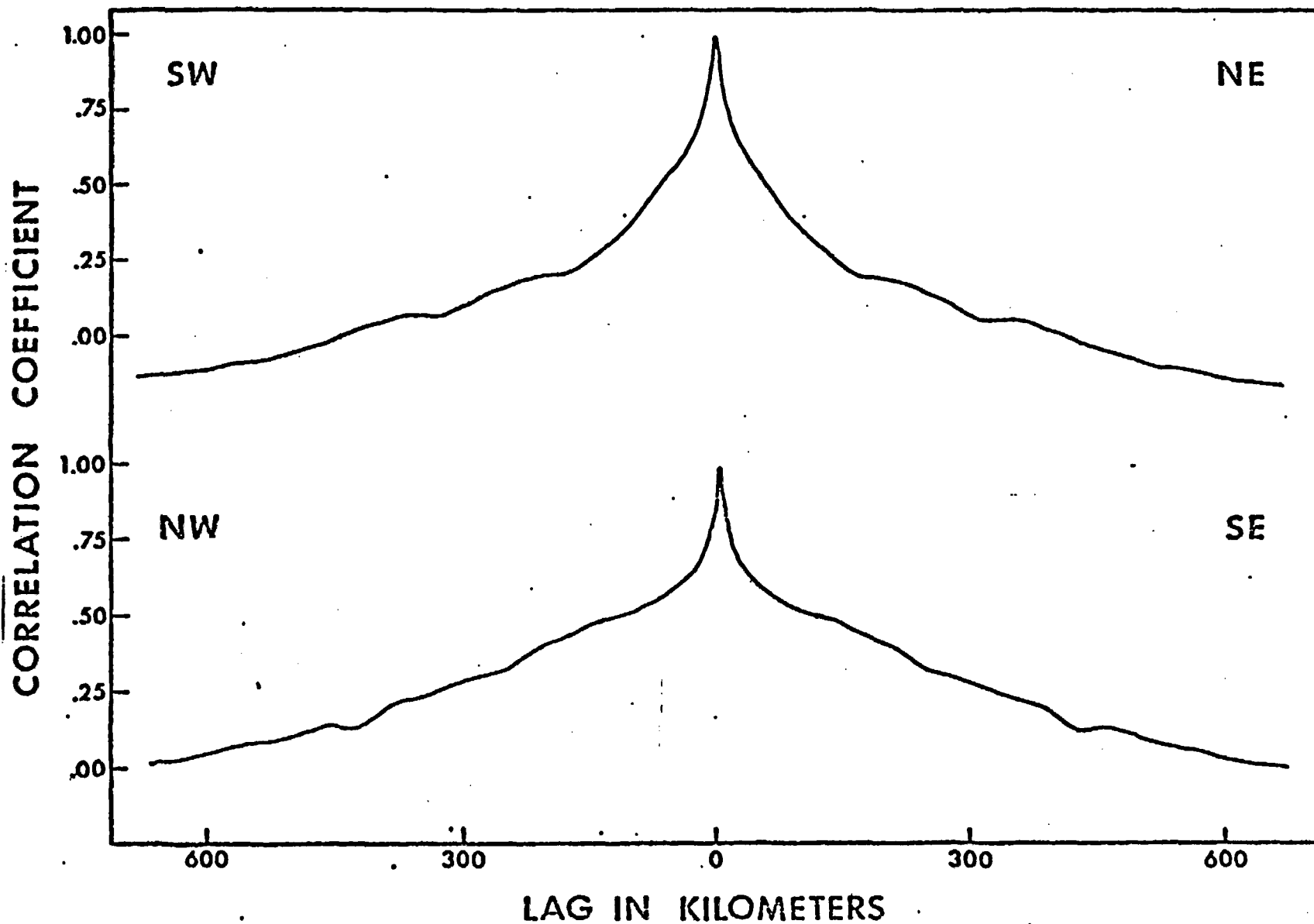


Figure 3.4-9. Plot of the autocorrelation function of the 1963 through 1972 decibel values calculated from the cumulative strain release for SW-NE and NW-SE lags in the California/Nevada area.

function of the cumulative strain release scaled in decibels, but is not observed for the autocorrelation function of strain release. The autocorrelation function of the strain release, in fact, approximates the autocorrelation function of random white noise. Therefore, cross-correlation of the strain release scaled in decibels appears to be the more useful and possibly the more significant seismic parameter to use in this study.

The correlation distance is arbitrarily defined as the distance from zero lag to a point at which the autocorrelation function decreases to 0.30. The correlation distance of the 1956 cumulative strain release in the NW-SE direction is approximately 30 km, whereas the correlation distance of the 1956 decibel values in the NW-SE direction is approximately 60 km. The correlation distances of the 1963-1972 cumulative strain release and decibel values are 20 and 240 km, respectively.

The maximum correlation coefficients obtained from the two-dimensional cross-correlation of the 1956 decibel values with the decibel values for each year, 1950 through 1973, are plotted in Figure 3.4-10. Lines connecting the correlation coefficients computed for each year are drawn for illustration purposes only. Correlation coefficients cannot be interpolated between points. The maximum correlation coefficients for all years occurred at the zero lag position, indicating that little or no movement has occurred in the seismic pattern as defined by strain release scaled in decibels. Also, the cross-correlation coefficients, ranging between 0.32 and 0.58, are indicative of a significant degree of correlation between the 1956 decibel values and those of the years 1950 through 1973. Therefore, the seismic pattern, as defined here, has not been measurably affected by nuclear testing at the Nevada Test Site. Notable also is the lack of a

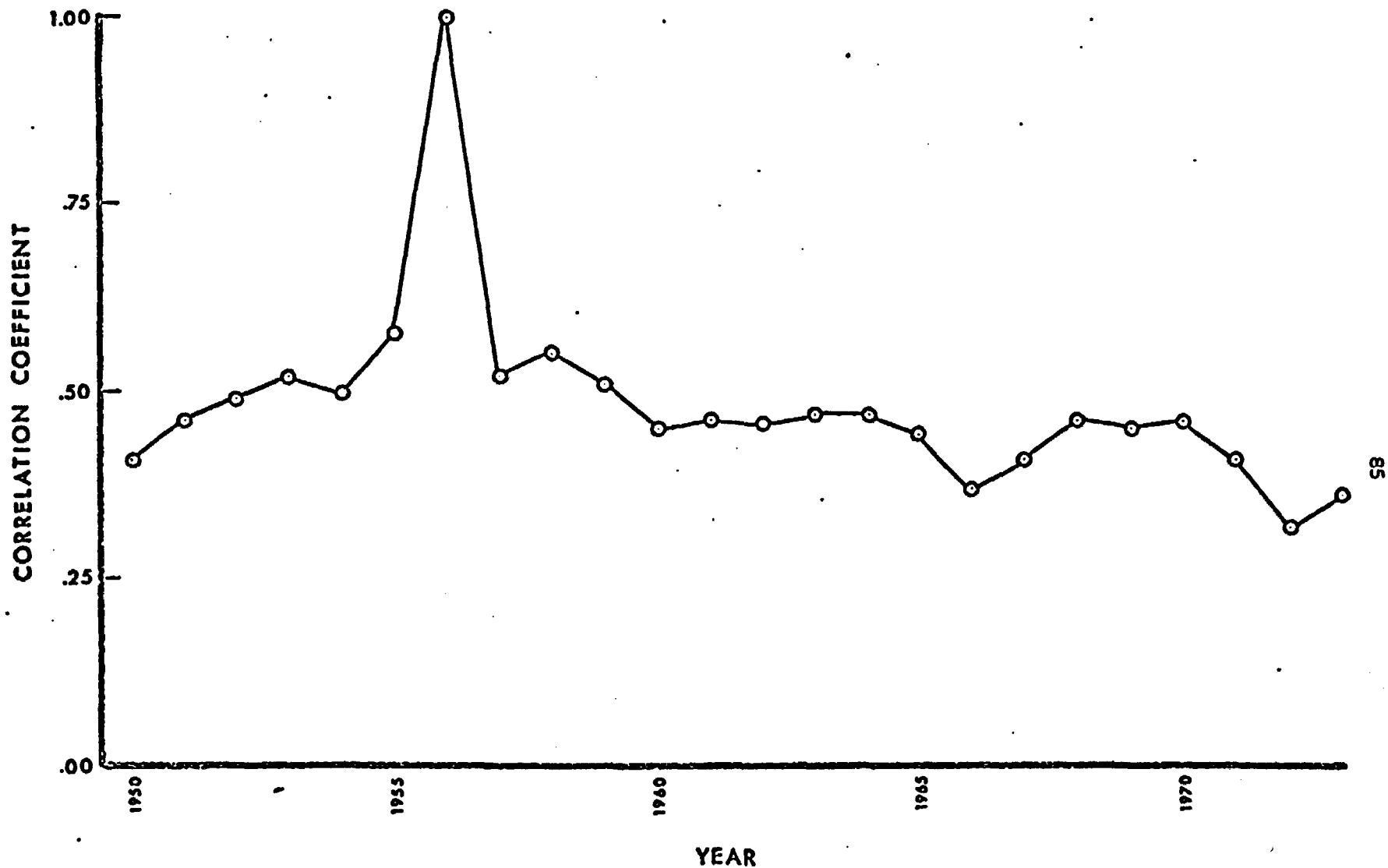


Figure 3.4-10. Maximum correlation coefficients obtained from the two-dimensional cross-correlation of the 1956 decibel values with the decibel values for each year, 1950 through 1973, in the California/Nevada area. Lines connecting the correlation coefficients computed for each year are drawn for illustrative purposes only. Correlation coefficients cannot be interpolated between points.

predominant period to the peak correlation coefficients, indicating the absence of a temporal cycle occurring during the years 1950 to 1973. This is not to say that no temporal cycle occurs. The 24-year window being examined may be a small part of a longer cycle. Wilson (1972), while studying the Chinese earthquake records, observed four stages of earthquake activity which repeated themselves every 370 to 380 years. Thus, the 24-year window may appear as a perturbation in a much longer 300 to 400 year cycle. A sample of the correlation coefficients obtained from the cross-correlation of the 1956 decibel values with the 1953 decibel values are shown in Figure 3.4-11. As previously noted, the maximum correlation coefficient occurs at the zero lag position located at the center of the plot. The NW-SE elongation of the 0.25 contour line is again present.

For comparison purposes, Figure 3.4-12, a sample of the correlation coefficients obtained from the cross-correlation of the strain release for the same years, 1956 and 1953, is included here. The maximum correlation coefficient occurs at a lag of 2° West and 1° North. This sample is typical of the cross-correlations for the 1956 strain release with the strain release of each year, 1950 through 1973, in that multiple peaks are observed at various latitudinal and longitudinal lags. These multiple peaks are probably due to the alignment of large magnitude earthquakes in the two years being cross-correlated. The effect of the alignment is decreased by cross-correlating the decibel equivalents of the strain release rather than strain release.

Maximum and zero lag correlation coefficients obtained from the two-dimensional cross-correlation of the 1956 strain release with the strain release of each year, 1950 through 1973, are presented in Figures

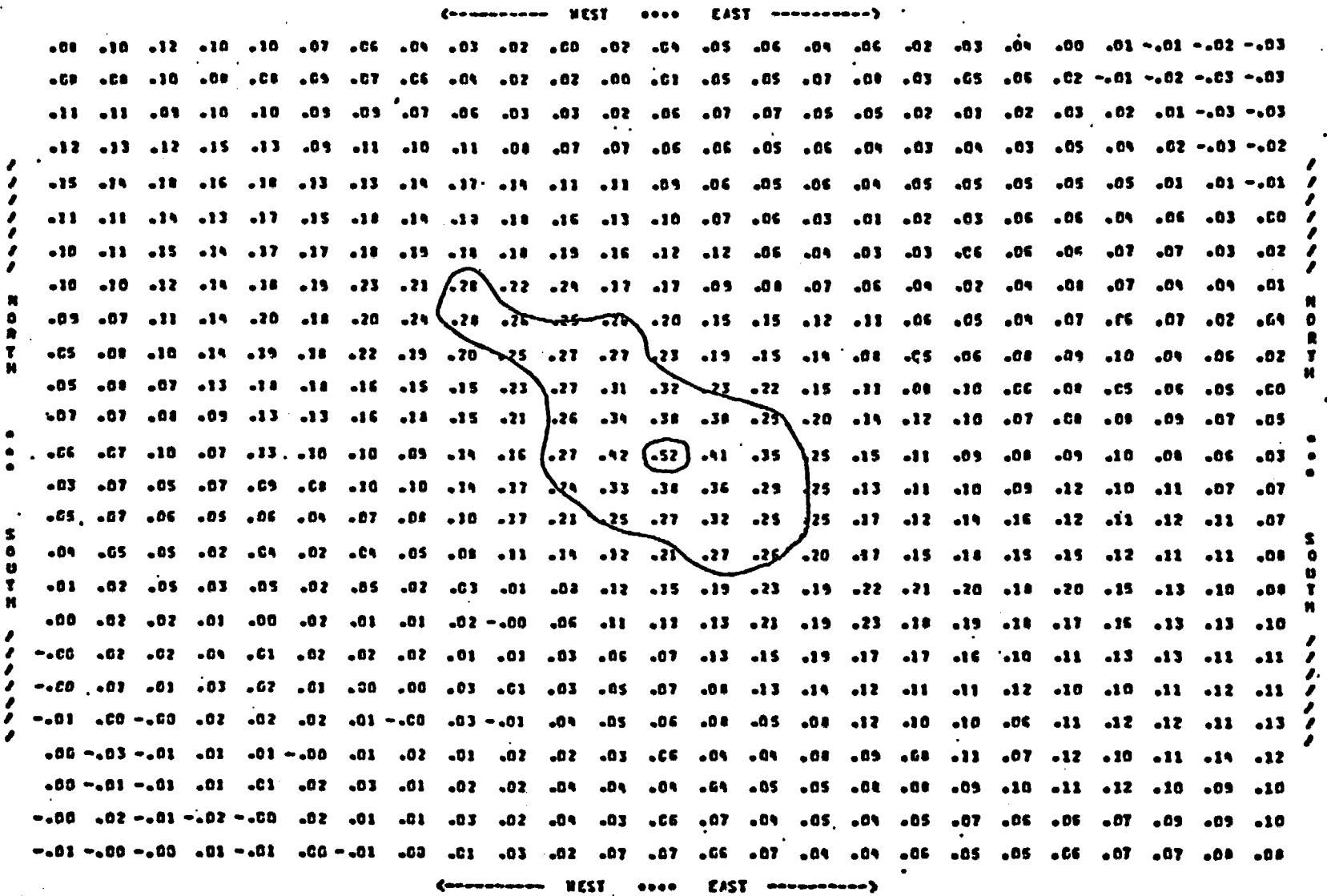


Figure 3.4-11. Sample of the correlation coefficients obtained from the two-dimensional cross-correlation of the 1956 decibel values with the 1953 decibel values calculated from the strain release in the California/Nevada area. Correlation coefficients are computed for each 1/4° of latitudinal and longitudinal lag. The zero lag position is at the center of the plot. The correlation coefficients are contoured at an interval of 0.25.

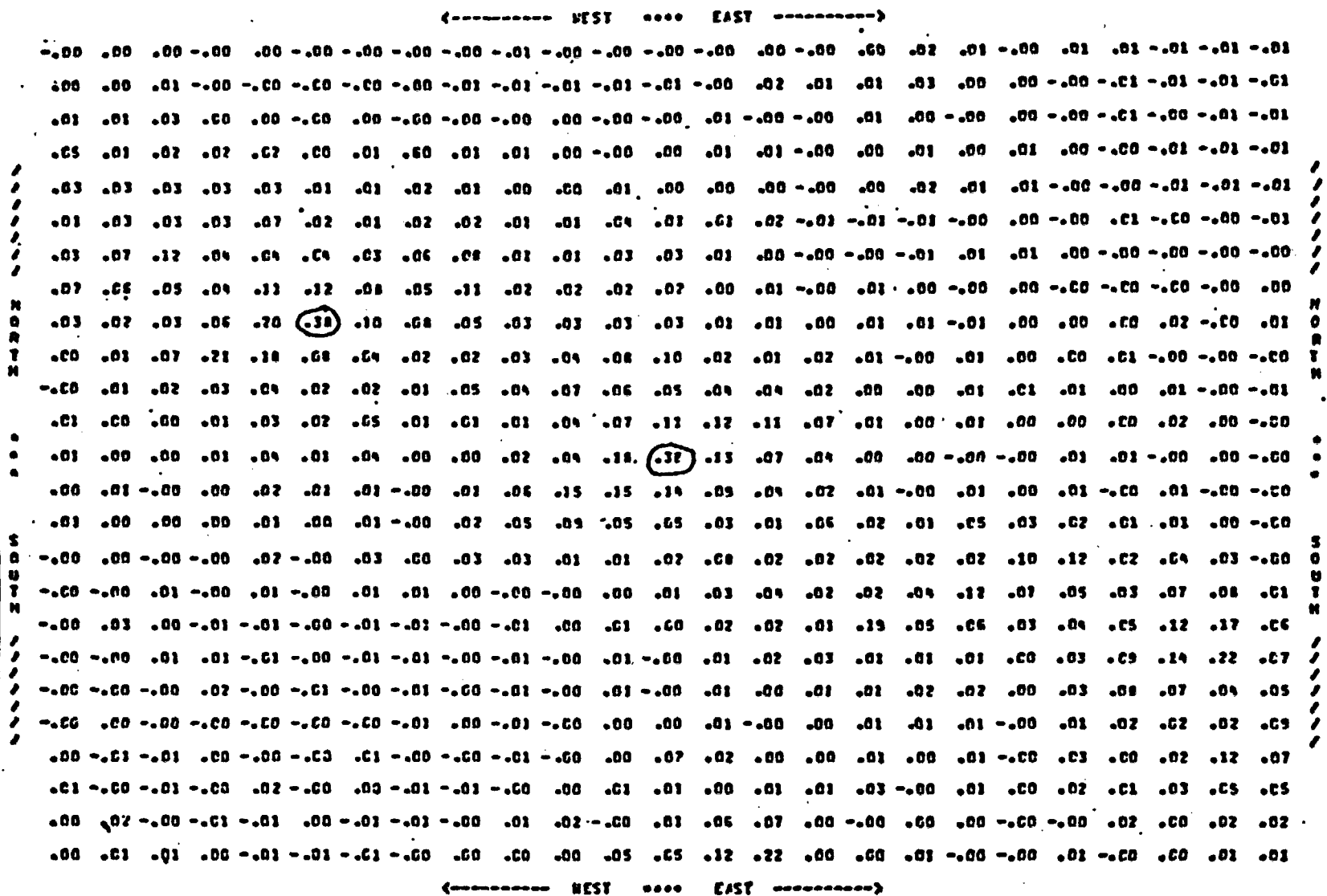


Figure 3.4-12. Sample of the correlation coefficients obtained from the two-dimensional cross-correlation of the 1956 strain release with the 1953 strain release in the California/Nevada area. Correlation coefficients are computed for each 1/4° of latitudinal and longitudinal lag. The zero lag position is at the center of the plot. The correlation coefficients are contoured at an interval of 0.25.

3.4-13 and 3.4-14, respectively. Although the zero lag coefficients appear to have no predominant period, the peak coefficients appear to repeat themselves every 5 to 6 years. This may be due to the reoccurrence every 5 or 6 years of one or more major earthquakes in the same grid units.

Figure 3.4-15 is a location plot of the maximum correlation coefficients shown in Figure 3.4-13. Migration of the maximum coefficients is, for the most part, NW-SE. This is due, in part, to the predominance of large earthquakes occurring along the NW-SE trending San Andreas fault system.

Figures 3.4-16 and 3.4-17 represent the yearly cumulative strain release for 1950 through 1973 and the 10-year cumulative strain release for 1933 through 1972, respectively. The strain release of 1952 and 1954 dominate the total strain release between 1950 and 1973. This is reflected in the 10-year cumulative strain release for the 10-year periods 1943-1952 and 1953-1962. The Kern Co. Earthquake of 1952, which occurred in southern California, had a reported magnitude of 7.7, while in 1954 four large earthquakes of magnitude 6.4, 6.8, 7.1, and 6.8 occurred in the general area east of Fallon, Nevada. The latter two occurred on the same day some 4 minutes apart in the Fairview Peak-Dixie Valley area. The epicenters were separated by a distance of approximately 38 miles.

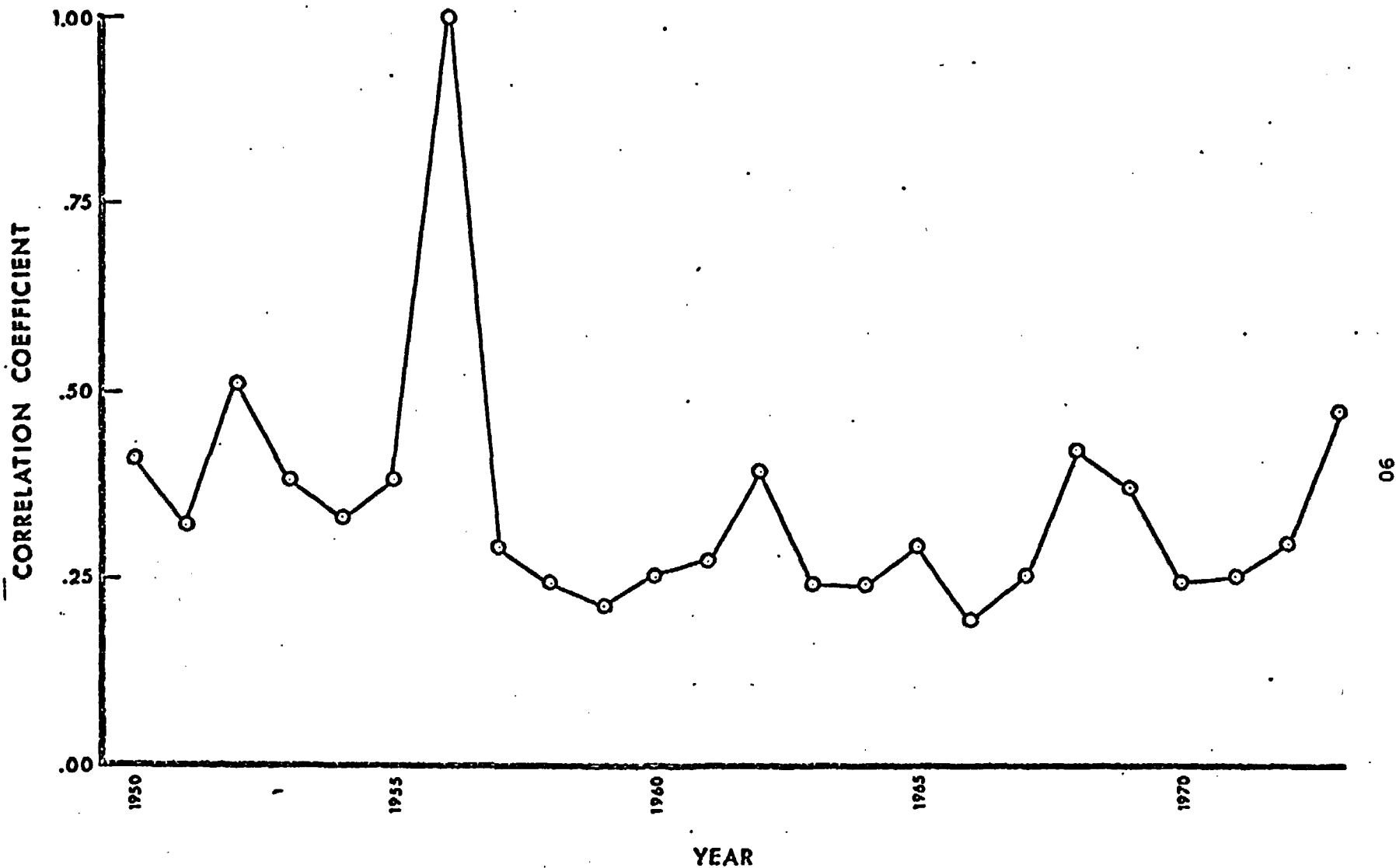


Figure 3.4-13. Maximum correlation coefficients obtained from the two-dimensional cross-correlation of the 1956 strain release with the strain release for each year, 1950 through 1973, in the California/Nevada area. Lines connecting the correlation coefficients computed for each year are drawn for illustrative purposes only. Correlation coefficients cannot be interpolated between points.

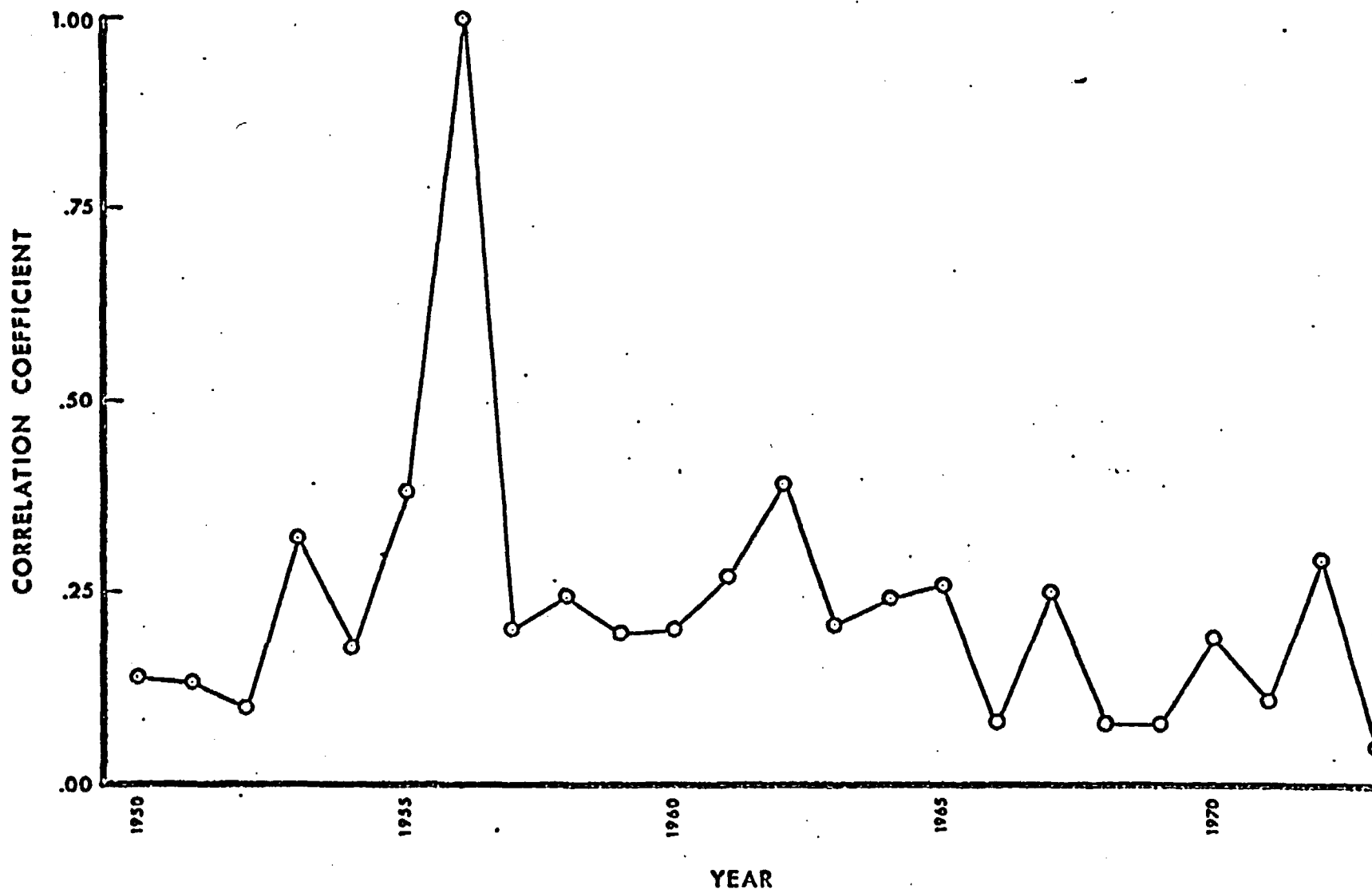


Figure 3.4-14. Zero-lag correlation coefficients obtained from the two-dimensional cross-correlation of the 1956 strain release with the strain release for each year, 1950 through 1973, in the California/Nevada area. Lines connecting the correlation coefficients computed for each year are drawn for illustrative purposes only. Correlation coefficients cannot be interpolated between points.

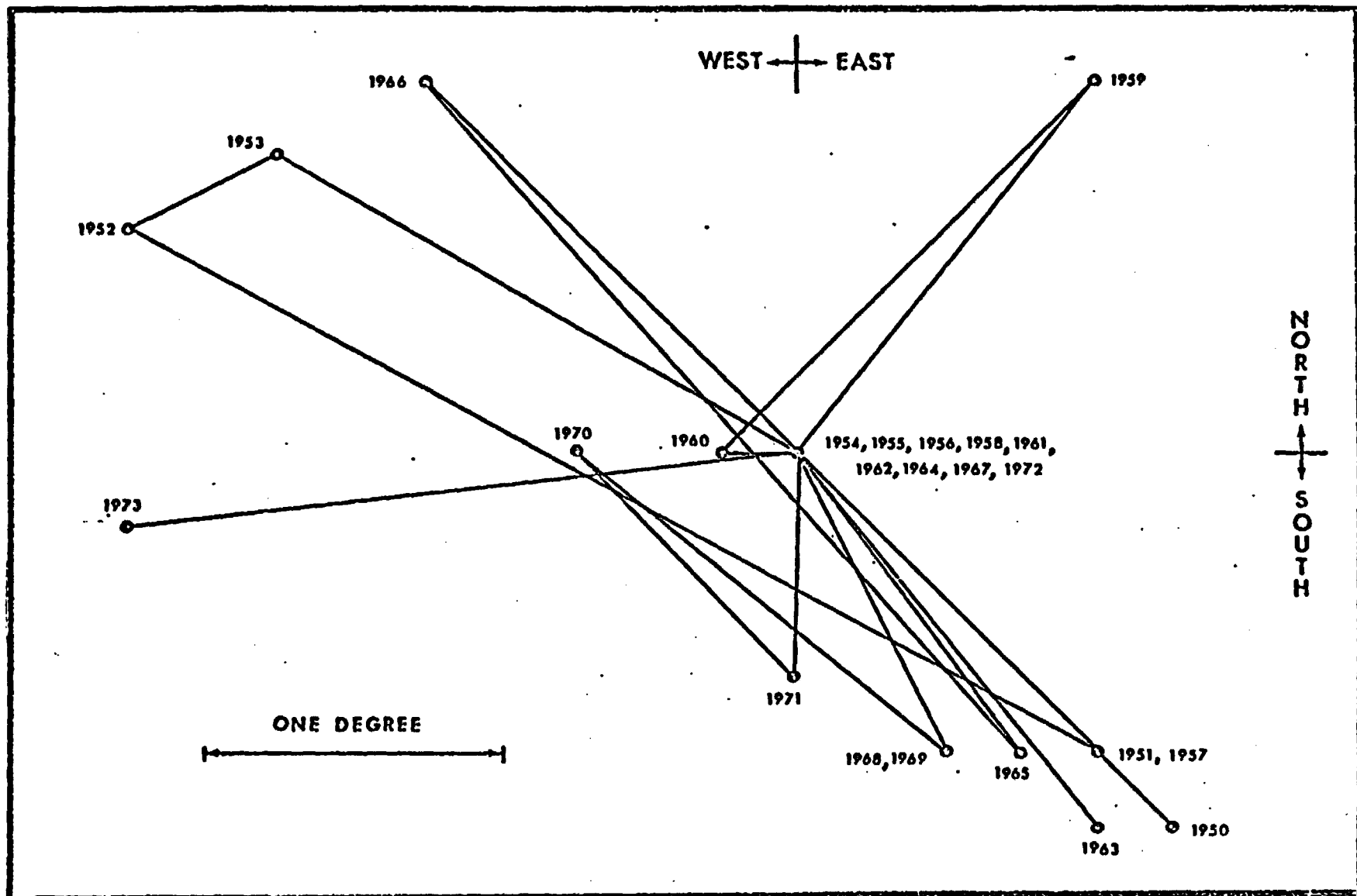


Figure 3.4-15. Plot of yearly peak correlation coefficient locations for cross-correlation of the 1956 strain release with the strain release of each year, 1950 through 1973.

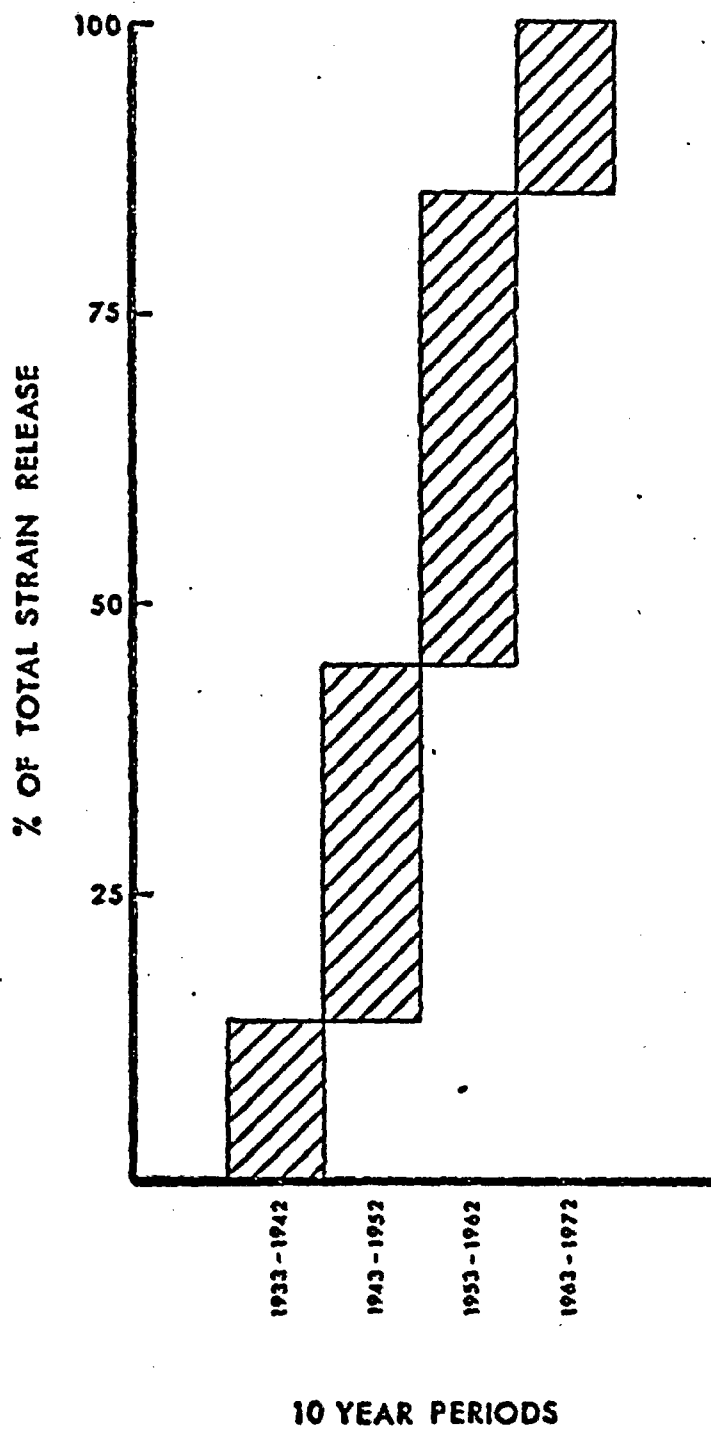


Figure 3.4-17. Cumulative strain release for each 10-year period for the California/Nevada area from 1933 through 1972.

Visual Analysis - Stereo Projections

A computer program was developed to portray the seismic activity in Nevada as a function of time and space by use of stereo projections. The program was later modified to accept the larger data base of the California/Nevada area. This program searches the data tape for the proper time window and assigns each earthquake within the given latitude and longitude a + or x symbol. The earthquakes are then plotted in a three-dimensional stereo reference frame as a stereo pair. The size of the + is proportional to magnitude, and events of unknown magnitude are shown by an x. The horizontal axes represent latitude and longitude, and the vertical axis represents time.

The seismicity of the general Nevada area is shown in Figures 3.4-18a and b and 3.4-19a and b for the time periods 1852-1962 and 1961-1973, respectively. These data are viewed from the southeast corner of the State. Similar plots viewed from the southwest, northwest, and northeast were also prepared. In the earlier period, 1852-1962, the activity at Lake Mead (Hoover Dam) is clearly evident as well as the improved seismograph station coverage. The intense activity in 1954 near Fallon corresponds to the Fairview Peak, Dixie Valley, and Rainbow Mt. earthquakes and their aftershocks. The later period, 1961-1973, reflects the activity at the Nevada Test Site when the resumption of the testing program started in September 1961. It can also be seen that there are more scattered lower magnitude earthquakes which can be directly related to the increased station coverage and hence lower detection thresholds. The vastly different time scale (110 years vs. 12 years) should be kept in mind when comparing these two figures. The area covered in Figure 3.4-18a and b is

restricted by the data set available to an area slightly larger than the Nevada State boundary, while Figure 3.4-19a and b includes that portion of California indicated by the coordinates shown in the figure.

Eight sets of stereo projections (Plates 2A and B through 9A and B) were constructed to view the California/Nevada area from the southeast with an expanded time scale, each pair extending over a 5-year time period. The total time period ranges from 1933 to 1973. The area included extends from 32.5°N to 42.5°N and 113.5°W to 124.5°W. Plate 1C is a plastic overlay for the right view that can be used with the above plates for geographical orientation purposes. This plate is located in the folder at the back of the report.

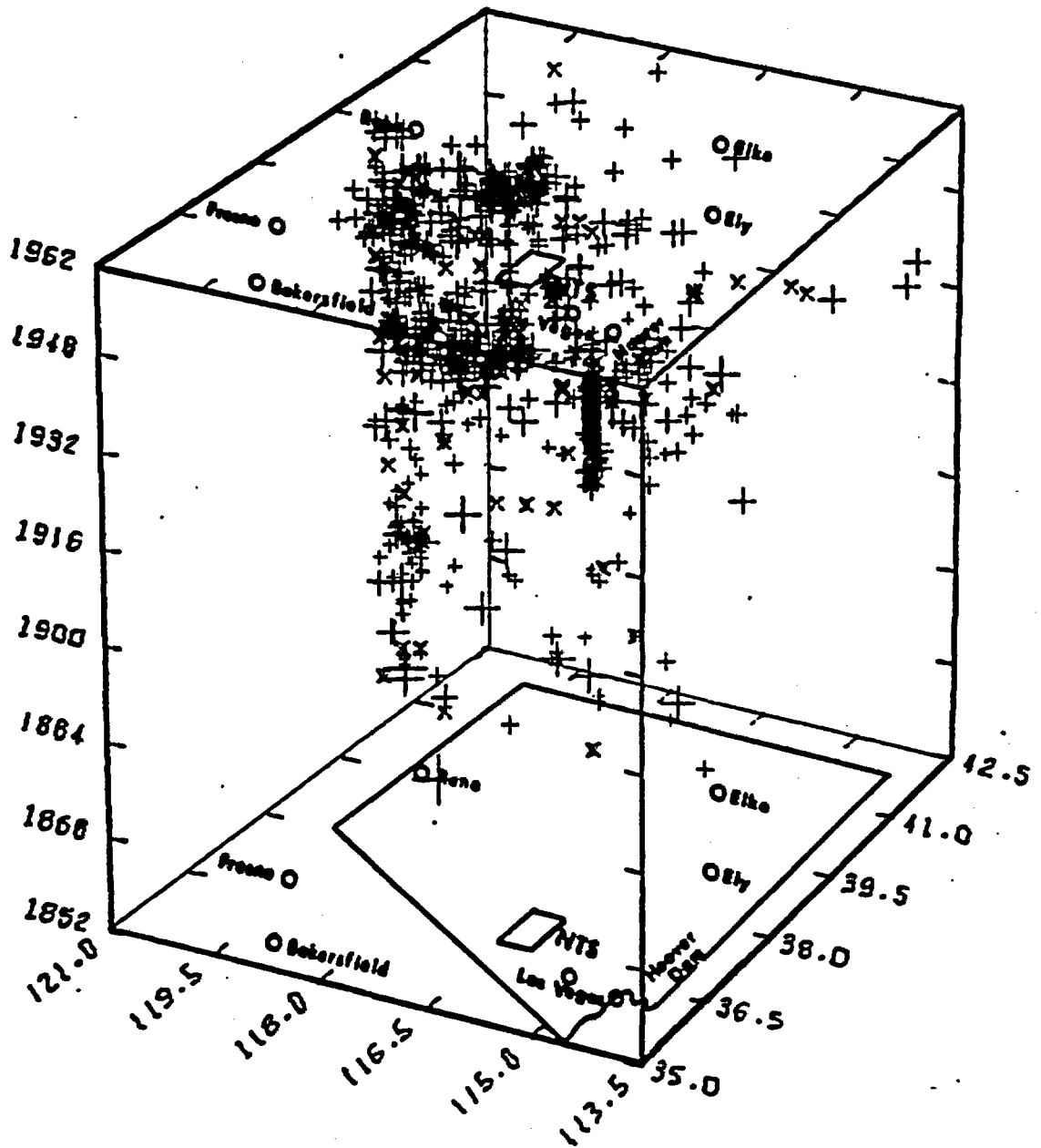


Figure 3.4-18a. Seismicity of Nevada from 1852 to 1962 using the catalog of Slemmons et al, 1965. The size of the + is proportional to magnitude, events of unknown magnitude are shown by an X. The figure is also the right view of the stereographic pair Figure 3.4-18a, Figure 3.4-18b.

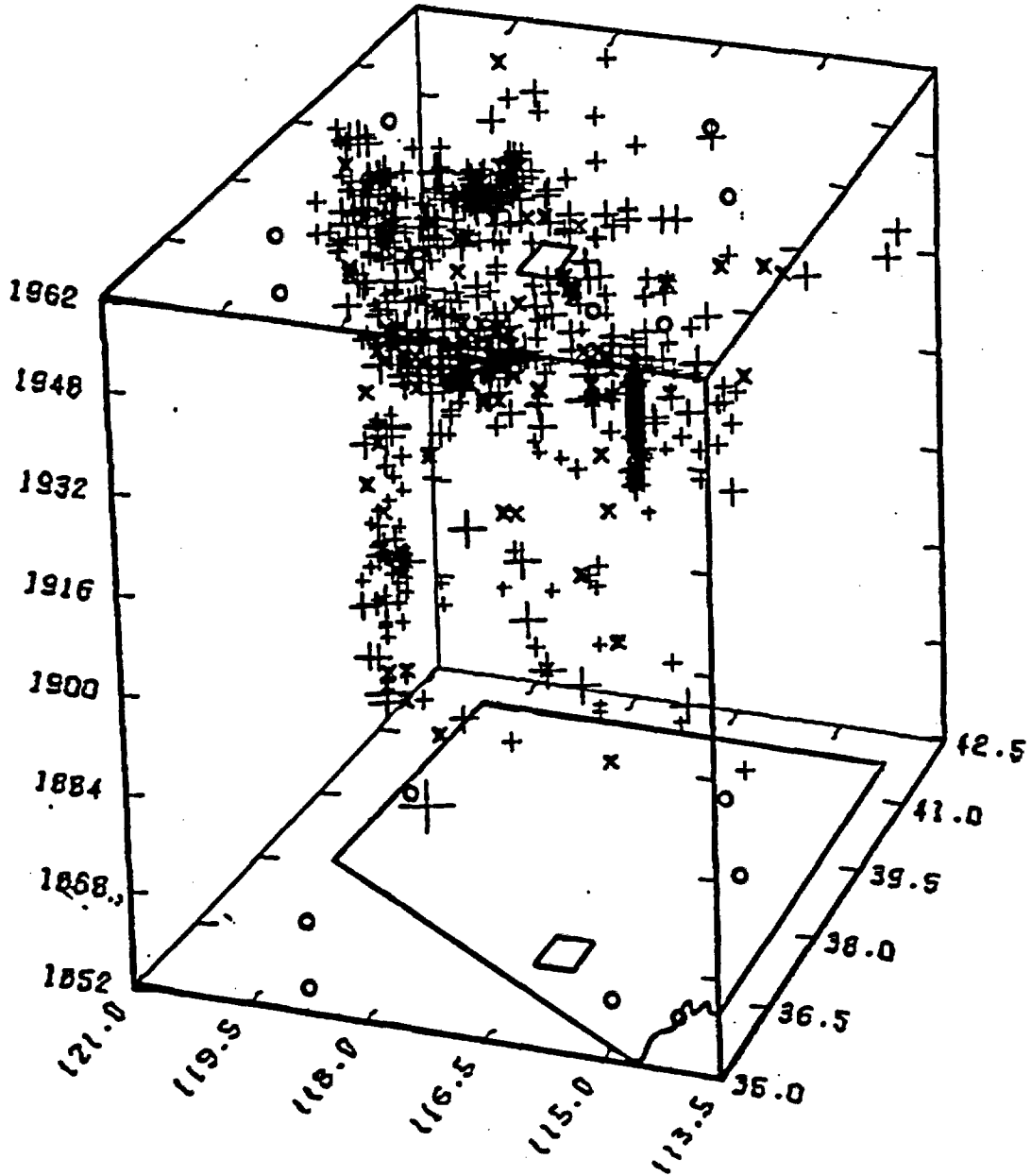


Figure 3.4-18b. Left view of stereographic pair Figure 3.4-18a, 3.4-18b.

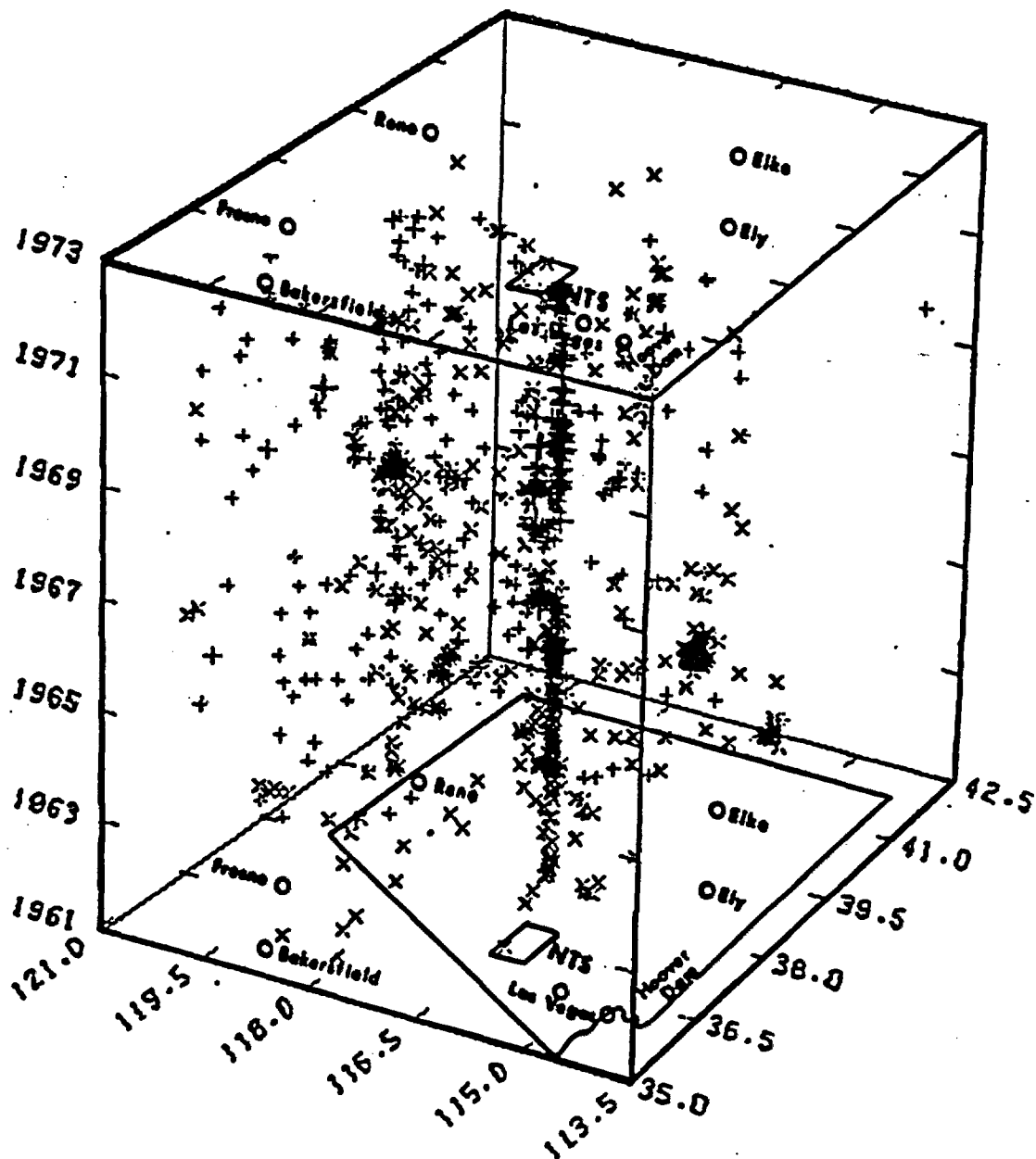


Figure 3.4-19a. Seismicity of Nevada from 1961 to 1973 using NEIS data. The size of the + is proportional to magnitude, events of unknown magnitude are shown by an X. The figure is also the right view of the stereographic pair Figure 3.4-19a, Figure 3.4-19b.

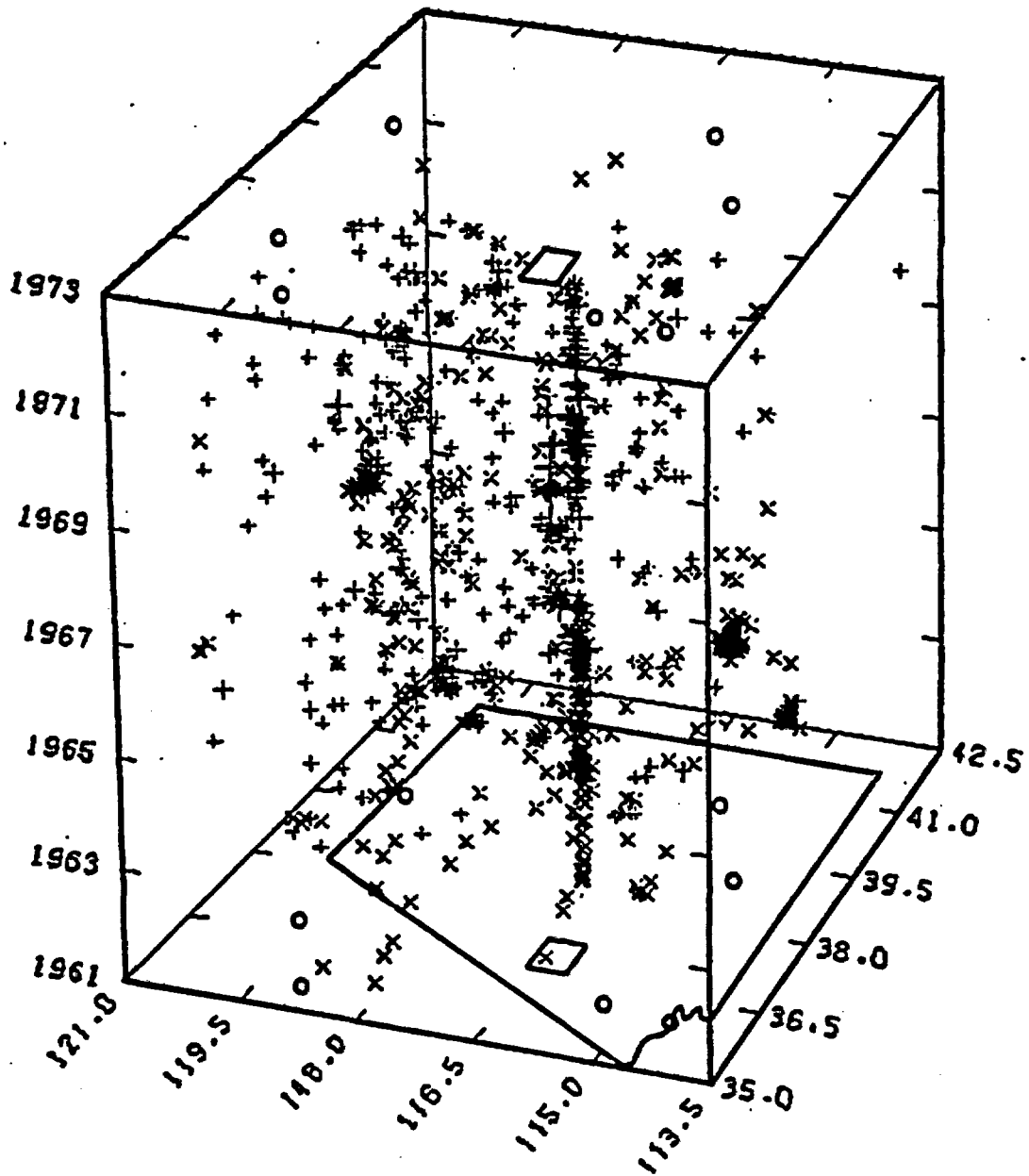


Figure 3.4-19b. Left view of stereographic pair Figure 3.4-19a, Figure 3.4-19b.

3.4.2 Nevada Test Site Seismicity

Earthquakes Detected by NTS Local Seismograph Networks

A detailed study was made of the Nevada Test Site seismicity for the time period 1 June 1969 through 1 March 1973. The earthquake data were obtained from the seismograph networks operated primarily by the U.S. Geological Survey-Menlo Park and the U.S. Geological Survey S.R.A.B.-Las Vegas (formerly the NOAA Special Projects Group). Some additional data were obtained from the University of California, Lawrence Livermore Laboratory network and the Sandia Laboratories network.

The area included in this study is primarily the area covered by the Pahute Mesa and Yucca Flats nets. The area extends from 36° to 37.5° North and 115.5° to 117° West. The seismicity is displayed in Figures 3.4-20 through 3.4-25 as either the total number of earthquakes per week, the total accumulative strain release per week, or as accumulative weekly percentages of each over different time periods.

The two largest peaks shown in Figure 3.4-20 reflect the aftershock activity following JORUM (16th week, $m_b = 6.2$) and HANDLEY (43rd week, $m_b = 6.5$). Figure 3.4-26 contains the magnitudes of all of the significant shots fired during this 200-week period. There were 60 shots during this time period that had body wave magnitudes that ranged from 3.5 to 6.5. There were five additional shots that were too small for magnitudes to be determined. The shots below 6.0 did not appear to influence significantly the normal seismicity for this area with the exception of the shot fired during the 173rd week and possibly the 110th week. The intense shot activity during the 47th through 53rd weeks may also have perturbed the natural seismic pattern. However, the perturbation may be part of the

Figure 3.4-20

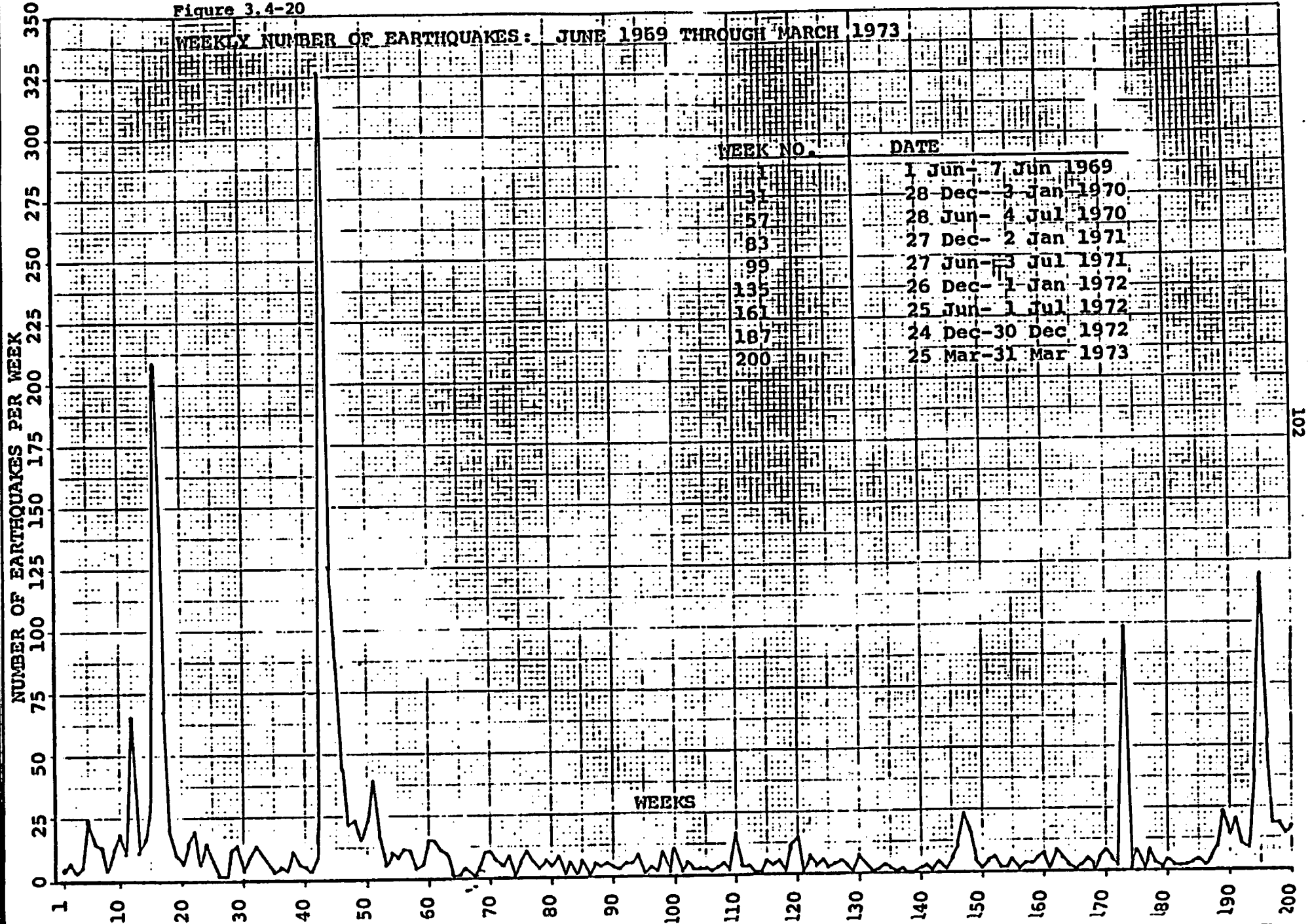
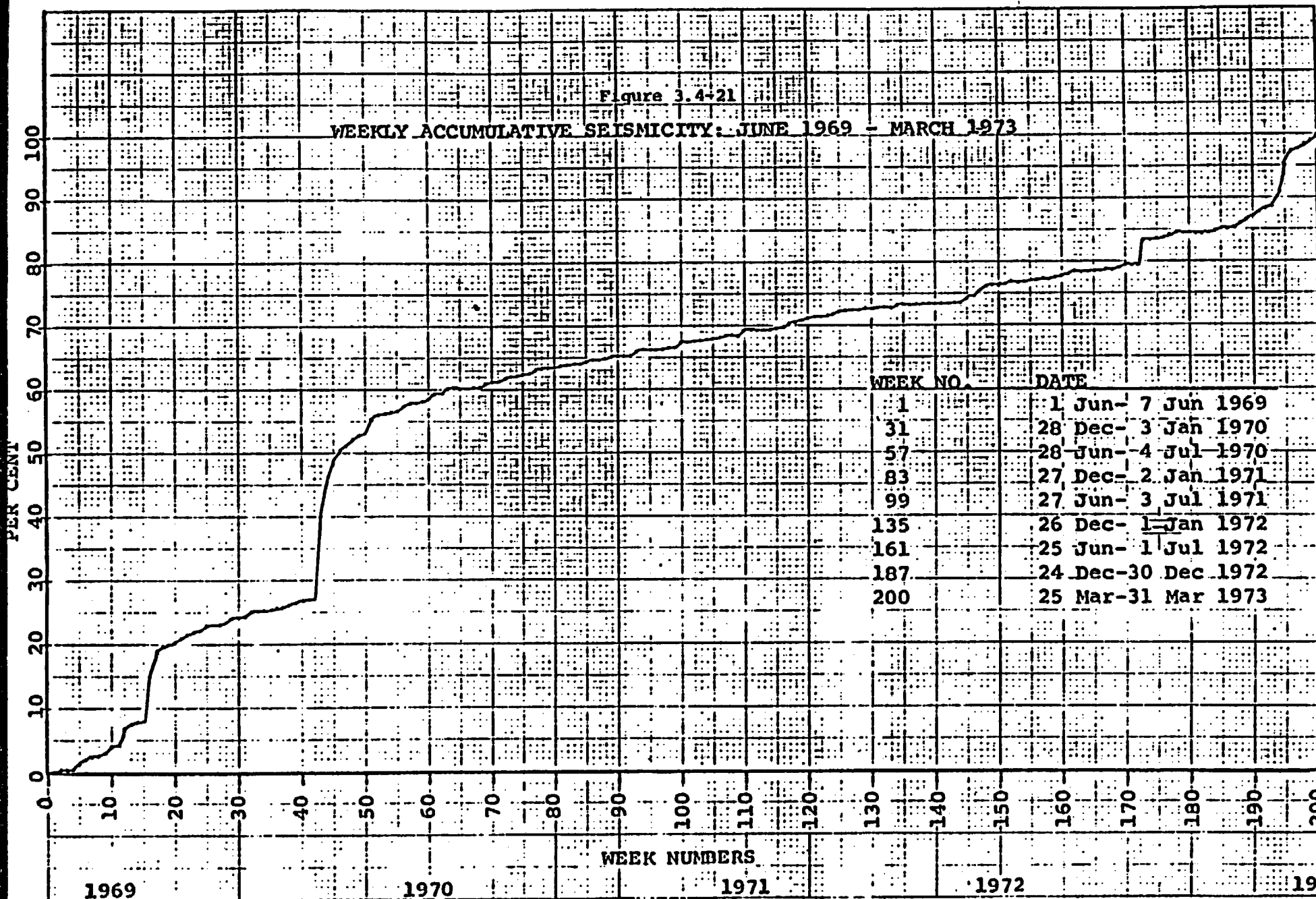


Figure 3.4-21

WEEKLY ACCUMULATIVE SEISMICITY: JUNE 1969 - MARCH 1973



103

1969

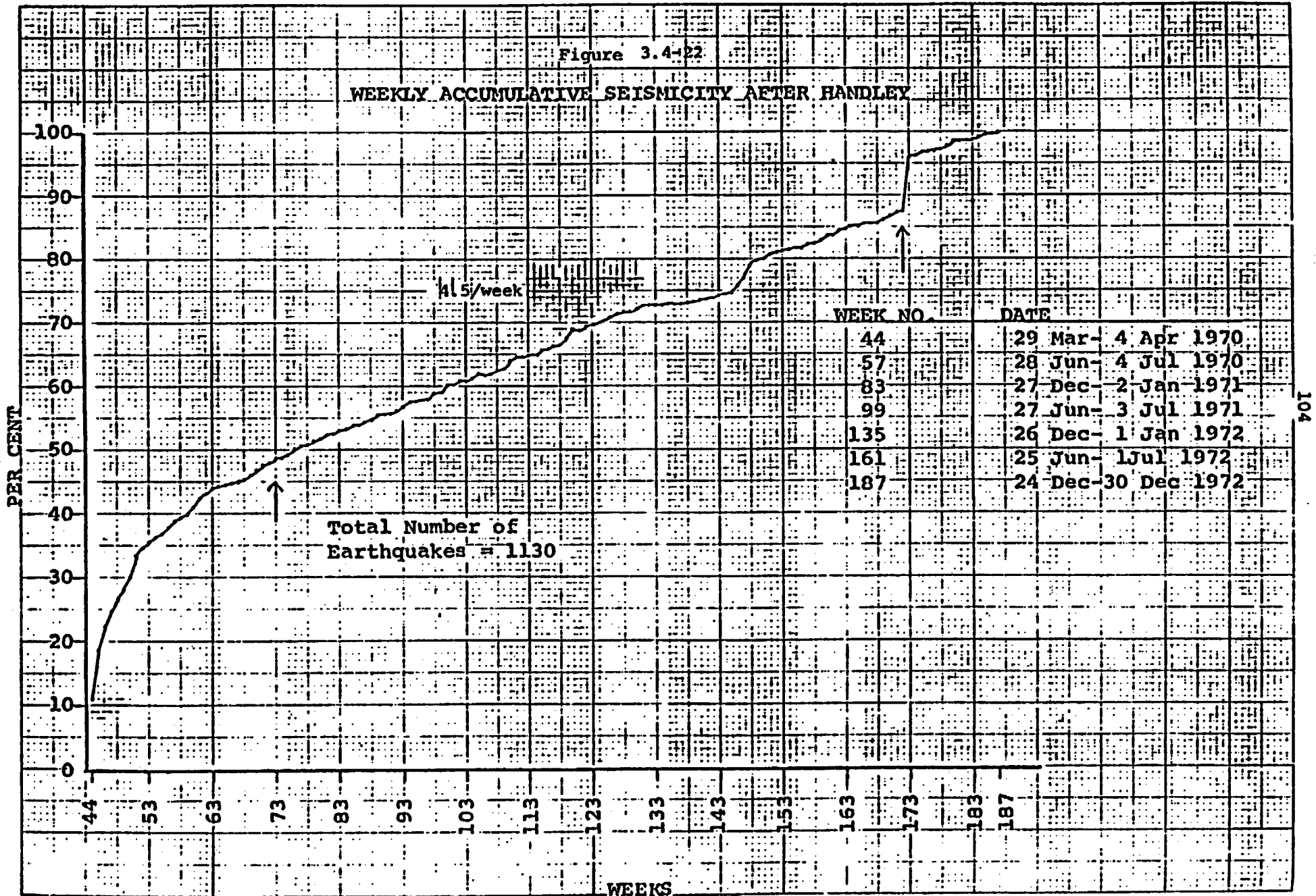
1970

1971

1972

1973

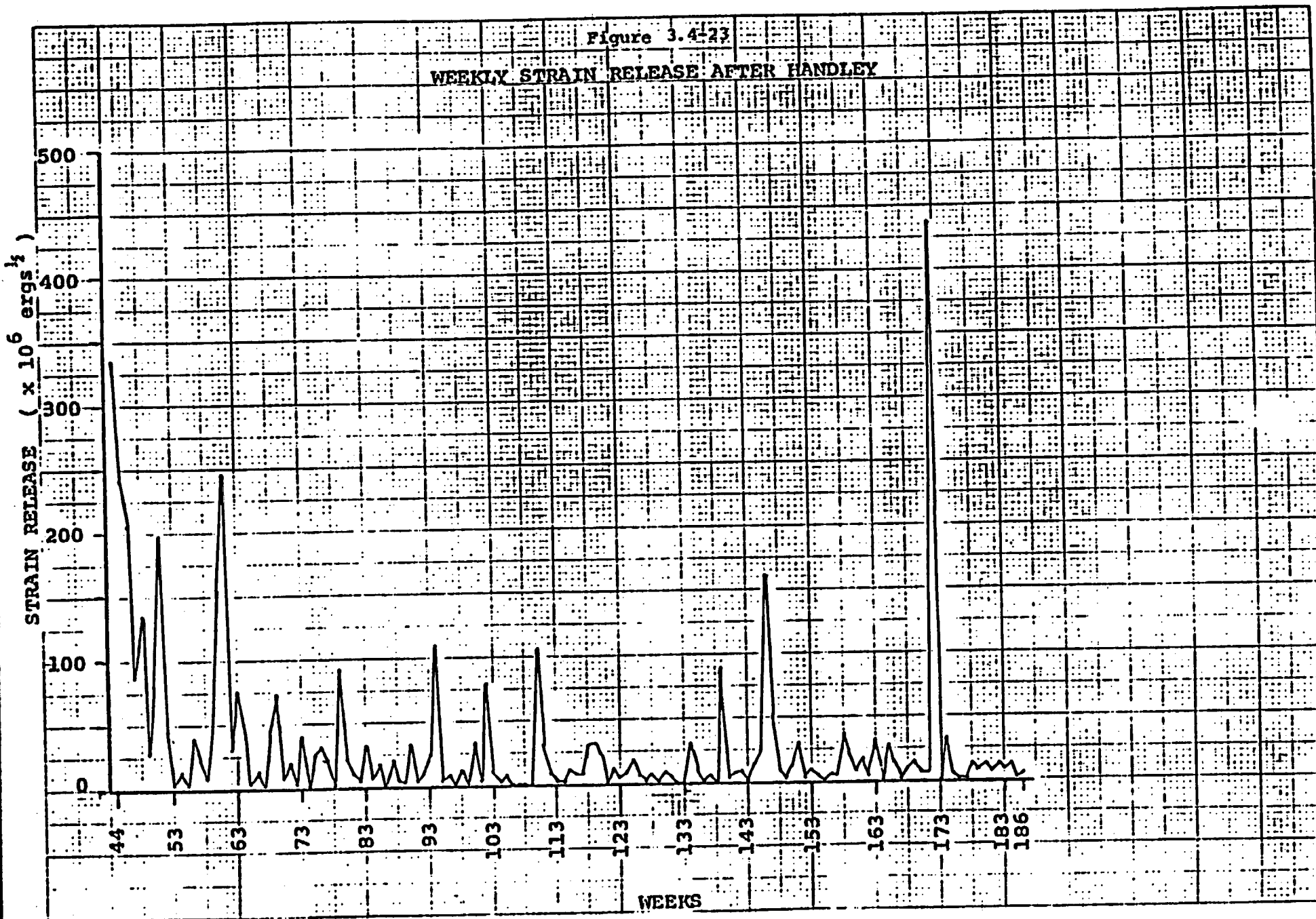
Figure 3.4-22
 WEEKLY ACCUMULATIVE SEISMICITY AFTER HANDLEY



101

Figure 3.4-23

WEEKLY STRAIN RELEASE AFTER HANDLEY



501

Figure 3.4-24

WEEKLY PER CENT STRAIN RELEASE ACCUMULATION
 1970-1972

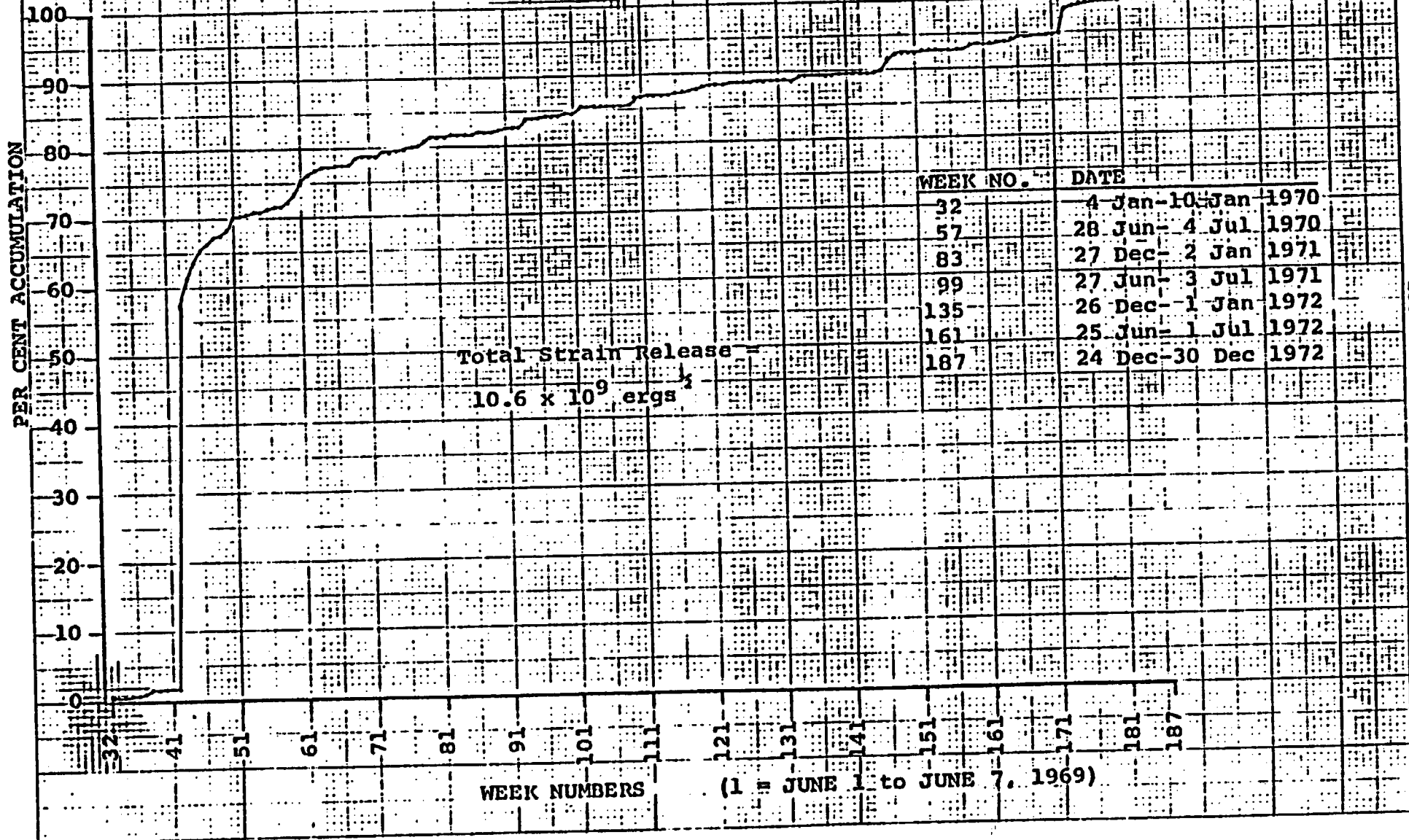
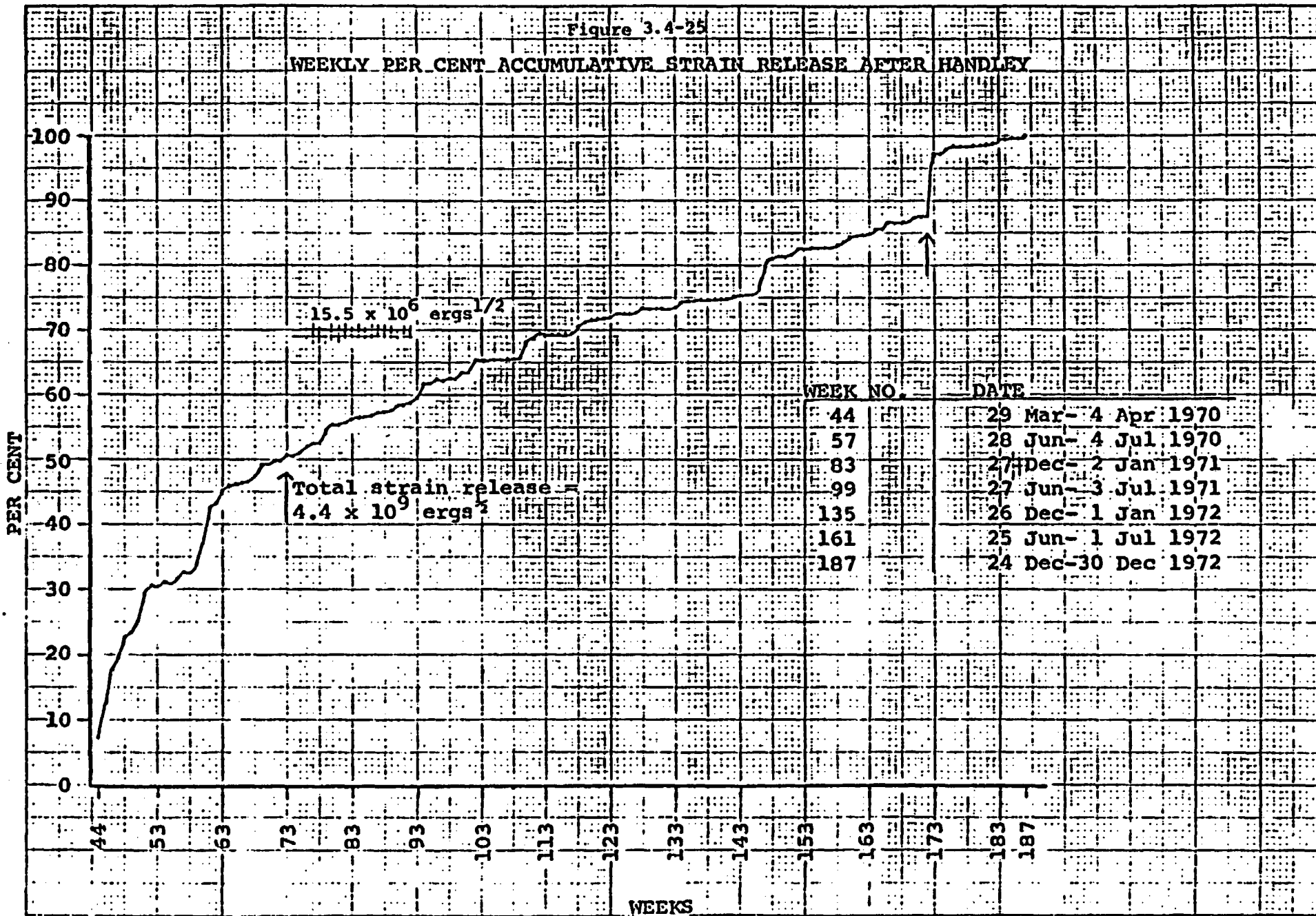
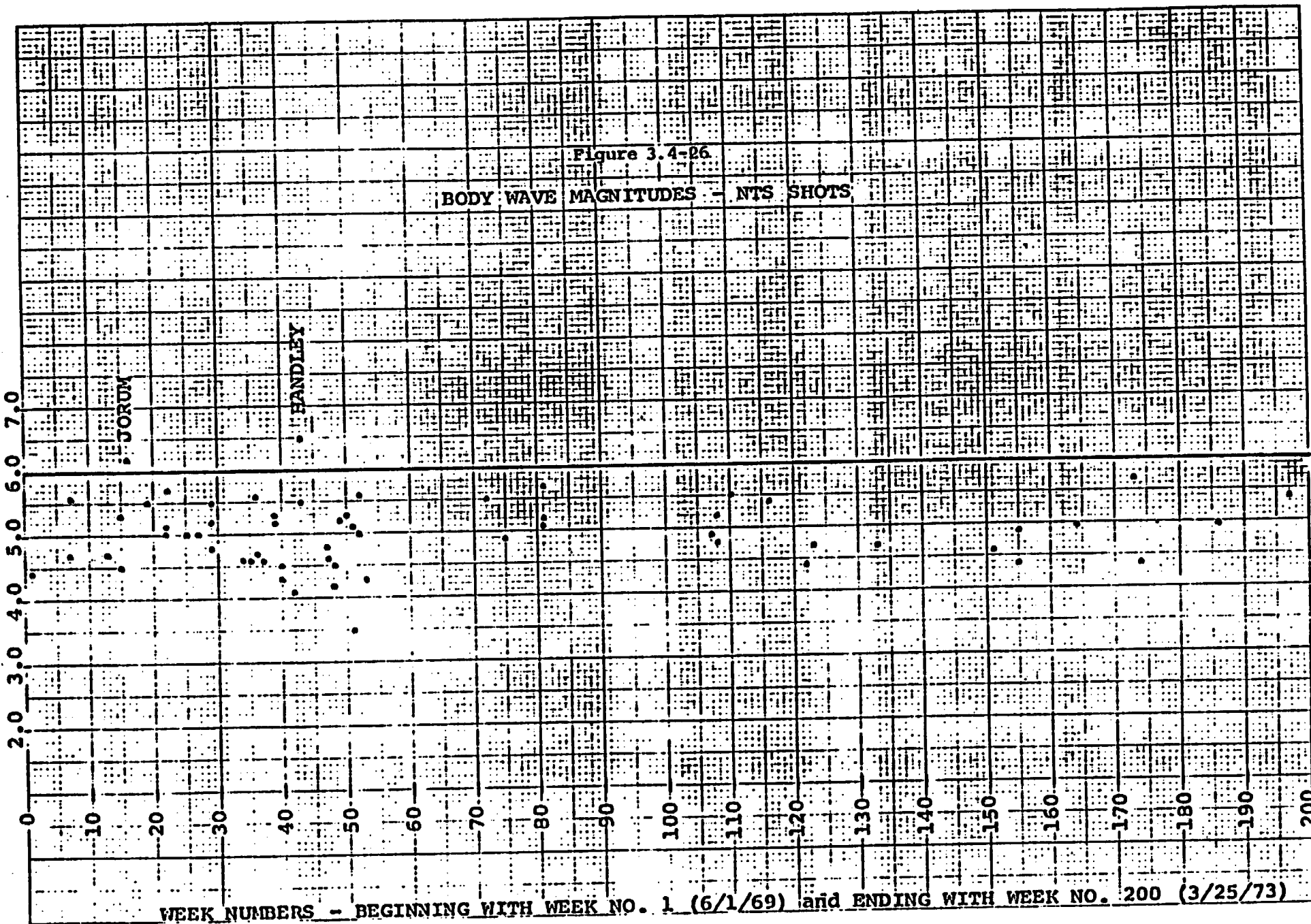


Figure 3.4-25

WEEKLY PER CENT ACCUMULATIVE STRAIN RELEASE AFTER HANDLEY



BODY WAVE MAGNITUDE - m0



aftershock activity caused by HANDLEY. The three large shots fired during the 81st week (the largest of which was 5.7) did not affect the seismic pattern as seen in both the strain release and weekly number of earthquakes.

The data base is not consistent throughout this 200-week period. Beginning at approximately the 188th week (Dec. 31, 1972) the number of seismograph stations in operation was reduced considerably by the closing of the U.S.G.S.-Menlo Park network. Hence, the weekly number of earthquakes shown for 1973 is a conservative number because of the smaller station control. It is interesting to note, however, that during this time period the number of earthquakes reported was higher than the average for the preceding 130 weeks indicating that there was a true increase in seismicity during the first 3 months of 1973. Strain release was not computed for this time period because most of the earthquakes reported did not have computed magnitudes. Those earthquakes that did have computed magnitudes ranged in value from 2.9 to 4.2. The number of earthquakes with magnitudes above 3.9 shows that the strain release for this period is also higher than average.

A Spearman's rank analysis for these data is shown below:

Time Period	Number of Earthquakes/Week Rho	Strain Release/Week Rho
1. 1 June 1969-25 March 1973 (Week No. 1 thru 200)	-.23	
2. 4 Jan. 1970-thru 1972 (Week No. 32 thru 187)	-.36	-.33
3. After HANDLEY-thru 1972 (Week No. 62 thru 187)	-.09	-.15
4. After HANDLEY-thru 25 March 1973 (Week No. 62 thru 200)	+.18	

Rho, the Spearman's rank correlation coefficient, can vary between +1 and -1. Rho near -1 is strong evidence of a decreasing trend, near +1 indicates strong evidence of an increasing trend. Overall the seismicity appears to be decreasing. Eliminating the 19 week time period following HANDLEY (see line 3 above) it can be seen that there is a relatively low level constant rate of seismic activity over a time period of 100 weeks. This is interpreted to represent more or less the natural seismicity for the area. Referring to Figures 3.4-22 and 3.4-25 for the time periods shown, the number of earthquakes per week and the strain release per week is approximately 4.5 and 15.5×10^6 ergs^{1/2}, respectively. The positive value of Rho is caused by the increased natural activity in early 1973.

Stereo Projections of NTS Activity

In order to examine in more detail the relationship between shot activity and earthquakes in the NTS area, stereo projections were made utilizing the local seismograph network which has a considerably lower magnitude detection threshold than most areas covered in our main file. Examples of these projections are shown in Plates 10A and B through 13A and B, which are located in the folder at the end of this report. Plate 10A and B is a stereo pair showing the shots fired at NTS during 1970-71 and -72. The large event in 1970 is HANDLEY. The area covered ranges from 36.0°N to 37.5°N and 115.5°W to 117.0°W. The same time and spatial configuration is shown in Plate 11A and B for all of the detected earthquakes in this area. The HANDLEY shot can be correlated with the intense earthquake activity in 1970. The time scale is expanded in Plates 12 and 13 to allow a more detailed examination of the seismicity in 1970. The after-shock activity following HANDLEY can be traced very clearly. An important

factor also clearly seen when these plates are viewed through a stereoscope is the limited areal extent of the aftershock activity. Immediately following the shot this activity is confined to a roughly circular area with a maximum diameter of approximately 45 km. Earthquake activity in this same general area can be seen in early 1970 prior to HANDLEY. Some of this activity is probably related to the aftershock sequence from JORUM.

3.5 Strain Measurements - Western U.S.

General Theory

The Nature of Strain

The deformation of a material body under the action of applied stresses produces a strain within that body. There are many sources of strain within the earth, most of which can be grouped into the five major sources listed in Table 3.5-1. In most strain studies, the periods or durations of interest to the geophysicist lie in the range of one second to a few years.

Strain within the earth can be represented by a nine-component symmetric tensor. Since all strainmeters are located on or near the surface of the earth, reduction then occurs in the strain field representation yielding a 2 x 2 symmetric tensor. This enables the strain field at the surface of the earth to be uniquely defined by three independent horizontal components. In strain measurement, the strain in a particular orientation is determined by measuring the change in length, Δl , of a reference and then dividing this change by the total reference length, l . From the mathematical expression, $\Delta l/l$, it is obvious that strain is a unitless quantity.

TABLE 3.5-1

Source and Duration of Earth Strains

<u>Source</u>	<u>Period or Duration</u>
Tectonic	$10^5 - 10^{10}$ Years
Extraterrestrial Bodies	8 Hours - 10^3 Years
Meteorological	8 Hours - 1 Year
Free Vibrations	10 Minutes - 24 Hours
Propagating Waves	.1 - 200 Seconds

Two categories into which measurements of the elastic deformation of the earth can be classified are geodetic measurements and strain measurements. Geodetic measurements are made over long base lines on a periodic basis with the intent of detecting any changes in the line length. Base lengths are on the order of one to ten kilometers and are usually measured once every half year to year. There are several drawbacks with geodetic measurements. Base lengths are often so long that only large scale deformations can be observed, and the length of time between surveys is often so great that the shorter period phenomena of Table 1 are not detected. Therefore, shorter base length instruments and continuous recording are necessary to resolve the smaller short period deformations. This is accomplished with strainmeters of which there are many types. Probably the most common, and the ones used in the daily and secular strain portions of this study, are the Benioff-type quartz-rod strainmeters (see Appendix D).

Strain Measurement

The solid earth tides produce the most obvious strain phenomenon that are observable on a strain record recorded on an instrument whose sensitivity is better than one part in a hundred million (10^8). Solid earth tides are the gravitational accelerations caused by the gravitational influence of the sun and moon, which produce a bulging of the earth with a maximum total magnitude of 36 cm (Melchior, 1966). It is this bulging or deformation which produces the earth tidal strains. Tidal strains are on the order of 5×10^{-8} (Knopoff, 1964), with diurnal and semi-diurnal components being predominant.

Secular strain is different from earth tidal strain in that it is the long term strain change associated with tectonic strain or some other

periodic or non-periodic source. Secular strain has been noted at a number of strainmeter sites over the past fifteen years. The values of secular strain vary from 10^{-8} per year in New York to 10^{-5} per year in southern Nevada (Major and others, 1964; Berger and Lovberg, 1970; Malone, 1972; Willis and others, 1973). Secular strain can be determined from both geodetic strain measurements and strainmeters.

Another area of strain research is the study of strain steps. It is thought that motion on a fault is triggered by an earthquake or nuclear event and the dislocation of the fault produces offsets on a strainmeter record. Wideman (1971) termed these offsets (i.e., residual strains) strain steps. Strain steps are well documented in the literature (Press, 1965; Wideman and Major, 1967; Romig and others, 1969a and b; Smith and others, 1969; Yeatts, 1973). Doubt as to the significance of the steps has persisted to the present due to the possibility of instrumental hysteresis, local readjustments of irregularly-coupled blocks of earth, or site-specific variations in elastic parameters (Kumamoto, 1973).

Nevada Strainmeter Deployment

In an attempt to evaluate the impact of nuclear testing on regional tectonics, a number of strainmeters were constructed by various groups⁻¹ in Nevada. Pertinent data on these installations is shown in Table 3.5-2. Instrument locations and component orientations are shown in Figure 3.5-1.

Short Period Strain Data

It is necessary before pursuing this study to determine the phase relationship between earth tides and earth tidal strain. A phase lag

⁻¹The former NOAA Earthquake Mechanisms Laboratory, Colorado School of Mines, the University of Nevada-Reno, and the California Institute of Technology.

TABLE 3.5-2

Nevada Strainmeter Installations

<u>Station</u>	<u>Station Code</u>	<u>North Latitude</u>	<u>West Longitude</u>	<u>Orientations</u>
Round Mountain	RMN	38°42.1'	117°04.6'	35.5, 288°, 347.5
Mina	MNN	38°26.3'	118°09.3'	137°, 203°, 254°
Ely	ELY	39°16.0'	114°56.7'	045°
Twin Springs	TSP	38°12.5'	116°09.2'	000°, 090°, 315°
Scotty's Junction*	SCT	37°05.4'	117°16.2'	Vertical, 039°, 084°, 309°, 354°
Sleeping Mountain	SPM	37°08.6'	116°46.0'	084°, 309°, 354°
Thirsty Canyon	THC	37°12.2'	116°34.7'	005°, 046°, 276°, 320°
Rawhide Mine	RH	38°13.6'	116°22.9'	325°
Kawich Peak	KP	37°53.8'	116°27.6'	356°
Quartzite Mine	QM	37°33.8'	116°19.1'	20°
Tolicha Peak	TI	37°17.1'	116°52.0'	266.5°
Yucca Mountain	YM	36°55.9'	116°33.2'	182.5°
Oak Spring Butte	OB	37°14.2'	116°03.2'	81°

* This site is located between Scotty's Castle and Scotty's Junction. It is actually closer to Scotty's Castle but is referred to as Scotty's Junction.

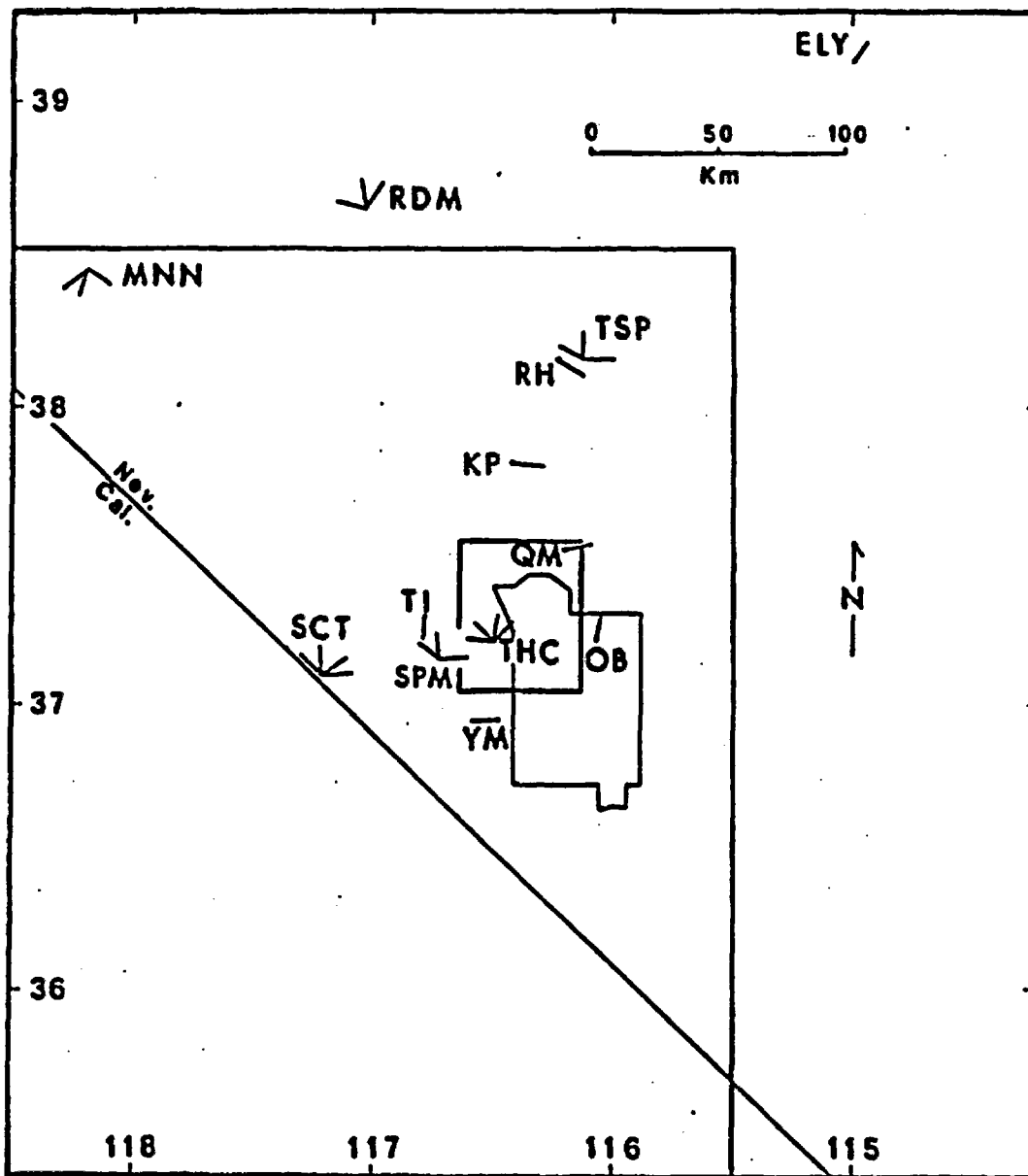


Figure 3.5-1. Locations of the thirteen Nevada strainmeter stations listed in Table 3.5-2.

will be present between earth tidal accelerations and strain as a result of energy dissipation in the solid earth. Harrison (1969) found the value of the phase lags between theoretical earth tidal accelerations and IGY world-wide tidal gravity data to be 0.8 ± 2.8 degrees. Priestly (1974) showed that the expected phase shift for the strain tide is approximately seven times larger than for the gravity tide. Since the phase lag is a small, rather variable and difficult quantity to measure, it will be assumed that the theoretical earth tides and earth tidal strains will not have any significant phase lags between them due to energy dissipation in the solid earth. Any phase lags between the earth tidal accelerations and recorded strain would then be due to site inhomogeneities (anisotropic response), data contamination, instrumental difficulties or station operator errors.

Empirical confirmation was sought for the earth tidal acceleration, earth tidal strain relationship. The theoretical earth strain, calculated using coordinates for Pinion Flats, California, was taken from a figure in Lee and Brown (1972) and digitized on a three hour interval with an accuracy of ± 2 hours. It was then cross-correlated with theoretical earth tides calculated over the same time interval and for the same station coordinates. It should be noted that cross-correlation is valid between any two data sets regardless of their scale (Tatar, 1974). Figure 3.5-2 shows the cross-correlation plot. The peak positive correlation of 0.78 occurs at +3 hours lag. It is believed that the observed phase lag is due to the inaccuracy in digitization of the figure in Lee and Brown and, to a lesser extent, the increment of digitization. Improvement in digitization would probably increase the correlation and reduce the lag.

PINION FLATS THEORETICAL STRAIN CROSS-CORRELATED
WITH THEORETICAL EARTH TIDES

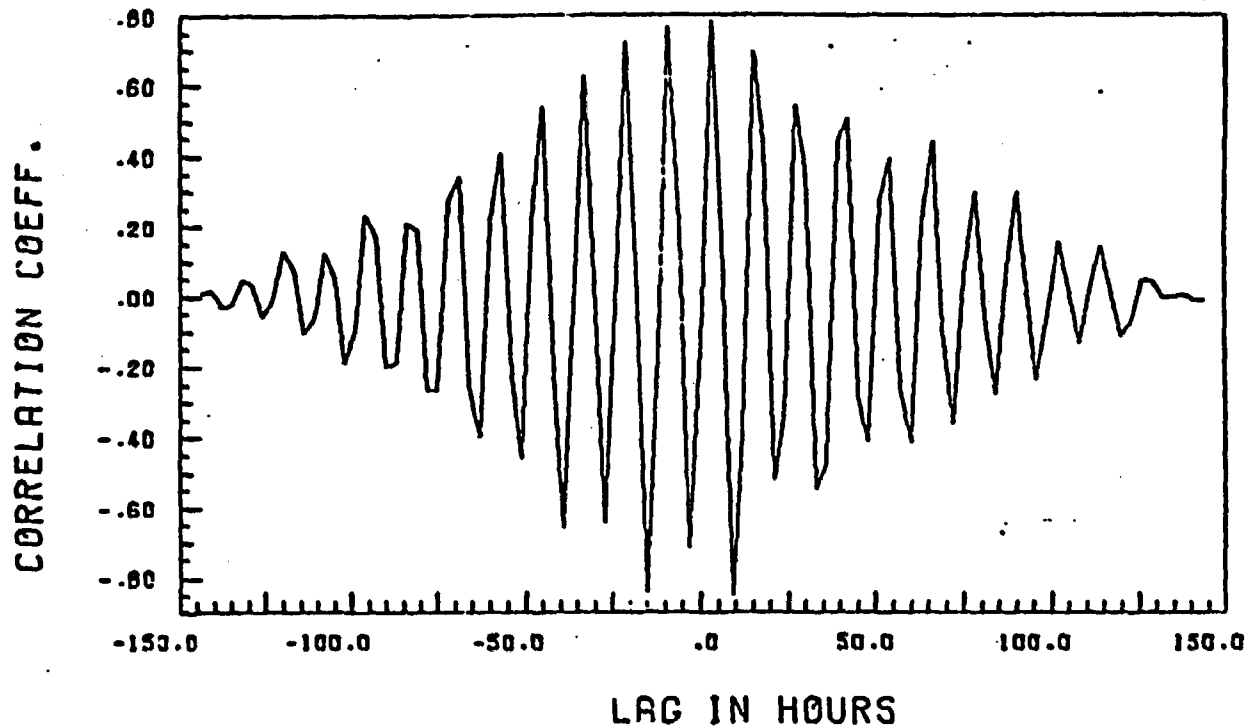


Figure 3.5-2. The cross-correlation function of Pinion Flats, California, north-south theoretical strain, cross-correlated with north-south theoretical earth tides calculated using Pinion Flats strainmeter coordinates. The data interval is from January 27, 1971 to February 2, 1971.

These results, however, are felt to support the statement that the theoretical earth tides and theoretical earth strains have no significant phase lags between them.

Another point of significance is to establish that the theoretical earth tidal periods, as calculated by the earth tidal program obtained from the former Earthquake Mechanisms Laboratory, NOAA, compare favorably with the observed earth tides. The earth tides of largest amplitudes (Melchior, 1966) and the only ones this study is concerned with are listed in Table 3.5-3.

There will be difficulties in the separation of the F_1 and two K_1 waves and the N_2 and M_2 in an earth tide generation program because of their close proximities to one another. It is important to note that if the program generated waves with these periods, the length of the data windows would not permit resolution in the power spectral density plots.

Figures 3.5-3, -6, -8, -10, and -12 are power spectral density plots of the autocorrelated theoretical earth tides. The peaks in these figures correspond closely to those listed by Melchior. The observed differences in period are probably due to the length of data windows (especially for SPM northwest and TSP north-south) and the intervals of digitization of the theoretical earth tidal data. The differences observed in the relative amplitudes of the various peaks from plot to plot are due to the different component orientations in the calculation of theoretical earth tides (Melchior, 1966). The close agreements of the theoretical periods to those of the observed periods indicates the theoretical earth tidal program is working properly.

TABLE 3.5-3

Diurnal and Semi-Diurnal Earth Tidal Components
and Their Associated Periods

DIURNAL

<u>Name</u>	<u>Period</u>	<u>Description</u>
Q_1	26.88	Lunar tide (elliptic wave of a)
O_1	25.82	Principal lunar wave
M_1	24.83	Elliptic lunar wave of K
P_1	24.07	Principal solar wave
S_1	24.00	Elliptic solar wave
K_1	23.93	Solar declinational wave
K_1	23.93	Lunar declinational wave
OO_1	22.31	Principal lunar declinational wave

SEMI-DIURNAL

<u>Name</u>	<u>Period</u>	<u>Description</u>
N_2	12.65	Lunar major elliptic wave of M_2
M_2	12.42	Lunar principal wave
S_2	12.00	Solar principal wave
K_2	11.97	Luni-solar declinational wave

TER-DIURNAL

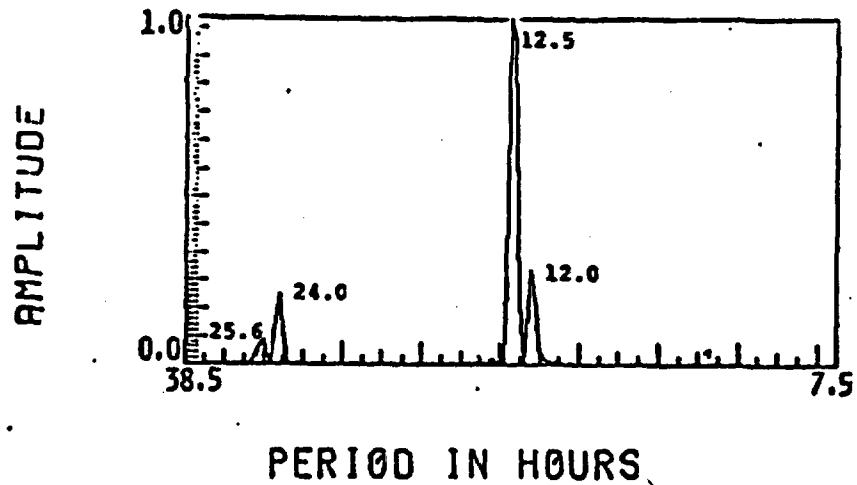
<u>Name</u>	<u>Period</u>	<u>Description</u>
M_3	8.28	Lunar principal wave
S_3	8.00	Solar principal wave

Short period data from Scotty's Junction, Sleeping Mountain, and Twin Springs strainmeter sites in southern Nevada (Table 3.5-3), operated by the Colorado School of Mines and the former NOAA Earthquake Mechanisms Laboratory, were analyzed. Detailed comparisons of the autocorrelated theoretical earth tides and the autocorrelated (detrended) strain are made to determine how well the observed strain periods and relative peak amplitudes compared to the theoretical earth tides. Rather than base correlation between the two on a visual qualitative basis, the data were cross-correlated to determine quantitatively the correlation coefficients. Power spectral density plots of the cross-correlation function yield the frequencies common to each, which contains the predominant short period energy.

Scotty's Junction Strain

Figure 3.5-3 is the power spectral density plots for the autocorrelated horizontal north-south theoretical earth tides and the autocorrelated detrended strain for the Scotty's Junction north-south horizontal component for the time period January 15, 1971 to February 12, 1971. The strain data were detrended using a least squares computer program. The power spectral density plots show, for the most part, very distinct peaks indicating strong periodic components in the data. The long period peak at 29.6 hours for Scotty's Junction north-south strain is believed to be noise related to the detrending of the strain data. The strain data peak with period 26.1 hours is thought to correspond to the 25.6 hour period present in the theoretical earth tidal data. The period at 22.3 hours in the strain data does not correspond to any peak present in the autocorrelated earth tidal data. However, there does exist an earth tidal

THEORETICAL EARTH TIDES POWER SPECTRA



SCT NS AUTOCORRELATION POWER SPECTRA

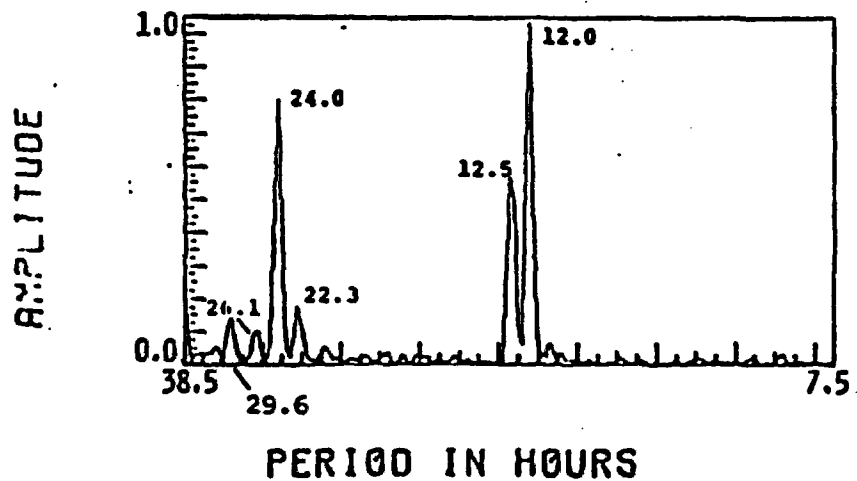


Figure 3.5-3. Power spectral density plots of the autocorrelation function for autocorrelated north-south horizontal theoretical earth tides (top), calculated using Scotty's Junction, Nevada, station coordinates and autocorrelated Scotty's Junction (SCT) north-south horizontal strain component (bottom). The data interval is from January 15, 1971 to February 12, 1971.

wave, the lunar declination wave OO_1 , which does have a period corresponding in value. The 22.3 hour peak does not appear in the plot since its amplitude, relative to the M_2 tidal peak at 12.5 hours, is 1/90 as great (Melchior, 1966). No explanation for the appearance of this period in the auto-correlated strain data other than an amplification phenomenon which may be possibly meteorological or site-related in nature can be determined.

While the two plots, in general, do compare favorably in terms of period, the plot of the autocorrelated strain does not maintain the same relative amplitude ratios between the peaks as might be expected if the earth tides were the only influencing factor. The observed strain has greater relative amplitudes than the corresponding earth tides at periods of 24.0 and 12.0 hours and a smaller relative amplitude at 12.5 hours. These observed variations in amplitude might be due to local site-related inhomogeneities or meteorological contamination of the data. Ozawa (in King and Bilham, 1973), using various instruments, compared theoretical with observed tides at various azimuths and as a function of the angle to the vertical. His results showed marked asymmetry about the vertical axis which was greater than 20 percent. This asymmetry of results was attributed by Ozawa to inhomogeneities in the region of his site or poor calibration of his instruments.

Cross-correlating theoretical earth tides with SCT north-south strain yielded Figure 3.5-4, which is the cross-correlation function. A peak positive correlation of 0.56 occurs at -3 hours lag indicating that the theoretical earth tides lead the strain by three hours. Table 3.5-4 also lists the values of the short period correlations and their associated

SCT NS CROSS-CORRELATED WITH THEORETICAL EARTH TIDES

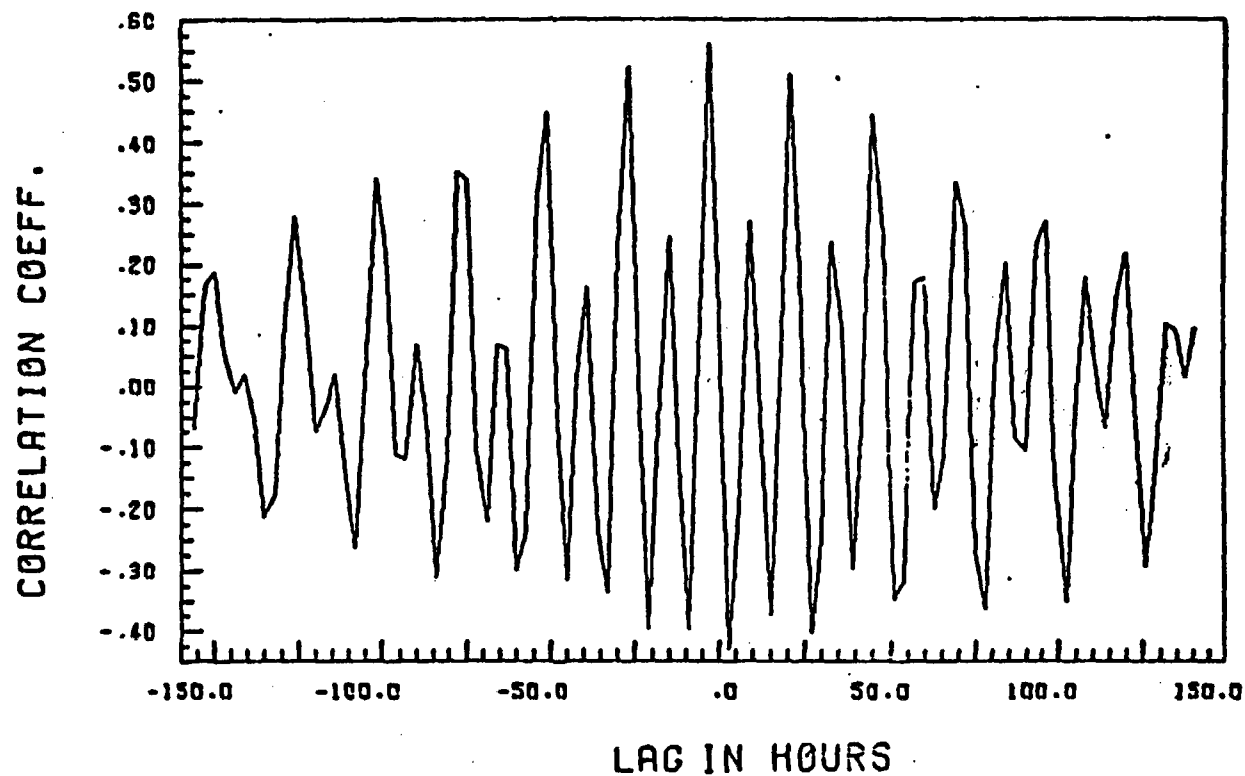


Figure 3.5-4. Plot of the cross-correlation function for Scotty's Junction, Nevada, (SCT) north-south horizontal strain component cross-correlated with the north-south theoretical earth tides, calculated using Scotty's Junction station coordinates. The data interval is from January 15, 1971 to February 12, 1971.

TABLE 3.5-4

Short-Period Cross-Correlation Coefficients for South-Central Nevada Strain Components, Yucca Flats, Nevada, Temperature and Groom Mine, Nevada, Microseismic Events, Cross-Correlated with Theoretical Earth Tides and Meteorological Data

Cross-Correlation			
<u>Data Set 1</u>	<u>Data Set 2</u>	<u>Correlation</u>	<u>Lag</u>
SCT NS	Earth Tides	0.56	-3.0 Hr
SCT Vertical	Earth Tides	0.39	-9.0 Hr
SCT NW	Earth Tides	0.35	0.0 Hr
SFM NW	Earth Tides	0.29	-9.0 Hr
TSP NS	Earth Tides	0.29	Inconcl.
SCT NS	Temperature	0.32	-6.0 Hr
SCT NS	Barometric Pressure	0.16	-4.5 Hr
Temperature	Earth Tides	0.51	6.0 Hr
Strain	Earth Tides	0.78	3.0 Hr
Groom Mine Microseisms	Earth Tides	0.52	4.0 Hr

lags. For the table as a whole, a negative lag means the first data set listed lags behind the second data set and for a positive lag the first data set leads the second data set in phase. It appears reasonable that the observed strain might lag theoretical earth tides to some extent since in the calculation of the tides a homogeneous elastic body is assumed. Elastic losses within the rock would lead to a lag between earth tidal maxima and a response to this stress, but it seems unlikely that it could produce a lag of -3 hours. Ocean loading may be responsible for some phase differences between the observed and theoretical data (Priestly, 1974); however, it is not felt to be a significant factor. It should be noted that the increment of digitization for this and all subsequent short period data sets only permits resolution of any peaks to within $\pm 1-1/2$ hours. Therefore, it is conceivable that the lag is as little as $1-1/2$ hours. For the length of the data window employed, the probability that the correlation resulted from chance is less than one in one thousand.

The power spectral density plot for the cross-correlation function described above is shown in Figure 3.5-5. All periods present are also present in the autocorrelated earth tides. The peak at 22.3 hours, by its existence, is correlative between the two data sets, meaning that the peak occurs in the earth tides. Due to its low amplitude, however, it is not visible in the autocorrelation plot (refer back to Figure 3.5-3). The 26.1 hour peak again most likely represents the 25.6 hour peak in the autocorrelated earth tides, but slightly shifted. The reason for this is not known. The longer period noise (29.6 hr) believed to be related to detrending has now vanished, meaning that it was non-correlative, thus lending support to the earlier hypothesis. In the cross-correlation power spectral density

SCT NS CROSS-CORRELATED WITH EARTH TIDES POWER SPECTRA

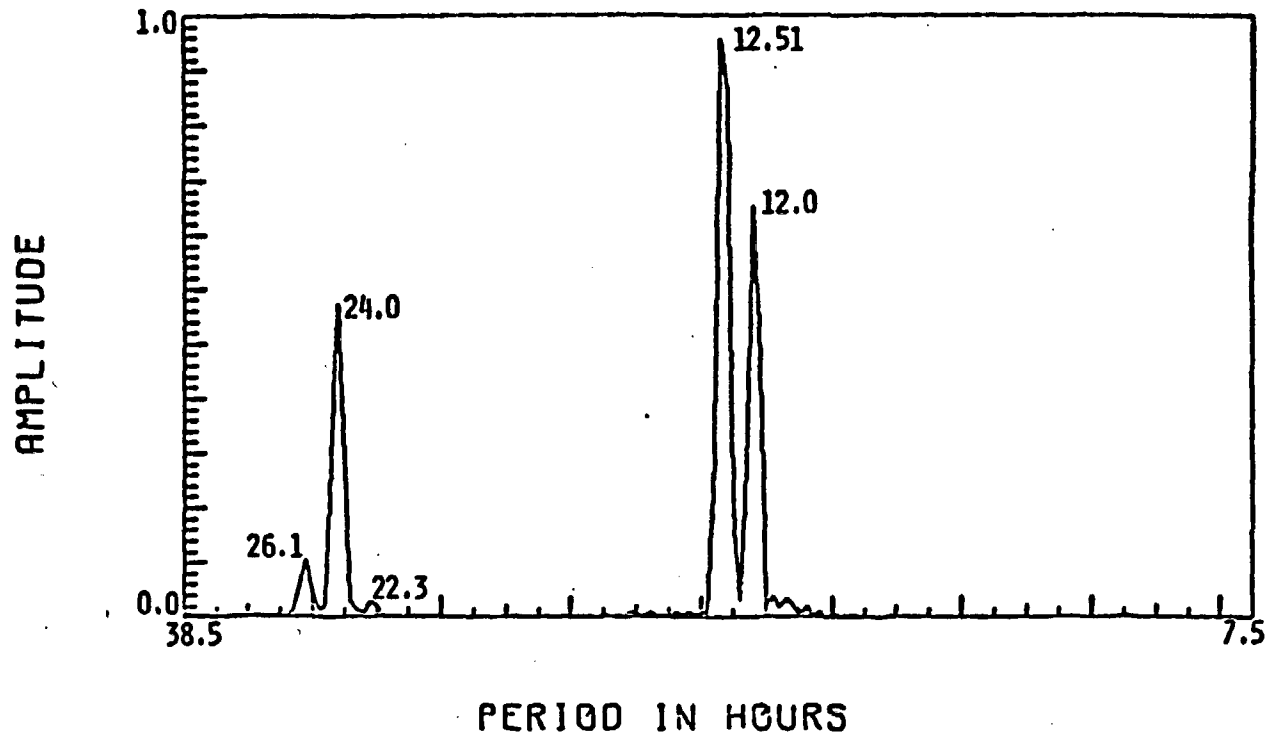


Figure 3.5-5. Power spectral density plot of the cross-correlation function for Scotty's Junction, Nevada, (SCT) north-south horizontal strain component cross-correlated with north-south horizontal theoretical earth tides, calculated using Scotty's Junction station coordinates. The data interval is from January 15, 1971 to February 12, 1971.

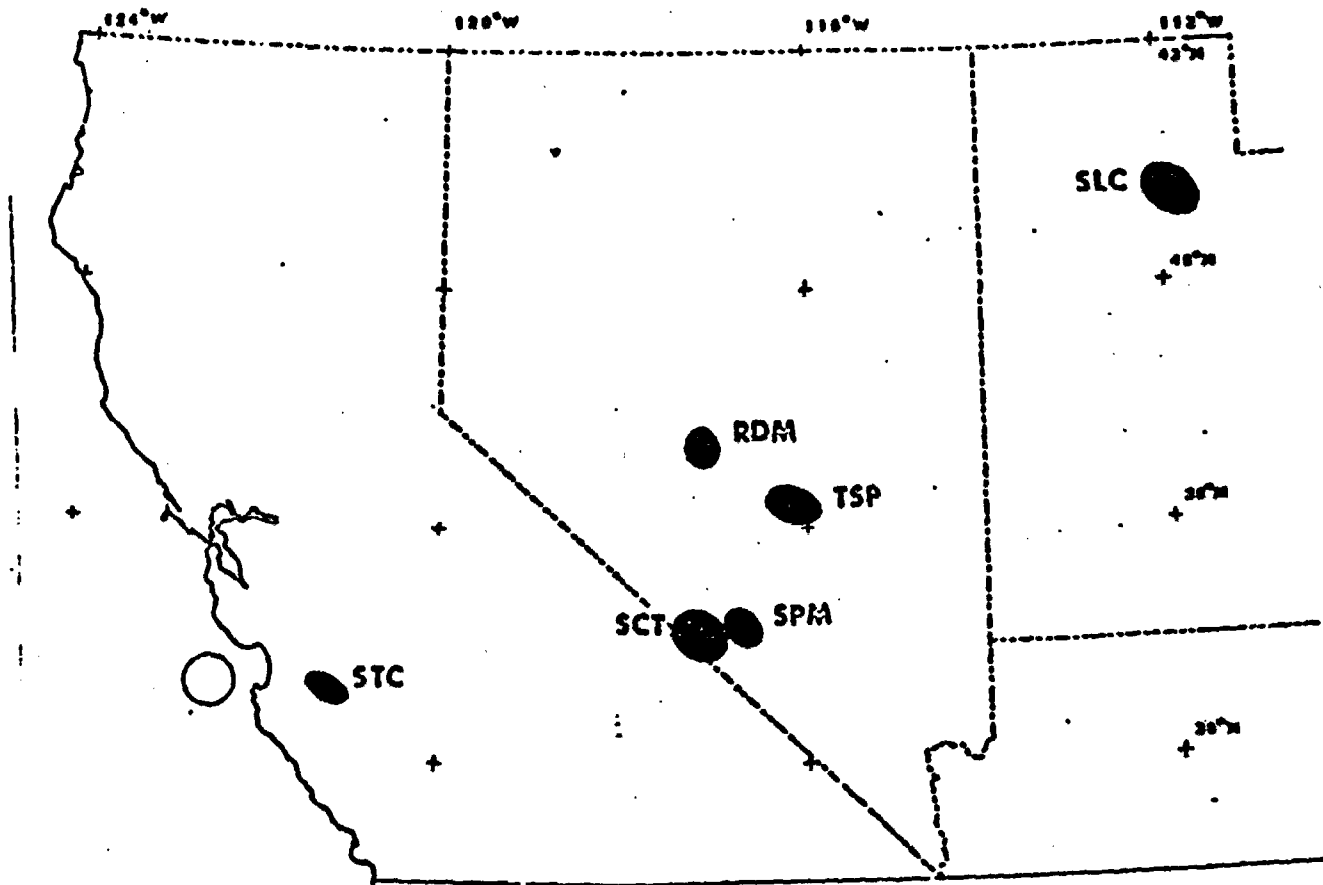


Figure 3.5-22. Secular strain change ellipses from short-base strainmeter data. The observational period was from June, 1970 to June, 1971, except at Salt Lake City, Utah, (SLC), where the period was from January, 1970 to January, 1971. Other strainmeter abbreviations: Scotty's Junction, Nevada, SCT, Sleeping Mountain, Nevada, SPM, Twin Springs, Nevada, TSP, Round Mountain, Nevada, RDM, and Stone Canyon, California, STC. The open circle is an undeformed reference. From Willis and others, 1973, Figure 51.

maximum compression (or minimum extension) trend north and east. Shorter term data from Smith and Kind (1972), and Kumamoto (1973) indicate a consistent tectonic strain trend agreeing with the above. Malone (1972) described strain observations at the Round Mountain and Mina sites north of the Nevada Test Site. He summarized data from a number of sources in a map reproduced here as Figure 3.5-23. The picture is dominantly one of northwest-southeast extension which is consistent with the previously determined extensional directions. Priestly (1974) computed strain change ellipses for two periods of time for the Mina, Nevada strainmeter station (described in Table 3.5-2). During the period February through September 1972, the Mina strainmeter data showed a strain field with a principal axis of extension oriented $N30^{\circ}E$ and a principal axis of compression oriented $N60^{\circ}W$ (Figure 3.5-24). This is opposite to the stress field indicated by earthquake focal mechanism (Priestly, 1974). During September and October 1972, this strain field broke down, and by November a new strain field was established. The new strain field had nearly identical orientations for the principal axes as before, but with the extensional and compressional directions switched (Figure 3.5-25). The field has remained essentially constant to the present time. Priestly (1974) believes this cycle would be seen repeated on a longer data sample.

Figure 3.5-26 shows the strain change ellipse for the Round Mountain, Nevada strainmeter data (Priestly, 1974). The focal mechanisms are not well determined due to the low seismicity in the area. The strain field observed has principal axes oriented $N15^{\circ}E$ and $N75^{\circ}W$. The $N15^{\circ}E$ axis is the principal axis of extension. Priestly has described the Round Mountain strain field as stable and concluded that Round Mountain and Mina, Nevada,

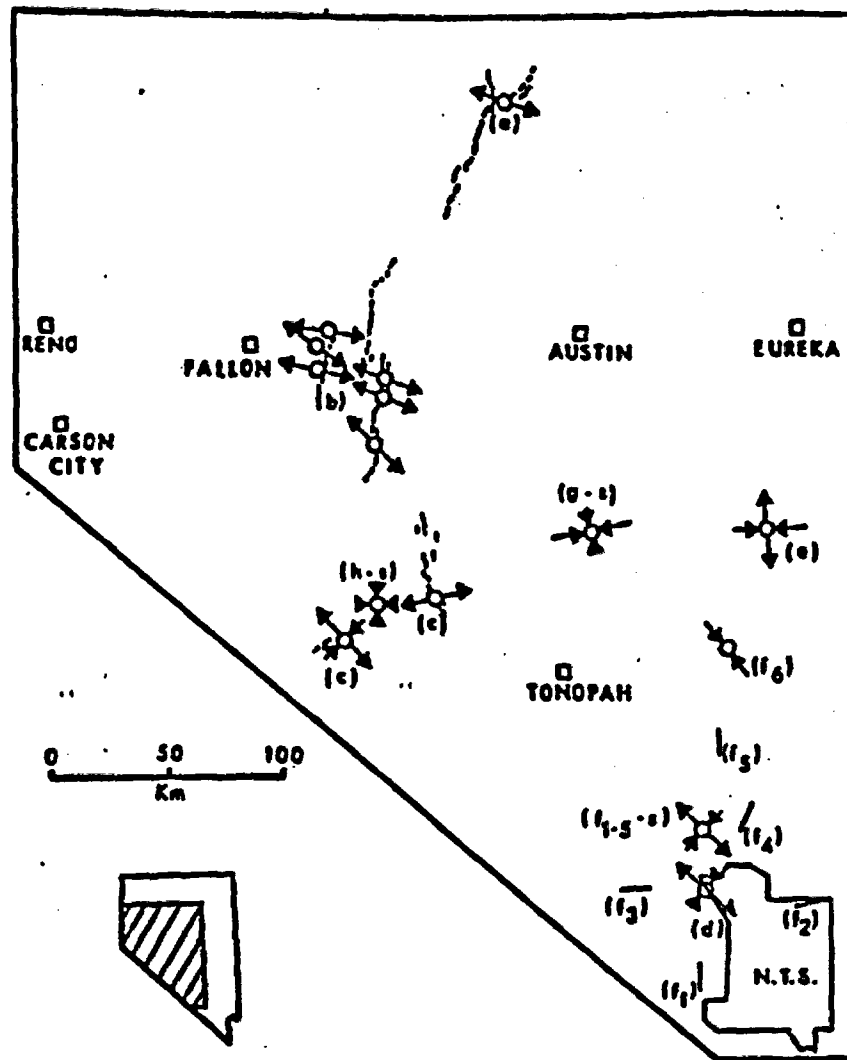


Figure 3.5-23. Stress patterns in Nevada. (a) Pleasant Valley earthquake, (b) Dixie Valley-Fairview Peak and Rainbow Mountain earthquakes and aftershocks, (c) Excelsior Mt. and Cedar Mt. aftershocks, (d) NTS microearthquakes, (e) Central Nevada Test Site microearthquakes, (f1-5) composite strain solution, (f6) one component strain-meter, (g) three component strain solution RDM, (h) three component strain solution MNN. From Malone, 1972, page 44.

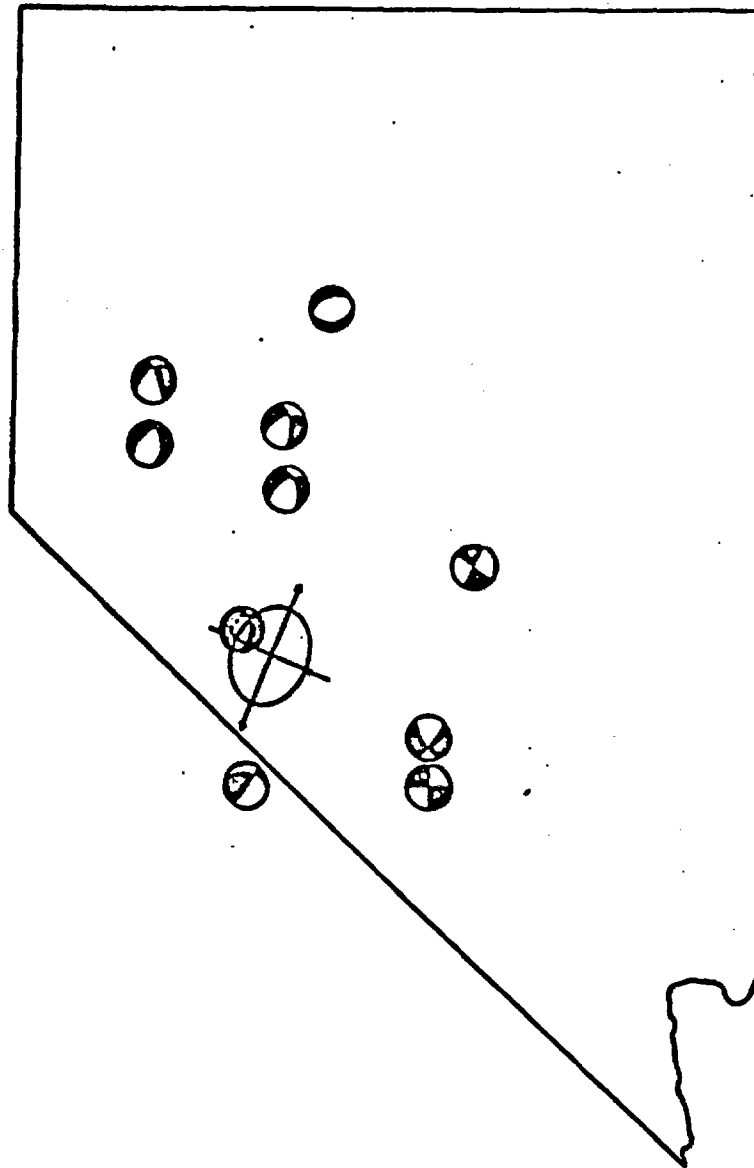


Figure 3.5-24. Comparison of the observed strain field at Mina indicated by strain change ellipses, and composite focal mechanism solutions for local microearthquakes. The darkened sector of the focal mechanism plot indicates the compression sector. The time period is from February through September, 1972. From Priestly, 1974, page 100.

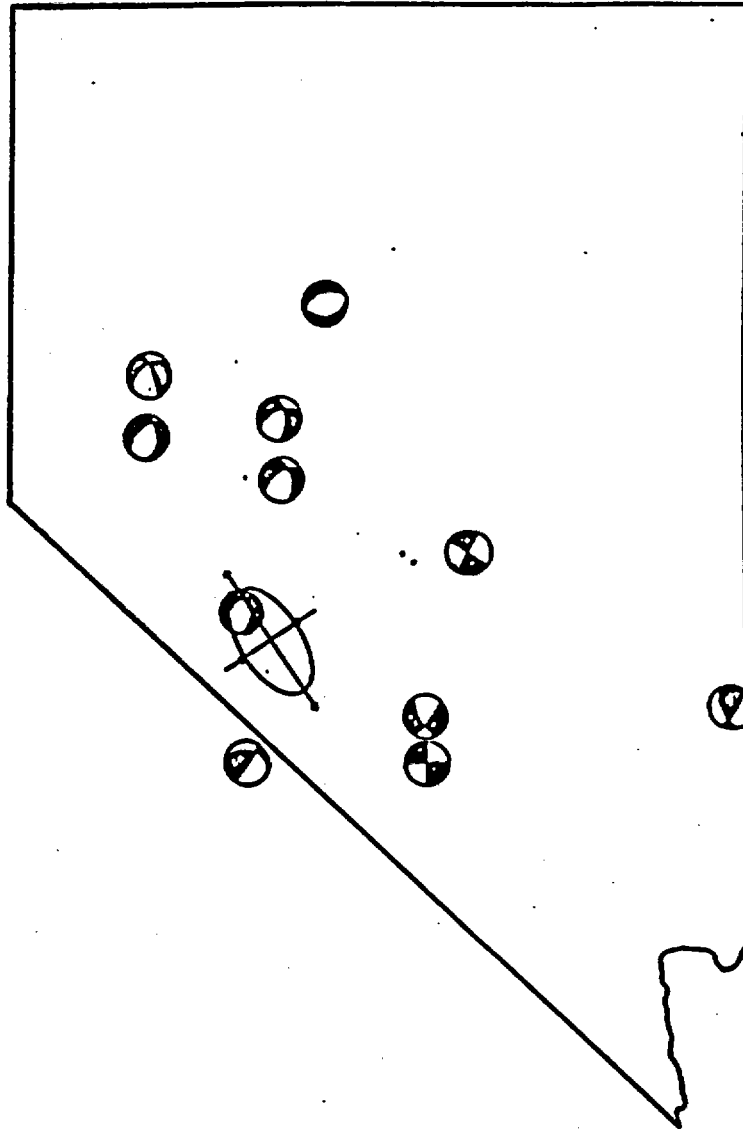


Figure 3.5-25. Comparison of the observed strain field at Mina indicated by strain change ellipses, and composite focal mechanism solutions for local microearthquakes. The darkened sector of the focal mechanism plot indicates the compression sector. The time period is from November, 1972 through October, 1973. From Priestly, 1974, page 101.

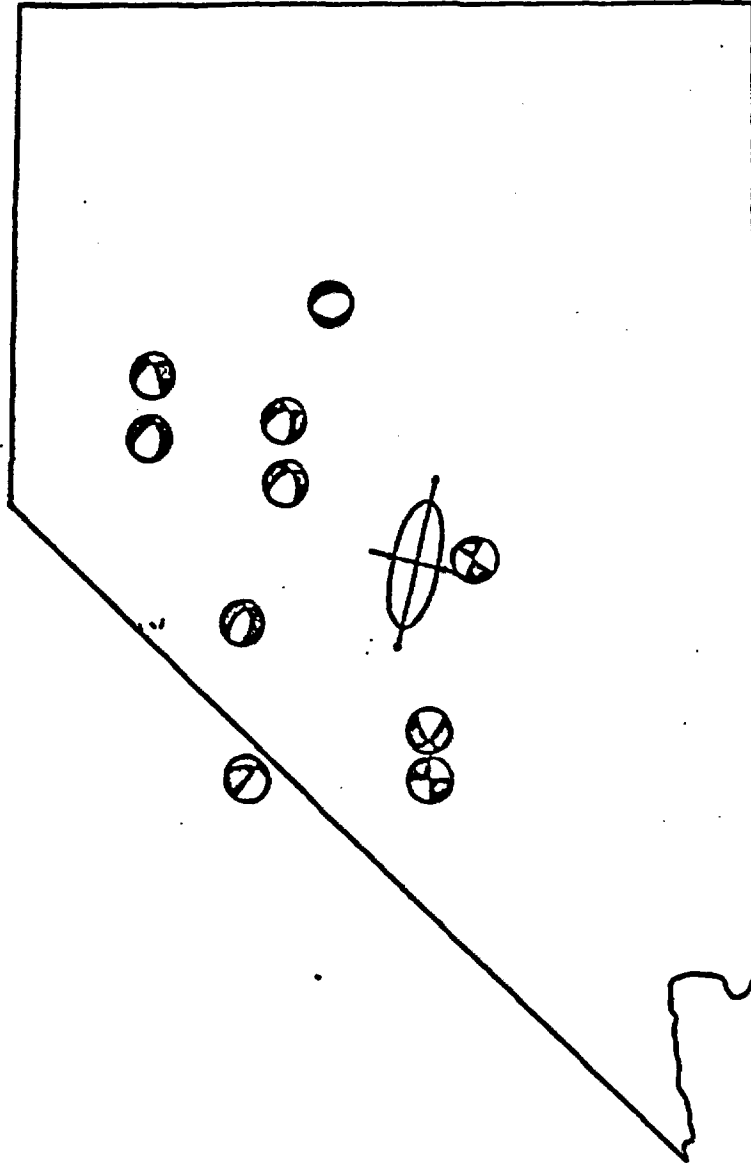


Figure 3.5-26. Comparison of the observed strain field at Round Mountain indicated by strain change ellipses, and composite focal mechanism solutions for local microearthquakes. From Priestly, 1974, Fig. 4-14.

data supports a general northwest-southeast extensional direction. Thompson and Burke (1973) have termed the Basin and Range Province an anomalous spreading zone with a spreading direction of about N55°W-S55°E. This is consistent with Atwater's (1970) description of relative motion between the Pacific and North American plates. Other studies in Pahute Mesa similarly reveal a northwest-southeast extension (Hamilton and Healy, 1969).

The secular strain data from Scotty's Junction, Sleeping Mountain, and Twin Springs is therefore in good agreement with present theories of plate tectonics and indicates a relatively coherent driving force for this region.

Geodetic Strain

Geodetic strain studies in south-central Nevada have been concentrated in the Nevada Test Site area (NTS). Investigators have measured geodetic strain before and after nuclear events to determine changes in the strain field induced by the shots (Dickey, 1969; Dickey, 1971; Savage and others, 1974).

Using a geodolite, Dickey (1969) measured six survey grids, Figure 3.5-27, before and after the BENHAM event. Maximum extension of 52.1×10^{-5} was measured one kilometer from ground zero and 3.3×10^{-5} was measured at 11 kilometers, indicating that the amount of strain diminished with distance from the shot, as would be anticipated for a spherical source. However, strain directions determined were not consistent and Dickey related this inconsistency to faulting in the area.

Dickey (1971) also made geodetic measurements of 10 strain grids before and after the JORUM event. The strains resulting from the test form a fairly consistent pattern which Dickey believes is related to

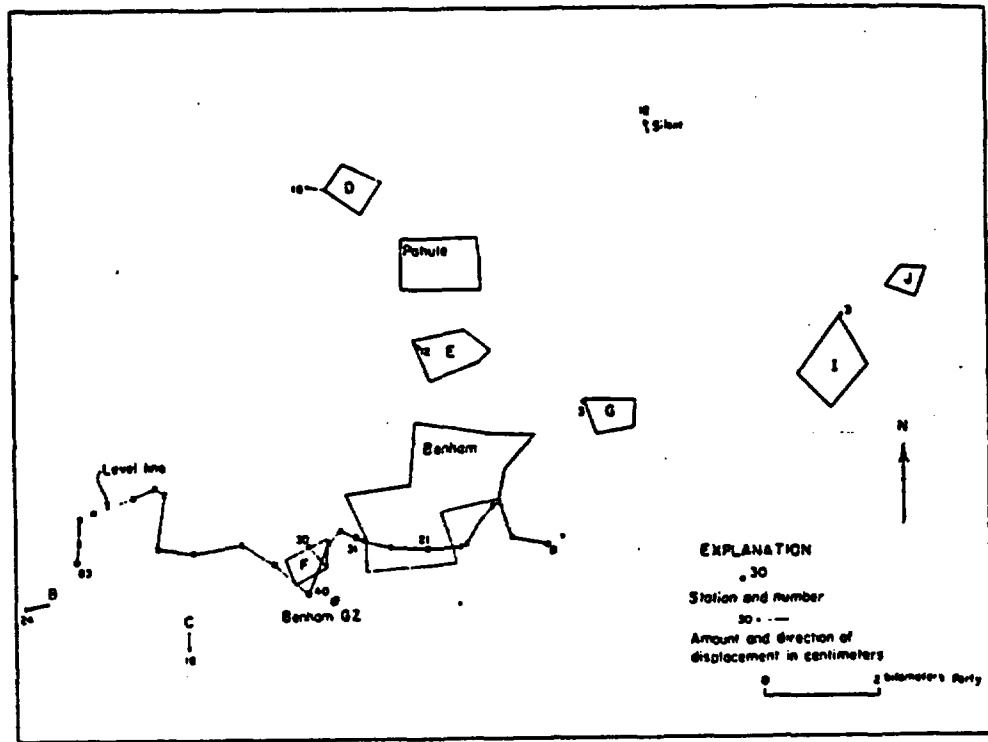


Figure 3.5-27. Index map showing location of strain nets and level line for BENHAM explosion. From Dickey, 1969, p. 2222.

caldera structures in the NTS area. Figure 3.5-28 displays the measured strains and the caldera boundaries. The Area 20 collapse zone of the Silent Canyon caldera had three grids with compressive strains oriented northwest and two other grids with extension in the northeast direction. Grid L, to the south in the Timber Mountain collapse area, had strain in the same direction as the Silent Canyon caldera. Grid G has northwest compressional strain associated with it. Dickey feels the other strains measured are too small to be meaningful, considering the probable error in strain measurement is 1×10^{-5} .

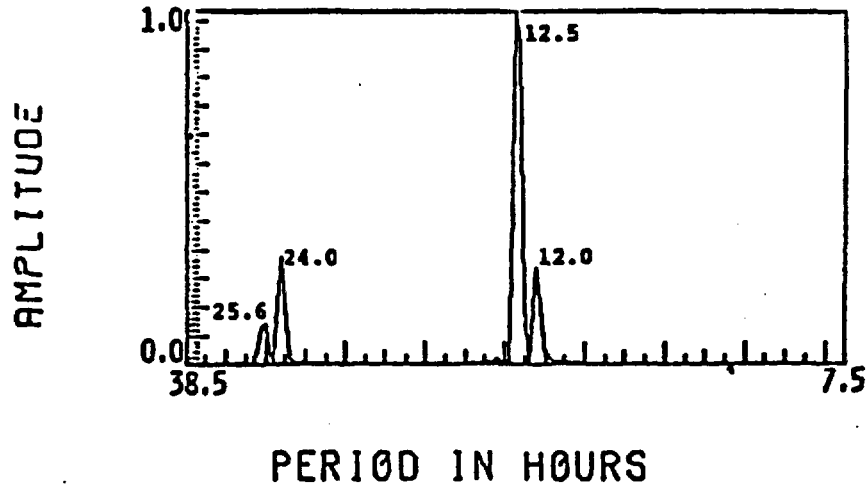
Dickey concluded that the close-in strain pattern which resulted from the JORUM explosion was controlled by the geologic features of the area. He further concluded that the caldera collapse zones have boundaries that are effective in separating stress-strain regimes into semi-independent entities. Dickey believes these boundaries are highly fractured rock zones which limit the transfer of stress from one block (caldera) to another.

Savage and others (1974) made repeated surveys of a trilateration network centered on ground zero, for the HANDLEY event. The network was surveyed two weeks before the test, two weeks after the test, and at approximately 6-month intervals through May 1973. The lines were measured with a geodolite having a precision of $\pm 2 \times 10^{-6}$. In Figure 3.5-29 are the station displacements as calculated by Savage and others for the time period March 1970 to April 1970. The large changes in length for this time period represent the deformation produced by the shot and the immediate post-shot relaxation. Note that for this time period encompassing the shot that the radial displacements increase with station distance from ground zero (with the exception of Micro). This is opposite to that anticipated for a spherical source mechanism.

plot, the relative amplitudes are now much closer to those predicted by the theoretical earth tides. The peaks at 24.0 and 12.0 hours are still somewhat anomalously high and may be an indication of some thermal contamination or site (local) inhomogeneities. As will be seen later, autocorrelation of temperature shows two peaks, the largest at 24.0 hours and another one-tenth the amplitude at 12.0 hours.

Figure 3.5-6 is the power spectral density plots for the autocorrelated horizontal northwest-southeast theoretical earth tides and the autocorrelated detrended strain for the Scotty's Junction northwest-southeast horizontal component for the time period January 15, 1971 to February 12, 1971. It is obvious that the autocorrelation of SCT NW contains high noise levels especially in the 38 to 15 hour range. This is probably attributable to problems associated with detrending of the strain data. The raw strain data for the NW component were plagued with many sharp changes in trend, most on the order of one to four days in length, making the detrending of the data exceedingly difficult. It is felt, however, that the peaks at 25.6 and 24.0 hours are real. If contamination of these peaks exists due to the detrending, it is of an indeterminable extent. Ignoring that which is believed to be noise, the two plots compare favorably in terms of period. While the relative amplitudes for the autocorrelated strain at the 25.6 and 24.0 hour peaks maintain the same general relationship as in the autocorrelated theoretical earth tides plot, the peak at 25.6 hours has increased, possibly due to long period contamination. The amplitude relationship between the 12.5 and 12.0 hour peaks for the detrended strain as compared to the autocorrelated earth tides is reversed. The increased amplitude at 12.0

THEORETICAL EARTH TIDES POWER SPECTRA



SCT NW AUTOCORRELATION POWER SPECTRA

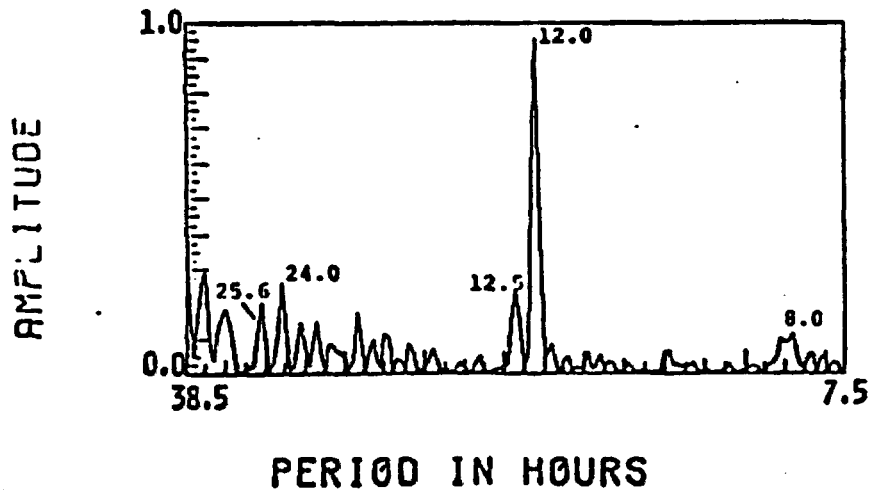


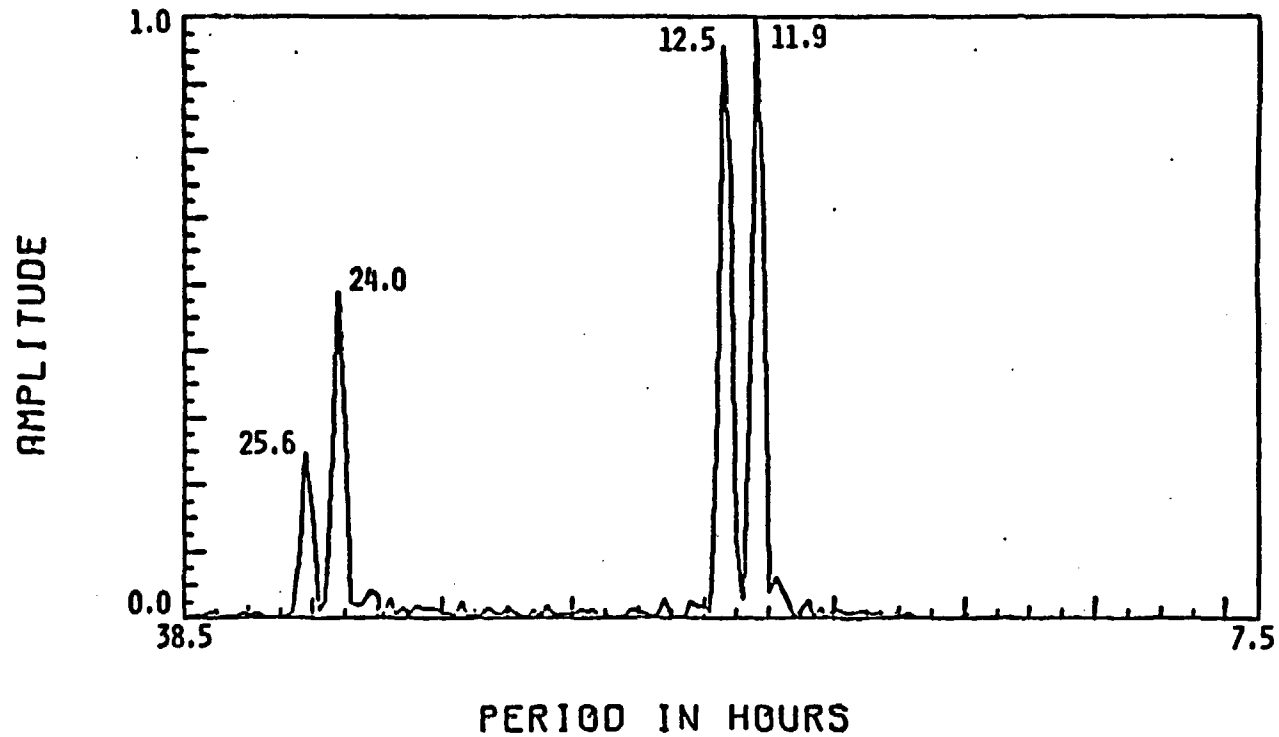
Figure 3.5-6. Power spectral density plots of the autocorrelation function for autocorrelated northwest-southeast horizontal theoretical earth tides (top), calculated using Scotty's Junction, Nevada, station coordinates and autocorrelated Scotty's Junction (SCT) northwest-southeast horizontal strain component (bottom). The data interval is from January 15, 1971 to February 12, 1971.

hours and the decrease at 12.5 hours might be explicable in terms of both in site inhomogeneities and thermal contamination. The peak at 8.0 hours may represent the terdiurnal component of the lunar principal wave M_3 , greatly amplified, or possibly noise related to the detrending. All the frequencies present in the strain data are contained in the earth tides but the strain data does not maintain the same relative amplitudes as might be expected if the earth tides were the only influencing factor.

The cross-correlation function will not be given for the cross-correlation of theoretical earth tides and Scotty's Junction northwest and vertical, Sleeping Mountain northwest and Twin Springs north-south strain components. Pertinent information related to the cross-correlation is listed in Table 3.5-4. A peak positive correlation of 0.35 occurs at 0 hours lag for Scotty's NW strain cross-correlated with theoretical earth tides, indicating that the earth tides and the strain data are in phase. The true phase lag differences between SCT NS and SCT NW cross-correlated with the earth tides may be zero or as much as 6 hours (refer back to the $\pm 1\frac{1}{2}$ hour uncertainty). For this data window length the probability that the correlation is due to random chance is less than 0.001. Hence, it appears that the SCT NW component is responding directly to the earth tides.

The power spectral density plot of the cross-correlation function (Figure 3.5-7) bears a closer relationship to the autocorrelated earth tides than to the autocorrelated strain. Peaks at 25.6, 24.0 and 12.5 have increased in relative amplitude, with those previously termed noise, greatly diminished, indicating they were noncorrelative with the earth tides. The peak at 11.9 hours corresponds to the predominant 12 hour peak in the autocorrelated strain power spectra. The same arguments explaining the observed differences between theoretical earth tides and SCT NS are applicable here.

SCT NW CROSS-CORRELATED WITH EARTH TIDES
POWER SPECTRA



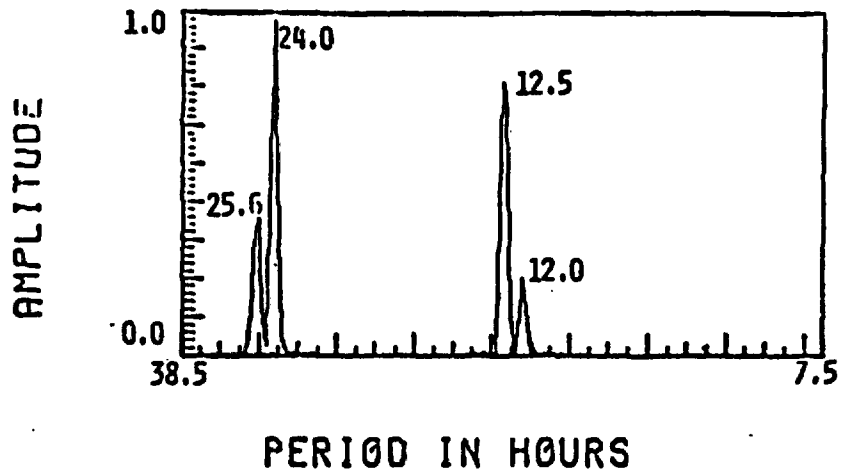
131

Figure 3.5-7. Power spectral density plot of the cross-correlation function for Scotty's Junction, Nevada, (SCT) northwest-southeast horizontal strain component cross-correlated with northwest-southeast horizontal theoretical earth tides, calculated using Scotty's Junction coordinates. The data interval is from January 15, 1971 to February 12, 1971.

The power spectral density plots for autocorrelated vertical theoretical earth tides and autocorrelated detrended strain for the Scotty's Junction (SCT) vertical component are given in Figure 3.5-8. The time period covered is from January 15, 1971 to February 12, 1971. Periods of 25.6 hours and 12.5 hours, corresponding to the O_1 and N_2, M_2 tidal peaks, are not visible in the SCT vertical strain autocorrelation. The relative amplitude ratio for the two peaks present, 24.0 and 12.0 hours, is approximately the same as in the autocorrelated earth tides. Great amplification at 24.0 and 12.0 hour periods might make the 25.6 and 12.5 hour peaks indistinguishable on the plot, but it is not certain what the cause of an amplification of this sort might be.

Table 3.5-4 lists the values of the correlation coefficient and the associated lag for this earth tide-strain cross-correlation. The maximum positive correlation of 0.39 occurs at a lag of -9 hours, which for this case is meaningless. The vertical strain measured by a vertical strainmeter results from cross-coupling with the horizontal areas strain (King and Bilham, 1973). This means that the vertical strain will be in phase with the total horizontal earth tidal strain or lag behind it by a small amount due to elastic losses in the rock. Therefore, the vertical strain will not be in phase with the vertical theoretical earth tides. Since the correlation coefficient for the earth tides total vertical component and the vertical strain result from the correlation of functions which are simply scaled through Poisson's ratio, the resulting correlation coefficients are still significant. The correlation coefficient 0.39 indicates that for the data window length, the probability that the correlation is due to chance is less than 0.001.

THEORETICAL EARTH TIDES POWER SPECTRA



SCT VERTICAL AUTOCORRELATION POWER SPECTRA

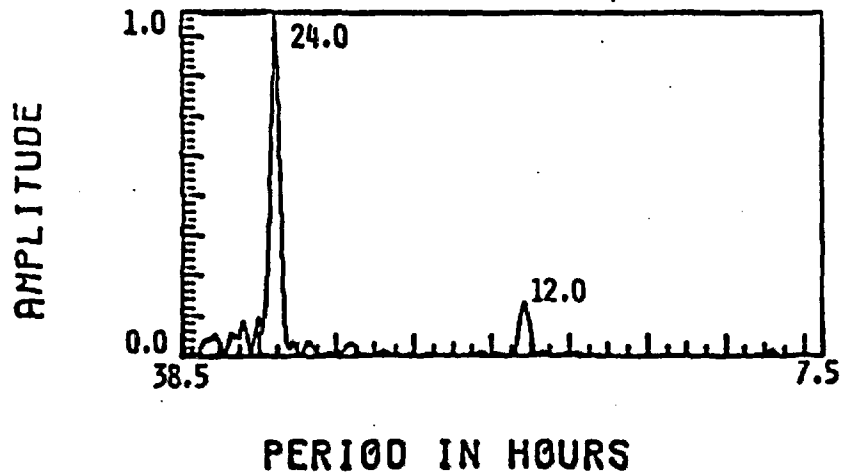


Figure 3.5-8. Power spectral density plots of the autocorrelation function for autocorrelated vertical theoretical earth tides (top), calculated using Scotty's Junction, Nevada, station coordinates and autocorrelated Scotty's Junction (SCT) vertical strain component (bottom). The data interval is from January 24, 1971 to February 12, 1971.

The power spectral density plot of Scotty's Junction vertical strain cross-correlated with theoretical earth tides is shown in Figure 3.5-9. This figure resembles closely that of SCT vertical strain autocorrelated in terms of relative amplitudes for the 24.0 and 12.0 hour peaks. The peaks at 25.6 hours and 12.5 hours indicate the existence of correlative data at these periods in the autocorrelated strain even though that plot did not show any visible peaks. Due to problems in data recording for the SCT site, the remaining two horizontal components (NE and EW) will not be treated.

Instrumental problems limited treatment of short period strain for the Sleeping Mountain and Twin Springs strainmeter stations to single 10 day intervals. This interval is December 3, 1970 to December 12, 1970 for Sleeping Mountain northwest and February 3, 1971 to February 12, 1971 for Twin Springs north-south.

Sleeping Mountain Strain

Figure 3.5-10 is the power spectral density plots of the autocorrelated horizontal northwest-southeast theoretical earth tides and the autocorrelated detrended strain for Sleeping Mountain northwest-southeast horizontal component for the time interval listed above. Immediately noticeable in both plots is the presence of only two peaks. This is due to the increment of digitization, the short data interval and plot resolution. The peaks in both the autocorrelated earth tides and the autocorrelated strain are broad in the sense of time. In the autocorrelated earth tide power spectral density plot, the peak with the period of 24.8 hours has half amplitude points of 27.5 and 23.3 hours and the peak at

SCT VERTICAL CROSS-CORRELATED WITH EARTH TIDES
POWER SPECTRA

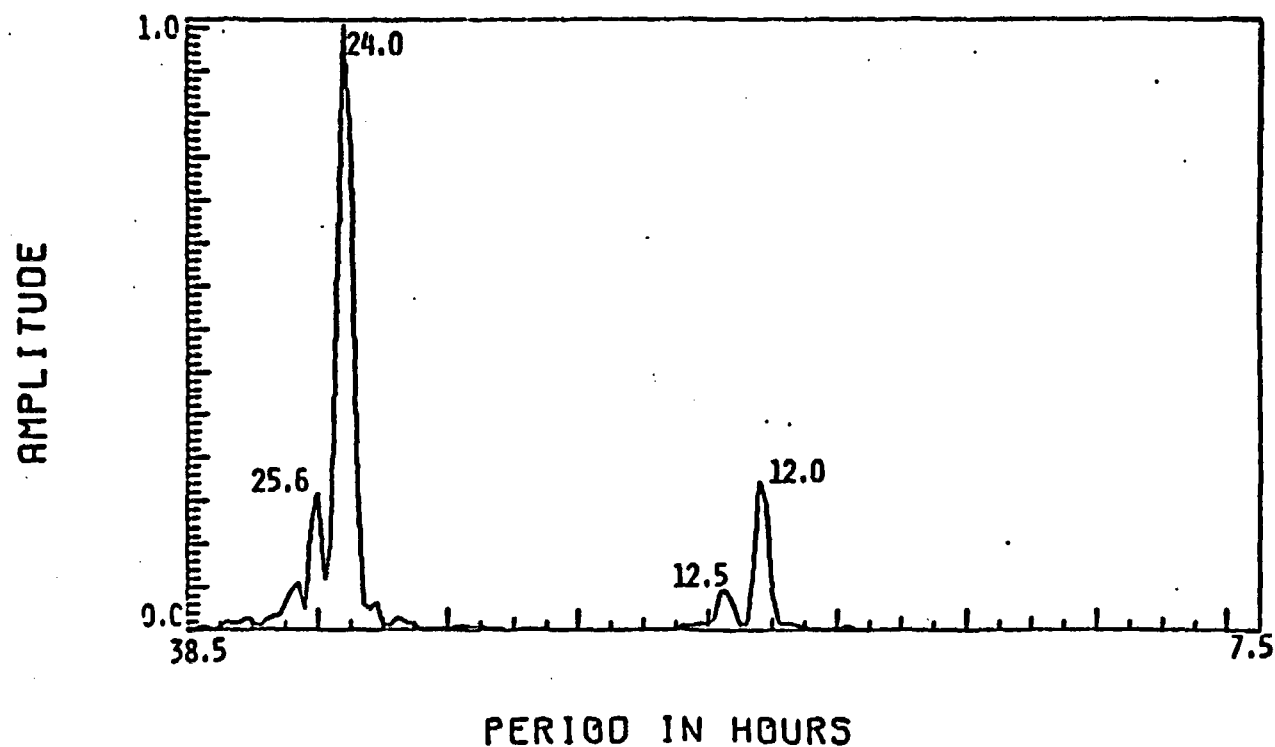
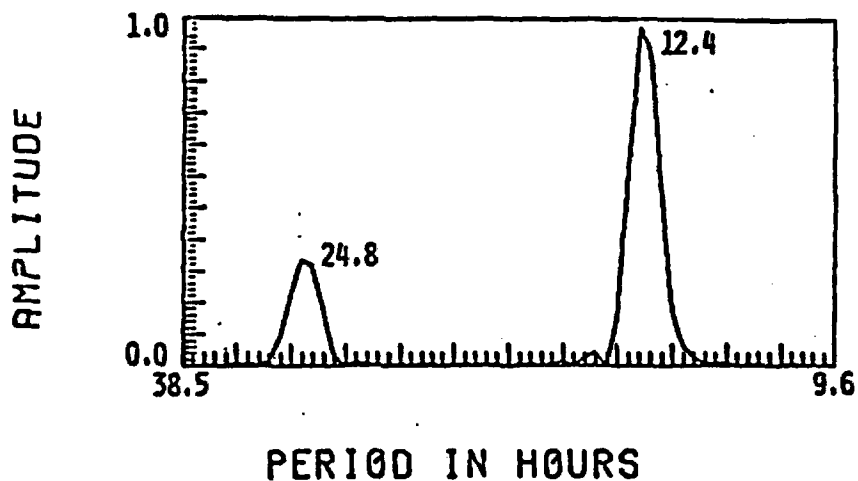


Figure 3.5-9. Power spectral density plot for Scotty's Junction, Nevada, (SCT) vertical strain component, cross-correlated with the vertical theoretical earth tides, calculated using Scotty's Junction station coordinates. The data interval is from January 24, 1971 to February 12, 1971.

THEORETICAL EARTH TIDES POWER SPECTRA



SPM NW AUTOCORRELATION POWER SPECTRA

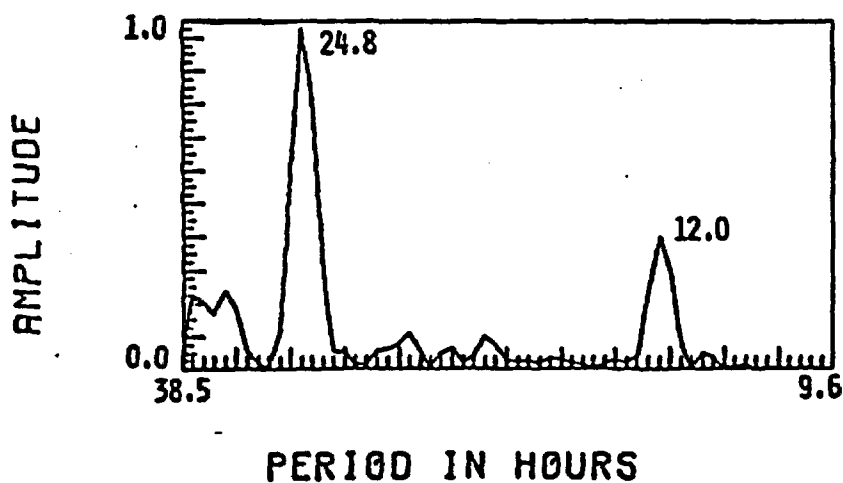


Figure 3.5-10. Power spectral density plots of the autocorrelated function for autocorrelated northwest horizontal theoretical earth tides calculated using Sleeping Mountain, Nevada, coordinates (top) and autocorrelated Sleeping Mountain (SPM) northwest horizontal strain (bottom). The data interval is from December 3, 1970 to December 12, 1971.

12.4 hours has the half amplitude points 12.6 and 12.0 hours. Similarly, the peaks in the autocorrelated strain have half amplitude points of 25.6 and 24.0 hours for the 24.2 hour peak and 12.5 and 11.7 hours for the 12.0 peak. The O_1 , P_1 , K_1 and S_1 tidal peaks occur within the 24 hour period range. Apart from the relative amplitudes of the two peaks, the period ranges in the plots agree quite well. Table 3.5-4 lists the peak positive correlation coefficient 0.29 occurring at -9 hours lag. This lag is larger than any lag attributable to the increment of digitization or short data window. This lag is also larger than can be attributable to site inhomogeneities. It would appear that serious problems are present with the data.

Figure 3.5-11 is a plot of the power spectral density of SPM north-west-southeast theoretical earth tides. Again the peaks are broad and encompass those periods present in the earth tidal components. The two peaks are approximately equal in amplitude. If the measured strain were entirely due to earth tides this would not be anticipated. Temperature contamination might possibly be the cause of the increase of the 24 hour peak, but it will be shown later that the temperature actually leads the earth tides at these sites so even a bigger phase problem would result.

Twin Springs Strain

Twin Springs strain data, in general, were poor. The power spectral density plots of the autocorrelation function for the north-south horizontal theoretical earth tides and the Twin Springs autocorrelated north-south strain are shown in Figure 3.5-12. There are several peaks of inexplicable origin about the 24 hour peak. These do not appear to be related to the autocorrelated theoretical earth tides. The peaks may be related to

SPM NW CROSS-CORRELATED WITH EARTH TIDES
POWER SPECTRA

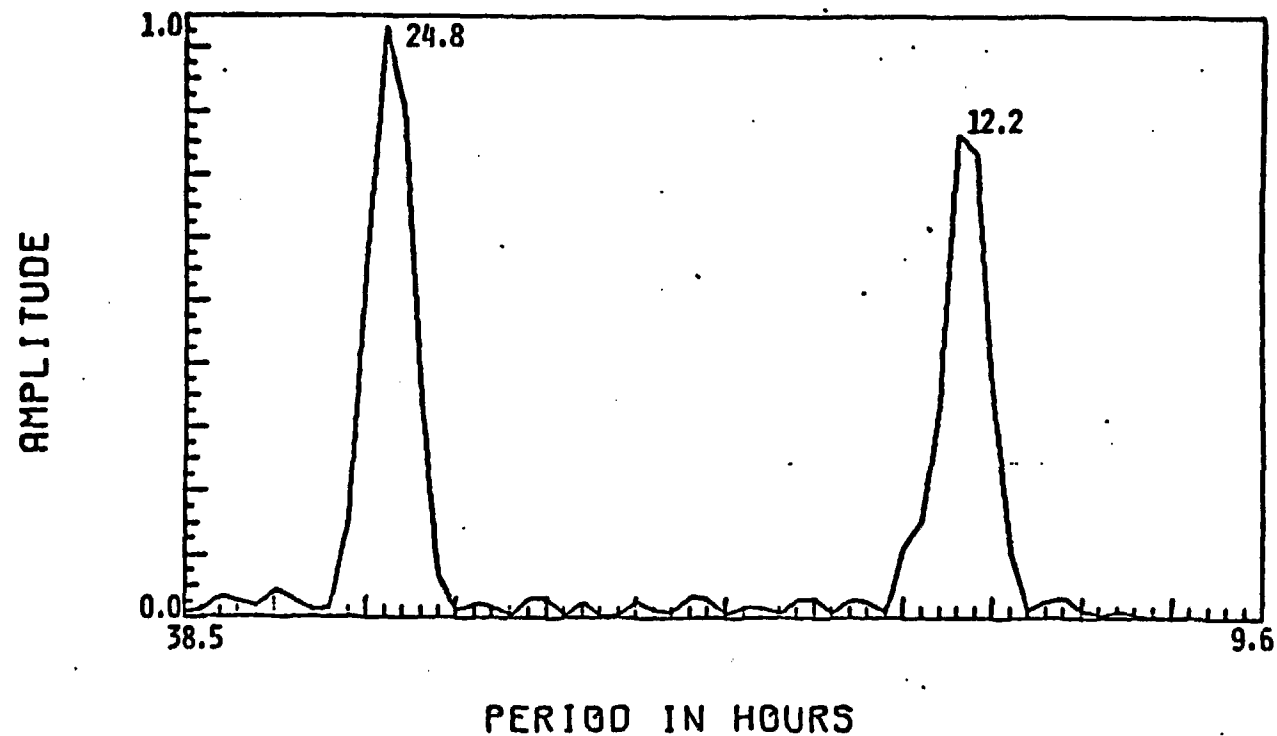
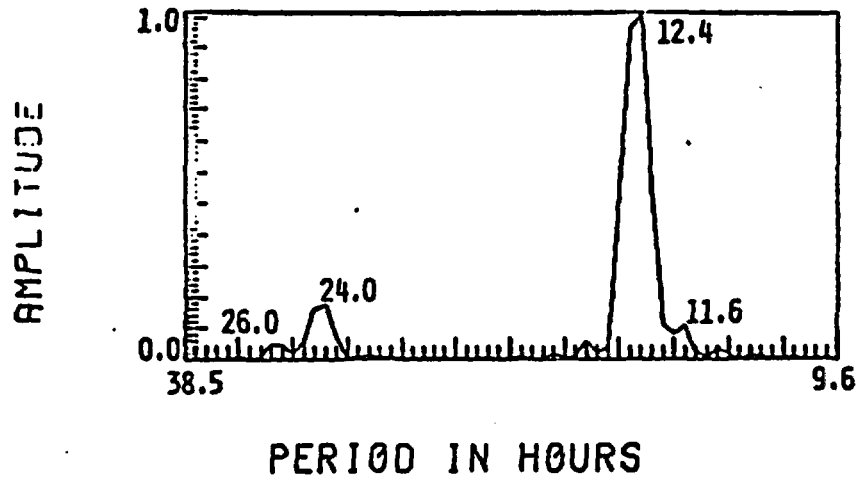


Figure 3.5-11. Power spectral density plot of the cross-correlation function for the northwest horizontal strain component at Sleeping Mountain, Nevada, (SPM), cross-correlated with the northwest horizontal theoretical earth tides, calculated using Sleeping Mountain station coordinates. The data interval is from December 3, 1970 to December 12, 1970.

THEORETICAL EARTH TIDES POWER SPECTRA



TSP NS AUTOCORRELATION POWER SPECTRA

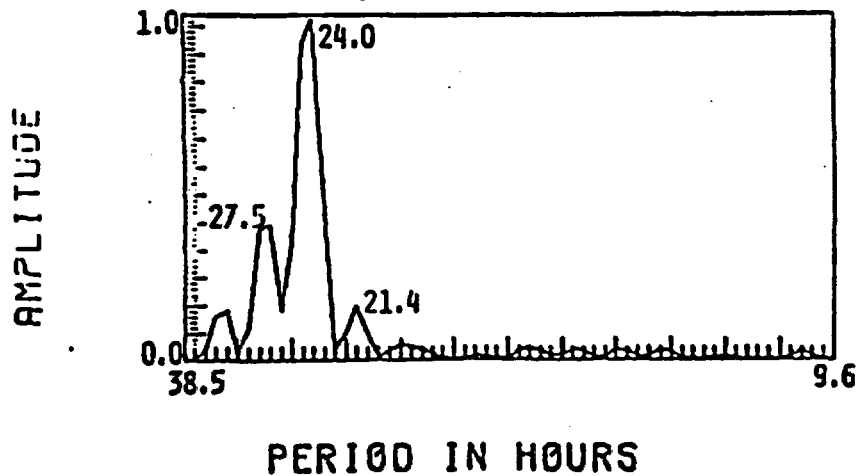


Figure 3.5-12. Power spectral density plots of the autocorrelation function for the autocorrelation of the north-south horizontal theoretical earth tides (top), calculated using the Twin Springs, Nevada, station coordinates and the autocorrelation of the Twin Springs (TSP) north-south horizontal strain component (bottom). The data interval is from February 3, 1971 to February 12, 1971.

detrending, but the data were detrended several different ways and the peaks remained. Any autocorrelation of the strain data failed to produce a visible peak in the 12 hour vicinity. Although the data appears that it will yield a poor correlation coefficient if cross-correlated with the earth tides, the peak at 24 hours is large enough, in combination with minor energy not visible in the autocorrelated strain at 12 hours, to produce a correlation coefficient of 0.29 (see Table 3.5-4). The peak positive correlation coefficient occurs at a lag of -108 hours. This is also indicative of poor quality data. The power spectral density plot for this cross-correlation is shown in Figure 3.5-13. The plot appears nearly the same as the autocorrelated strain data except for the peaks in the vicinity of 12 hours. The peaks indicate that there was correlative energy at these periods in the strain data not previously visible in the plot of the autocorrelated strain. It appears from the above analysis that there were serious problems present in the data.

Yucca Flats Temperature and Barometric Pressure

The power spectral density plots for autocorrelated temperature and barometric pressure for the time period January 15 to February 12, 1971, as recorded at the Yucca Flats weather station are shown in Figure 3.5-14. Although the weather station is as distant as 50 km from the strainmeter stations, it is felt that due to similar elevations and moderately close proximity, the actual temperature and pressure would correspond sufficiently to allow use in this study. The peak energy in the temperature power spectral density plot occurs at 24.0 hours (a solar day). A minor peak also exists at 12.0 hours. The barometric pressure power spectral density plot displays strong peaks at 24.0 and 12.0 hours with a minor

TSP NS CROSS-CORRELATED WITH EARTH TIDES
POWER SPECTRA

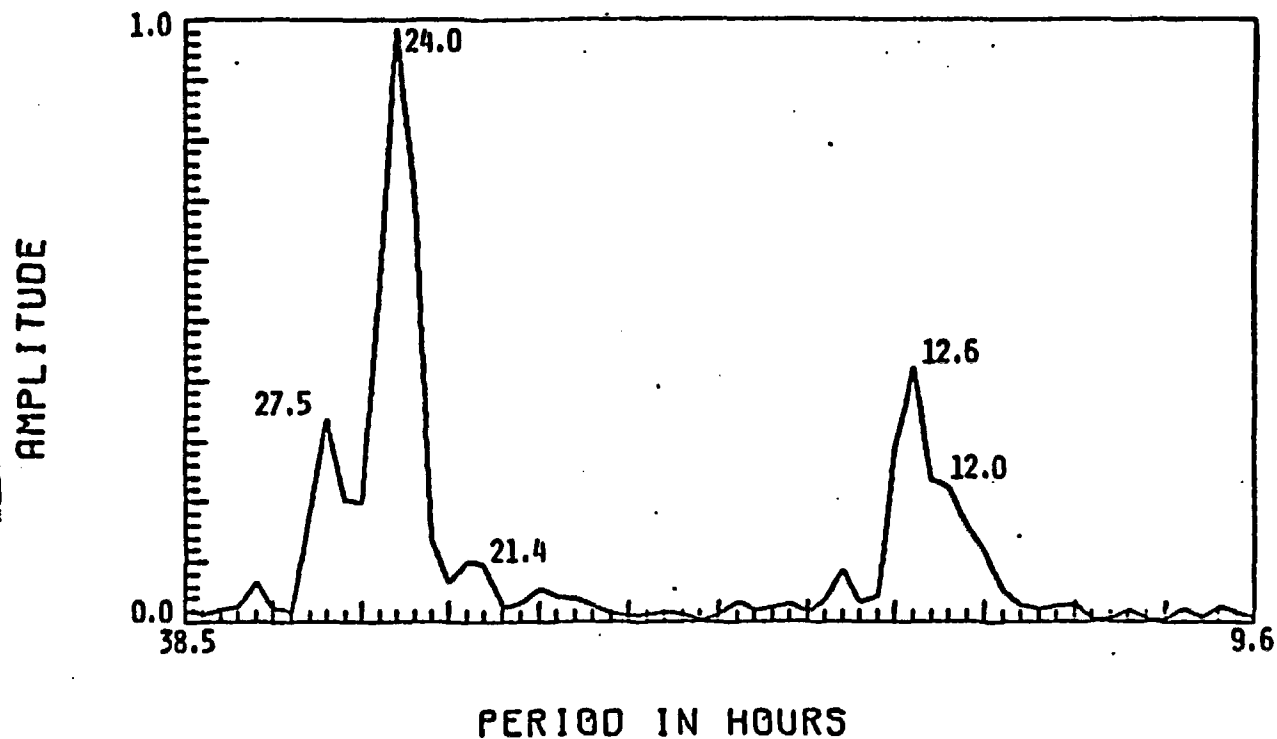
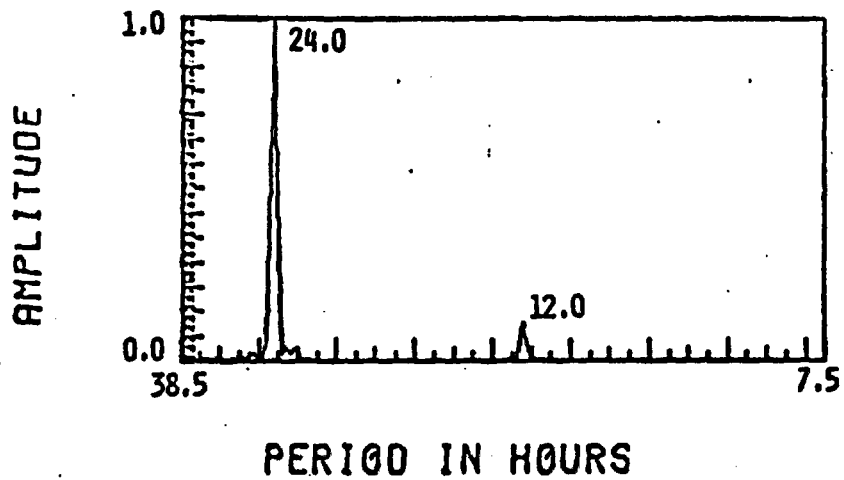


Figure 3.5-13. Power spectral density plot of the cross-correlation function for Twin Springs, Nevada, (TSP) north-south horizontal strain component, cross-correlated with the north-south horizontal theoretical earth tides, calculated using the Twin Springs station coordinates. The data interval is from February 3, 1971 to February 12, 1971.

OBSERVED TEMPERATURE POWER SPECTRA



OBSERVED BARO. PRESS. POWER SPECTRA

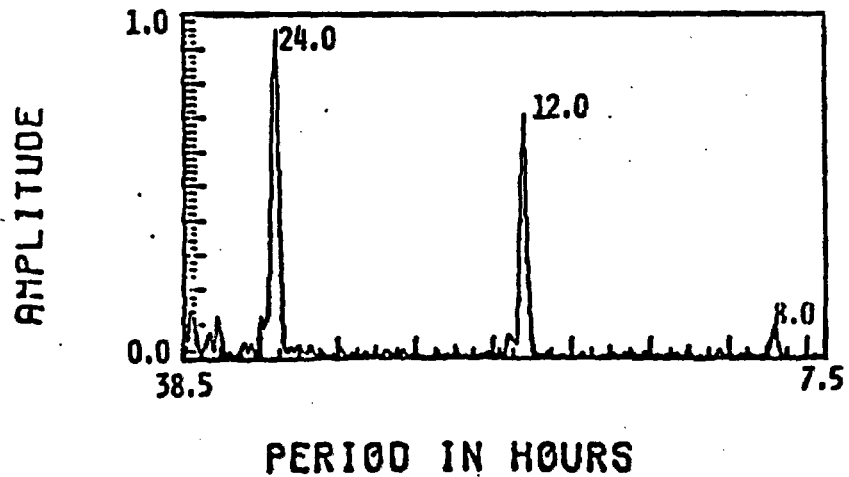


Figure 3.5-14. Power spectral density plots of the autocorrelation function for autocorrelated temperature (top) and barometric pressure (bottom) as recorded at the Yucca Flats, Nevada, weather station. The data interval is from January 15, 1971 to February 12, 1971.

one at 8.0 hours. These three peaks also coincide in period with the S_1 , S_2 and S_3 solar principal waves present in the earth tides. As stated previously, atmospheric tides have been estimated and observed to be up to 20 percent of the solid earth tides. This possibly explains the large peak in autocorrelated barometric pressure at 12.0 hours and the smaller one at 8.0 hours. The 24.0 hour peak is most probably generated by a combination of the solar day and atmospheric tides.

Since the temperature autocorrelation contains components equivalent to at least two peaks present in autocorrelated earth tides, a cross-correlation of the two was made. The results, shown in Figure 3.5-15 and listed in Table 3.5-4, show a positive correlation coefficient of 0.51 occurs at a lag of 6 hours, indicating that for the earth tidal component in question, the earth tides lag the temperature by 6 hours. This is of no real interest at this time. For this data window length, the probability that the correlation is due to chance is less than one in one thousand. The power spectral density plot for the above cross-correlation is shown in Figure 3.5-16. The point should be made that the fact that two variables are correlative does not necessarily indicate interdependence of one on the other. Associated phase lags, however, can be useful in determination of any dependency. Therefore, the high correlation coefficient between earth tides and temperature does not indicate that the earth tides are caused by the temperature cycle or vice versa. However, both are physically related through the planet's rotation (i.e., the solar day).

A one-inch change in mercury will cause an observable strain of 10^{-8} (Romig and Kumamoto, 1972). This degree of change is achieved only in seasonal variations, or on a short-term basis, when a weather system moves through an area and is nonperiodic in nature. Since actual strains

YUCCA FLATS TEMPERATURE CROSS-CORRELATED
WITH THEORETICAL EARTH TIDES

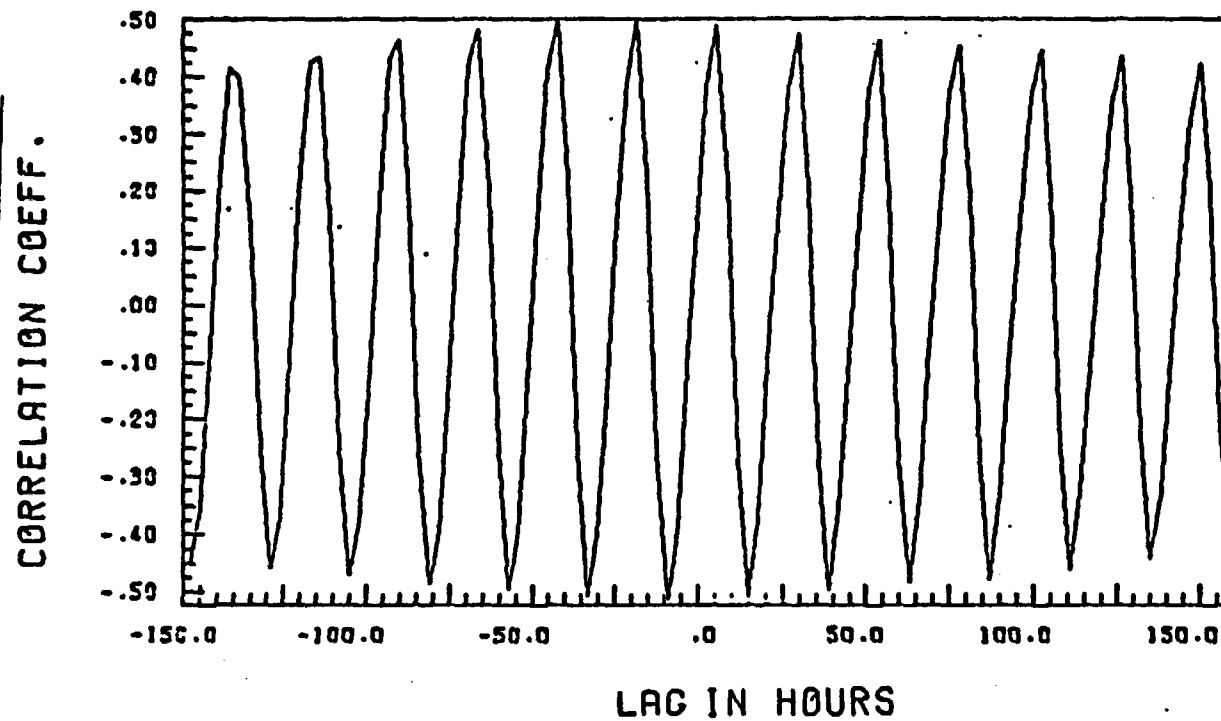


Figure 3.5-15. Plot of the cross-correlation function for Yucca Flats, Nevada, temperature, cross-correlated with the vertical theoretical earth tides, calculated using the Yucca Flats weather station coordinates. The data interval is from January 15, 1971 to February 12, 1971.

TEMPERATURE CROSS-CORRELATED WITH EARTH TIDES
POWER SPECTRA

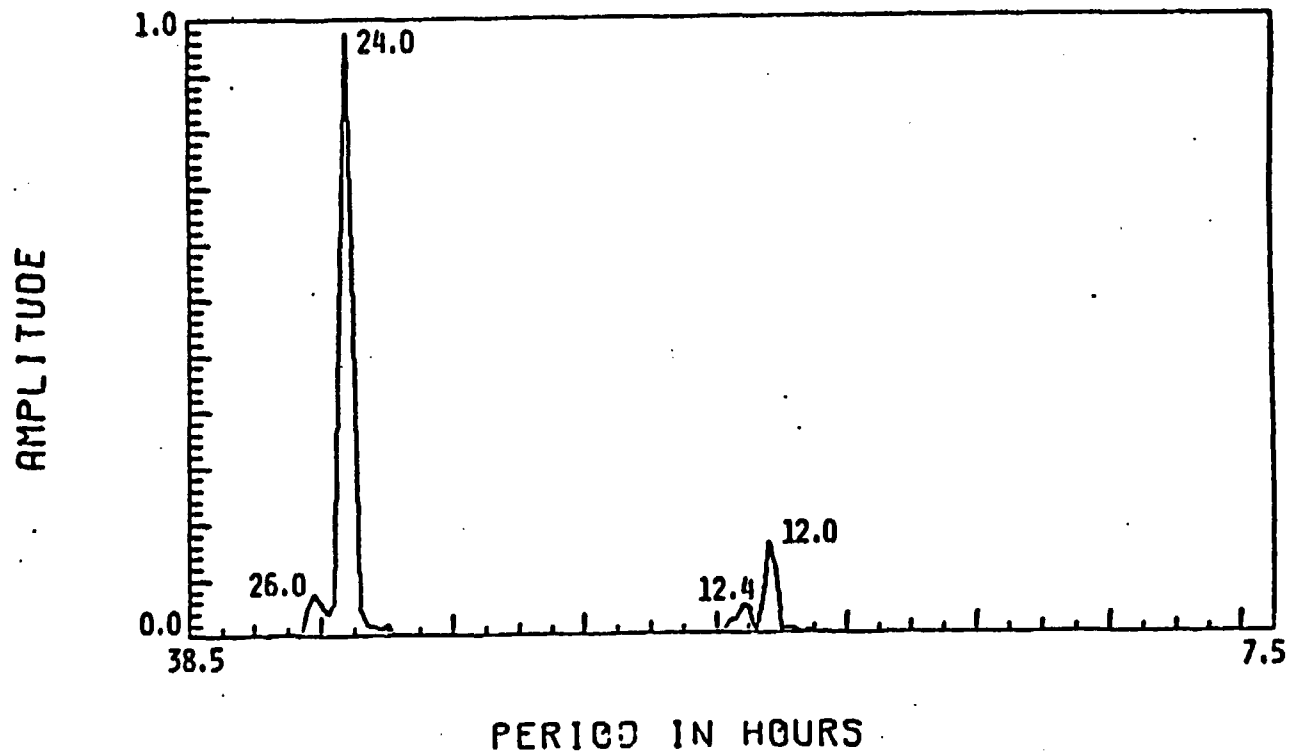


Figure 3.5-16. Power spectral density plot of the cross-correlation function of Yucca Flats, Nevada, temperature, cross-correlated with vertical theoretical earth tides calculated using Yucca Flats weather station coordinates. The data interval is from January 15, 1971 to February 12, 1971.

observed on a daily basis are periodic and on the order of 10^{-8} , it was felt that barometric pressure would contribute little to the measured strain. Therefore, no cross-correlation between barometric pressure and theoretical earth tides was performed, since the resulting high correlation would simply reflect the relationship of the pressure to earth tides as indicated in Figure 3.5-14.

Table 3.5-4 lists the values of the correlation coefficients and associated lags for the cross-correlation of Scotty's Junction NS horizontal strain with the Yucca Flats temperature and barometric pressure. The values of the correlation coefficients are high, 0.32 and 0.16, respectively, but neither are as high as the values of the cross-correlations of SCT NS and theoretical earth tides. Considering the physical nature of the temperature, barometric pressure, and the earth tides, indications from the correlation coefficients are that the earth tides exert the greatest influence on the recorded strain.

Examination of the phase lags is in order. Referring to Table 3.5-4, SCT NS cross-correlated with earth tides produces a phase lag of -3 hours. It was shown earlier that this lag could be as low as -1-1/2 hours, strain behind earth tides. The maximum positive correlation coefficient of Scotty's NS strain cross-correlated with temperature occurs at a lag of -6 hours. This means the measured strain lags behind the temperature by six hours. It would appear then from the phase lags that the strainmeter is responding more directly to earth tides than to temperature, although it is possible that both have phase lags of -4-1/2 hours.

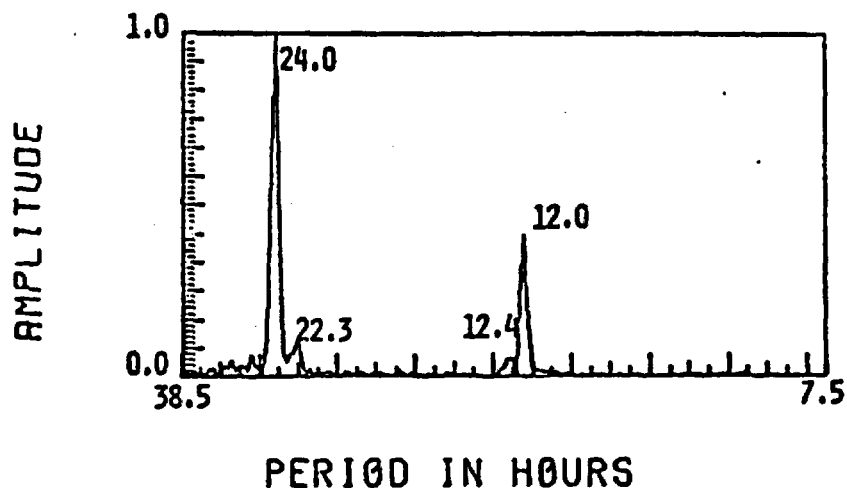
The temperature might affect the recorded strain in two possible ways. First, there could be thermal contamination of the instrument. A second

manner in which the strain record could be affected by temperature would be a direct thermoelastic effect on the earth's surface (Berger and Wyatt, 1973). Berger and Wyatt, at Pinion Flats, California, have shown a daily temperature fluctuation of 10°C will produce thermoelastic strain with a magnitude of 2.5×10^{-9} . Daily temperature fluctuations at Yucca Flats range as high as $25^{\circ}\text{-}30^{\circ}\text{C}$. Temperature might contribute to the recorded strain in this manner. Brown (1974, personal communication), monitoring vault temperatures in the Aleutian strainmeter network, has not observed any daily temperature cycles. The Aleutian instruments are of the same Colorado School of Mines design and are similar in construction and vault insulation. Daily temperature variations in the Aleutians are on the order of 10°C (Brown, 1974, personal communication). If one can assume instrumental response to temperature will be the same for similar instruments with similar site installation, it would appear that the majority of the thermal contribution to the strain on a daily basis would be through thermoelastic strains caused by the daily heating and cooling cycle and not through thermal contamination.

The maximum positive cross-correlation coefficient for the cross-correlation of SCT NS horizontal strain and barometric pressure occurs at a lag of -4.5 hours. The low coefficient value of 0.16 was anticipated and is not considered significant.

Figure 3.5-17 shows the power spectral density plots of SCT NS strain cross-correlated with temperature and barometric pressure. The figures are very similar to the temperature and barometric pressure autocorrelation power spectral density plots. However, the peaks in plots at 12.0

SCT NS CROSS-CORREL. TEMP.
POWER SPECTRA



SCT NS CROSS-CORREL. BARO. PRESS.
POWER SPECTRA

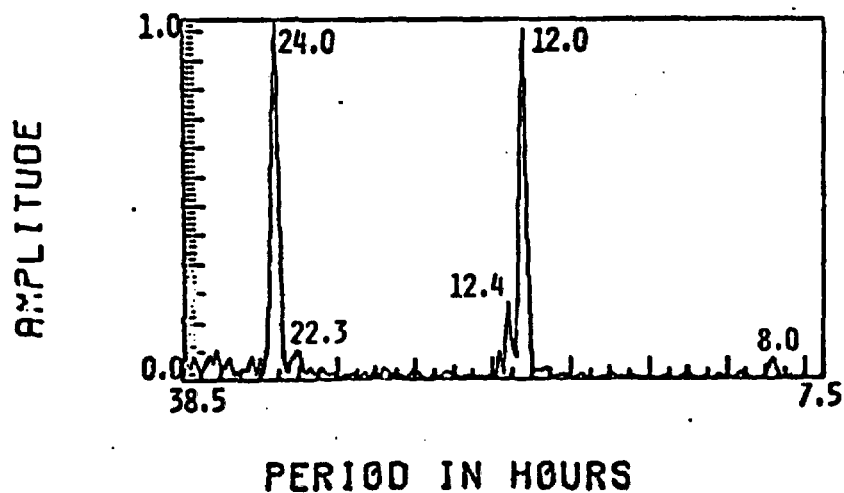


Figure 3.5-17. Power spectral density plots of the cross-correlation function for Scotty's Junction, Nevada, (SCT) north-south horizontal strain component, cross-correlated with Yucca Flats temperature (top) and barometric pressure (bottom). The data interval is from January 15, 1971 to February 12, 1971.

hours are greater. This may result from the strong peak present at this period in the autocorrelated SCT NS strain data (see Figure 3.5-3).

The above discussion has shown that the earth tides, temperature, and barometric pressure have similar periodic components. In the cases examined, measured strain always lags behind the above three factors. Aside from the anomalous lag of strain behind earth tides at SPM NW and TSP NS it appears that the strainmeters are responding more directly to earth tides than to temperature and barometric pressure. In addition, if the strainmeter vault temperatures are similar in response to the daily heating and cooling cycle as those described by Brown (1974, personal communication), then the thermal influence will be from thermoelastic strains induced in the ground from the daily temperature cycle. These thermoelastic strains, however, have periodic components equivalent to those of surface temperature (Berger and Wyatt, 1973). It does not appear possible at this time to separate earth tidal from thermoelastic influence, since considerable uncertainty is involved in the calculation of thermal and elastic behavior due to the lack of knowledge of the elastic and thermal parameters and the nature of the surface material at the strainmeter sites.

Secular Strain Data

Strainmeter data from the previously described sites (Scotty's Junction, Sleeping Mountain, and Twin Springs) were, in addition to the short period examinations, examined in terms of long period strain. The data analyzed is independent of Kumamoto's (1973), which was utilized in an earlier report (Willis et al, 1973). Figures 3.5-18, -19, and -20 are secular strain plots for Scotty's Junction, Sleeping Mountain, and Twin Springs, respectively. The most prominent feature common to these plots

SCOTTY'S JUNCTION SECULAR STRAIN

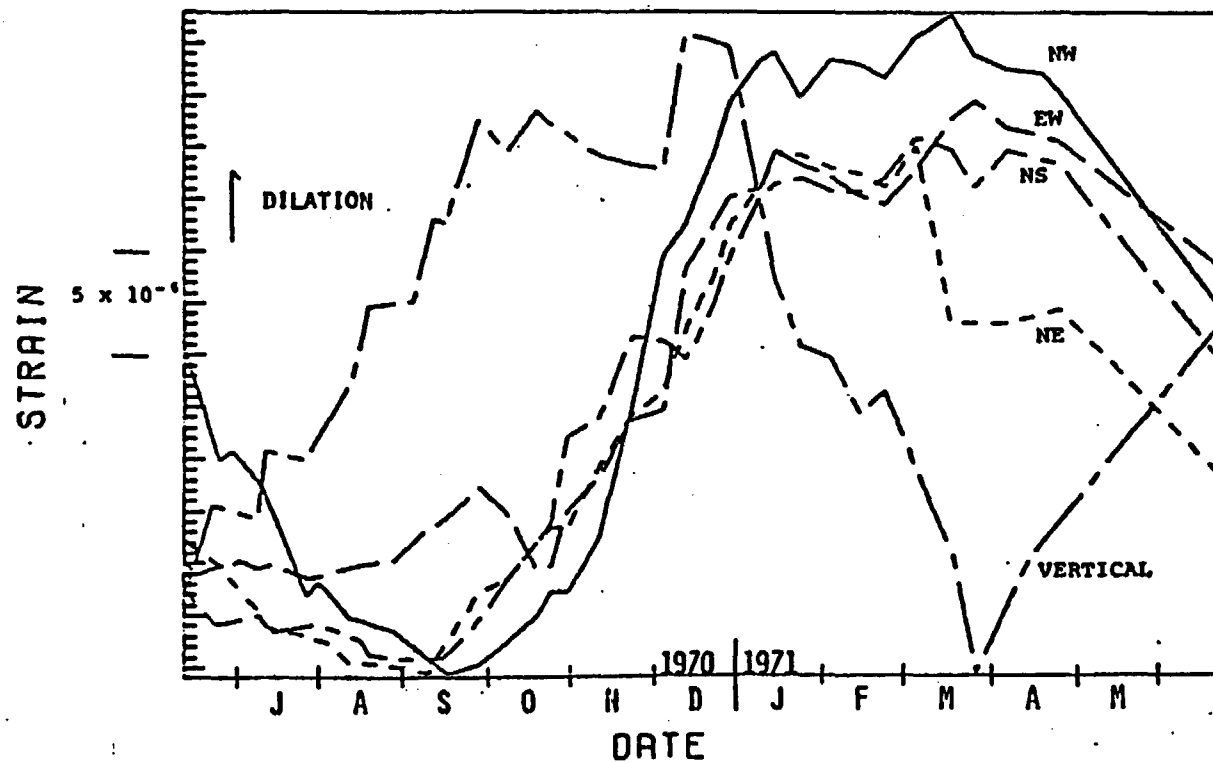


Figure 3.5-18. Secular strain at the Scotty's Junction, Nevada, strainmeter site, from June, 1970 to June, 1971.

SLEEPING MOUNTAIN SECULAR STRAIN

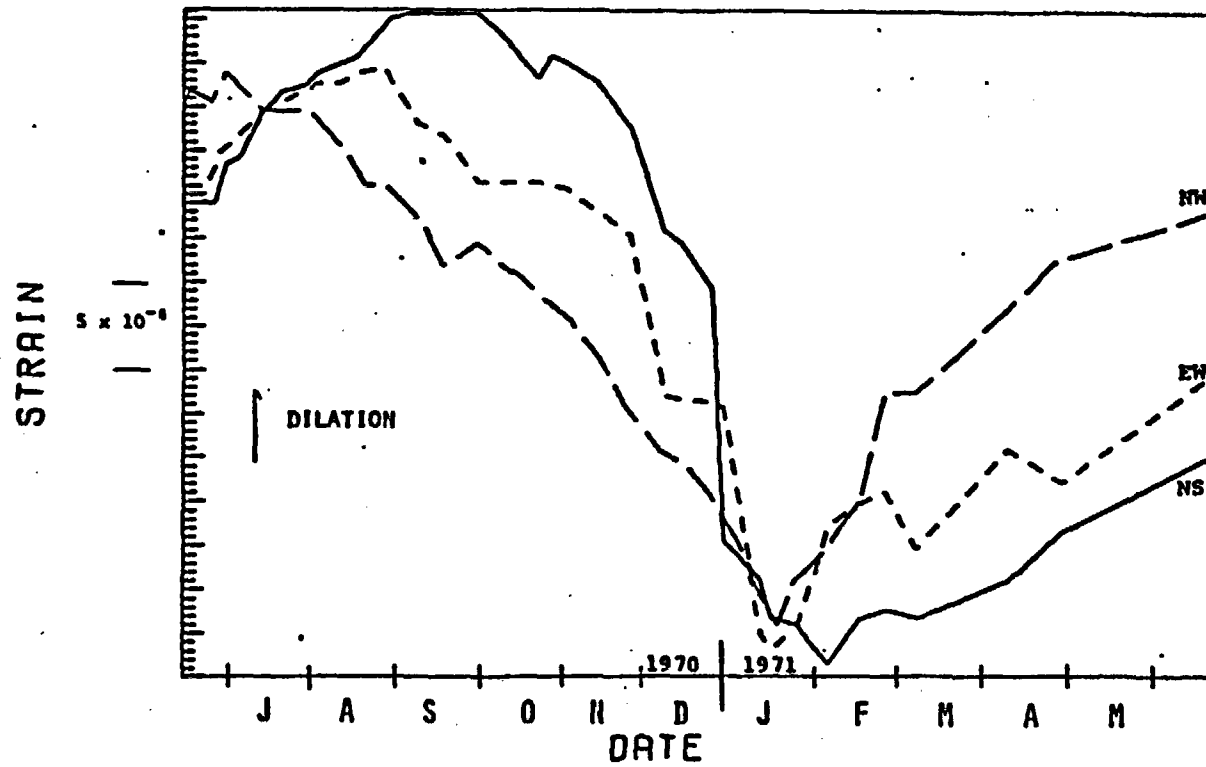


Figure 3.5-19. Secular strain at the Sleeping Mountain, Nevada, strainmeter site, from June, 1970 to June, 1971.

TWIN SPRINGS SECULAR STRAIN

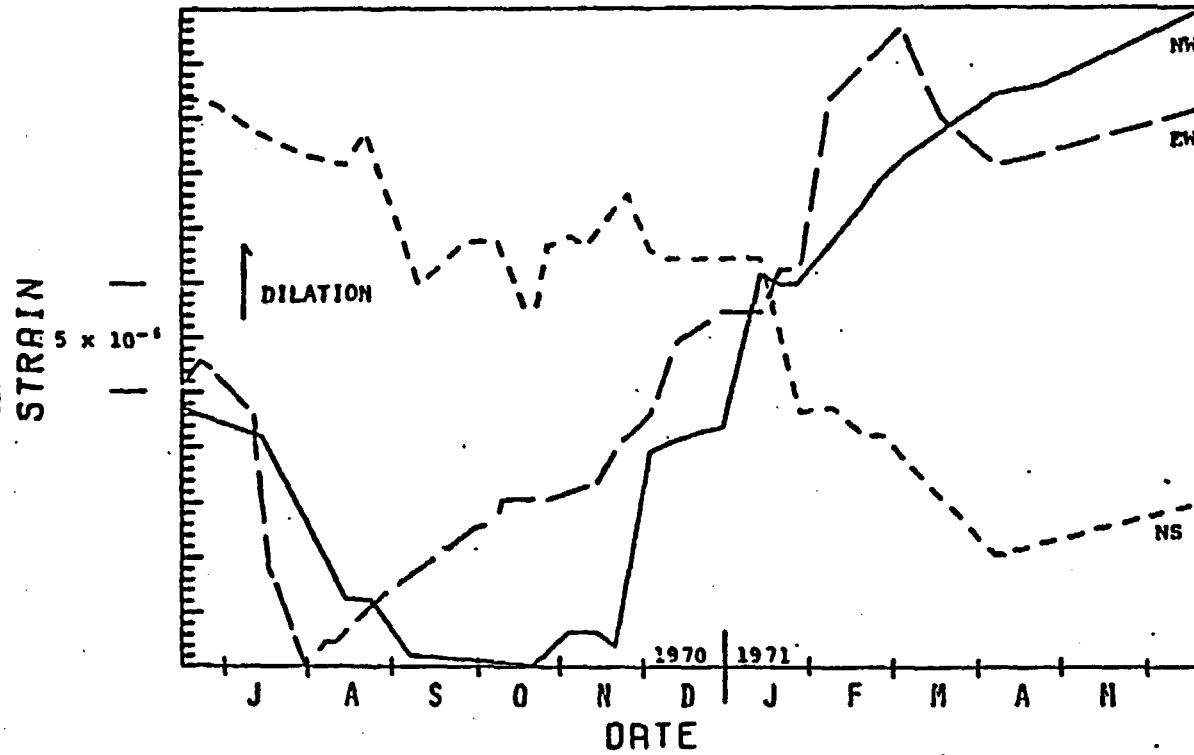


Figure 3.5-20. Secular strain at the Twin Springs, Nevada, strainmeter site, from June, 1970 to June, 1971.

is a cyclic, apparently seasonal variation in strain on the order of 1.0 to 3.7×10^{-5} . This cyclic phenomenon appears to be a feature common to many strainmeter sites and possibly some geodimeter lines (Berger, 1972; Berger and Wyatt, 1973; Pfluke and Stewart, 1973; Brown, 1974, personal communication). The question of whether this phenomenon represents instrumental or earth strain effects has remained unanswered. The amplitude of the apparently seasonal variation generally decreases as the base length or depth of the instrument increases.

Figure 3.5-21 is a plot of Yucca Flats surface air temperature averaged at ten-day intervals for a period of one year. Visual comparison of the seasonal strain variations at Sleeping Mountain and the temperature appears to show a good correlation. The other two strain stations show a fair negative correlation with temperature. In order to quantitatively establish the existence of a correlation between the two, a series of cross-correlations was made. Table 3.5-5 is a listing of the results of the long period cross-correlations between strain and temperature. Note that the correlations are both positive and negative corresponding to the obvious overall phase relationship between the two, as is evident in Figures 3.5-18, -19, and -20.

It is not precisely known what causes this 180° phase shift between various strain components. The most obvious suggestion is instrumental in origin, for one would not expect strain response to the same phenomenon to be in opposition at different sites. Brown (1974, personal communication) has identified a similar phenomenon in the Aleutian Islands with trenched strainmeters of the Colorado School of Mines design. He believes the cause of phase reversal to be related to the orientation of the micrometer mounting. Diurnal variations (such as earth tidal variations) and shorter period strain sense do not appear dependent on the mechanical orientation.

YUCCA FLATS TEMPERATURE

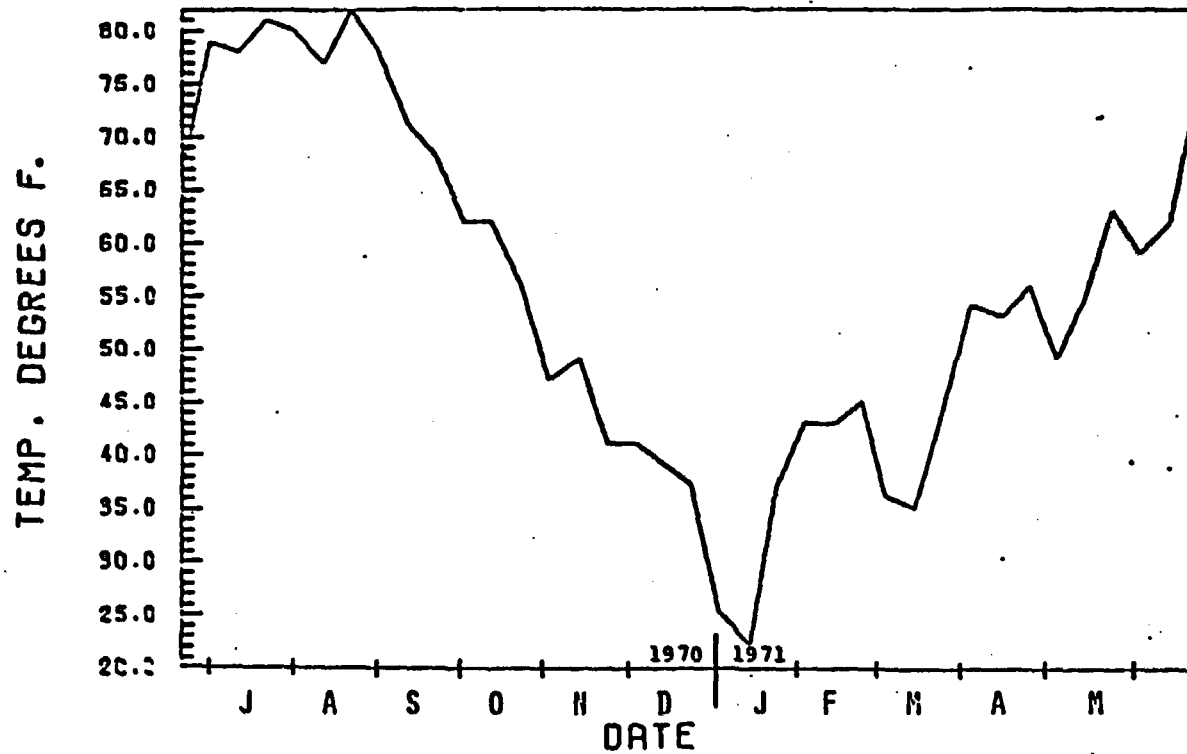


Figure 3.5-21. Plot of Yucca Flats, Nevada, surface temperature averaged over 10 day intervals, from June, 1970 to July, 1971.

TABLE 3.5-5

Long Period Cross-Correlation Coefficients for
South-Central Nevada Strainmeter Stations Strain
Components Cross-Correlation with Temperature

<u>Cross-Correlation</u>		<u>Correlation</u>	<u>Lag</u>
<u>Data Set 1</u>	<u>Data Set 2</u>		
SCT NS	Temperature	-0.83	-40 Days
SCT NE	Temperature	-0.88	-25 Days
SCT EW	Temperature	-0.78	-45 Days
SCT NW	Temperature	-0.88	-45 Days
SCT Vertical	Temperature	0.79	-95 Days
SPM NS	Temperature	0.85	-50 Days
SPM EW	Temperature	0.84	-25 Days
SPM NW	Temperature	0.89	0 Days
TSP NS	Temperature	0.68	-95 Days
TSP EW	Temperature	-0.79	-50 Days
TSP NW	Temperature	-0.82	-80 Days

The values of the cross-correlations are nowhere less than ± 0.68 , which indicates that for the data window length, the probability that the correlation is due to chance, is much less than one in one thousand. Also listed in the table are the lags associated with each cross-correlation value. The negative lags indicate that the recorded strain lags behind the temperature. Comparison of the lags shows a range from 0 lag at Sleeping Mountain northwest-southeast component to -95 days lag at Scotty's Junction vertical and Twin Springs north-south components. The median lag value is approximately -45 days.

Brown (1974, personal communication) has compared vault temperatures to surface temperature at the Aleutian strainmeter sites and has observed a lag of 40-45 days, vault temperature behind surface temperature. He believes the seasonal strain cycle to be related to vault temperature effects on the strainmeters. It would appear impossible, however, to determine exactly how much of the seasonal strain cycle is related to instrumental contamination by temperature and how much is attributable to thermal strains induced in the ground by the temperature field.

Phase lags have also been observed at other strainmeter stations. Berger and Wyatt (1973) monitored both strain and surface temperature at Pinion Flats, California, and observed a lag of the strain behind the temperature of two months. The lag is not believed to be instrumental in origin. It should also be noted that the yearly strain plots for Scotty's Junction, Sleeping Mountain and Twin Springs are without strain episodes such as those reported in the Aleutians (Major, 1971). The Aleutian records contain strain episodes with variations of up to 1×10^{-6} in the time span of hours to days. The Aleutian episodes are suspected to have

a relationship to precipitation. Kumamoto (1973), in an examination of precipitation data from Yucca Weather Station and continuous strain records from SCT, TSP and SPM, noted there was no unusual behavior in the observed strain with the occurrence of precipitation.

In determining secular strain trends, the effect of the seasonal cycle can be reduced, but not eliminated, by observing strain changes occurring over one or more years. Table 3.5-6 lists the yearly strain difference for Scotty's Junction, Sleeping Mountain, and Twin Springs strainmeter stations as determined from Figures 3.5-18, -19, and -20.

The secular strain change rates for these sites in southern Nevada are consistent and are reflected on all components. Therefore, it appears unlikely that these strains are instrumental in origin. Although these strain magnitudes ($\times 10^{-5}$) are large compared to other strainmeter sites (10^{-6} , 10^{-7}), they are considered to reflect real ground deformation.

Strain change ellipses have been calculated using data from this study and that from other three component strainmeter sites which were in operation for a year or more, by Willis and others (1973). Figure 3.5-22 displays these calculated strain change ellipses. (Exaggeration for this strain ellipse figure is $\times 10,000$ for shallow strainmeters and $\times 200,000$ for the deep sites.) The period covered was from June, 1970 to June, 1971 for all sites except Salt Lake City (SLC), where the data are from Anderson (1972) for the period January, 1970 to January, 1971. The Round Mountain, Nevada, data are from Malone (1972) and the Stone Canyon data are described by Bufe (1972).

The axes of maximum extension (or minimum compression) at strainmeter sites in California, Nevada, and Utah trend north and west, while axes of

TABLE 3.5-6

Yearly Strain Differences for Strainmeter
Stations in South-Central Nevada

<u>Station</u>	<u>Component</u>	<u>Strain</u>
Scotty's Junction	NS	0.9×10^{-5} Dilation
	EW	1.5×10^{-5} Dilation
	NE	0.6×10^{-5} Dilation
	NW	0.4×10^{-5} Dilation
	Vertical	1.6×10^{-5} Dilation
Sleeping Mountain	NS	1.4×10^{-5} Compression
	EW	1.8×10^{-5} Compression
	NW	0.8×10^{-5} Compression
Twin Springs	NS	1.6×10^{-5} Compression
	EW	0.8×10^{-5} Dilation
	NW	1.6×10^{-5} Dilation

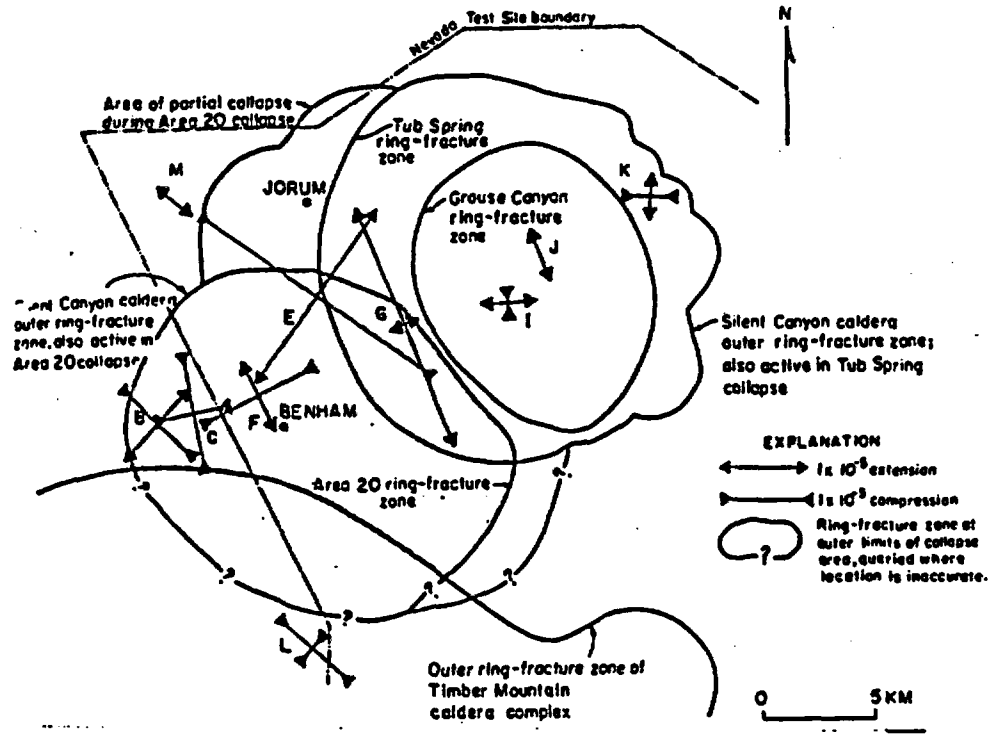


Figure 3.5-28. Caldera boundaries in Pahute Mesa area and strains related to the JORUM explosion. From Dickey, 1971, p. 1577.

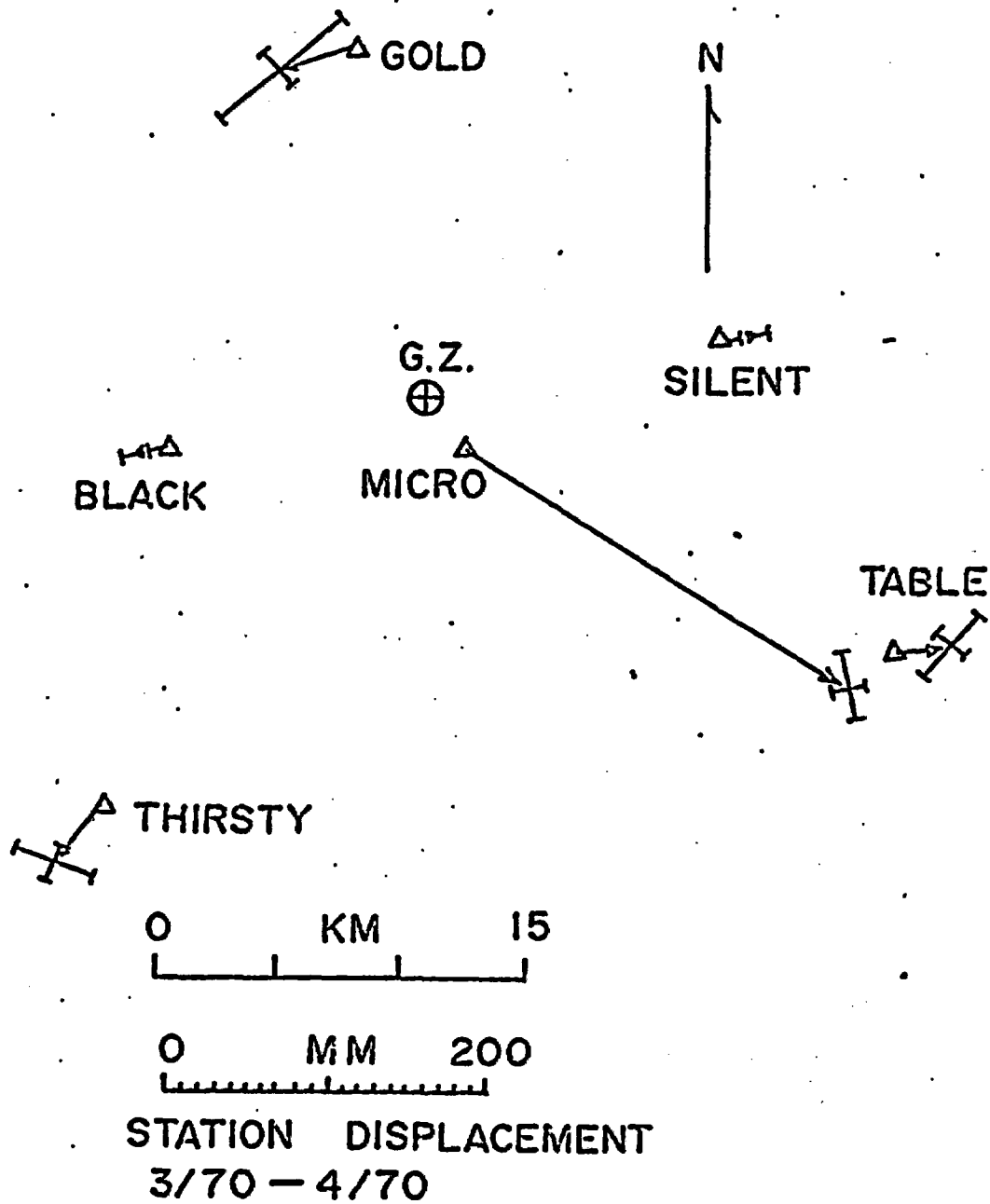


Figure 3.5-29. Station displacements (arrows) calculated from a least squares adjustment of the observed changes in line length between March 1970 and April 1970 (includes HANDLEY event). The orthogonal error bars indicate the principal axes of the error ellipse (95% confidence level in displacement). From Savage and others, 1974, figure 5.

The relaxation of the shot imposed deformation for April 1970 to May 1971 is shown in Figure 3.5-30. Savage and others have hypothesized that the relaxation is from creep on those faults which were previously stressed by the shot. It should be recognized that the magnitude of the recovery is greater at all stations, except Micro, than the shot-induced displacements. It was postulated that part of the relaxation observed was due to post-shot relaxation present from the BENHAM and JORUM nuclear tests detonated on Pahute Mesa within a 15 month period previous to HANDLEY.

In the subsequent two year period, May 1971 to May 1973, only small changes in the strain field were noted. Calculated strains were small for this time period, on the order of $.1 \pm .2 \times 10^{-6}$. Thus, Savage and others concluded the overall response of Pahute Mesa to the HANDLEY event as stable. In none of the time periods examined by Savage and others, did there appear a relation between the strain field and caldera structure in the NTS area.

Residual Strain

Strainmeters can detect residual strains on the order of 10^{-8} to 10^{-9} under normal conditions. Displacements of up to 1/2 cm accompanying major earthquakes and large nuclear detonations, can occur at distances on the order of thousands of kilometers (Press, 1965). These displacements appear as sudden offsets, termed strain steps, indicating that there are permanent adjustments in the strain field of the earth. Strain steps have been observed to follow both earthquakes and nuclear detonations (Press, 1965; Romig et al, 1969; Romig et al, 1969; Smith and others, 1969; Kumamoto, 1973; Yeatts, 1973). Their speed of propagation is approximately 3 km/sec and their offset amplitude is dependent on distance and appears to generally follow the relation $R^{-3/2}$ (Wideman and Major, 1967).

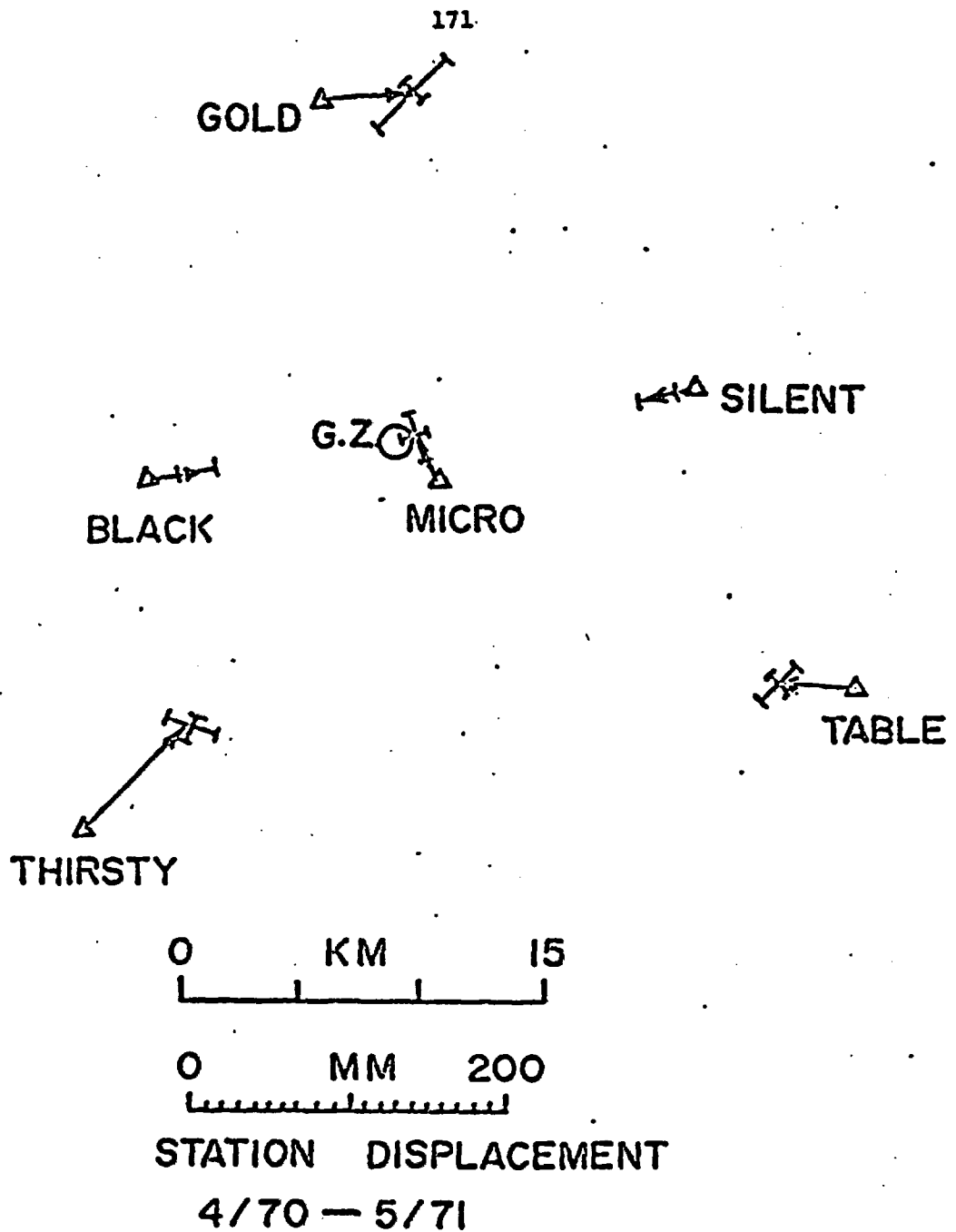


Figure 3.5-30. Station displacements (arrows) calculated from a least squares adjustment of the observed changes in line length between April 1970 and May 1971, the year following the HANDLEY event. The orthogonal error bars indicate the principal axes of the error ellipse (95% confidence level in displacement). From Savage and others, 1974, figure 6.

There has been some question as to the reality of the steps. As the instruments are highly sensitive, it is possible that they will undergo a permanent mechanical or electrical offset following the passage of seismic waves. However, it has been shown by various authors (Press, 1965; Kumamoto, 1973) that the strain steps are most probably representative of real ground deformation.

Four nuclear detonations at the Nevada Test Site have been monitored using strainmeter stations in the south-central Nevada area (Smith and others, 1969a and b, Romig and others, 1969a and b; Yeatts, 1973; Kumamoto, 1973). The earliest shot studied was the BOXCAR underground nuclear event which was detonated on April 26, 1968 (see Table 3.5-7). The device had an m_b of 6.3. Smith and others (1969a) monitored the explosion with strain and tilt meters at Isabella, California, to see whether a permanent change in the existing strain field could be measured. The measurements showed that if any change occurred within the first few minutes after the detonation, it would have to be smaller than 2×10^{-10} . This is 2 orders of magnitude smaller than the earth tidal strain. They therefore concluded that the residual strain induced by the shot could in no way alter the tectonic environment of the seismically active area surrounding Isabella, California.

The dynamic strain produced by the passage of seismic waves will be larger than the residual strain. At Isabella, California, Smith and others (1969a) observed a dynamic strain of 2×10^{-8} accompanying the S waves produced by the BOXCAR nuclear event. While 2 orders of magnitude greater than the permanent strain recorded at this site, Smith and others reported that this dynamic loading did not affect the local strain field.

TABLE 3.5-7

<u>SHOT</u>	<u>DATE</u>	<u>GMT TIME</u>	<u>APPROXIMATE YIELD (KT)</u>	<u>MEDIUM</u>	<u>LOCATION</u>	<u>m_b</u>	<u>M_B</u>	<u>M_L</u>
BOXCAR	26 Apr 68	15:00:00	1200	rhyolite	37°17'43.5" N 116°27'20.5" W	6.3	6.3	5.4
BENHAM	19 Dec 68	16:30:00	1100	tuff	37°13'53.3" N 116°28'24.9" W	6.3	5.6	6.2
JORUM	16 Sep 69	14:30:00	<1000	tuff	37°18'50.9" N 116°27'38.4" W	6.2	5.1	6.3
HANDLEY	26 Mar 70	19:00:00	>1000	tuff	37°18'01.7" N 116°32'02.8" W	6.5	5.3	6.2

Their monitoring of the 1872 fault scarp in Owens Valley in the time window surrounding the shot showed visible shaking from the explosion, but no measurable displacements. They concluded from this study that tectonic stress changes associated with large explosions are confined to distance of 100 km, and perhaps much less.

Romig and others (1969), using two strainmeters at locations designated Site 1 and Site 2 observed steplike compressive strains following the BENHAM event. Site 1 corresponds to the component oriented N84°E at Sleeping Mountain (see Table 3.5-2) and the latter is oriented N84°E at Scotty's Junction (a component not previously described in this report). Initial strain amplitudes were 1.8×10^{-7} at Site 1, 28 kilometers from ground zero, and 0.35×10^{-7} at Site 2, 71 kilometers from ground zero (Figure 3.5-31). The amplitude decrease with increasing distance (Figure 3.5-32) follows closely that predicted ($R^{-3/2}$) by Wideman and Major (1967) for earthquakes. Beyond 60 km from the shot, the residual strains are less than those strains induced by the earth tides.

The most significant observation, Romig and others concluded, was that the strain decayed at Site 1 to near-zero amplitude within 1/2 hour. The strain step at Site 2 was not observed to decay noticeably during the first few days after the shot.

Examination of records from a library at the Colorado School of Mines consisting of earthquakes strain steps showed that in no case had any earthquake strain step decayed in time. It was therefore concluded that the phenomenon was associated with the explosive source. Figure 3.5-31 also shows the pressure decay history curves for a shot 6.5 kilotons in

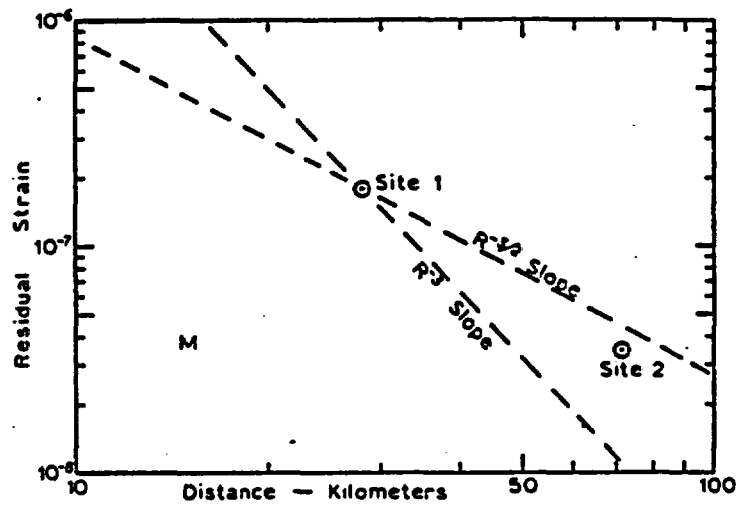


Figure 3.5-32. Variation of strain step amplitude with distance. Dashed lines drawn through Site 1 have slopes corresponding to decay with distance laws of R^{-3} and $R^{-3/2}$. From Romig and others, 1969a, p. 2172.

size (Olsen, 1967) and a theoretical one calculated for BENHAM. The strain decay curve is intermediate between the two time constants of the pressure decay curves. Romig and others (1969) concluded that the strain decay at Site 1 was therefore a reflection of the pressure history of the BENHAM cavity.

Smith and others (1969), monitoring the BENHAM event on strainmeters 20 and 250 km from ground zero, observed a peak "quasi-static" radial strain of 1.2×10^{-7} at 29 km. The strain transient decayed exponentially to zero with a time constant of 13 minutes. This further supports Romig and others (1969) findings and the interpretation of the phenomenon as a direct elastic response of the medium to the pressure decay of the BENHAM cavity. However, using the residual strain value of 1.2×10^{-7} at 29 km and the residual value determined at Isabella, California, for the BOXCAR nuclear event, they determined that the strain decrease with distance followed more closely R^{-3} , which is the theoretically determined decrease in strain with distance.

Smith and others (1969) have conjectured that previous observations of a strain distance variation of $R^{-3/2}$ are the result of permanent strain changes near the recording site induced by the dynamic overloading of near surface fractures that occur with the passage of large amplitude surface waves. Such a phenomenon, they concluded, would be expected to show the same velocity of surface waves and to have an amplitude-distance relationship of $R^{-3/2}$. Therefore, there is some conflict as to the extrapolation of strain with distance for the BENHAM shot.

Because of the interest generated by the "quasi-static" strain step associated with the BENHAM test, the strainmeter coverage was expanded for

the JORUM nuclear event. The strainmeter station at Sleeping Mountain was expanded to three components, and three components were also installed near Twin Springs (see Table 3.5-2 for locations and orientations).

Romig and others (1969), in an analysis of the strain recordings for the time period surrounding JORUM at these sites, observed non-decaying strain steps of 3×10^{-7} at 34 km, the Sleeping Mountain site, and 1×10^{-7} at 102 km, the Twin Springs site (Figures 3.5-33 and -34). By the non-decaying nature of the strain steps and the fact that the resulting principal axes of strain determined from the steps were not consistent with an explosive point source mechanism, Romig and others concluded that fault movement occurred in the vicinity of the test. The associated earthquake, they suggested, had a magnitude at least as large as the JORUM test (6.2 m_b). Assuming a fault centered near the test location, preliminary interpretation by Romig and others suggested a fault approximately 30 km long oriented NS with an average displacement of about 0.3 meters. Movement was estimated to be 2/3 dip-slip (west side down) and 1/3 left-lateral strike-slip. Surface mapping by U.S.G.S. (Hamilton and others, 1969) has demonstrated that there is indeed up to 1 meter surface displacement along pre-existing faults following some of the larger underground nuclear tests.

Major and others (1969) monitored strains on Amchitka Island during the MILROW test, October 2, 1969. Within 50 km of ground zero, strain records showed the superposition of two types of residual strain. A "quasi-static" component similar to that recorded for the BENHAM event was observed and similarly interpreted to represent the pressure decay history of the shot cavity. A permanent strain step, approximately 4 times as large as the "quasi-static" step, was also observed. The large permanent steps were interpreted to be due to an earthquake hypothesized to have occurred within 1 minute post shot.

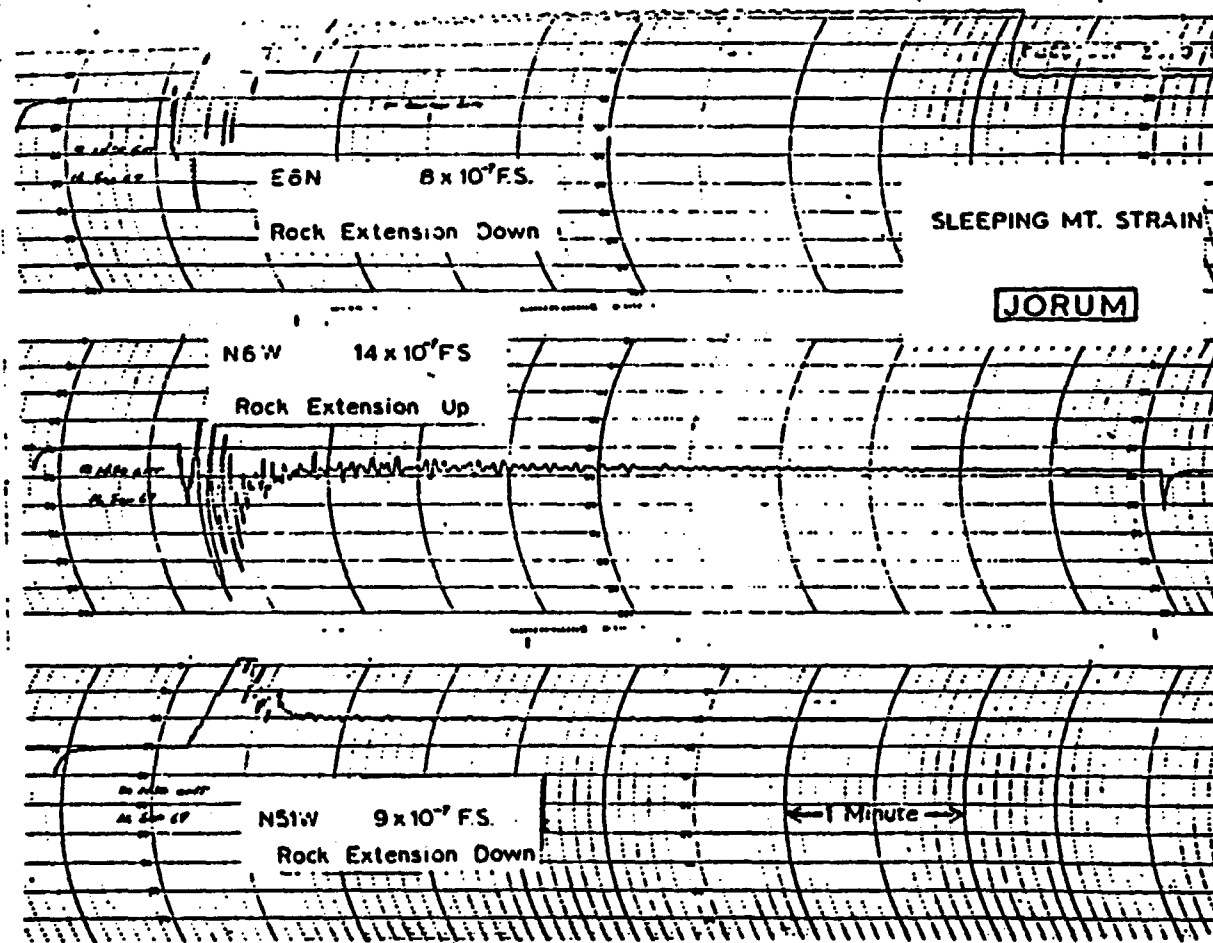


Figure 3.5-33. Records from short-base strainmeters located at Sleeping Mountain, Nevada, for the time period immediately surrounding the JORUM event.

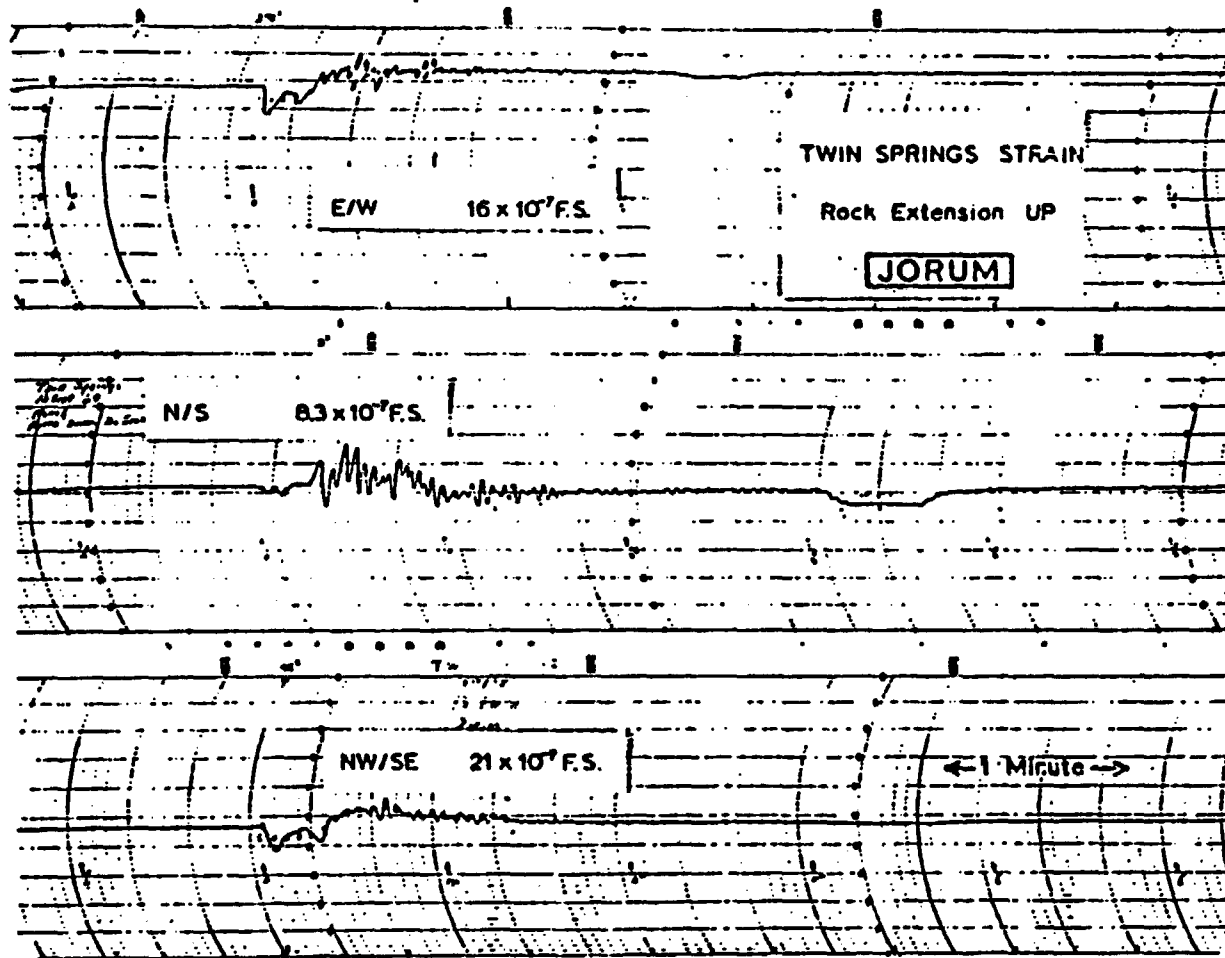


Figure 3.5-34. Records from short-base strainmeters located at Twin Springs, Nevada, for the time period immediately surrounding the JORUM event.

Amplitudes of the strains associated with the MILROW event were compared by Major and others (1969) with the BENHAM observations (Figure 3.5-35). The slopes of the four lines represent various rates of decay with distance, R^{-3} , R^{-2} , $R^{-3/2}$, and R^{-1} . The data supports an $R^{-3/2}$ law.

The HANDLEY event, detonated March 26, 1970, was monitored by a total of 18 strainmeters in the Nevada Test Site area, making it one of the best monitored shots (Table 3.5-8). Kumamoto (1973), in a detailed analysis of the non-decaying strain steps at the Scotty's Junction strainmeter site, concluded from the consistency of the data and the realizable Poisson's ratio (.453) calculated from the recorded strain steps, that the steps are measures of true ground deformation and not instrumental eccentricities.

Yeatts (1970) has concluded, using a least-square analysis of the HANDLEY non-decaying strain steps from the 18 station network, that significant fault movement at the source was necessary to explain the field effects. Therefore, he concluded that an earthquake was triggered by the nuclear explosion. (The amount of fault movement required is less than the $6.5 m_0$ of the shot.) Interpretation by Yeatts suggested a fault 2-10 km long striking $N20^\circ E$. Movement was estimated to be 1 meter left-lateral strike-slip and 1 meter dip-slip (east block up). The inferred fault length and displacement yields an m_0 of 3.8 to 5.0.

From the study of residual strains there has been interest in what order of magnitude strain will affect seismicity. Smith et al (1969) have concluded that strains of 10^{-7} to 10^{-8} have little or no effect since earth tidal strains are of this magnitude and the crust is constantly subject to them. However, it should be noted that the time involved with

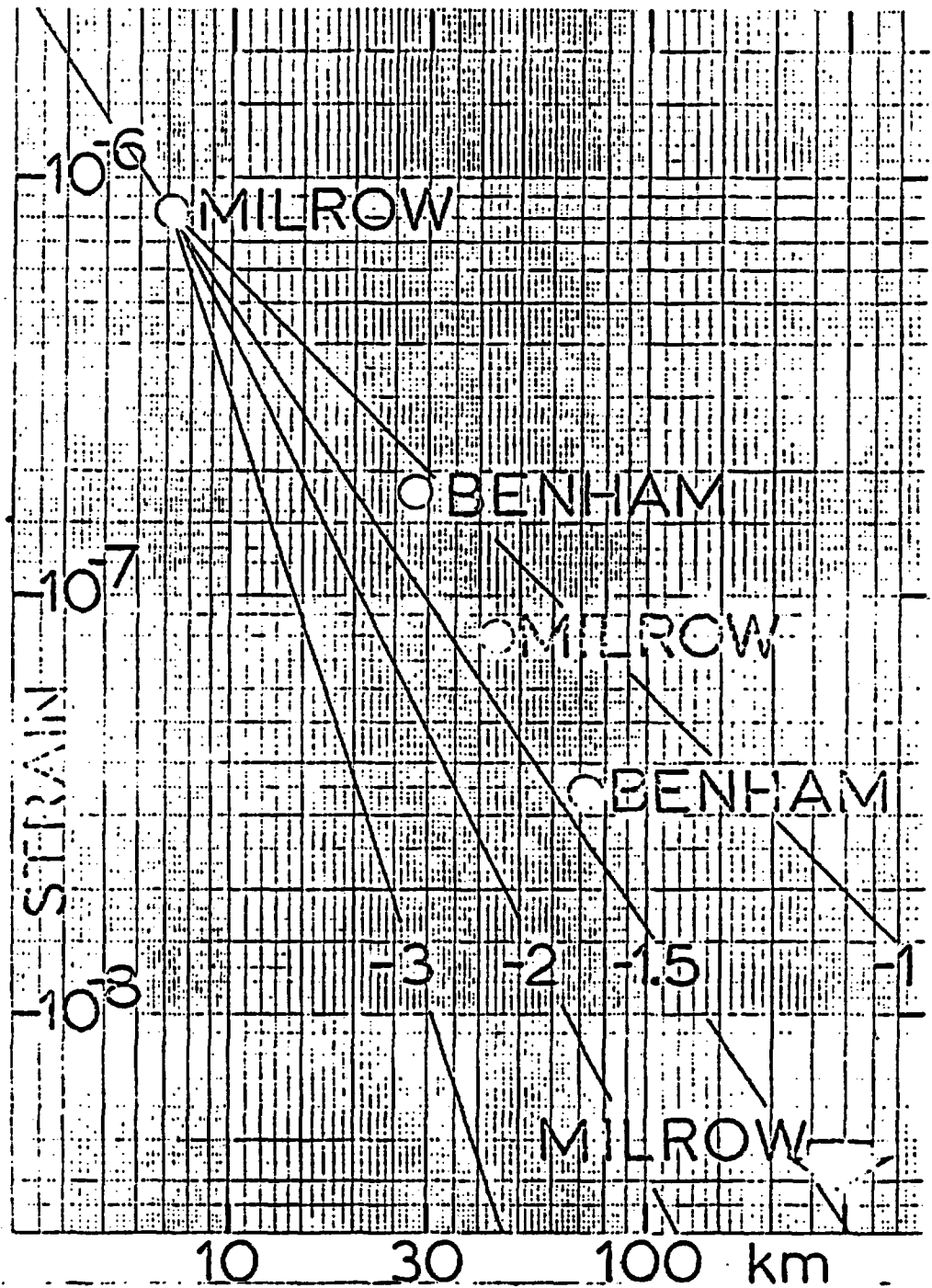


Figure 3.5-35. Quasi-static strain vs. distance plot for MILROW and BENHAM nuclear events. From Major and others, 1969, figure 11.

TABLE 3.5-8

HANDLEY Strainmeter Site and Strain-Step Data

Site	Distance (km)	Azimuth (deg)	Component (deg)	Strain Step ($\times 10^{-7}$)
Sleeping Mountain	26.9	230	84	-9.0
			-6	0.58
			-51	6.2
Survey Butte	28.0	105	75	-1.6
			15	1.0
			-45	0.05
Tolicha Peak	29.6	267	-94	-9.8
Quartzite Mountain	34.8	33	20	-2.2
Yucca Mountain	41.1	183	3	1.0
Oak Springs	43.3	100	-99	-0.75
Yucca Flat	48.0	114	90	-0.80
			0	0.05
			45	0.50
Kawich Peak	66.5	6	-4	1.2
Scotty's	69.5	250	84	0.067
			-51	0.55
			39	0.27
Rawhide Mountain	103.6	8	-35	3.8
Twin Springs	106.0	18	90	0.93
			0	0.034
			45	0.85
Round Mountain	162.0	343	-72	0.047
			-13	0.10
			36	-0.04
Mina	183.0	313	70	0.026

(from Yeatts, 1970, p. 222)

a strain change due to a large explosion or earthquake is on the order of seconds rather than the 6 hours required for a 10^{-8} strain change due to the earth tides. This time factor may be significant for triggering of earthquakes.

In the Nevada Test Site area a strain of 10^{-3} would be expected to cause an earthquake without faults or prestress present in the region (Smith and others, 1969). A smaller strain might cause an earthquake in a prestressed medium, especially where a fault zone concentrates the stress.. A lower limit on strain necessary to activate an existent fault in the NTS region would be 10^{-6} (Smith and others, 1969). This strain could be expected at distances of less than 15 km from shots of the order of one megaton if a distance decay law of R^{-3} is assumed. The distance, however, would be greater if an $R^{-3/2}$ decay law is utilized.

Dynamic strain, produced by seismic waves may be the most important factor as a trigger. In studies where records of the strain steps and dynamic strain are presented, the dynamic strain is, in general, an order of magnitude greater than the static strain. It would appear then, that the dynamic strain would be at least as important a triggering mechanism as static strain. Whether the near field dynamic strain follows the $R^{-3/2}$ or R^{-3} dependence on distance, one can expect very high strain levels in the near source region.

It is concluded from the analysis of strain from 4 nuclear shots detonated at the Nevada Test Site, the strain decrease with distance follows more closely the $R^{-3/2}$ decay law and that JORUM and HANDLEY generated earthquakes near ground zero upon detonation.

3.6 Triggering of Earthquakes by Natural and Man-Made Forces

3.6.1 Earthquake Triggering by Underground Nuclear Detonations

The question concerning the triggering of earthquakes by underground nuclear detonations is not, "Does the process occur?" but, "When, to what degree, and at what distance from the detonation does the process occur?"

Large nuclear detonations at the Nevada Test Site have stimulated (triggered) earthquake activity within the area of the shot point immediately after the detonations. This earthquake activity has continued for lengths of time in some cases in excess of six months, but the magnitudes of these events are so small that most of them are not detectable by the regional network which reports to the National Earthquake Information Service (NEIS).

In addition to the immediate occurrence of earthquakes, a delayed triggering effect may be present. The frequency of aftershocks following the nuclear detonation BENHAM did not decay as a "normal" aftershock sequence does, but instead, the number of aftershocks appeared to periodically increase. The periodicity was reported to be about 20 days (Hamilton and others, 1972). The authors were hesitant to attribute this to an effect of the explosion. In their words (p. 1330), "it is difficult to imagine an effect of the explosion that could have such a long period and that could continue to manifest itself for approximately four months."

Engdahl (1972) reported a delayed triggering effect for some near-cavity, explosion-stimulated tectonic events following the nuclear detonation CANNIKIN on Amchitka Island. These triggered earthquakes did not commence until the seventh day after the detonation, and the last event occurred about 3 months after CANNIKIN.

Several methods have been used to examine the possibility that triggering effects took place outside of the area near the detonations.

One method, which was given additional stimulus by the large after-shock sequence observed after the detonation of BOXCAR, was to establish a sensitive seismographic network within a local area remote from the test site. The seismic activity of this local area was then monitored for a period of time before and after a nuclear detonation. These small networks have been located at distances up to 620 km from the Nevada Test Site. This type of study was conducted by Boucher and others (1969), Molnar (1969), Willis (1970), and Hamilton and others (1972). The results of these studies led the investigators to conclude that there was no triggering effect observed in these areas resulting from the nuclear detonation.

The second method of studying the possible triggering effect of underground nuclear detonations at distance from the shot point was to examine the earthquake data obtained from a regional seismographic network during time periods before and after selected nuclear detonations.

Regional networks that supplied the earthquake data necessary for such a study were the University of Nevada seismic network, reported by Boucher and others (1969), who concluded that there was "no consistent effect"; the California seismic network, reported by Bolt and Miller (1971), who concluded that in the northern California area, the number of earthquakes within one-week periods following six large nuclear detonations at the Nevada Test Site was not significantly greater than the number of earthquakes that occurred in any other week; and the NEIS regional stations. Emiliani and others (1969), using data from the latter, concluded that underground nuclear detonations trigger significant seismic activity for

up to 32 hours afterward, at distances up to 860 km from the Nevada Test Site. Their conclusions were refuted by Healy and Marshall (1970), Anderson and others (1970), Allen and Bailey (1970), and Ryall and Boucher (1969).

In addition to the previously stated stimulation of earthquake activity in the area of the shot point, a release of tectonic energy occurred simultaneously with some nuclear detonations. Primary evidence for this simultaneous release includes the observation of anomalous primary Love waves (Brune and Pomeroy, 1963), and an azimuthal variation in the Rayleigh wave pattern (Toksöz and Kehrler, 1971), in addition to the strain release discussed earlier.

This tectonic energy release cannot always be described as resulting from an earthquake. Archambeau (1972) pointed out that because of the fracture zone set up by the explosion shock wave, tectonic energy release always occurs for an explosion detonated in a prestressed media. He stated that in addition to this release of prestress in the fracture zone, the explosion may or may not induce an earthquake (which he described as rapid faulting), that would release an additional amount of tectonic energy.

Even though the model of stress relaxation brought about by the formation of a crushed zone is similar to the model for stress relaxation resulting from an earthquake, Archambeau (1972) stated that the total tectonic energy release accompanying nuclear detonations must be considered the result of one or both of the above processes, rather than due simply to the occurrence of an induced earthquake. Archambeau also added that the major difference between the two models is geometrical; that being the shape of the region of failure.

The amount of tectonic strain energy released by an explosion is strongly dependent upon the properties of the material in which the shot is fired and the level of ambient tectonic stress present (Toksöz and others, 1971). The site of the tectonic energy release is the vicinity of the nuclear detonations, and as Toksöz and Kehrler (1971) point out, the energy release cannot be interpreted as resulting from a triggered earthquake at a distance of 10 km or more from the detonation.

Regional Seismic Activity: BOXCAR, BENHAM, JORUM, and HANDLEY

Method of Analysis

The largest underground nuclear detonations (explosive yields of the order of 1 megaton) at the Nevada Test Site were BOXCAR, BENHAM, JORUM, and HANDLEY. The locations, explosive yields, shot mediums, and the equivalent m_b and M_s magnitudes for each of these detonations are listed in Table 3.5-7.

The largest nuclear detonations were selected for the study since any triggering effect at distance is probably a function of the magnitude of the initiating event. Therefore, any examination of the seismic activity following large nuclear detonations should present the best opportunity to determine if a triggering effect took place.

All earthquakes reported by NEIS and located within 1000 km of 37.3°N latitude, 116.5°W longitude (the mean location of the four shot points), during the 30 days before and after each of the detonations, were selected for study.

The cumulative strain release parameter developed by Benioff (1949) is used in this study to depict the seismic activity in the region of interest. The parameter is defined as the cumulative summation of the

square roots of the seismic wave energy generated by each earthquake within the sequence under investigation, and is discussed in more detail in Sec. 3.4.1.

Although the physical significance of the parameter is subject to question when applied to earthquakes with a wide range of magnitudes and hypocentral locations, the parameter is still a useful method of depicting seismic activity.

The equation used to calculate the seismic wave energy from which the strain release parameter is obtained has the general form

$$\log E = bM + a$$

and

$$E = 10^{(bM + A)}$$

Hence, the strain release is

$$\sqrt{E} = 10^{1/2(bM + A)}$$

In this relationship, M is a general expression for earthquake magnitude. The constants a and b are dependent on the magnitude scale used for any individual study.

Simplistically, strain release may be viewed as a non-linear weighting function of the earthquakes within a sequence. The degree of weighting is such that for 2 earthquakes with magnitude M_1 and M_2 , when $(M_1 - M_2) = 1$,

$$(E_1/E_2)^{1/2} = 10^{b/2}$$

Hence, the number of earthquakes of any magnitude required to equal the equivalent amount of strain release of an earthquake one magnitude unit greater is $10^{b/2}$.

The magnitude reported by NEIS for most earthquakes is termed the body wave magnitude and is represented by the symbol m_b . NEIS reports the arithmetic mean of the body wave magnitudes reported by the individual cooperating stations. These stations determine m_b from the amplitude of the largest pulse within the first 5 cycles of the compressional body wave.

The strain release parameter used in the study was obtained by taking the square root of the seismic wave energy, in ergs, defined by

$$\log E = 12.24 + 1.44 M_s \quad (\text{B\aa}th, 1958)$$

M_s is the surface wave magnitude, usually calculated from the maximum amplitude of the surface waves in the 20 second period window. To calculate the seismic wave energy from the m_b values reported by NEIS, the B\aa th equation above was rewritten in terms of m_b using the relationship

$$M_s = 1.59 m_b - 3.97 \quad (\text{Richter, 1958})$$

Therefore,

$$\log E = 2.29 m_b + 6.53$$

Hence, $10^{b/2}$, the number of earthquakes of any m_b magnitude required to equal the equivalent amount of strain release of an earthquake one m_b unit larger, is about 14.

The daily strain release for any area of interest was obtained by summing the square roots of the energies of the earthquakes within each 24-hour period, and determining a cumulative summation, in percent, of the total strain release within that area during each 60-day period.

The daily seismic activity during each 60-day period was observed by classifying the earthquakes as increments of $N\Delta t$, with Δt equal to 24 hours, and N taking all integer values from -30 to +30 relative to t_0 ,

the time of each detonation. The daily strain release was calculated using the relationship described earlier in this section except when no m_b was reported, M_L (local magnitude) was used to calculate m_b by the relationship $m_b = 1.7 + .8 M_L - .01 M_L^2$ (Richter, 1958).

Accumulated Seismicity: Four 60-Day Periods

Because the same regional area was considered for each 60-day period, an examination of the total seismic activity summed over all four periods was possible. The summation allows a possible observation of any triggering effect that might not be observed if each period was examined separately. In addition, by summing the seismic activity over all four periods, a longer period of time is used to observe the seismicity within the region at distances less than 1000 km from the detonations.

During the four 60-day periods, 192 earthquakes were reported from the area within 1000 km of the Nevada Test Site. The number of earthquakes, summed over the four periods during each 24-hour period can be seen in Figure 3.6-1a.

The rise in seismic activity following t_0 is not a result of earthquake triggering within the region at distances from 50 to 1000 km of the detonations. Instead, the increased seismicity results from aftershocks within the area near the shot point.

The number of earthquakes at distances between 50 km and 1000 km from the detonations and at distances less than 50 km are pictured in Figures 3.6-1b and 3.6-1c, respectively. The earthquakes located within 50 km of the detonations (Figure 3.6-1c) all took place during the periods following the events and by these criteria may be considered aftershocks of the detonations.

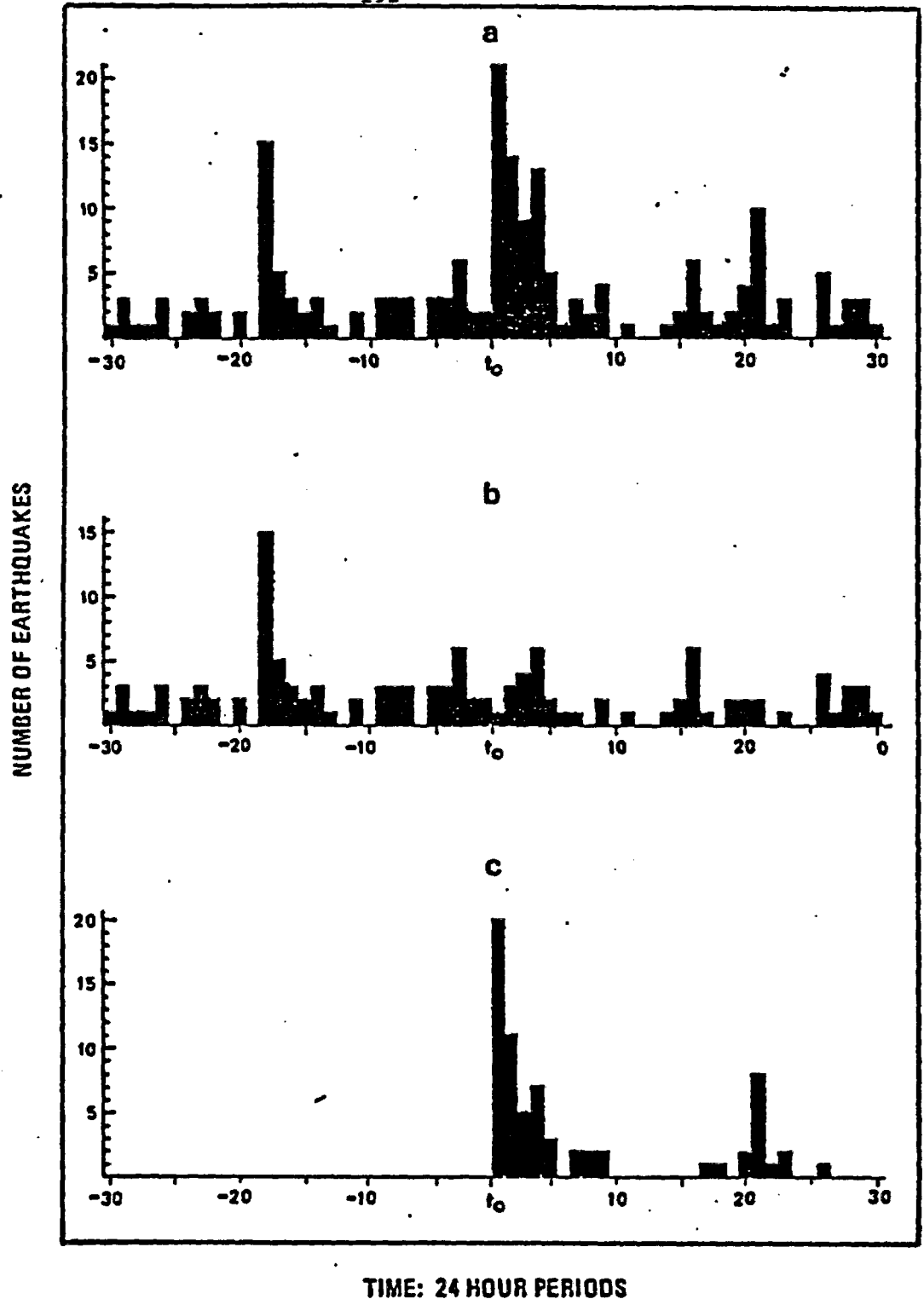


Figure 3.6-1. Total number of earthquakes that occurred during each 24-hour period relative to the detonation times of BOXCAR, BENHAM, JORUM, and HANDLEY. The daily number of earthquakes totaled for the four 60-day periods is shown for all earthquakes that were located (a) within 1000 km of the detonations, (b) at distances between 50 km and 1000 km from the detonations, and (c) at distances less than 50 km from the detonations.

Aftershocks within the area near the detonations were previously described in studies such as Boucher and others (1969). These known aftershocks must be eliminated from the earthquake data for the area within 1000 km of the detonations to allow observation of the seismicity at distances greater than 50 km; the area in which the occurrence of triggered earthquakes is questioned.

Examination of Figure 3.6-1b, the daily number of earthquakes at distances greater than 50 km during the four 60-day periods selected, does not lead one to conclude that a triggering effect is present, because the number of earthquakes did not noticeably increase following the nuclear detonations. During the 5-day period following the detonations, a total of 16 earthquakes took place; the same number of earthquakes that was reported during the preceding 5-day period. Using the strain release parameter (see Figure 3.6-2) for the four cumulative 60-day time periods centered on these shots, more than 70% of the strain release occurred during the 30 day periods prior to the detonations. No rapid increase in strain release pattern was observed following t_0 .

Although the total seismic activity summed over these four 60-day periods does not indicate that any triggering effect has occurred following the large nuclear detonations, the 60-day period around each nuclear detonation was examined to see if the same conclusion was warranted for each of the periods.

BOXCAR

Sixty-two earthquakes were reported within 1000 km of BOXCAR during the 60-day period centered on the shot (Figure 3.6-3). Fifteen of the earthquakes occurred within 50 km of the shot point, and these events can be considered a result of the detonation.

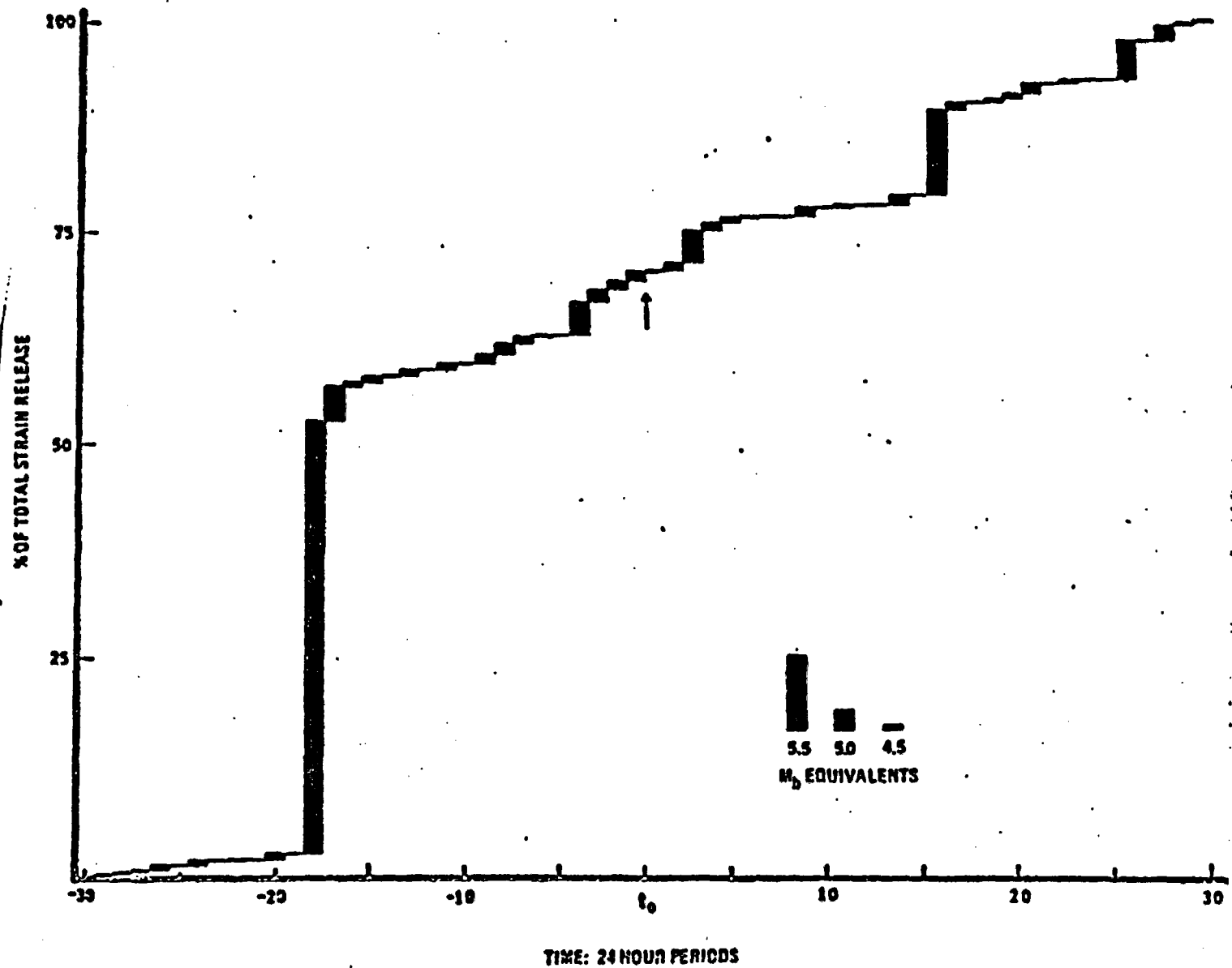


Figure 3.6-2. Cumulative daily strain release for the area between 50 and 1000 km of BOXCAR, BENHAM, JORUM, and HANDLEY. The daily strain release was calculated for each 24-hour period relative to the time of each detonation (t_0) and summed for the four 60-day periods centered on each t_0 .

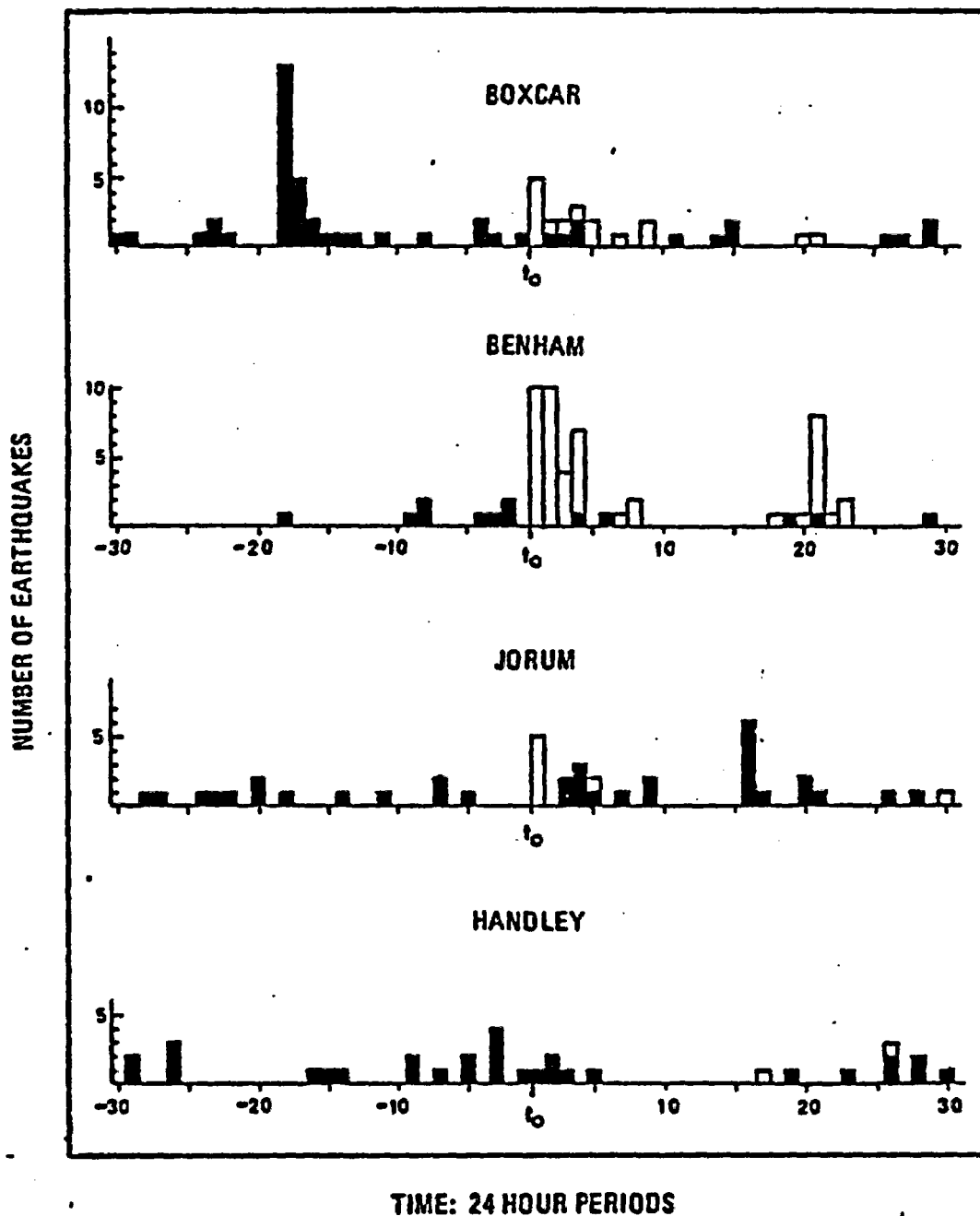


Figure 3.6-3. Number of earthquakes that occurred during 24-hour periods relative to t_0 , the detonation time of BOXCAR, BENHAM, JORUM, and HANDLEY. The solid bars are the number of earthquakes located at distances between 50 and 1000 km of the shot points, and the open bars are the number of earthquakes located at distances less than 50 km of the shot points.

The regional picture of seismic activity obtained from the remaining 47 earthquakes that were located at distances greater than 50 km from BOXCAR during the 60-day period does not indicate that a triggering effect took place. Thirty-five of these earthquakes were reported during the 30-day period prior to t_0 , and the remaining twelve events were reported during the 30-day period after the detonation.

In addition, there was not an increase in the number of earthquakes immediately following t_0 . During the 4-day period after the shot, 4 earthquakes took place, the same number of earthquakes that took place during the four days before the shot (Figure 3.6-3).

The regional picture of seismic activity presented by the cumulative daily strain release (Figure 3.6-4) also indicates that an increase in seismicity did not take place following BOXCAR. About 90 percent of the strain release during the 60-day period occurred during the 30-day period preceding the detonation, and a rapid increase in strain release did not occur following t_0 .

BENHAM

Fifty-eight earthquakes were reported within 1000 km of BENHAM during the 60-day period centered on the shot (Figure 3.6-3). Only thirteen of the earthquakes were located at distances greater than 50 km from the shot and the remaining 45 earthquakes were part of the BENHAM aftershock sequence.

Not all of the aftershocks reported by the NEIS during the BENHAM 60-day period took place immediately following the shot. Thirteen of these aftershocks took place during the period from the eighteenth to the twenty-third day after the time of BENHAM (Figure 3.6-3). These

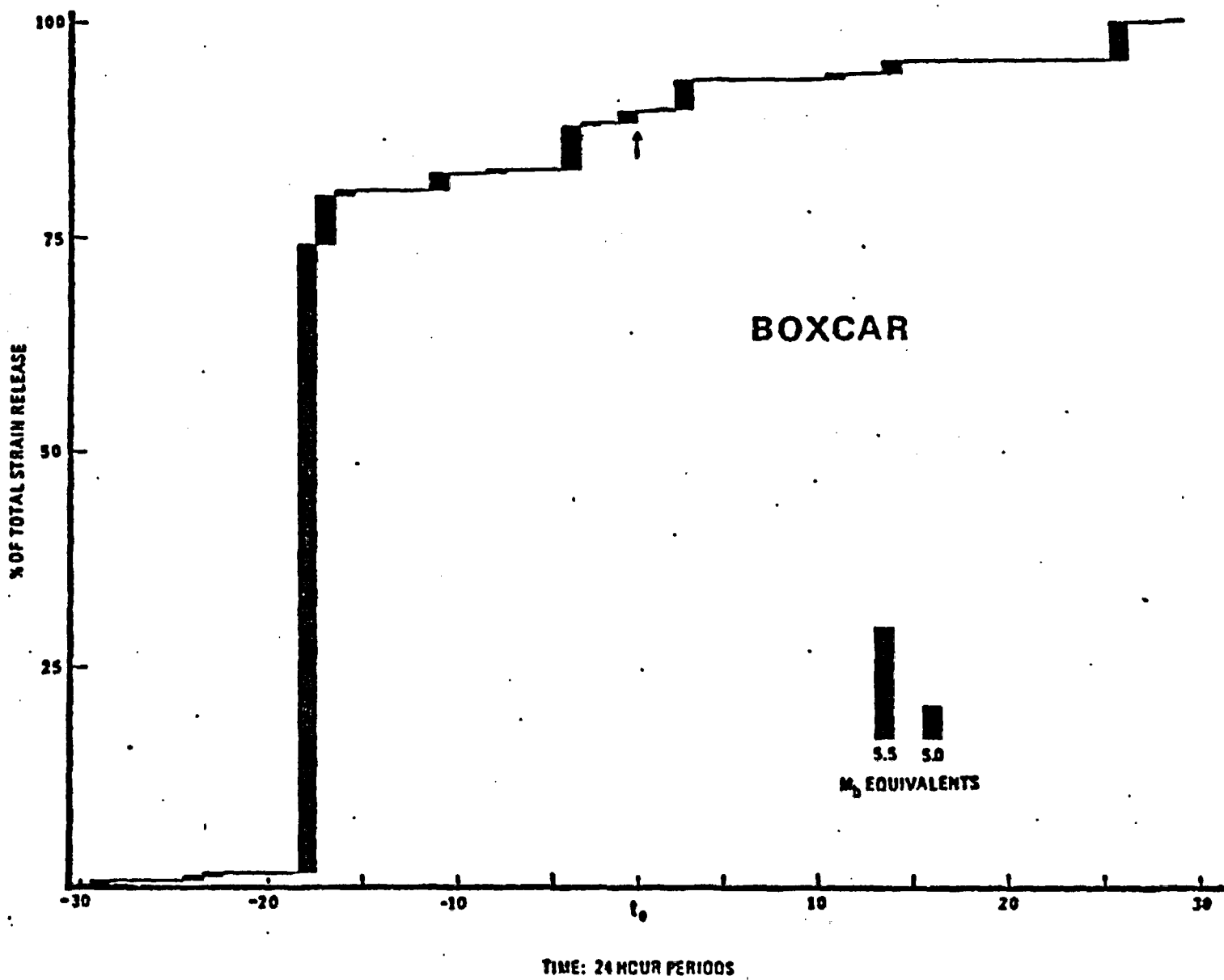


Figure 3.6-4. Cumulative daily strain release for the area between 50 and 1000 km of the BOXCAR nuclear detonation. The cumulative daily strain release was calculated for each 24-hour period relative to t_0 , the time of BOXCAR.

earthquakes are part of the periodically increasing aftershock sequence of BENHAM as reported by Hamilton and others (1972).

The regional seismic activity depicted by the earthquake frequency, although limited to 13 earthquakes, does not increase following t_0 . Two earthquakes were reported during the 6-day period following t_0 , while four earthquakes were reported during the same time period before t_0 (Figure 3.6-3).

The regional seismicity depicted by the cumulative daily strain release (Figure 3.6-5) also reflects the lack of increased seismicity following t_0 . About 80 percent of the strain release during the 60-day period took place during the 30-day period preceding the detonation, and a rapid increase in strain release was not present following t_0 .

JORUM

Forty earthquakes were reported within 1000 km of JORUM during the 60-day period centered on the detonation. Thirty-four of the earthquakes were located at distances greater than 50 km from the shot, and the remaining six earthquakes were part of the JORUM aftershock sequence (Figure 3.6-3).

The regional seismic activity depicted by the number of earthquakes per day that occurred at distances between 50 and 1000 km of the detonations does increase following t_0 . Nine of the earthquakes took place during the 9-day period following the detonation compared to 3 earthquakes that took place during the same period prior to the detonation.

The seismic activity depicted by the cumulative daily strain release (Figure 3.6-6) does not completely reflect the increased number of earthquakes seen following t_0 . Although the rate of cumulative daily strain

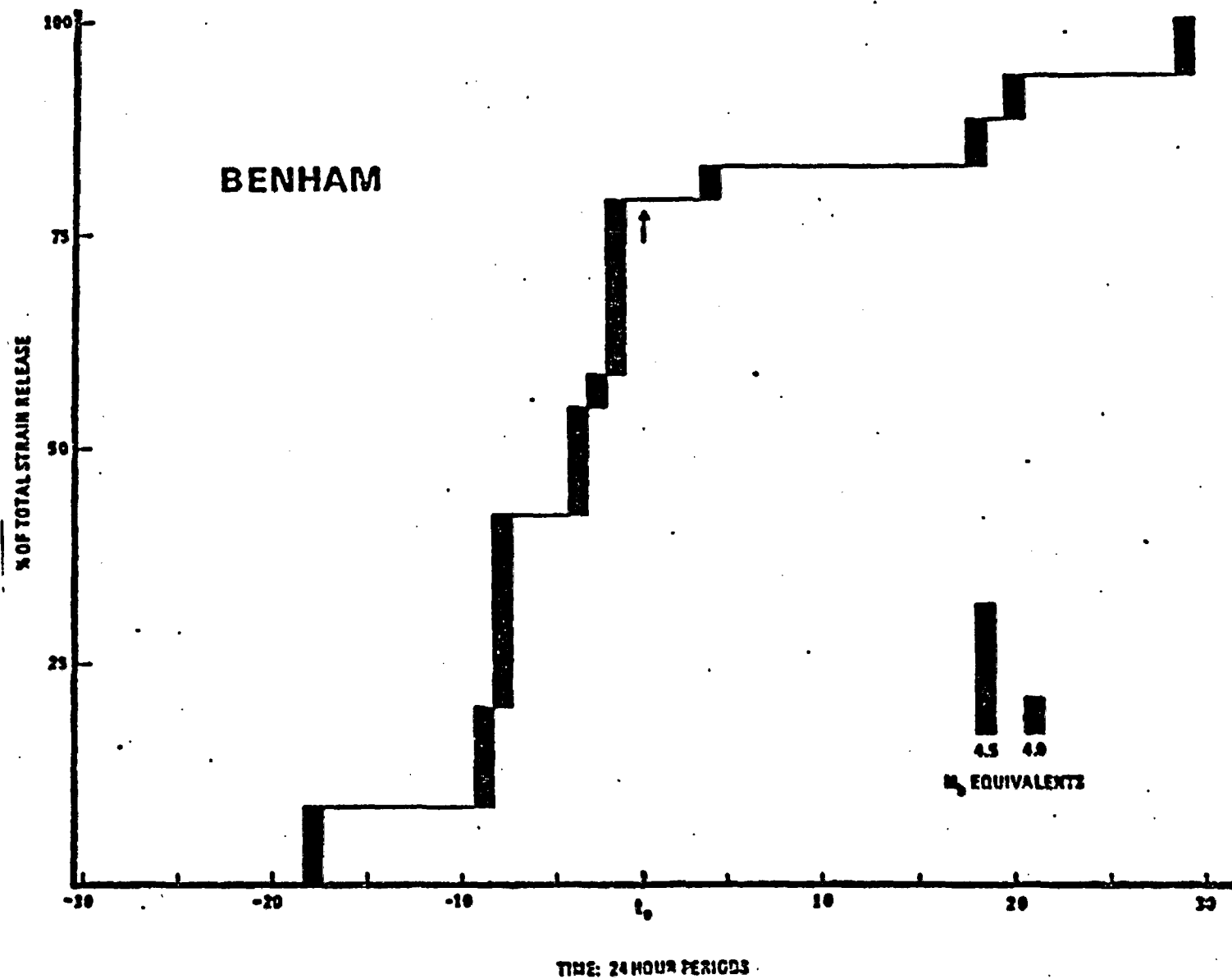


Figure 3.6-5. Cumulative daily strain release for the area between 50 and 1000 km of the BENHAM nuclear detonation. The cumulative daily strain release was calculated for each 24-hour period relative to t_0 , the time of BENHAM.

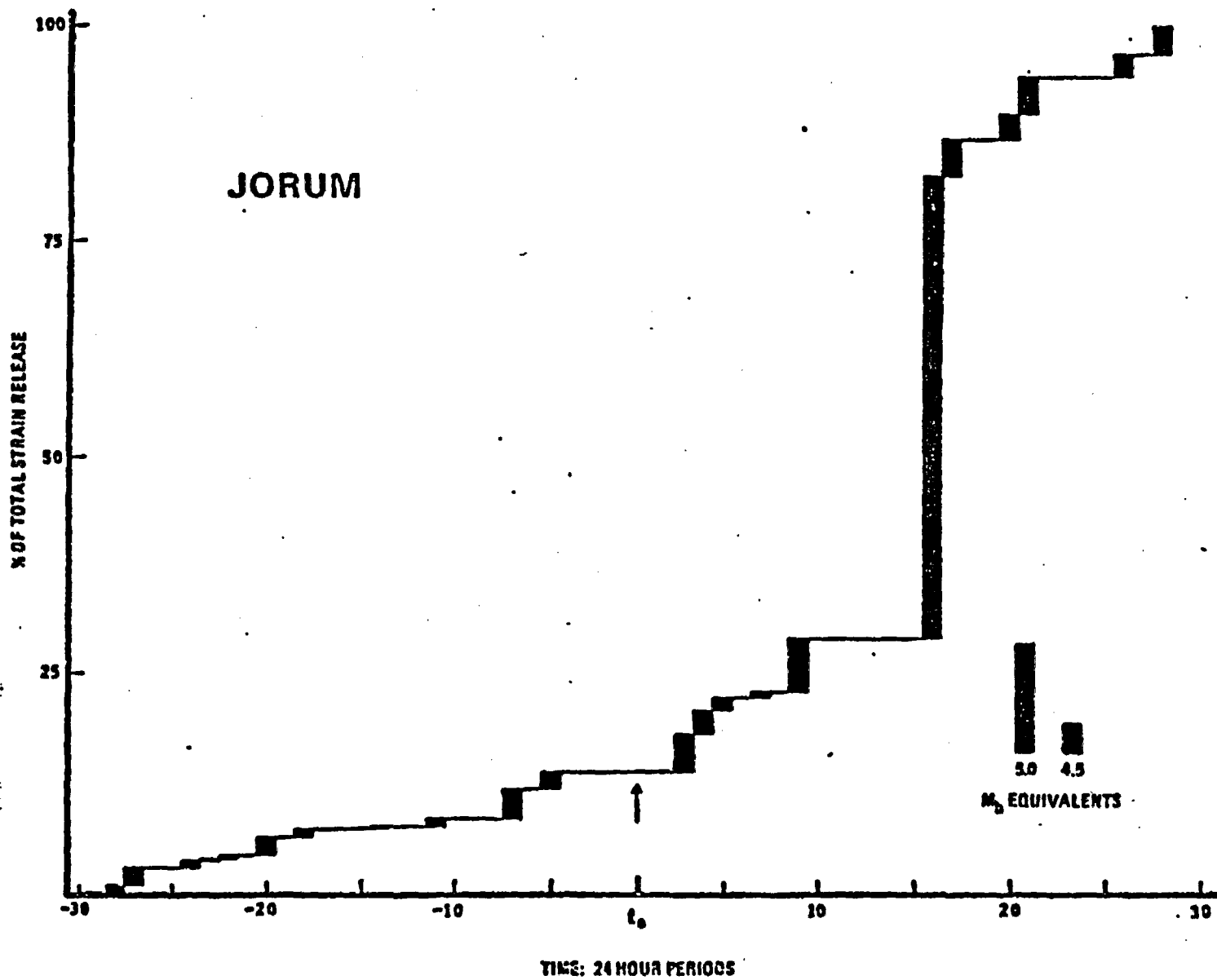


Figure 3.6-6. Cumulative daily strain release for the area between 50 and 1000 km of the JORUM nuclear detonation. The cumulative daily strain release was calculated for each 24-hour period relative to t_0 , the time of JORUM.

release does slightly increase following t_0 , compared to the rate during the 30-day period prior to t_0 , the amount of strain release during the nine days following the detonation (about 13 percent of the total strain release during the 60-day period) was not large compared to the observed strain release increase within the regional areas following the major earthquakes.

HANDLEY

Thirty-two earthquakes occurred within 1000 km of HANDLEY during the 60-day period centered on the detonation. Thirty of the earthquakes took place within the area at distances greater than 50 km from the shot point, and the remaining two earthquakes, aftershocks of the nuclear detonation, were located at distances less than 50 km.

The regional seismic activity depicted by the earthquake frequency does not increase following t_0 . Five earthquakes took place during the 5-day period following t_0 , compared to the seven earthquakes that took place during the 5-day period preceding t_0 .

The regional seismic activity depicted by the cumulative daily strain release does not rapidly increase following t_0 , even though 60 percent of the total strain release did take place during the 30 days following the detonation (Figure 3.6-7).

Discussion of the Regional Seismic Activity

A consistent pattern of regional seismic activity depicted as either the daily number of earthquakes or the cumulative daily strain release was not present among the four 60-day periods centered on BOXCAR, BENHAM, JORUM, and HANDLEY.

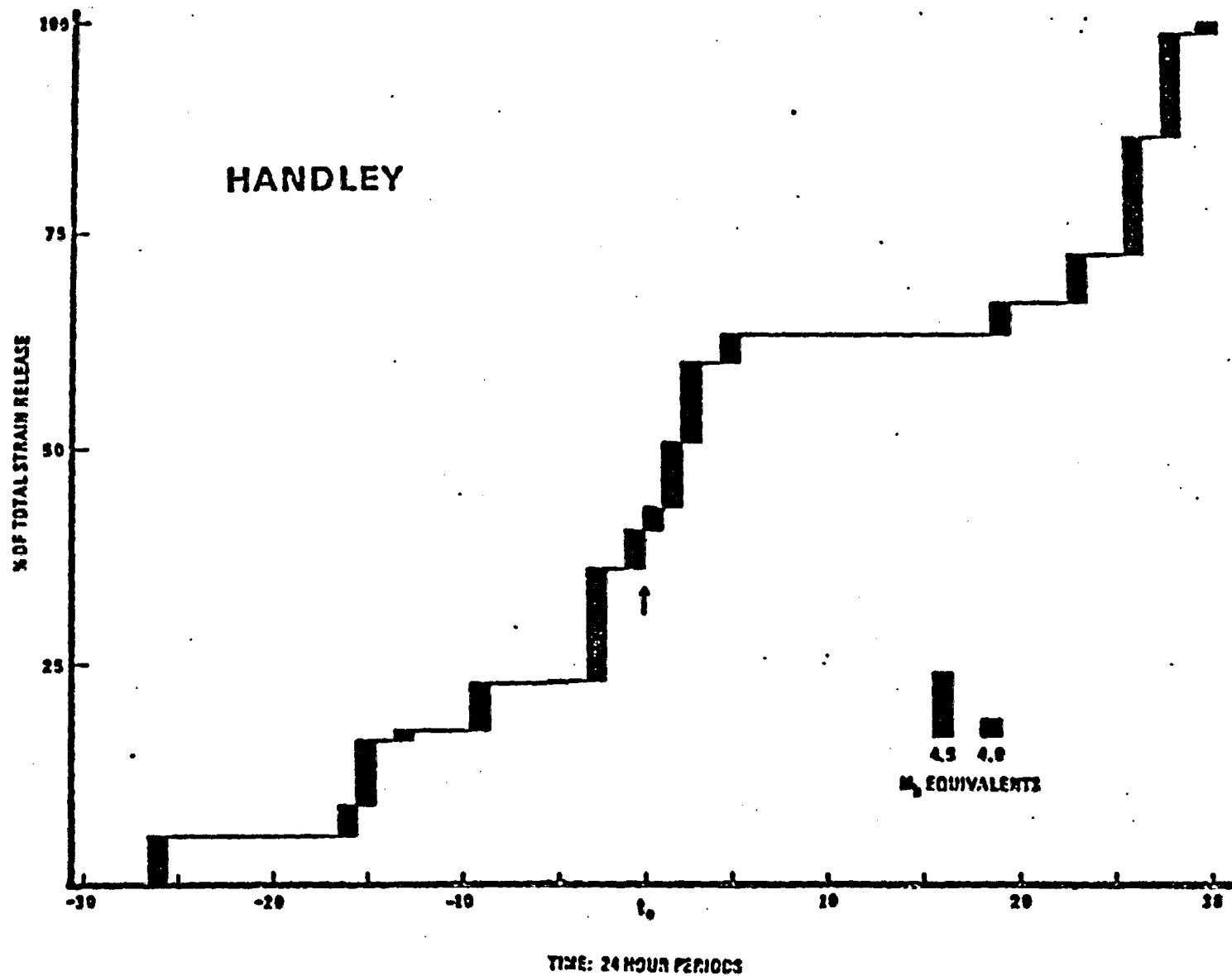


Figure 3.6-7. Cumulative daily strain release for the area between 50 and 1000 km of the HANDLEY nuclear detonation. The cumulative daily strain release was calculated for each 24-hour period relative to t_0 , the time of HANDLEY.

The same type of regional seismicity analysis, based on earthquakes reported by NEIS, was applied to the 60-day periods centered on the shot times of MILROW and CANNIKIN (two nuclear detonations that took place on Amchitka Island, about 50 km from the epicenter of the February 4, 1965 earthquake) by Willis and others (1972). MILROW was detonated on October 2, 1969, and with a yield of about 1 megaton, and CANNIKIN, the United States' largest underground nuclear detonation, was fired on November 6, 1971, with a yield of slightly less than 5 megatons.

The results of that seismicity study led to the conclusion that neither detonation affected the regional seismic activity, a conclusion also reported by Engdahl (1972) based on data obtained from the NOAA local Aleutian seismic station network.

3.6.2 Triggering of Microearthquakes by Tidal Forces

Groom Mine Microearthquake Activity

Many authors have investigated possible earthquake triggering by earth tides (Allen, 1936; Allen, 1958; Tamrazan, 1967, 1968; Dix, 1969). The term "trigger" refers to "that which initiates an event." To this date, on a global basis, no definite correlation has been shown to exist between earth tides and earthquakes. Allen (1936) pointed out that in attempts to cross-correlate earthquakes and earth tides, authors have concerned themselves with a region of too great an areal extent. Carrying the idea further, cross-correlation between earth tides and earthquakes would be best attempted when earthquake activity is abundant and confined in area. In a region of limited areal extent, the earth tides will be in phase and will potentially affect all the events at the same time. After-shock sequences or microseismic events, confined in area, would be best suited for this type of cross-correlation study.

In cross-correlation of aftershock sequences with earth tides, it is important that the orientation of the fault system along which the aftershocks are occurring be known. The best cross-correlation in terms of phase and lag will result when the aftershocks and the horizontal component of the earth tides parallel or normal to the orientation of the fault system are cross-correlated (Allen, 1936; Malone, 1972).

In a manner basically similar to that of Ryall, Van Wormer and Jones (1968), an hourly count of high frequency microearthquakes recorded by a high gain, high frequency seismograph station (Willis, 1970) located in an abandoned mine shaft at Groom Mine, Nevada, was cross-correlated with the theoretical total vertical earth tidal acceleration calculated at the seismograph station coordinates. Since most faulting in the Groom Mine area is dip-slip, vertical theoretical earth tides were used for this cross-correlation.

Figure 3.6-8 is a plot of the cross-correlation function. The time encompassed is from October 2, 1969 to October 5, 1969, in which 255 distinct microseismic events were recorded. The maximum positive correlation of 0.52 occurs at +4 hours lag and maximum negative correlation exists at -6 hours lag. This means the microearthquake activity peak leads the theoretical earth tidal acceleration maxima by four hours or lags behind an earth tidal acceleration minima by 6 hours. For the time window encompassed by the data, the probability that the two variables are uncorrelated is less than 0.001.

Since most microearthquakes are considered to have their origin below the surface affected by the daily heating and cooling cycle, it was felt that temperature triggering was not a likely cause of the microseisms.

GROOM MINE MICROEARTHQUAKE HOURLY COUNT
CROSS-CORRELATED WITH THEORETICAL EARTH TIDES

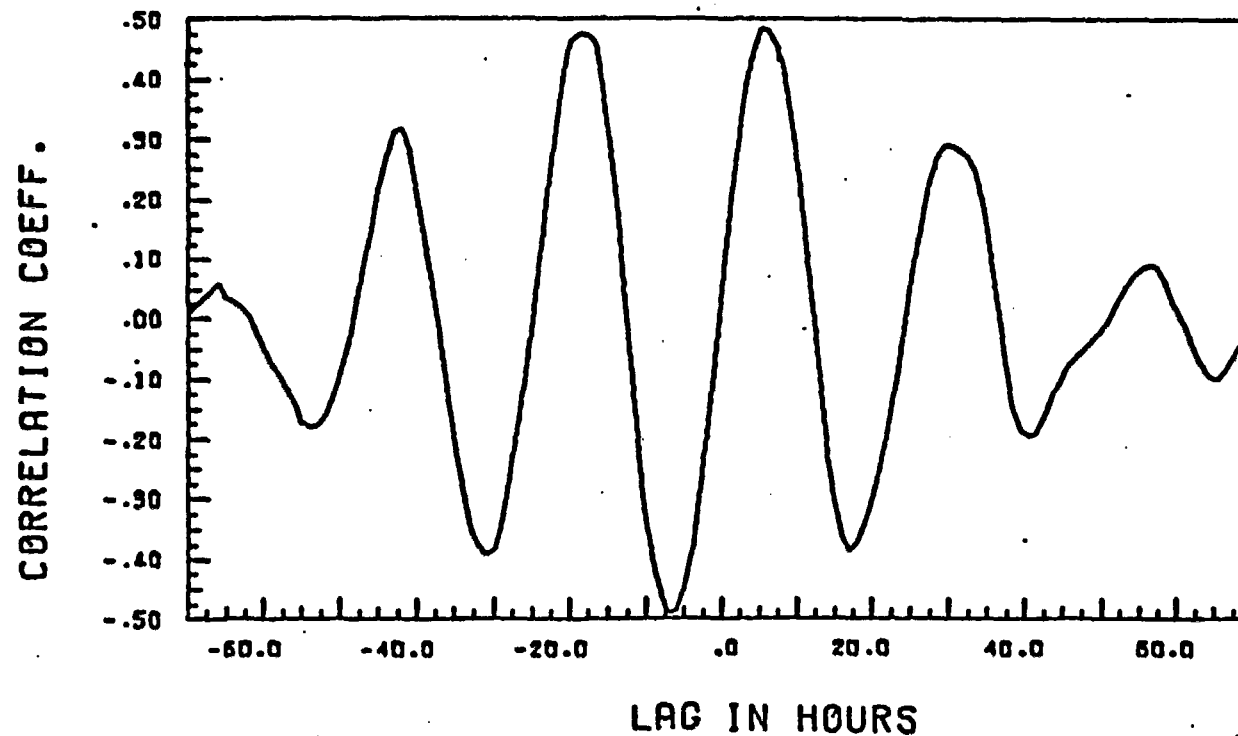
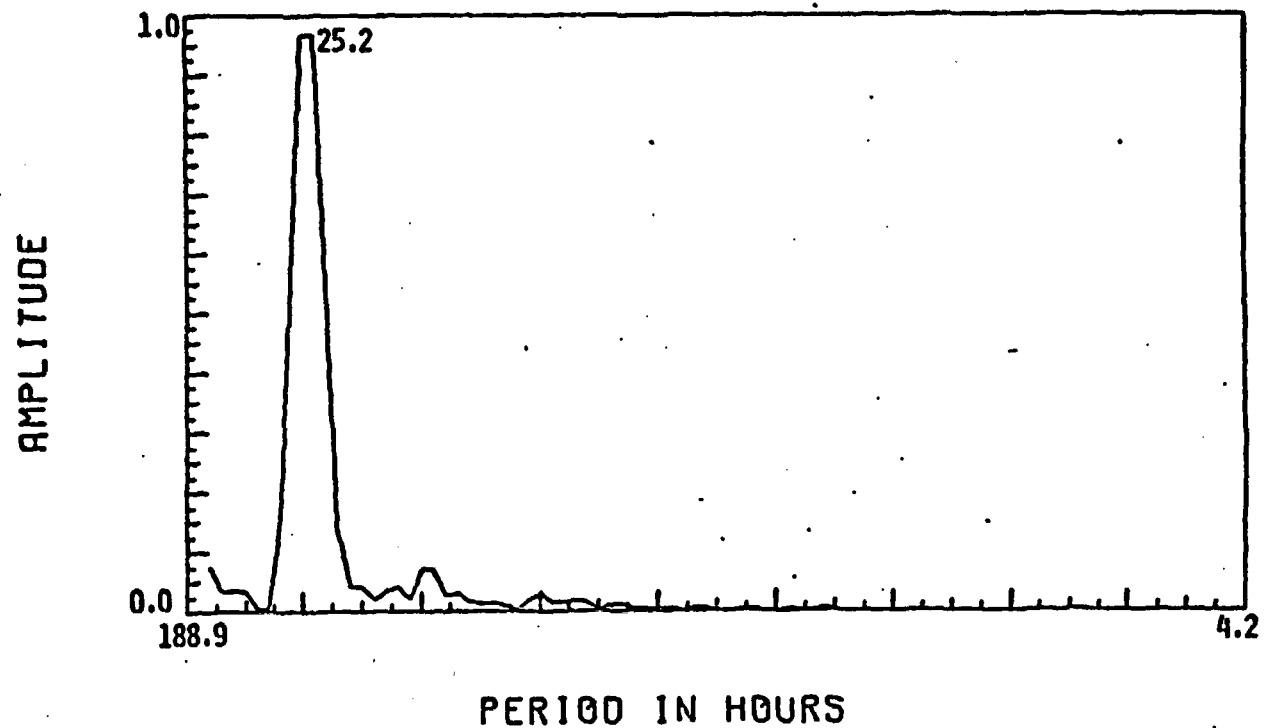


Figure 3.6-8. Plot of the cross-correlation function for Groom Mine, Nevada, microearthquake hourly count, cross-correlated with vertical theoretical earth tides, calculated using the Groom Mine seismograph station coordinates. The data interval is from October 2, 1969 to October 5, 1969.

Figure 3.6-9 shows the power spectral density plot for the cross-correlation of the microearthquake activity and theoretical earth tidal acceleration. The pronounced peak at 25.2 hours also serves to eliminate temperature as a possible cause for the microearthquakes. At the time increment of digitization used for this data, the peak value may be ± 0.75 hours from the time peaks shown. Referring back to Figure 3.5-14, note that the autocorrelation of the temperature shows a very narrow high peak at 24.0 hours which is outside the peak range for this cross-correlation. However, the O_1 tidal component (diurnal principle lunar wave) with a period of 25.81 hours falls within this range. The "triggering" of microearthquakes may be related more to the change in stress than to the actual peak stress value.

Figure 3.6-10 is a plot of the derivative of the theoretical earth tidal acceleration and the microearthquakes. There is a strong visual positive correlation between them, with the highest rate of change in the positive direction of earth tidal stress corresponding to the maximum microearthquake activity. Cross-correlating the derivative of the theoretical earth tides with the microearthquakes results in Figure 3.6-11. The maximum positive correlation of 0.38 occurs at 0 lag indicating the earth tidal derivative and microearthquake maxima are in phase. The correlation value has dropped from that of 0.52. In view of the additional high frequency noise which will result from differentiation of the earth tidal data, the difference between 0.52 and 0.38 is considered negligible. It is concluded from these data that for the Groom Mine area, the microearthquakes are strongly correlative with and possibly triggered by the rate of change of stress due to the solid earth tides.

GM MICROEQ. HOURLY COUNT CROSS-CORRELATED
WITH EARTH TIDES - POWER SPECTRA



207

Figure 3.6-9. Power spectral density plot of the cross-correlation function of Groom Mine, Nevada, (GM) microearthquake hourly count, cross-correlated with the vertical theoretical earth tides, calculated using Groom Mine seismograph station coordinates for the time period October 2, 1969 to October 5, 1969.

GROOM MINE MICROEARTHQUAKES
 PLOTTED AGAINST EARTH TIDES DERIVATIVE

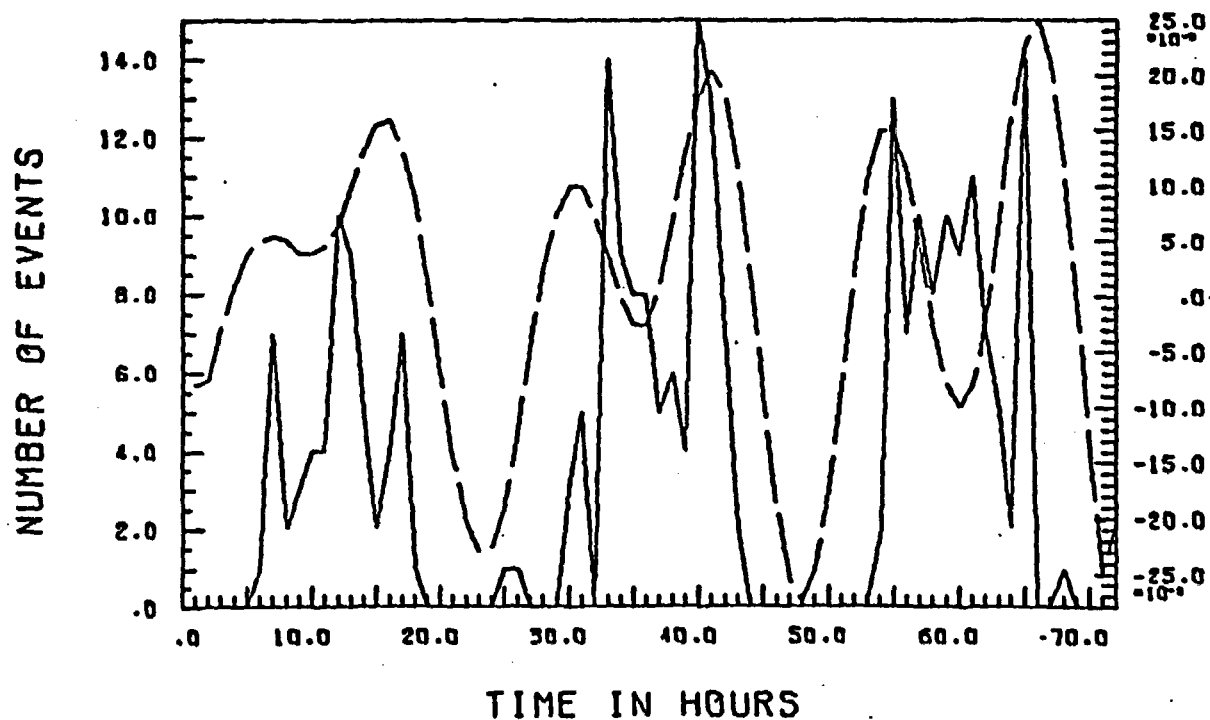


Figure 3.6-10. Overlay plot of Groom Mine, Nevada, microearthquake hourly count (solid line) and the derivative of the vertical component of the theoretical earth tides (dashed line), calculated using the Groom Mine seismograph station coordinates. The data interval is from October 2, 1969 to October 5, 1969. 0 time corresponds to 21:00 hours GMT, October 2, 1969.

GROOM MINE MICROEARTHQUAKES
CROSS-CORRELATED WITH EARTH TIDES DERIVATIVE

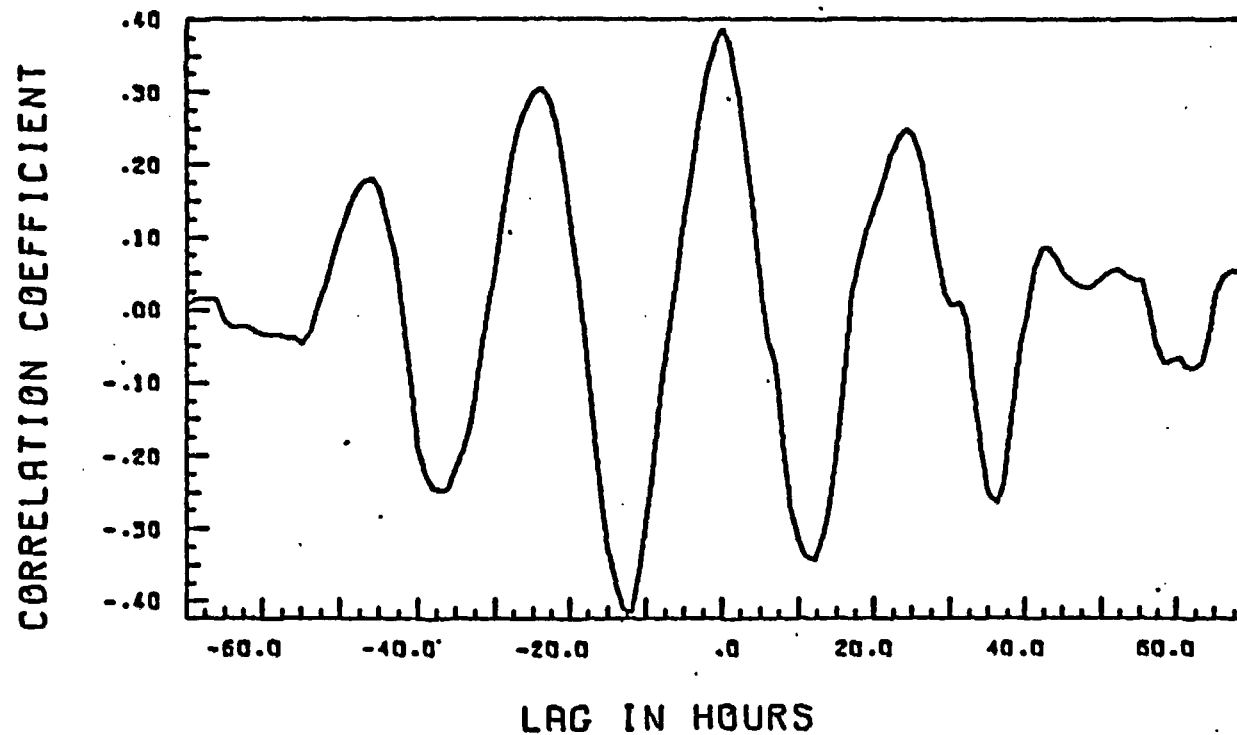


Figure 3.6-11. Plot of the cross-correlation function for Groom Mine, Nevada, microearthquakes hourly count, cross-correlated with the derivative of the vertical theoretical earth tides, calculated by using the Groom Mine seismograph station coordinates. The data interval is from October 2, 1969 to October 5, 1969.

To investigate this correlation further, horizontal theoretical strain data were obtained from Dr. C. G. Bufe of the U.S.G.S. for the Groom Mine site for the same time period mentioned above. These data were cross-correlated with the seismicity. The results are summarized in Table 3.6-1.

TABLE 3.6-1

Correlation between Seismicity and Horizontal Strain

Horizontal Strain Component	0°	45°	90°	315°
Cross-Correlation Coefficient	.55	.60	.62	.58
Seismicity Lead Ahead of Maximum Strain (Hours)	5-6	6	6	5

3.6.3 Triggering of Earthquakes in the Central California Area

In the two previous parts of this section, triggering of earthquakes by nuclear shots at distances out to 1000 km and the triggering of micro-earthquakes by tidal forces over a small area, were discussed. The seismograph station coverage for these two cases was quite different. In the first case, the stations of the WSSN and the Cal Tech-Berkeley nets were used, while the latter case involved a very high gain station monitoring events that were located within several kilometers of the station. This portion of the report deals with an area in central California that has a high density of seismograph station coverage. This is in an active seismic area and includes a portion of the San Andreas fault and the Calaveras and Hayward faults. The study area is shown in Figure 3.6-12. The recording stations range in distance from 400 to 500 km from the Nevada Test Site.

The period of time covered by this study is two years, 1969 and 1970. The U.S.G.S. National Center for Earthquake Research and other institutions operated 83 short-period vertical seismographs in this area during 1969. They recorded and located 1190 earthquakes in the study area during 1969. In 1970 their seismograph network was expanded to include 109 stations in the same area. Because of the increased station coverage the zone of reliable location was increased by 119 percent. A total of 2319 earthquakes were recorded in 1970 in the study area, an increase of 95 percent over the previous year. The magnitudes ranged from -0.1 to 5.8.

This high density of seismograph stations that were in continuous operation over a two year time period provided an opportunity to correlate the seismicity of the area with the underground nuclear testing program

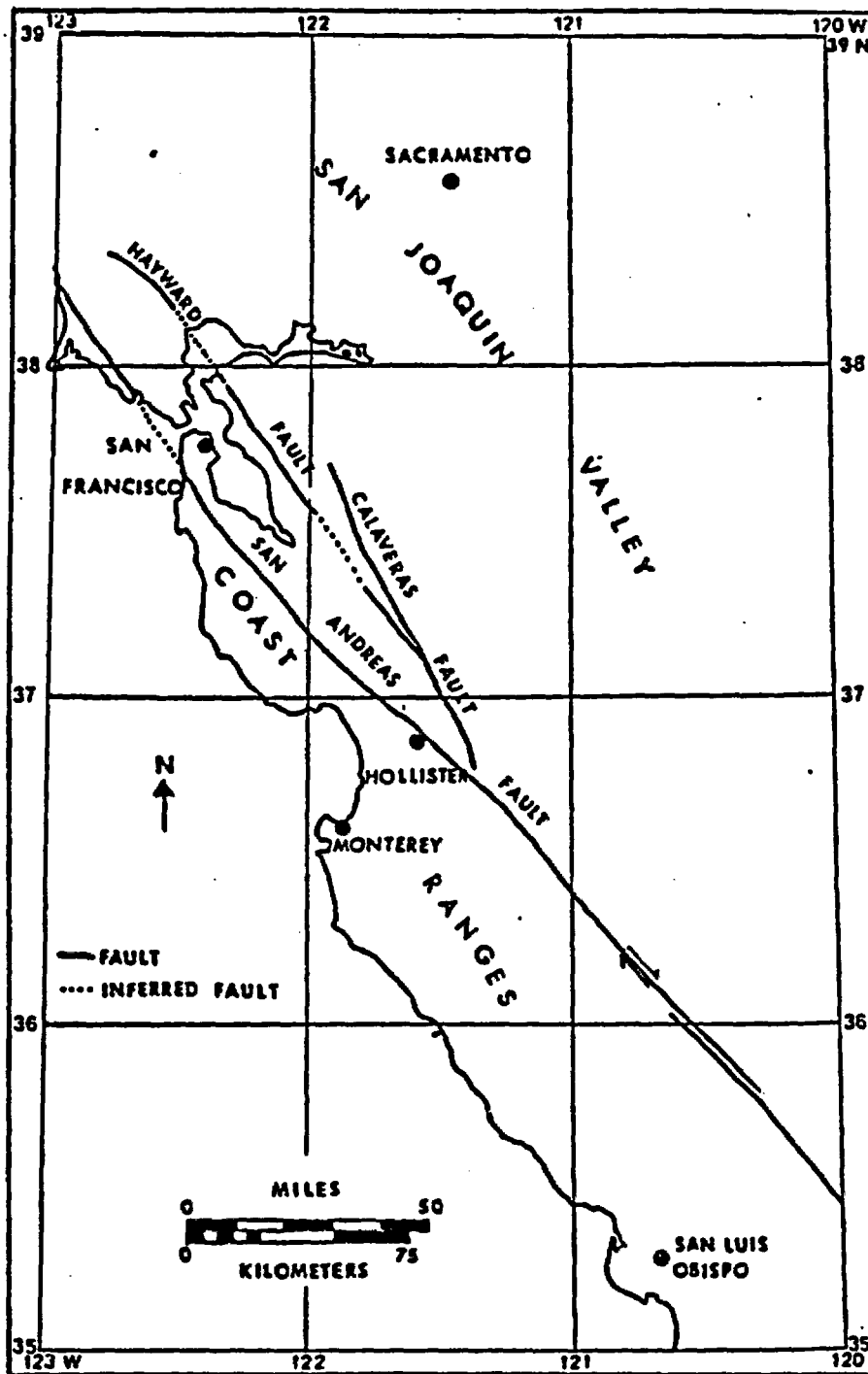


Figure 3.6-12. Location of the San Andreas Fault System in Central California, 35°N, 120°W, to 39°N, 123°W.

at the Nevada Test Site and with the solid earth tides in order to determine if there were any triggering effects. The gravity data were obtained from published tidal tables and from a theoretical tidal acceleration computer program obtained from the National Center for Earthquake Research. Information on daily celestial events were obtained from Long (1968, 1969, 1970).

A detailed study was made (Revoek, 1974) of the relationship between the number and time of occurrence of earthquakes in the study area and the vertical component of gravity along with the occurrence of celestial events and underground nuclear shots. A total of 730 24-hour data sets were plotted in order to investigate any possible correlation of these parameters. Examples are shown in Figures 3.6-13 to -15. The latter two figures cover the time periods when JORUM and HANDLEY were detonated. It can be seen that the shots caused no detectable increase in seismicity in the study area. The cumulative results from all of the hourly studies of graph sets for days of nuclear detonations are as follows: 19% of the detonations were followed by an increase in the seismicity pattern of the study area, 9% were followed by a decrease in seismicity, 36% had no change in the seismicity pattern, and 36% had no earthquakes before and after the detonation; hence, there was no change in the seismicity pattern. The results from this part of the investigation indicate clearly that at least 81% of the 1969-70 NTS detonations did not trigger any significant earthquake activity in the study area within the day of the detonation. The remaining 19% did not include any of the larger shots. Hence, this increase in seismic activity following these shots is interpreted to reflect the random nature of the seismicity and not reflect a triggering mechanism caused by the shots.

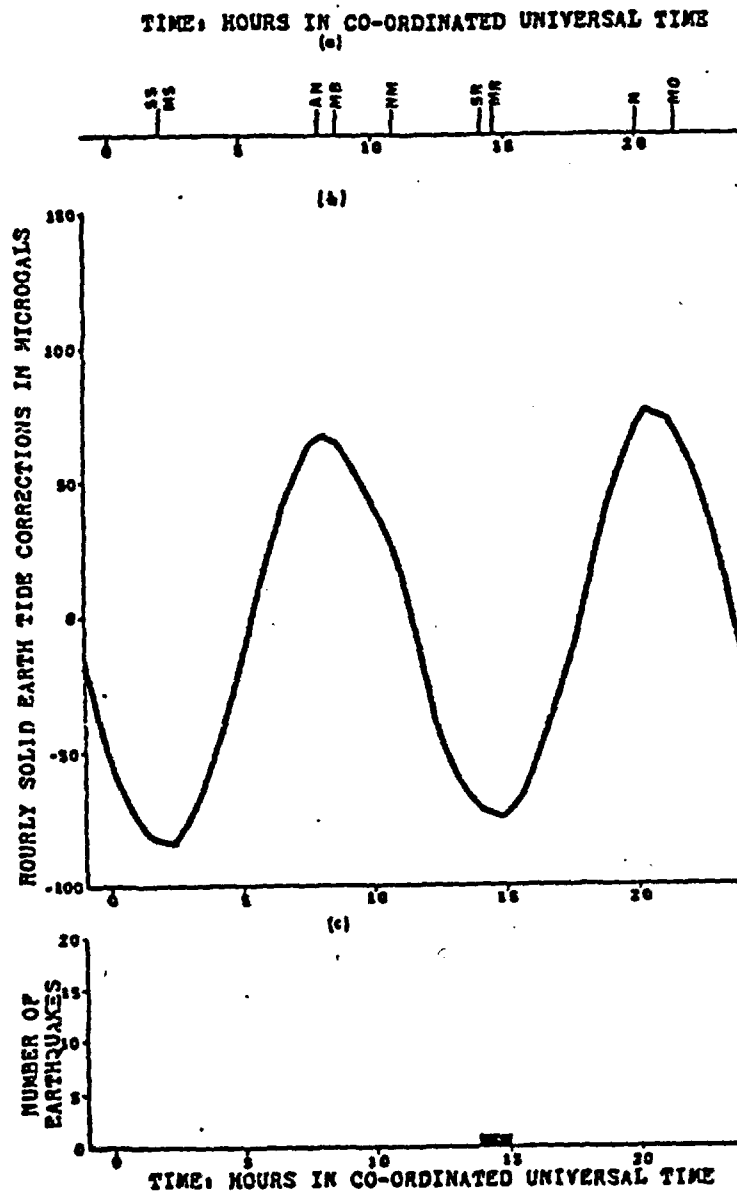


Figure 3.6-13. Celestial events, hourly variations in gravity, and number of earthquakes in the San Andreas Fault System study area during day number 77, Mar. 18, 1969. (a) Celestial events: SS = sunset, MS = moonset, AN = midnight, MB = moon-midnight, NM = new moon, SR = sunrise, MR = moonrise, N = noon, and MO = moon-noon. (b) Hourly variations in the vertical component of gravity at locality 37°N , 120°W , sea level. (c) Number of earthquakes within each hour.

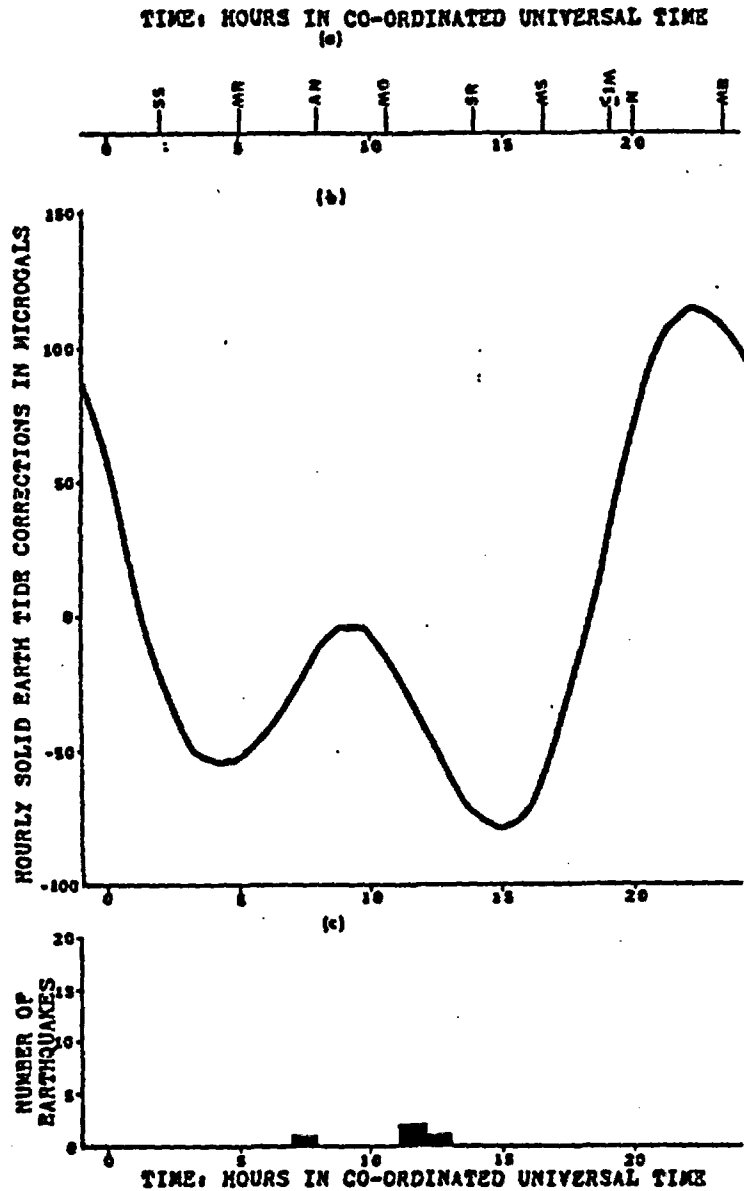


Figure 3.6-15. Celestial events, hourly variations in gravity, and number of earthquakes in the San Andreas Fault System study area during day number 450, Mar. 26, 1970, the day of the nuclear event HANDLEY. (a) Celestial events: SS = sunset, MR = moonrise, AN = midnight, MO = moon-noon, SR = sunrise, MS = moonset, N = noon, and MB = moon-midnight. Nuclear event HANDLEY: ≥ 1 M = greater than or equal to one megaton. (b) Hourly variations in the vertical component of gravity at locality 37°N , 120°W , sea level. (c) Number of earthquakes within each hour.

These graphs also showed a very low degree of correlation between seismicity during the two year period and the theoretical vertical component of earth tides. However, some increase in seismicity was observed during the periods when the first time derivative of the theoretical vertical earth tides was near zero.

Figures 3.6-16A through -16L are 60-day daily data sets for the first 720 days of the 730 day study. Part A shows the celestial event times; vertical ticks correspond to the days of the lunar phases and apsides, earth apsides, solstices, and equinoxes. Part B shows the days that underground nuclear detonations occurred. Part C is a display of the daily cumulative earthquake elastic strain release. The 60-day total cumulative elastic strain release for the 60-day sequence is at the upper left corner of the graph. Part D is the daily seismicity during the interval. The bar graph represents the number of earthquakes per day, the curved line the five day moving point average number of earthquakes per day, and the horizontal line the average number of earthquakes per day for the entire 60-day interval.

Using the data in Figure 3.6-16 a longer time window was examined to investigate any delayed effects that the underground testing program might have had on the natural seismicity in the study area. The time window that was used, centered on each shot, was 2-3 days before and 3 days after the shot. Both the number of earthquakes and the strain release were computed for each time period. The results are summarized in Table 3.6-2.

It can be seen from the above that 45% of the nuclear shots were followed by an increase in seismicity, 17% of the shots were followed by a decrease in seismicity, and 38% were followed by no change. The 45%/55%

- Figure 3.6-16
- A. Time period 1/1/69 through 3/1/69.
 - B. Time period 3/2/69 through 4/30/69.
 - C. Time period 5/1/69 through 6/29/69.
 - D. Time period 6/30/69 through 8/28/69.
 - E. Time period 8/29/69 through 10/27/69.
 - F. Time period 10/28/69 through 12/26/69.
 - G. Time period 12/27/69 through 2/24/70.
 - H. Time period 2/25/70 through 4/25/70.
 - I. Time period 4/26/70 through 6/24/70.
 - J. Time period 6/25/70 through 8/23/70.
 - K. Time period 8/24/70 through 10/22/70.
 - L. Time period 10/23/70 through 12/21/70.

Celestial events, nuclear events, strain release, and number of earthquakes in the central California study area.

- A. Celestial events: FQ = first quarter, LQ = last quarter, FM = full moon, NM = new moon, A = apogee, P = perigee, VE = vernal equinox, AE = autumnal equinox, SS = summer solstice, WS = winter solstice, AP = aphelion, PE = perihelion.
- B. Nuclear events in relative yield categories: L = low, L-I = low-intermediate, I = intermediate, L-M = low megaton, M = megaton.
- C. Cumulative strain release during 60-day interval.
- D. Number of earthquakes within each 24-hour period. The curved line is the five-day moving point average number of earthquakes per day, and the horizontal line is the average number of earthquakes per day during the 60-day interval.

Figure 3.6-16A

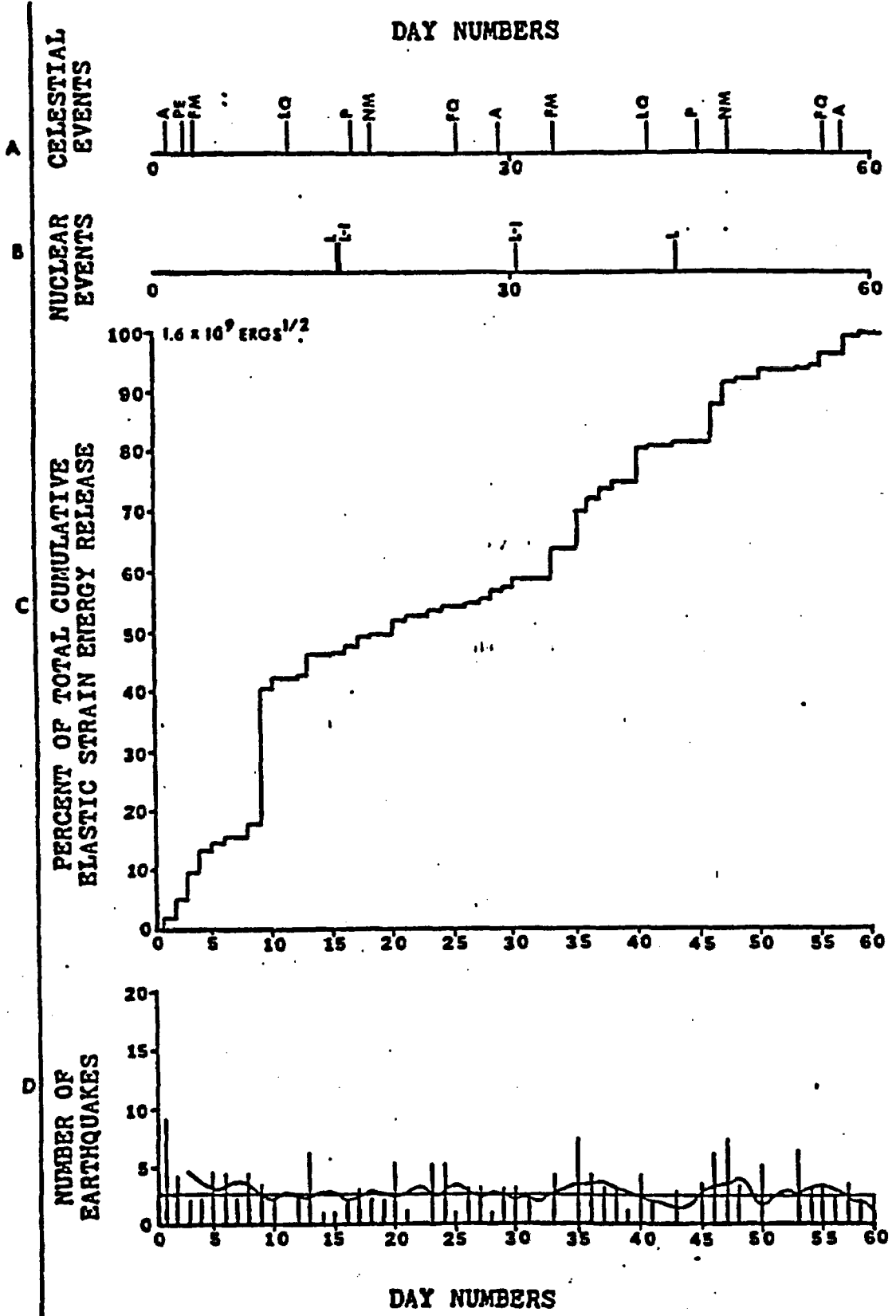


Figure 3.6-16B

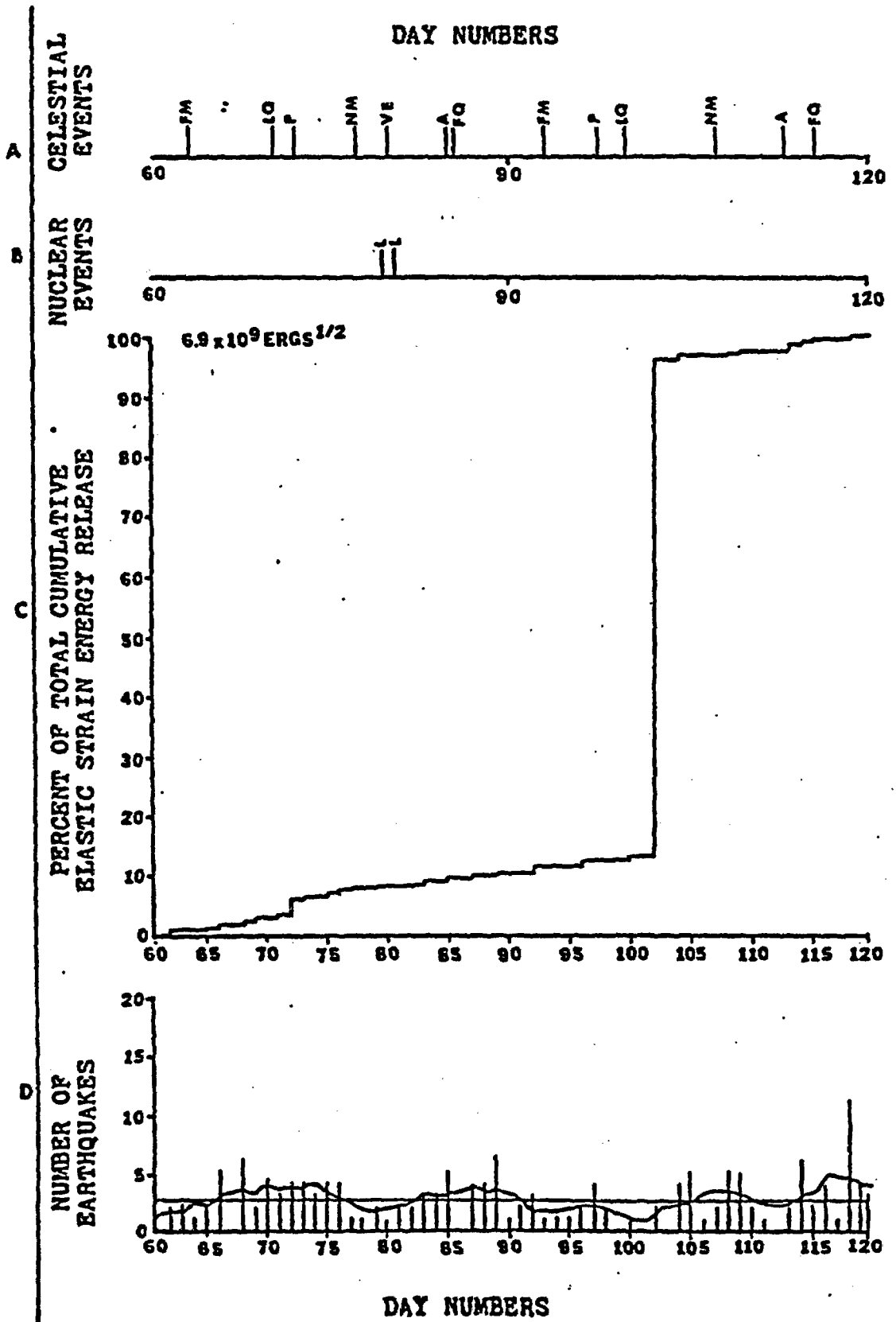


Figure 3.6-16C

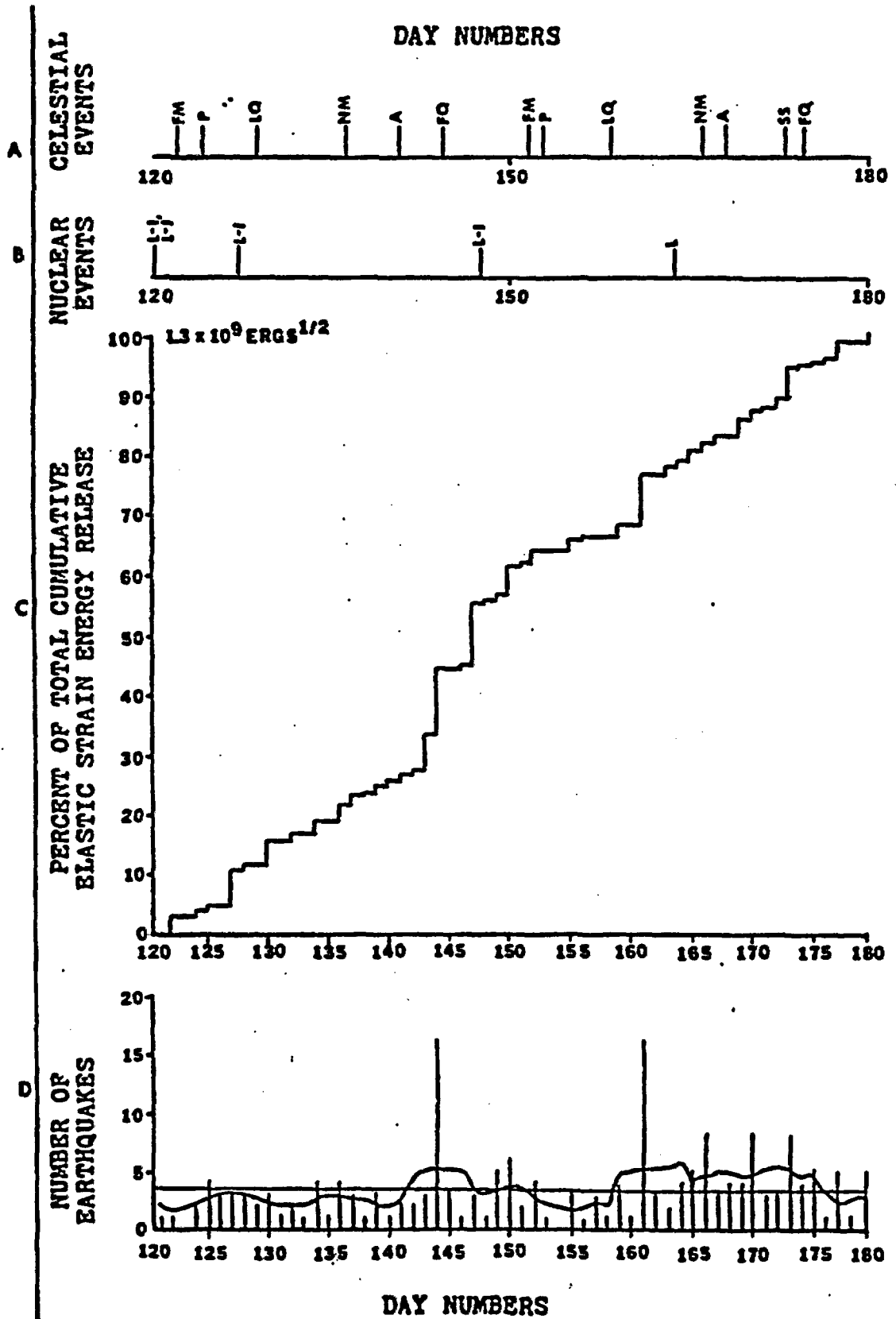


Figure 3.6-16D

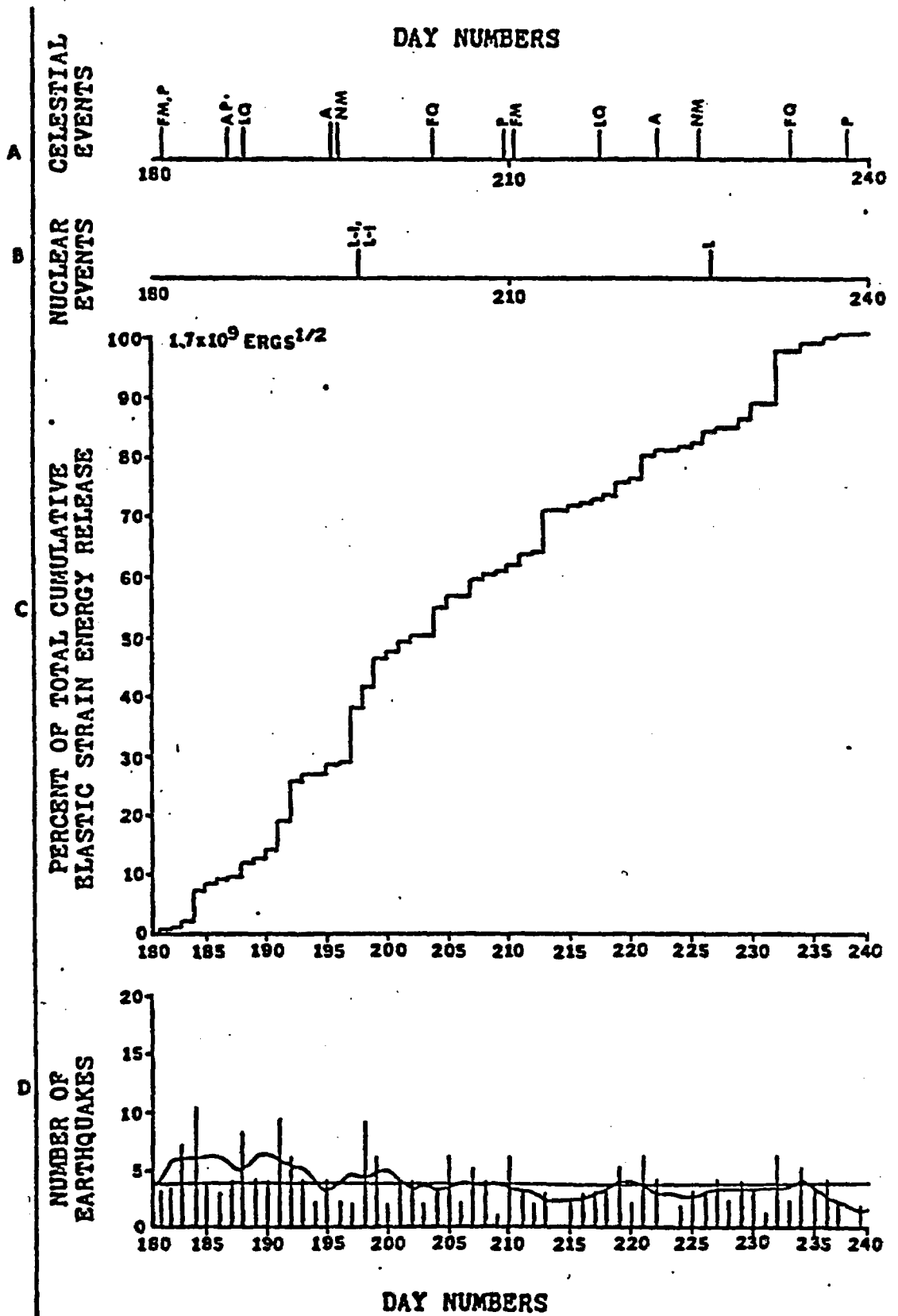


Figure 3.6-16E

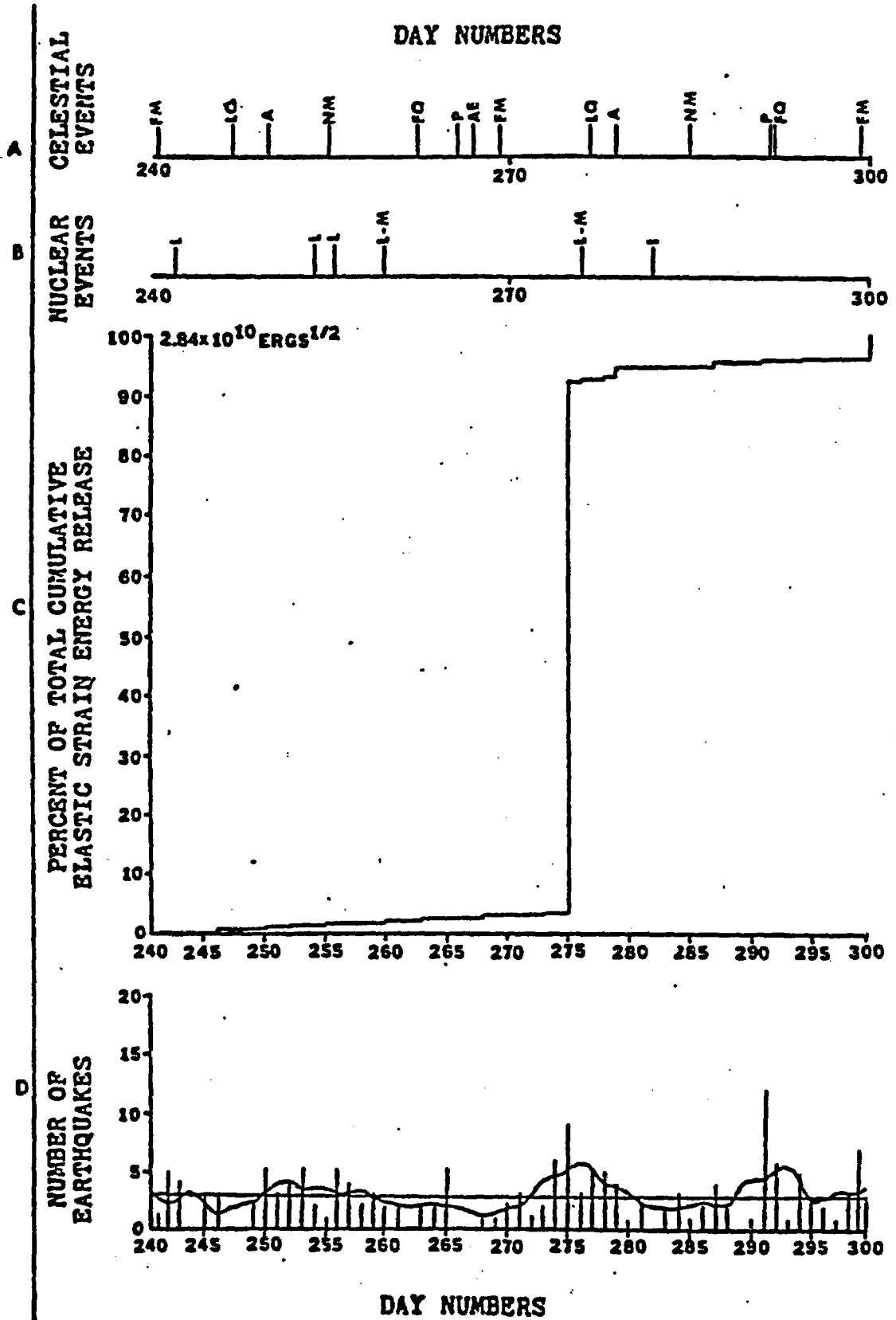


Figure 3.6-16F

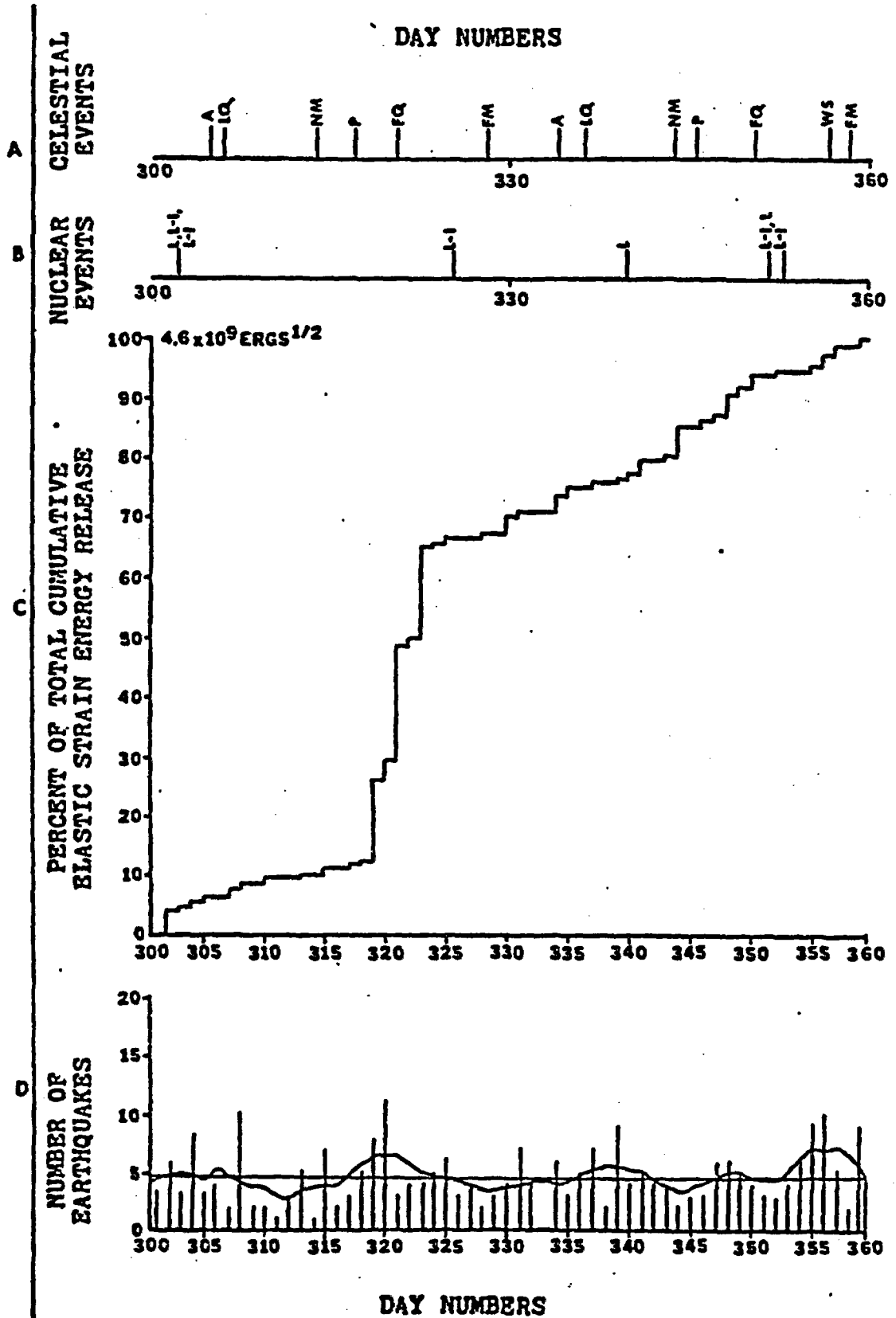


Figure 3.6-16G

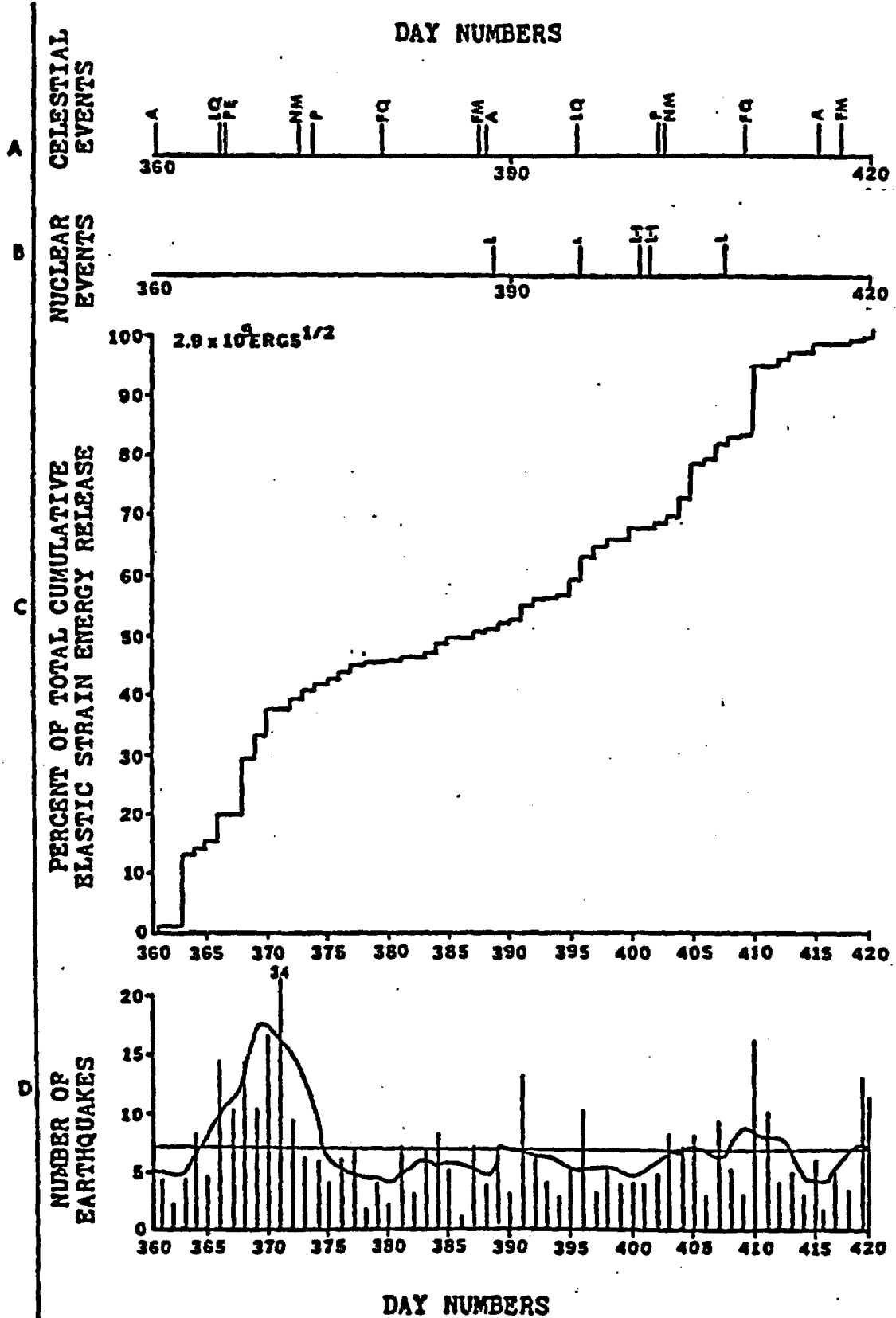


Figure 3.6-16I

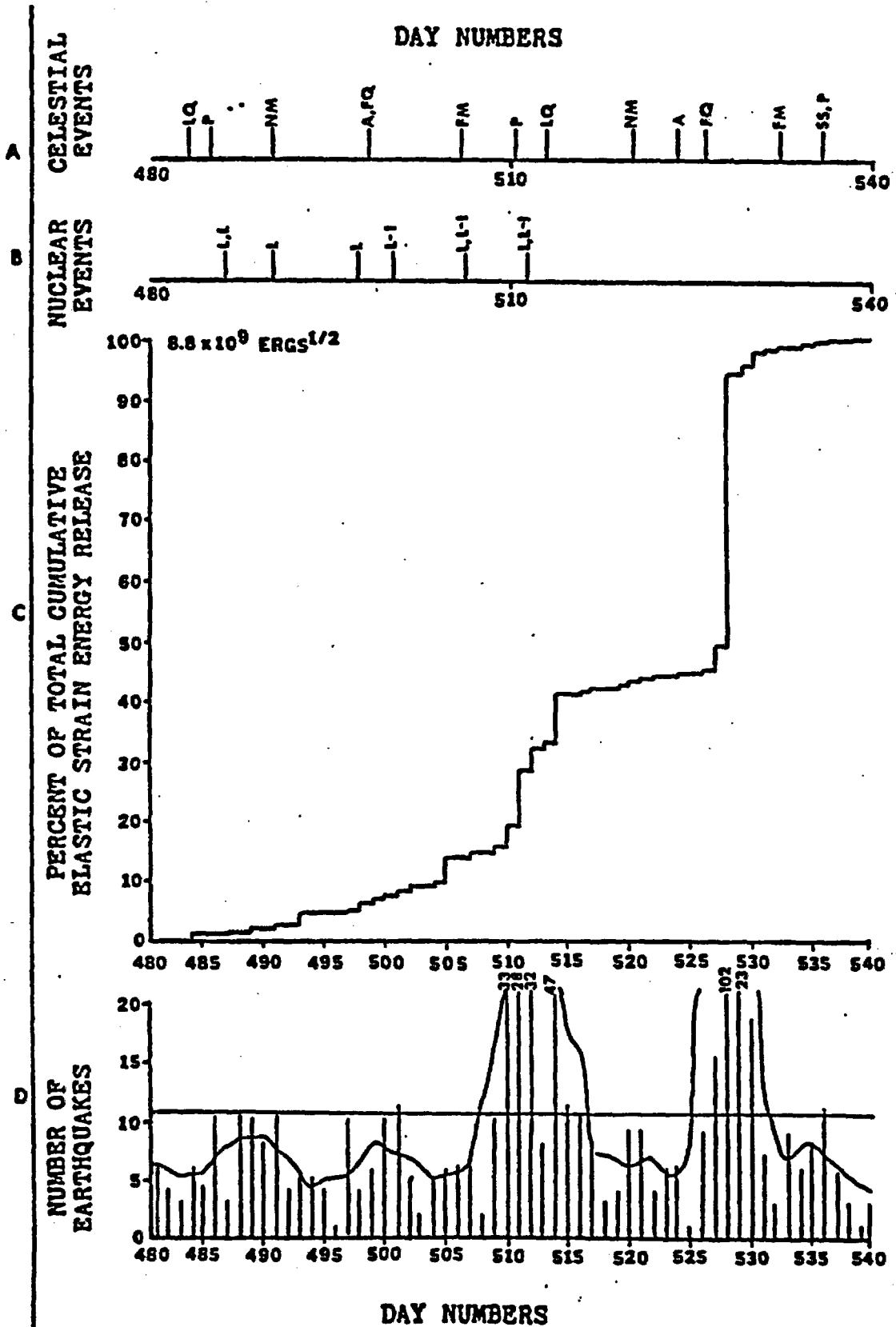


Figure 3.6-16J

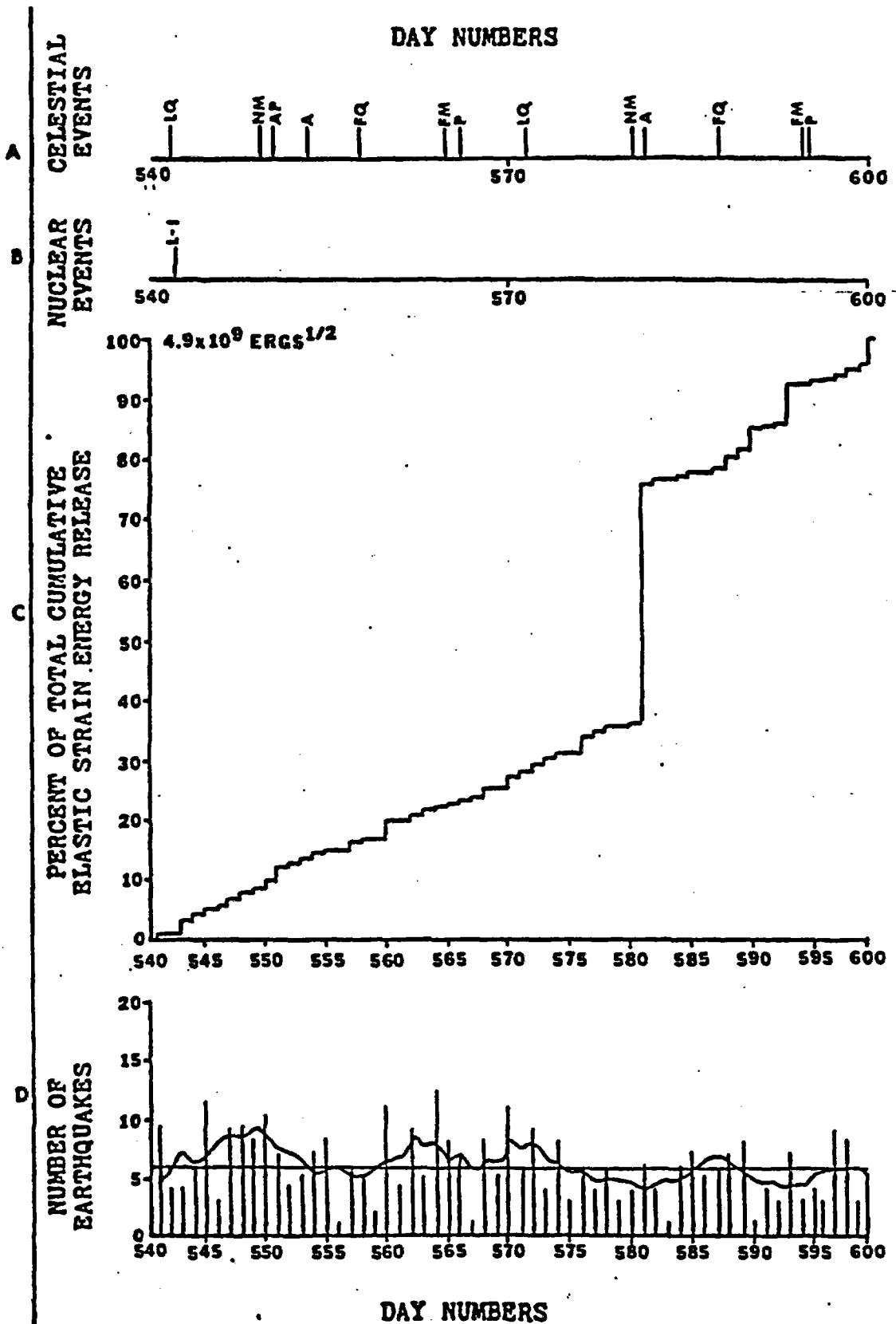


Figure 3.6-16K

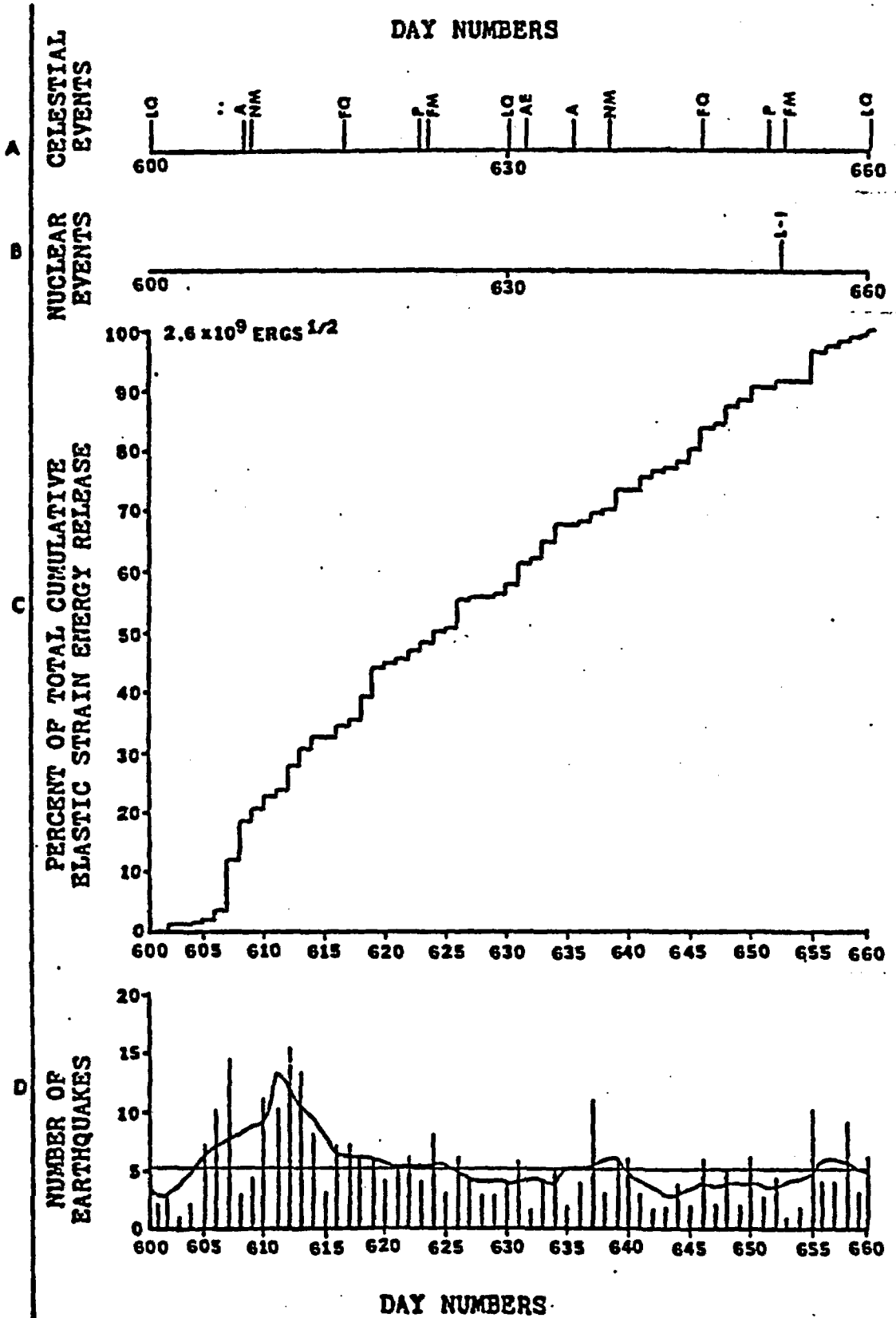
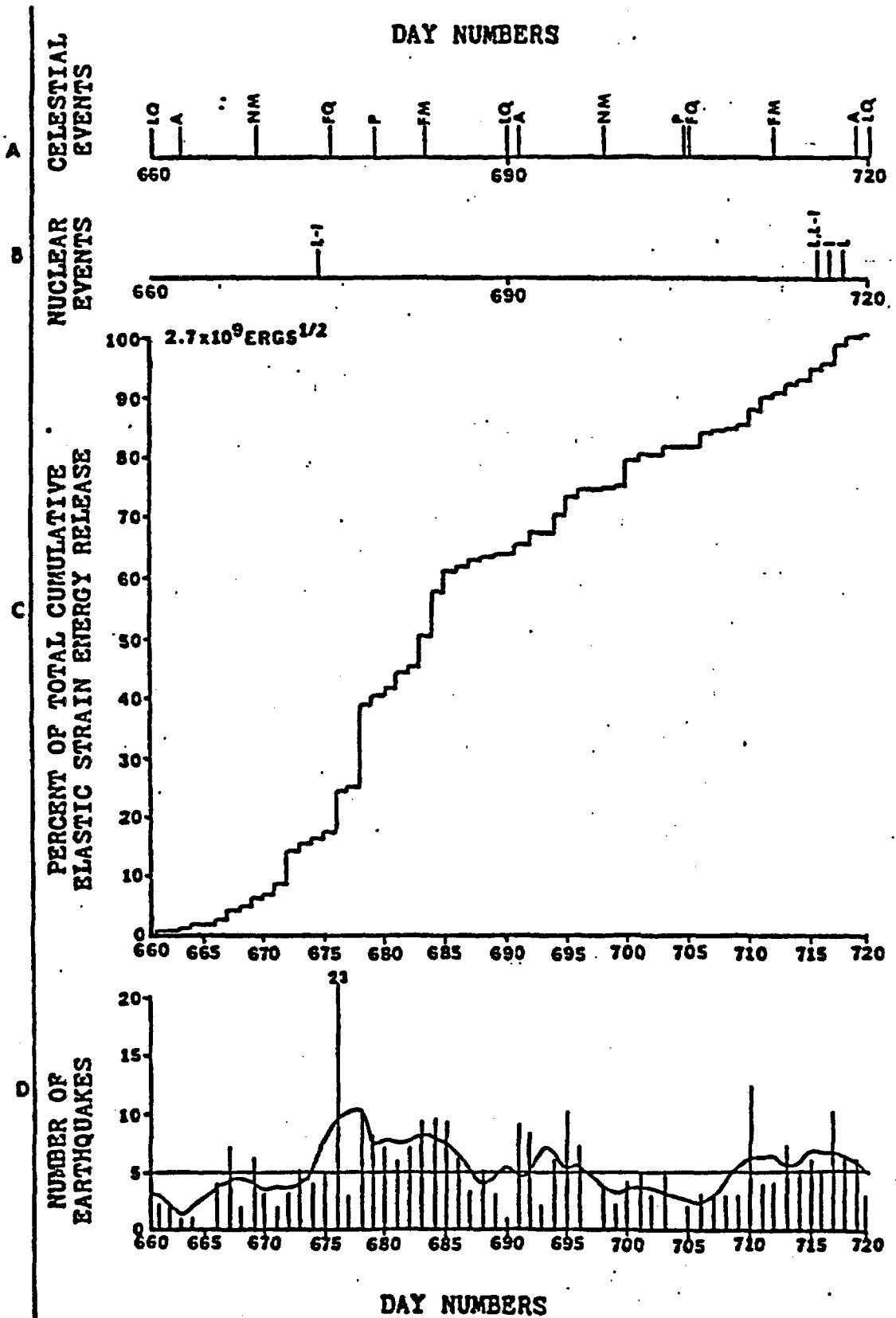


Figure 3.6-16L



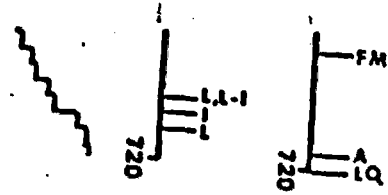


TABLE 3.6-2

Visual Comparison between Nuclear Detonations, Seismicity and Strain Release

Visual Window Number	Number of Nuclear Events	Seismicity			Earthquake Elastic Strain Release		
		% Increase	% Decrease	% Same	% Increase	% Decrease	% Same
1	4	0	50	50	50	0	50
2	2	100	0	0	0	0	100
3	5	80	20	0	40	20	40
4	3	100	0	0	0	0	100
5	6	17	17	66	0	33	67
6	8	37	25	38	12	88	0
7	5	20	0	80	80	20	0
8	9	33	22	45	33	0	67
9	9	78	22	0	33	11	56
10	1	0	0	100	0	0	100
11	1	100	0	0	0	0	100
12	5	20	0	80	20	0	80
13	0	-	-	-	-	-	-
2-Year Total Events		58					
		26	10	22	16	12	30
2-Year Total Percentage							
		45	17	38	27	21	52

relationship is close to the 50%/50% relationship one would expect for a random pattern of seismicity. The elastic strain release percentages also clearly show no increased seismic activity following the shots.

Similar comparisons were made for the 60-day data sets (Figure 3.6-16) between elastic strain release and lunar episodes (apogee and perigee), syzygy and quadrature. Only low degrees of correlation were found. More information on this subject may be found in Revock (1974).

Figure 3.6-17 is a display of the monthly average number of earthquakes per day for the 1969-70 study interval. The secular celestial events have been included also. This graph was produced to show the 1969-70 cumulative seismicity.

Figure 3.6-18 is a display of the 30-day increases in elastic strain energy release for 1969-70. This graph was produced in order to show the relationship between the 60-day elastic strain energy release graphs. A change in the rate of elastic strain energy release at the end of 1969 was observed. The rate increases at the end of 1969 and remains at the higher level throughout the rest of the study interval. This increased rate can be directly correlated with the 119% increase in the zone of reliable location at the end of 1969 due to the increased number of seismograph stations put into operation. The number of study area earthquakes detected in 1970 was 95% greater than the number of study area earthquakes detected in 1969.

In order to obtain quantitative results to compare with the visual correlations discussed above, approximately 58% of the two-year data set was digitized to facilitate computational procedures. Seven 60 to 62 day sub-data sets were compiled. Seismicity and strain release were cross-correlated with the theoretical vertical and horizontal components of the

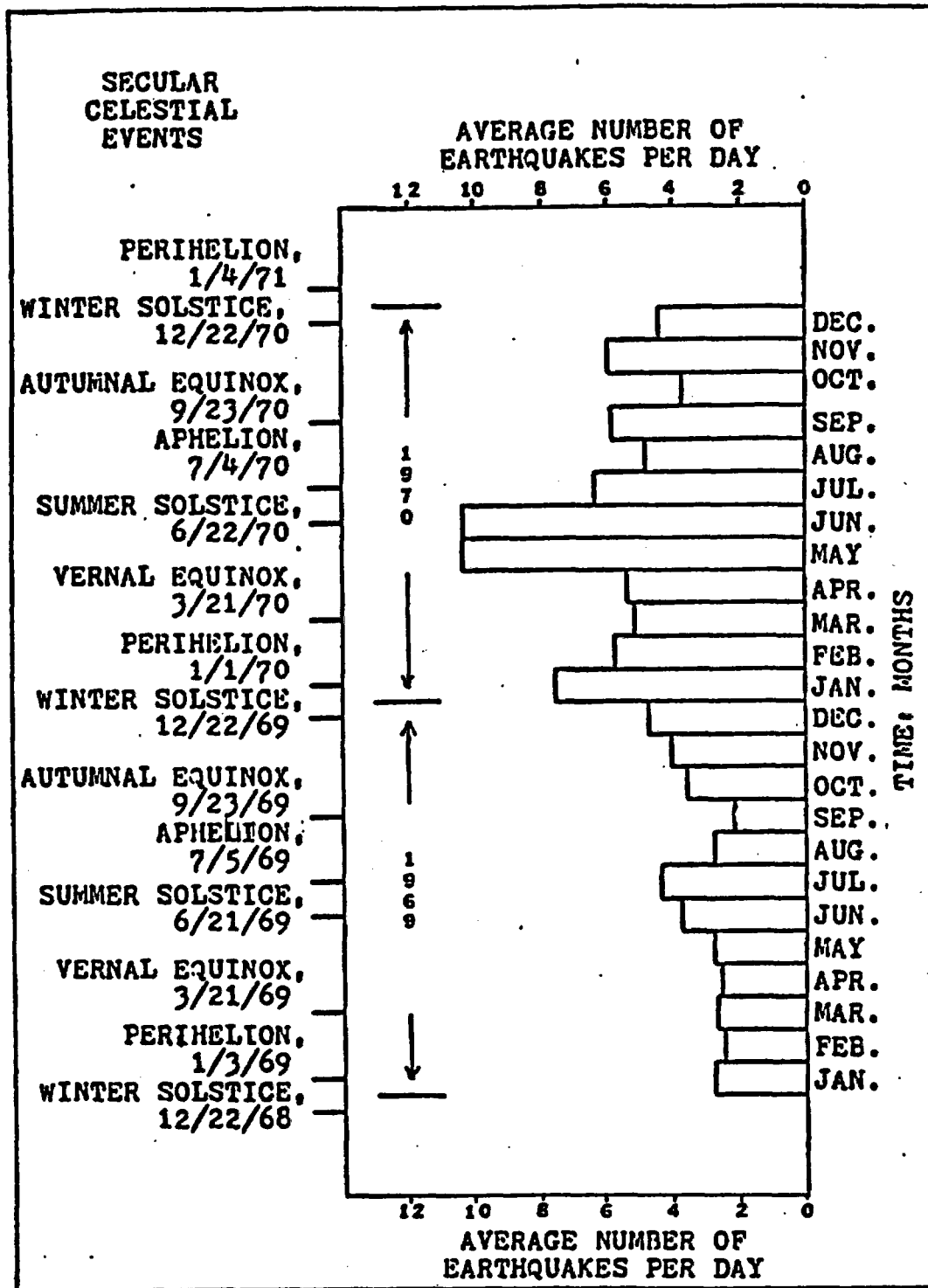


Figure 3.6-17. Two year, 1969-70, average monthly seismicity and secular celestial events in the central California study area.

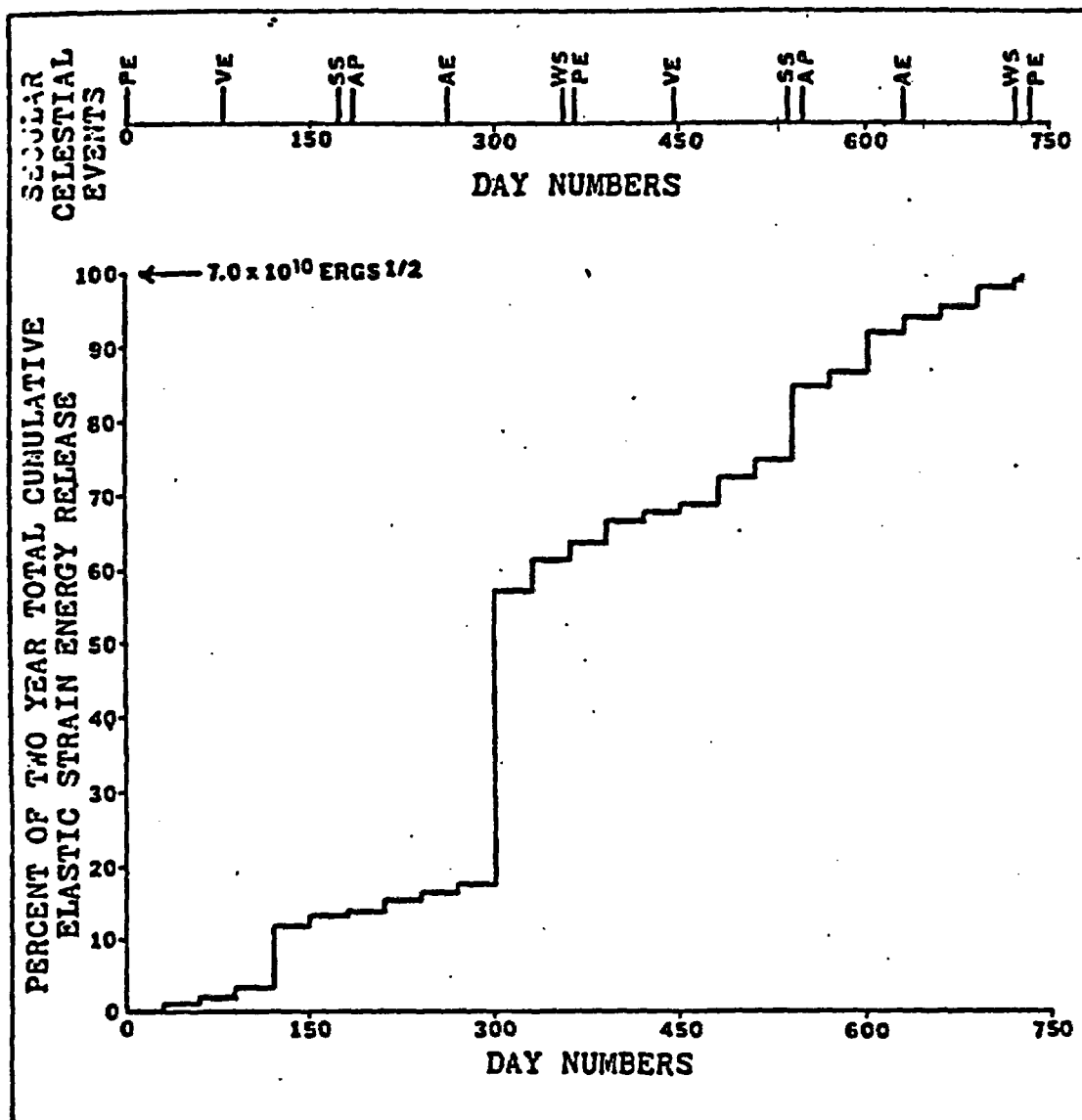


Figure 3.6-18. Two year, 1969-70, total cumulative elastic strain energy release in the central California study area. Secular celestial events within the time interval are initialed as follows: PE = perihelion, VE = vernal equinox, SS = summer solstice, AP = aphelion, AE = autumnal equinox, and WS = winter solstice.

tidal acceleration. A partial listing of these results is shown in Table 3.6-3. It can be seen that the seismicity (and the strain release) had a low degree of correlation with the vertical and horizontal components of tidal accelerations in the study area. Other horizontal components orientated perpendicular and at 45° to the major trend of the San Andreas Fault showed the same low correlation with seismicity.

Power spectra were computed for the autocorrelations of the seismicity and strain release. An example is shown in Figure 3.6-19. These analyses disclosed that the peak periods of the seismicity varied between sub-data sets and that their periods were different from the predominant periods of the principal solar and lunar tidal components of the solid earth tides (11.97 to 12.66 hours and 23.93 to 25.82 hours). The latter also include components with periods of 14.75 and 27.6 days. The maximum period that can be reliably resolved in the power spectra of the cross- and auto-correlations is one-quarter of the window length. Since the time interval of the sub-data sets was 60 days, the maximum period would be 15 days. Limitations of time and funds prevented analyzing the longer time periods.

TABLE 3.6-3

Cross-Correlation Coefficients between Seismicity, Strain Release and Tidal Accelerations

Sub-Data Sets	Starting Date	Ending Date	Number of Days	Number of Data Points	Data Sets Cross-Correlated	Correlation Coefficient Maximum	Correlation Coefficient Minimum
1	Aug. 1, 1969	Sept. 30, 1969	61	488	S X g_v	+0.07	-0.10
					S X g_h	+0.07	-0.07
					SR X g_v	+0.11	-0.09
					SR X g_h	+0.09	-0.10
2	Oct. 1, 1969	Nov. 29, 1969	60	480	S X g_v	+0.09	-0.09
3	Nov. 30, 1969	Jan. 30, 1970	62	496	S X g_v	+0.10	-0.10
4	Jan. 31, 1970	Mar. 31, 1970	60	480	S X g_v	+0.11	-0.10
5	Apr. 1, 1970	May 30, 1970	60	480	S X g_v	+0.12	-0.14
6	May 31, 1970	July 29, 1970	60	480	S X g_v	+0.09	-0.12
7	July 30, 1970	Sept. 27, 1970	60	480	S X g_v	+0.05	-0.07

S = seismicity, SR = strain release, g_v = vertical gravity, g_h = horizontal gravity parallel to fault strike, and X = cross-correlated.

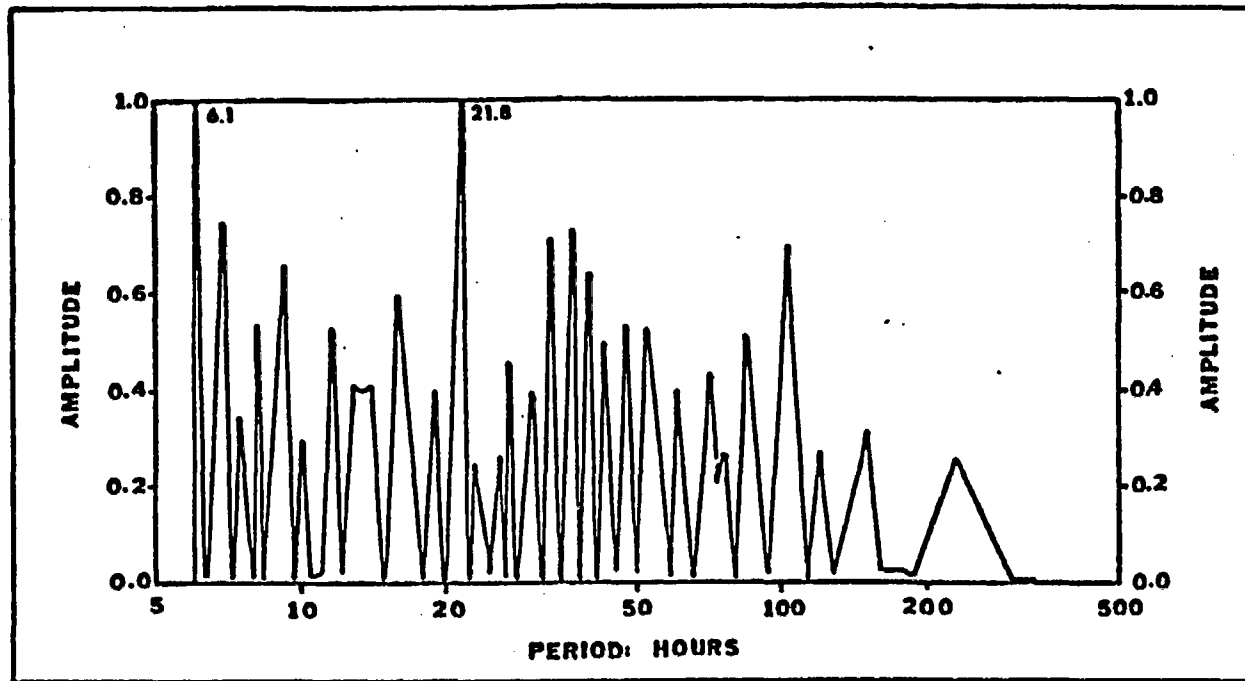


Figure 3.6-19. Strain release power spectrum of the central California study area events within the interval from day number 213, Aug. 1, 1969, through day number 273, Sept. 30, 1969.

3.7 Magnitude Variations

Earthquake magnitudes which are determined directly from seismic wave amplitudes on seismograph recordings allow a better understanding and interpretation of earthquakes. Richter's (1935) original magnitude scale (M_L - local magnitude) was developed for use in southern California and was limited to earthquakes with epicentral distances of less than 600 kilometers. Magnitude scales (body wave - m_b and surface wave - M_s) were later developed for use at greater distances and other regions. Some inconsistencies arose in the use of these different scales due primarily to the widely fluctuating geologic environments in the earthquake source regions, at the recording stations and along the intervening transmission paths. Richter's equations for the scales have been modified to fit restricted regions in North America by Bath (1969), Evernden (1967), and von Seggern (1970), among others.

Magnitude estimates for any one event (earthquake or underground explosion) commonly vary by one unit between seismograph stations and have been found to vary by as much as three or more units. Magnitude determinations are influenced by several factors including (1) instrument response, (2) nature of the propagation path, (3) the geology in the source region, and (4) the local geology in the vicinity of the seismograph station.

Gutenberg and Richter (1958) used a term, $\log A/T$, in their magnitude equations because of the "considerable variation in prevailing periods determined from instruments of widely different characteristics." A is the amplitude of the seismic signal and T is its period. Instrumentation variability has been minimized in this report by using only data from

World Wide Standard Seismograph Network (WSSN) and Canadian Seismograph Network (CSN) stations. Seismograms obtained from short-period and long-period narrow-band seismometers were used exclusively for body and surface wave magnitude calculations, respectively.

The geological conditions at the recording site, along the entire propagation path, and in the epicentral region affect the seismic amplitudes and hence the magnitude estimates. Seismic sources originating in granite, for example, are coupled more efficiently than in alluvium. Table 3.7-1 shows the percentage of energy radiated as seismic waves for the same size explosive source detonated in different rock media.

TABLE 3.7-1

Percentage of Energy Radiated as Seismic Waves in Various Source Rocks (after Environmental Research Corporation, 1974)

<u>Source Rock</u>	<u>Percentage of Energy Radiated as Seismic Waves</u>
Granite	2%
Salt	3%
Tuff	0.1 - 3.0%
Alluvium	0.05 - 0.15%

From the epicenter to the recording station several geologic and geophysical factors can alter the character and amplitude of the seismic signal. These include the crustal-upper mantle structure and thickness, surface layering, absorption and scattering (Long and Berg, 1969).

Both surface and subsurface topography have been associated with the attenuation/amplification of seismic waves. Simon (1968) has found that the waves passing under the Rocky Mountains are severely attenuated. According to Davis and West (1973), "topography plays a significant role and is an important consideration in determining the seismic motion that a particular site sees." This is especially true of topographic features in the area of the recording site. Van Nostrand (1966) found resonance to be the most significant factor in amplitude variation as a result of near-surface local geologic changes. Frequency of the signal is important, however, and topographic variations lose their importance when the wavelength of the seismic signal is much larger than the dimensions of the topographic feature.

The character of the crust and uppermost mantle west of the Rockies to the Sierra Nevadas is in sharp contrast to that found in the eastern United States. As seen in Figure 3.7-1, Pn velocities are lower in the western United States than in the eastern United States. Pn velocities range from a high in the eastern U.S. of 8.4 km/sec to a low in the west-central U.S. of 7.7 km/sec. These regional variations correlate quite well with the general topography. Pn velocities are very low in the mountainous western states and variations in crustal structures appear to be associated with properties in the upper mantle. The mountain ranges in the West under isostatic compensation have a low-density, low-velocity upper mantle and a thick crust. This is opposed to a crust of more average thickness and density across the eastern two-thirds of the U.S.

Over the past few decades seismologists have found it useful to refer to a dimensionless quantity, Q , sometimes called specific dissipation, when

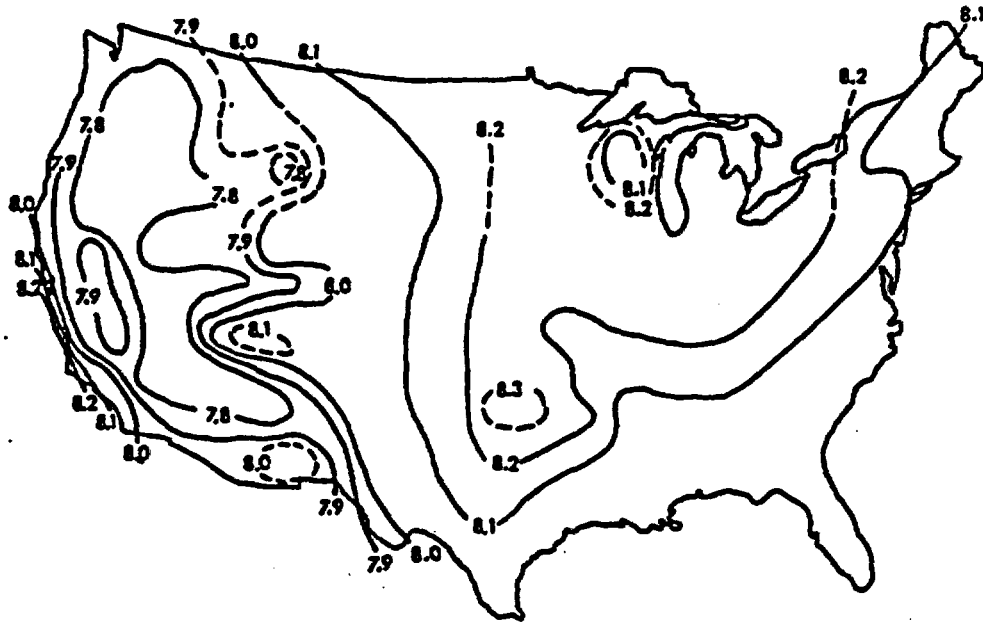


Figure 3.7-1. Estimated P_n velocity in the United States, based on data from deep seismic soundings, underground nuclear explosions, and earthquakes. After Herrin, 1969.

describing the absorption of seismic signals along a propagation path. Mathematically, Q can be represented as

$$Q = \pi/UT\gamma$$

where U is the group velocity of the signal, T its period, and γ the coefficient of anelastic attenuation (Ben-Menahem, 1965). Apparent attenuation includes losses due to geometrical spreading, absorption, reflection, and scattering. In a homogeneous medium absorption increases with a decreasing wave period. Long period surface waves are affected by the attenuative properties of both the crust and the upper mantle.

Pakiser and Zietz (1965) found that the attenuation of short-period Rayleigh waves was significantly higher west of the Rocky Mountains than to the east. The Q for a wave with a period of one second is ten times larger in the East than in the West. Hence, the radius of perceptibility in the eastern United States for an earthquake or explosion is as much as ten times larger than that in the western U.S.

Lateral variation of P and S wave differential attenuation as reported by Solomon and Toksöz (1970) is shown in Figures 3.7-2 and 3.7-3. From these figures, high attenuation is observed in the region from the Rocky Mountains to the Sierra Nevada-Cascade ranges and in the northeast section of the U.S. The abnormally high attenuation in the latter region was noted as possibly due to spatial fluctuations near the source. The far west, the central and eastern parts of the country exhibit low attenuation for both P and S waves. In large part this delineates the changing Q of the crust and upper mantle across the continental U.S.

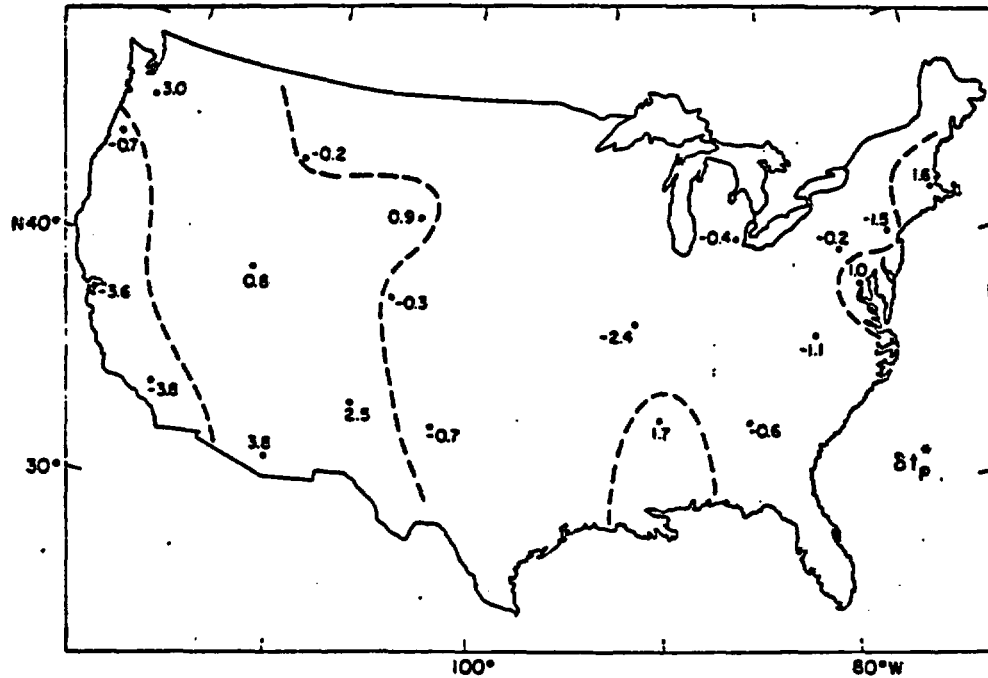


Figure 3.7-2. Lateral variation of P wave differential attenuation at U.S. stations. δt_p^* is the average of attenuation measurements from two deep earthquakes in the Peru-Brazil border region. After Solomon and Toksöz, 1970.

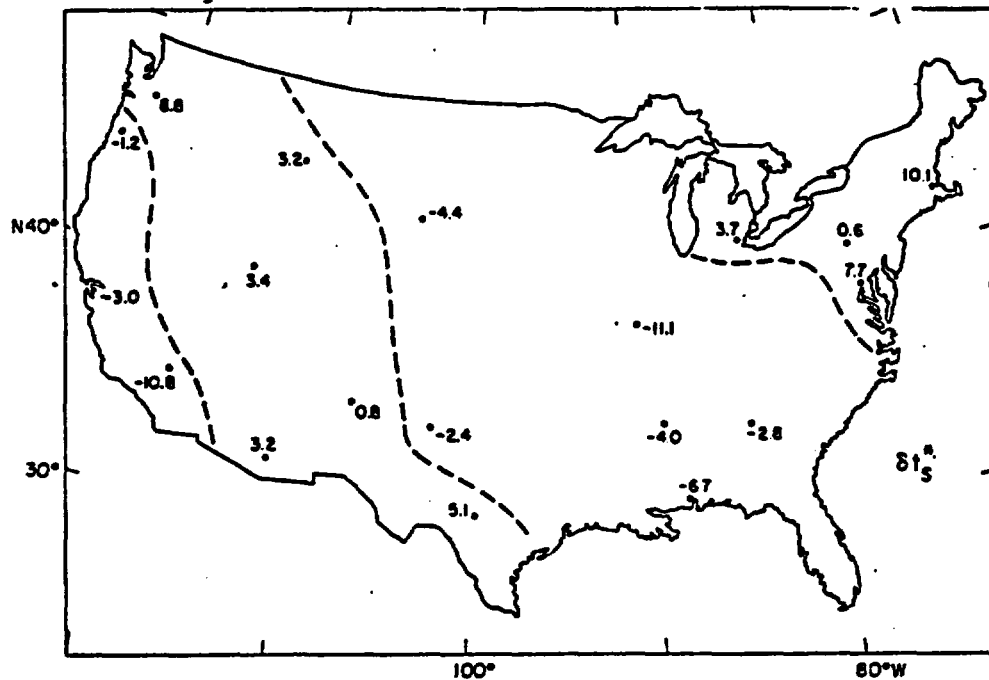


Figure 3.7-3. Lateral variation of S wave differential attenuation at two U.S. stations. δt_s^* is the average of attenuation measurements from two deep earthquakes in the Peru-Brazil border region. After Solomon and Toksöz, 1970.

Attenuation constants have been determined by Oliver (1964) along various profiles across the U.S. using PL waves. In order of increasing Q , the profiles are: Rocky Mountain front, Colorado Plateau, the Mid-Continent region, and the Appalachian region.

Nuclear-explosion seismologists have for years applied the basic earthquake magnitude equations to the measurement of underground nuclear explosions (Basham, 1969; Båth, 1952, 1969; Carpenter and others, 1962; Evernden, 1967; Evernden and Filson, 1971). The point source function of a nuclear detonation consists of "the superposition of an isotropic dilatational component due to the explosion and a multipolar component due to the release of some tectonic strain energy" (Toksöz and others, 1964). Because the source time function for explosions is known, variation due to the source character is generally reduced. However, radiation patterns from explosive sources, as shown by Ben-Menahem and Harkrider (1964), Brune and Pomeroy (1963), von Seggern (1970), and Willis and others (1972), show azimuthally dependent magnitudes.

Studies of magnitude variations for earthquakes generally show significant variations due to the source mechanism. Both surface and body-wave magnitudes for earthquakes show more scatter than similar magnitudes from explosions because of source radiation patterns, which are influenced by the source depth, fault plane dip angle, angle of slip motion, and fault rupture velocity (von Seggern, 1970). Deep earthquakes generate less surface wave energy than shallow earthquakes. Underground nuclear explosions are considered to be shallow focus events (shallow compared with earthquakes).

Magnitude estimates from underground nuclear explosions have been found to exhibit regional patterns of highs and lows across the United

States (Mickey, 1963; Guyton, 1964; Willis and others, 1973). Asymmetry in radiation patterns from a radially symmetric source could result from the relaxation of prestress in the source region, changing geologic conditions along the transmission path, or differences in local geology at the seismograph stations.

Propagation of seismic waves from an ideal point source such as an explosion would be radially symmetric except that prestress in the source region affects the radiation pattern, particularly of surface waves. Radiation patterns for Rayleigh and Love waves in a prestressed medium from the BILBY explosion are shown in Figures 3.7-4 and -5. Note in both patterns the superposition of a double couple and a compressional source, the former causing asymmetry in the radiation pattern from the release of local tectonic strain.

Seismograms from 23 WSSN and 26 CSN stations in North America were analyzed in determining magnitudes from six NTS shots (PILE DRIVER, GREELEY, BOXCAR, BENHAM, JORUM, and HANDLEY) and two explosions on Amchitka Island (MILROW and CANNIKIN). Station names and locations are given in Table 3.7-2. Source parameters for the shots are shown in Table 3.7-3. M_s and m_b radiation patterns for many of the individual shots have been presented in previous reports (Willis and others, 1972, 1973).

To get an overall perspective of the patterns of magnitude distribution, the amount of deviation of each station's magnitude from the published magnitude was determined. The average deviation for each station was then calculated and plotted. Figure 3.7-6 is a contoured map of these average deviations from published M_s magnitudes. Regions of high and low deviations are broad, and extremes vary by approximately one unit

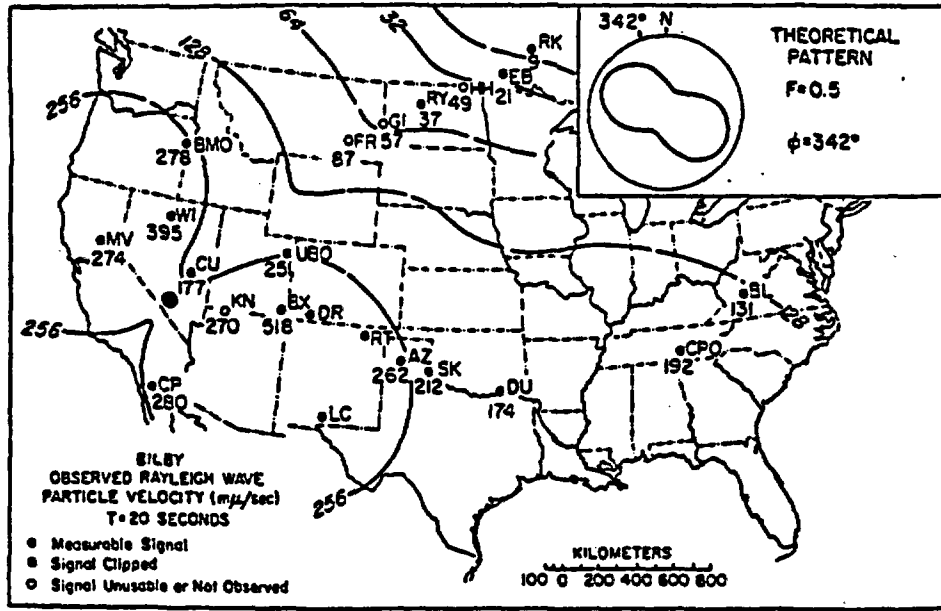


Figure 3.7-4. Rayleigh wave radiation pattern at $T = 20$ sec. observed from the BILBY nuclear explosion. The theoretical pattern shown in the inset corresponds to the superposition of a double couple and a compressional point source. The azimuth of the equivalent double couple is $\phi = 342^\circ$ and the relative excitation of the double couple to compressional point source equivalent is $F = 0.5$. After Archambeau and Sammis, 1970.

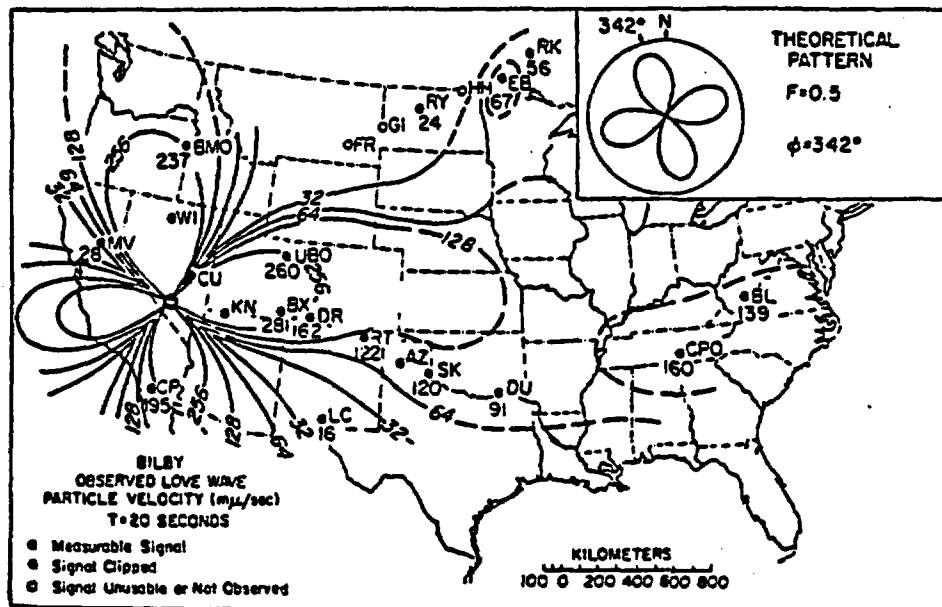


Figure 3.7-5. Love wave radiation pattern at $T = 20$ sec. observed from the BILBY nuclear explosion. The theoretical pattern shown in the inset corresponds to the superposition of a double couple and a compressional point source. The azimuth of the equivalent double couple is $\phi = 342^\circ$ and the relative excitation of the double couple to the compressional point source equivalent is $F = 0.5$. After Archambeau and Sammis, 1970.

TABLE 3.7-2

Names and Locations of Seismograph Stations

Station Designation	Seismic Network	Location	Coordinates	
			Lat. °N	Long. °W
AAM	WWSSN	Ann Arbor, Michigan	42.3	83.7
ALE	CSN	Alert, Northwest Terr.	82.5	62.4
ALQ	WWSSN	Albuquerque, New Mexico	34.9	106.5
ATL	WWSSN	Atlanta, Georgia	33.4	84.3
BKS	WWSSN	Byerly, California	37.9	122.2
BLA	WWSSN	Blacksburg, Virginia	37.2	80.4
BLC	CSN	Baker Lake, N.W. Terr.	64.3	96.0
BOZ	WWSSN	Bozeman, Montana	45.6	111.6
CMC	CSN	Copper Mine, N.W. Terr.	67.8	115.1
COL	WWSSN	College Outpost, Alaska	64.9	147.8
COR	WWSSN	Corvallis, Oregon	44.6	123.3
DAL	WWSSN	Dallas, Texas	32.8	96.8
DUG	WWSSN	Dugway, Utah	40.2	112.6
EDM	CSN	Edmonton, Alberta	53.2	113.4
FBC	CSN	Frobisher Bay, N.W. Terr.	63.7	68.5
FCC	CSN	Fort Churchill, Manitoba	58.8	94.1
FFC	CSN	Flin Flon, Manitoba	54.7	102.0
FLO	WWSSN	Florissant, Missouri	38.8	90.4
FSJ	CSN	Fort St. James, B.C.	54.4	124.3
GEO	WWSSN	Georgetown, D.C.	38.9	77.1
GOL	WWSSN	Golden, Colorado	39.7	105.4
GWC	CSN	Great Whale River, Quebec	55.3	77.8
HAL	CSN	Halifax, Nova Scotia	44.6	63.6
INK	CSN	Inuvick, N.W. Territory	68.3	133.5
JCT	WWSSN	Junction City, Texas	30.5	99.8
LHC	CSN	Lakehead Univ., Ontario	48.4	89.3
LON	WWSSN	Longmire, Washington	46.8	121.8
LUB	WWSSN	Lubbock, Texas	33.6	101.9
MBC	CSN	Mould Bay, N.W. Territory	76.2	119.4
MCC	CSN	Mica Creek, B.C.	52.1	118.6
MNT	CSN	Montreal, Quebec	45.5	73.6
OGD	WWSSN	Ogdensburg, New Jersey	41.1	74.6
OTT	CSN	Ottawa, Ontario	45.4	75.7
OXF	WWSSN	Oxford, Mississippi	34.5	89.4
PHC	CSN	Port Hardy, B.C.	50.7	127.4
PNT	CSN	Penticton, B.C.	49.3	119.6
RCD	WWSSN	Rapid City, South Dakota	44.1	103.2
RES	CSN	Resolute, Northwest Terr.	74.7	94.9
SCB	CSN	Scarborough, Ontario	43.7	79.2
SCH	CSN	Schefferville, Labrador	54.8	66.8
SCP	WWSSN	State College, Penn.	40.8	77.9
SES	CSN	Suffield, Alberta	50.4	111.0
SFA	CSN	Seven Falls, Quebec	47.1	70.8
SHA	WWSSN	Spring Hill, Alabama	30.7	88.1
SUD	CSN	Sudbury, Ontario	46.5	81.0
TUC	WWSSN	Tucson, Arizona	32.3	110.8
VIC	CSN	Victoria, B.C.	48.5	123.4
WES	WWSSN	Weston, Massachusetts	42.4	71.3
YKC	CSN	Yellowknife, N.W. Terr.	62.5	114.5

TABLE 3.7-3

Source Parameters for U.S. Underground Nuclear Explosions

<u>Shot</u>	<u>Date</u>	<u>GMT Time</u>	<u>Approx. Yield (Kilotons)</u>	<u>Medium</u>	<u>Location</u>	<u>Region</u>
PILE DRIVER	2 JUN 66	15:30:00	56	Granite	37°22'42" N 116°56'00" W	Yucca Flat
GREELEY	20 DEC 66	15:30:00	825	Tuff	37°18'07.4" N 116°24'29.9" W	Pahute Mesa
BOXCAR	26 APR 68	15:00:00	1200	Rhyolite	37°17'43.5" N 116°27'20.5" W	Pahute Mesa
BENHAM	19 DEC 68	16:30:00	1100	Tuff	37°13'53.3" N 116°28'24.9" W	Pahute Mesa
JORUM	16 SEP 69	14:30:00	1000	Tuff	37°18'50.9" N 116°27'38.4" W	Pahute Mesa
MILROW	2 OCT 69	22:06:00	1000	Andesite	51°25'01.6" N 179°10'56.3" E	Amchitka Island
HANDLEY	26 MAR 70	19:00:00	1000	Tuff	37°18'01.7" N 116°32'02.8" W	Pahute Mesa
CANNIKIN	6 NOV 71	22:00:00	5000	Andesite	51°28'18.7" N 179°06'24.3" E	Amchitka Island

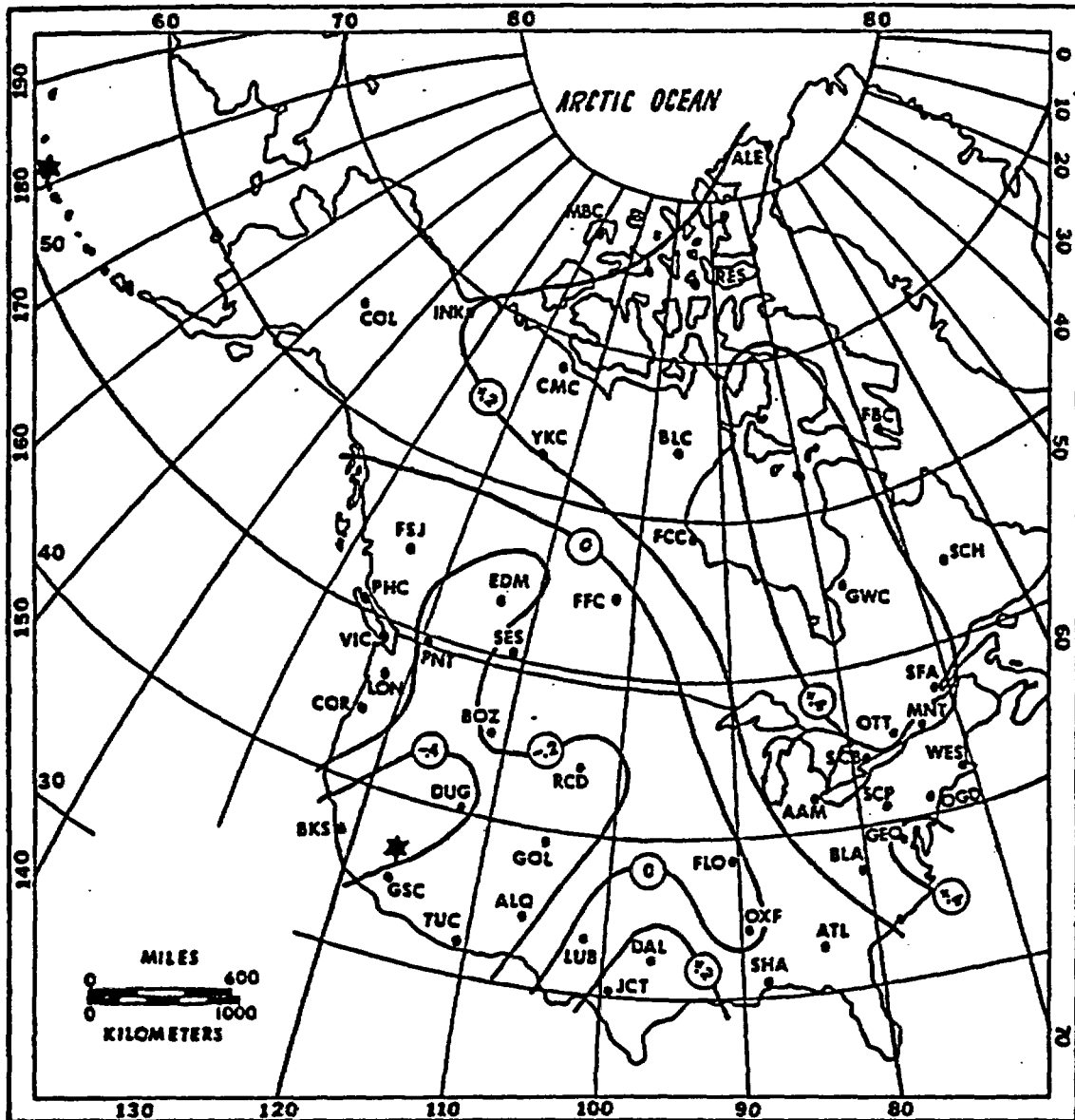


Figure 3.7-6. Contour map of average deviations from published M_s magnitudes of six NTS explosions (FILE DRIVER, GREELEY, BOXCAR, JORUM, HANDLEY) and two explosions on Amchitka Island (MILROW and CANNIKIN). The stars indicate the shot locations and the dots show the distribution of seismograph stations used in magnitude calculations.

of magnitude. All of the negative deviations are in the western U.S. and the southwest corner of Canada, approximately within the boundaries of 89°-130° West Longitude and 30°-60° North Latitude.

These negative deviations in the western U.S. correlate very well with its thinner crust and lower crustal and upper mantle P velocities. Low upper mantle Q values in the West, which cause greater attenuation for the 20 second period surface waves, are very likely caused by the low velocity layer in the upper mantle. The West is also more fractured by younger fault systems and has higher heat flow values than the East, both of which tend to increase the attenuation of seismic waves.

The topography of North America is shown in Figure 3.7-7. Note that the high relief of the Rocky Mountains and the Sierra-Nevadas correlates with the region of most negative anomalies. However, this is not the case in western Canada and Alaska.

Relatively high deviations are concentrated in the eastern U.S. and eastern Canada. This is likely a reflection of several factors: a thicker, older and more stable crust; the absence of a low velocity layer in the upper mantle as is evident in the western U.S., and lower heat flow values. The stable Canadian Shield, represented by the striped and speckled area in the tectonic map of North America (Figure 3.7-8), encompasses most of the high positive magnitude deviations in the continent. Highest values are concentrated in southeastern Canada and northeastern United States.

Zero and near-zero deviation values lie generally within the internal plains of North America, again referring to Figure 3.7-8.

It was reported in an earlier report by Willis and others (1972) that surface wave magnitudes from the CANNIKIN shot increased with distance. A

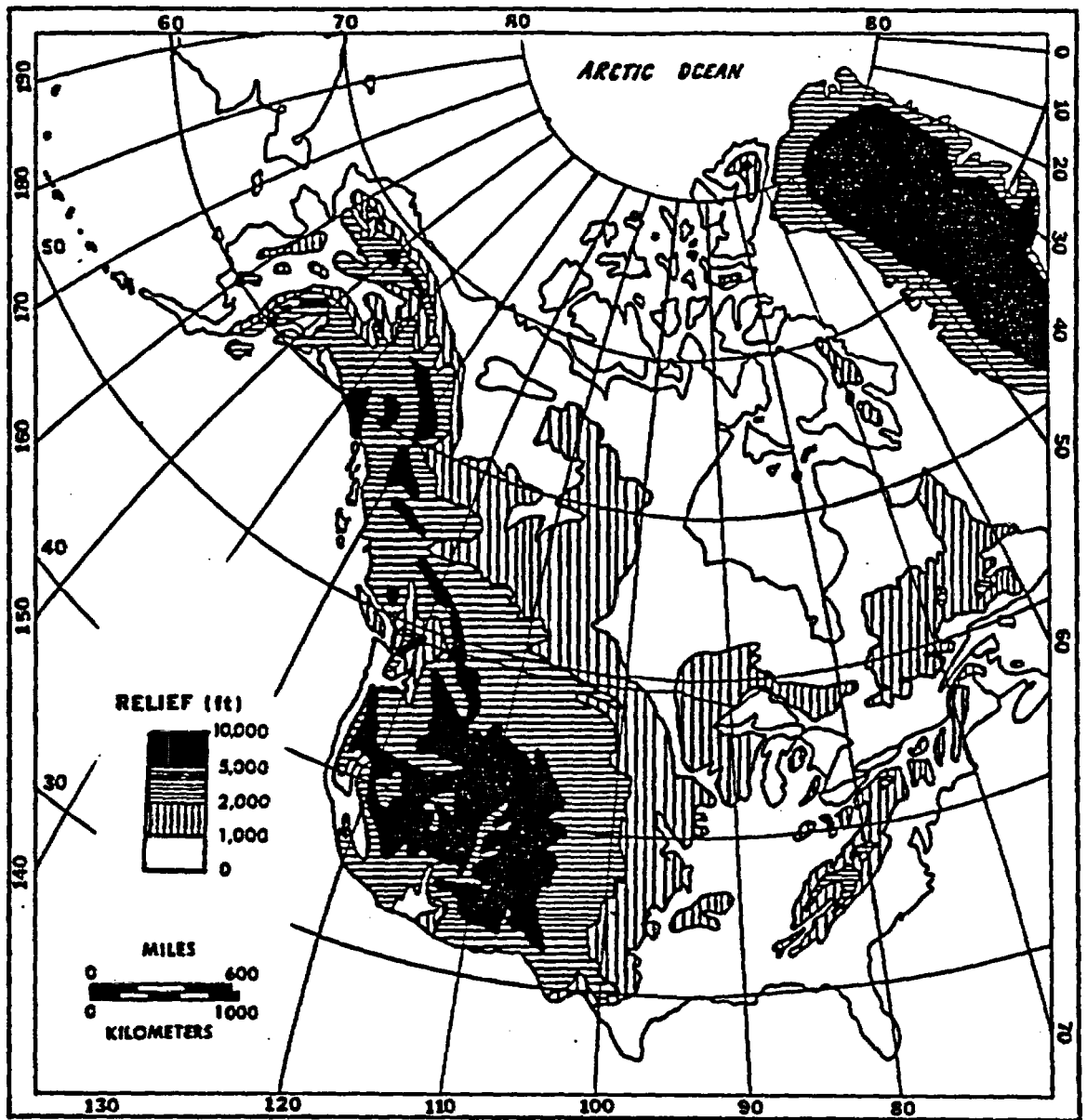
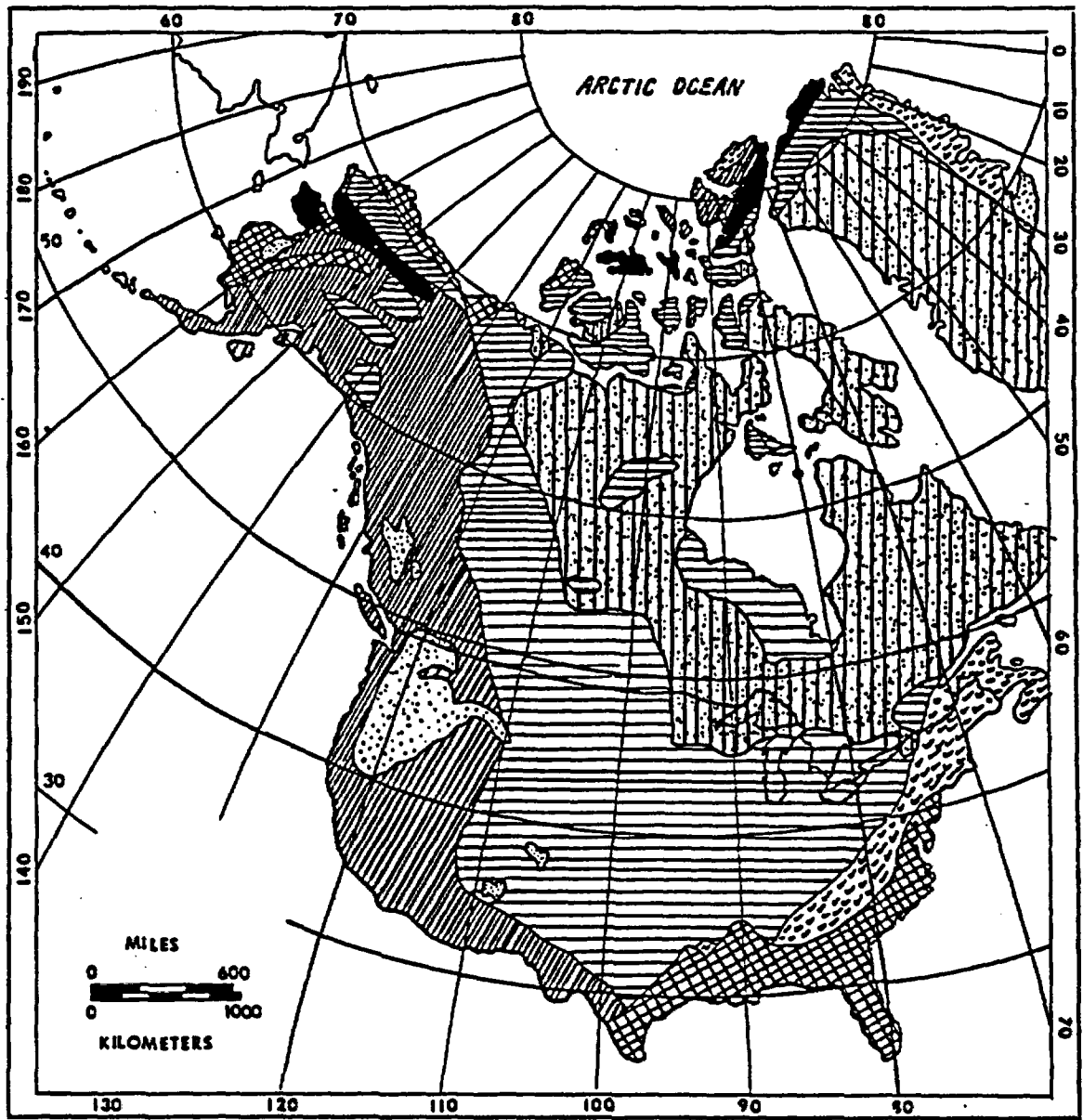


Figure 3.7-7. Topographic map of North America.



- | | | | | | |
|---|-----------------|---|--------------------------|---|------------------------|
|  | SHIELDS |  | EARLY & MIDDLE PALEOZOIC |  | MESOZOIC AND CENOZOIC |
|  | INTERNAL PLAINS |  | LATE PALEOZOIC |  | EXTINCT VOLCANIC AREAS |
|  | COASTAL PLAINS | | | | |

Figure 3.7-8. Tectonic map of North America.

plot of the average station deviation vs. distance for the six NTS events is shown in Figure 3.7-9. While this suggests an increasing magnitude effect with distance, it could be explained in part as lateral changes in the thickness and structure of the crust and upper mantle, as was pointed out previously when describing differences in the eastern and western United States.

Station deviations for body wave magnitudes are contoured in Figure 3.7-10. The regional anomaly patterns are not consistent with those found using surface wave magnitude deviations. In analyzing this map, it should be noted that the average of all body wave magnitudes calculated for this report was .2 magnitude units above the published values. This is due in part to the consistent high anomalies in Corvallis, Oregon (COR) and Longmire, Washington (LON). Figure 3.7-11, a plot of average body wave magnitude deviation versus distance for the six NTS shots, reveals considerable scatter but a least squares linear fit of the data indicates a decrease in the deviation with distance. Part of this variation may be due to first arrivals being refracted from increasingly deeper refractors with the increasing epicentral distance.

Referring to Figure 3.7-10, it can be seen that the highest positive deviations are found in the southern states and in Washington and Oregon, as mentioned previously. The central section of the U.S. and Canada have only slightly positive deviations. The only apparent negative deviations are limited to northern and western Canada, except for the lone station of Halifax, Nova Scotia (HAL). Willis and DeNoyer (1966) reported that three of these same stations (RES, ALE, MBC) show high attenuation from the GNOME, HAYMAKER, and SHOAL blasts.

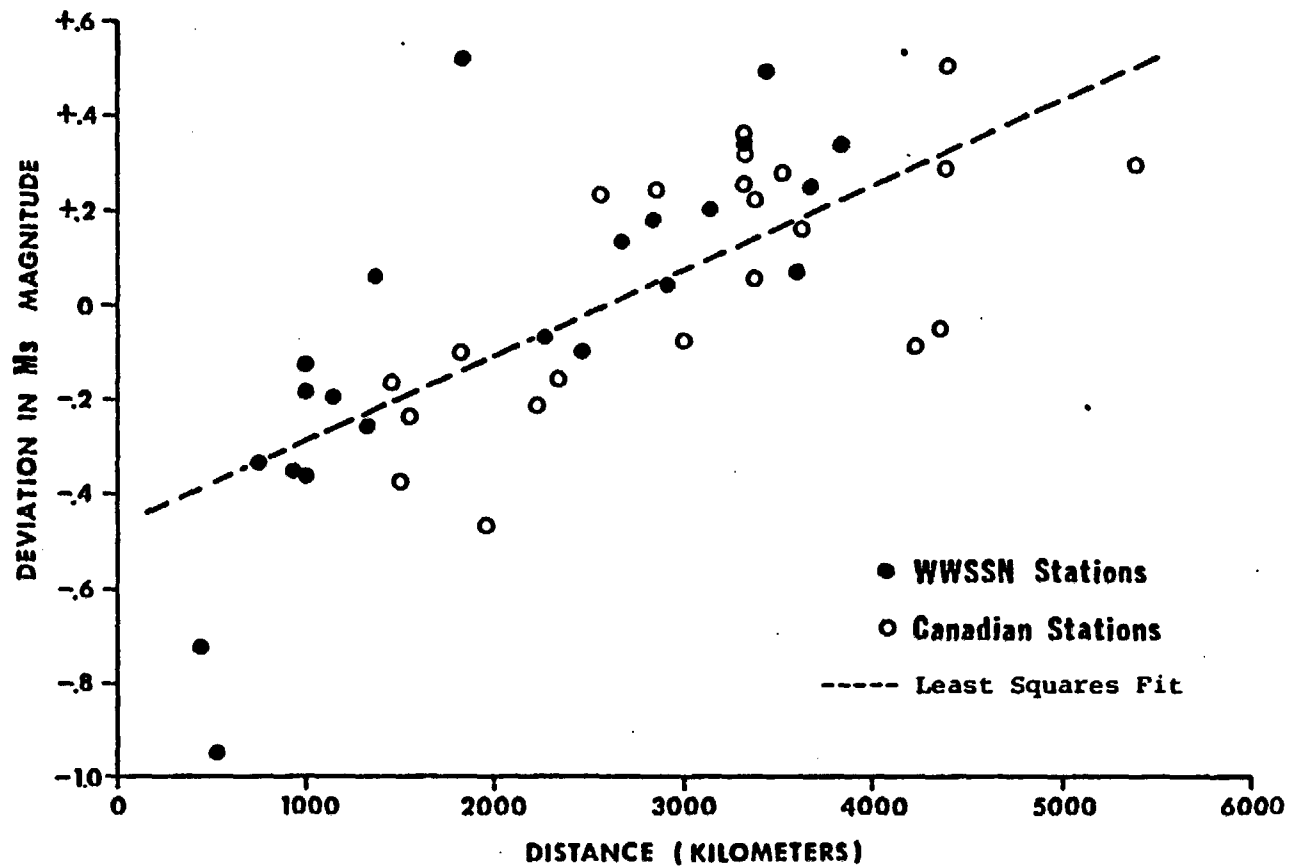


Figure 3.7-9. Comparison of epicentral distance average deviations from published M_S magnitudes of six NTS explosions (PILE DRIVER, GREELEY, BOXCAR, BENHAM, JORUM, HANDLEY) using 22 WWSSN and 22 CSN stations.

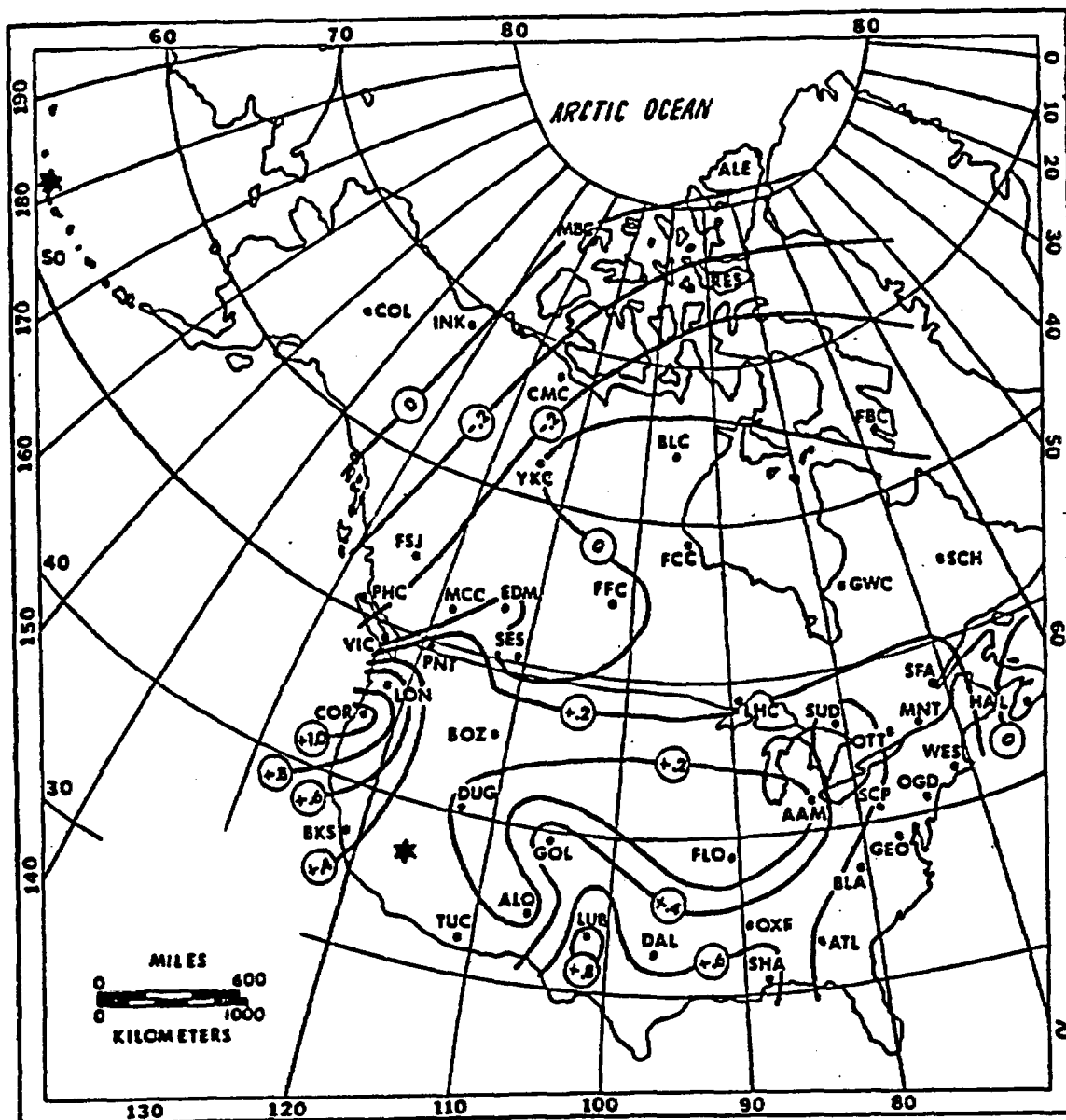


Figure 3.7-10. Contour map of average deviations from published m_b magnitudes of six NTS explosions (PILE DRIVER, GREELEY, BOXCAR, BENHAM, JORUM, HANDLEY) and two explosions on Amchitka Island (MILROW and CANNIKIN). The stars indicate the shot locations and the dots show the distribution of seismograph stations used in magnitude calculations.

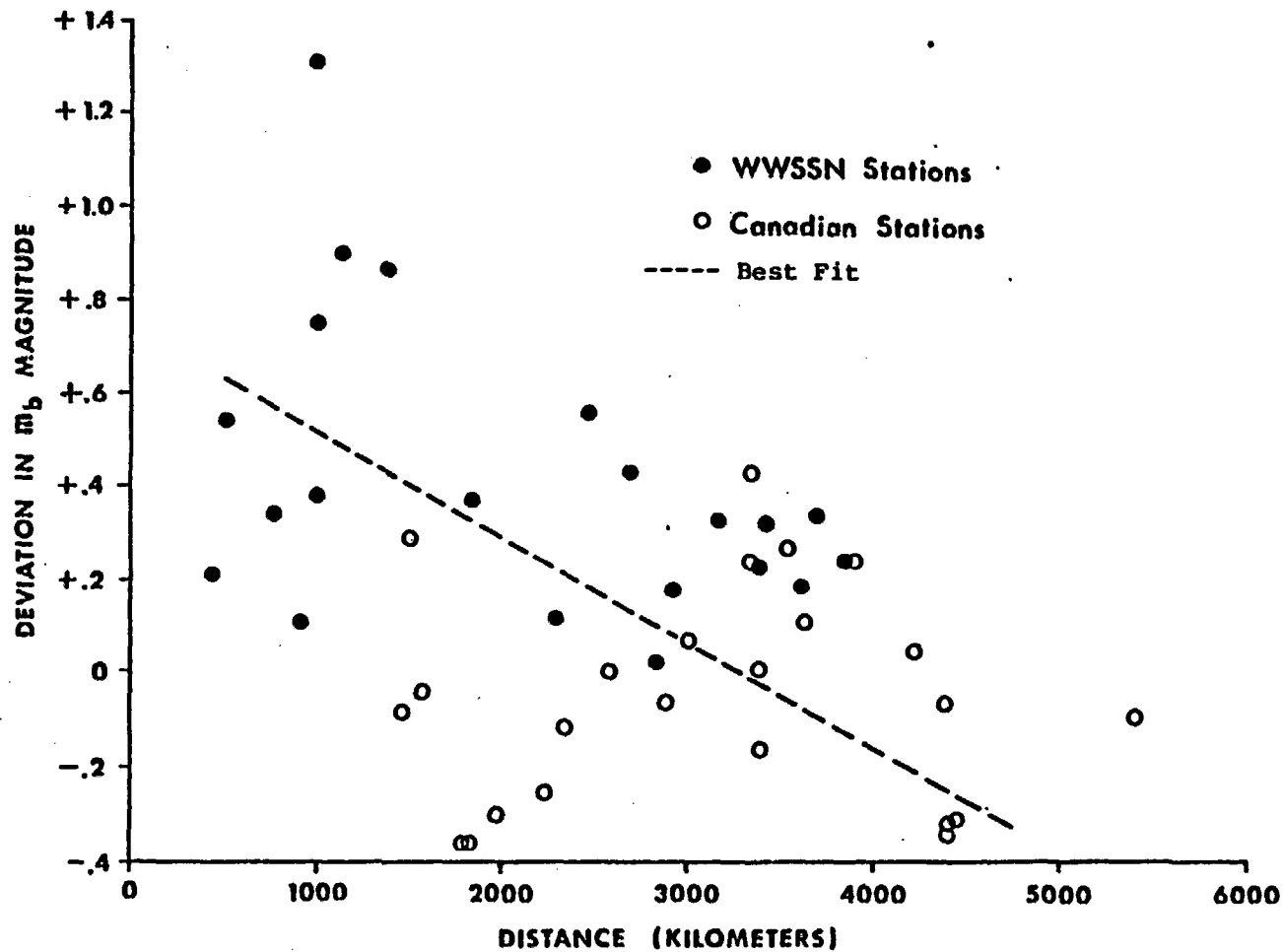


Figure 3.7-11. Comparison of average magnitude deviations from published m_b magnitudes of six NTS explosions (PILE DRIVER, GREELEY, BOXCAR, BENHAM, JORUM, HANDLEY) vs. epicentral distance using 24 WWSSN and 22 CSN stations.

Although only limited data were available, an analysis was made of seismograms from the south-central Illinois earthquake of November 9, 1968, $m_b = 5.5$, to see if the patterns of magnitude variations would be similar using a source with an epicenter in the eastern section of the U.S. A map of the major faults in the epicentral region is given in Figure 3.7-12. Iso-magnitude contour maps of surface and body wave magnitudes for the earthquake are presented in Figures 3.7-13 and 3.7-14, respectively.

The surface wave magnitudes distributed across the United States show apparent highs in the eastern section of the country. This is in general agreement with the positive highs shown in Figure 3.7-6. The distribution of body wave magnitudes does not agree well with the m_b deviations shown in Figure 3.7-10. Hence, either the source region or the type of source would appear to influence the m_b radiation pattern. If time would permit, an analysis should be made of existing seismograms of explosions from such sources as Project Early Rise (see Willis, 1968) and the nuclear detonations SALMON and RIO BLANCO to better understand the effect of the source region on magnitude distribution. Also, this would allow a correlation between point sources rather than between a point source and an earthquake. At present it is difficult to determine how much the radiation pattern is affected by the source mechanism.

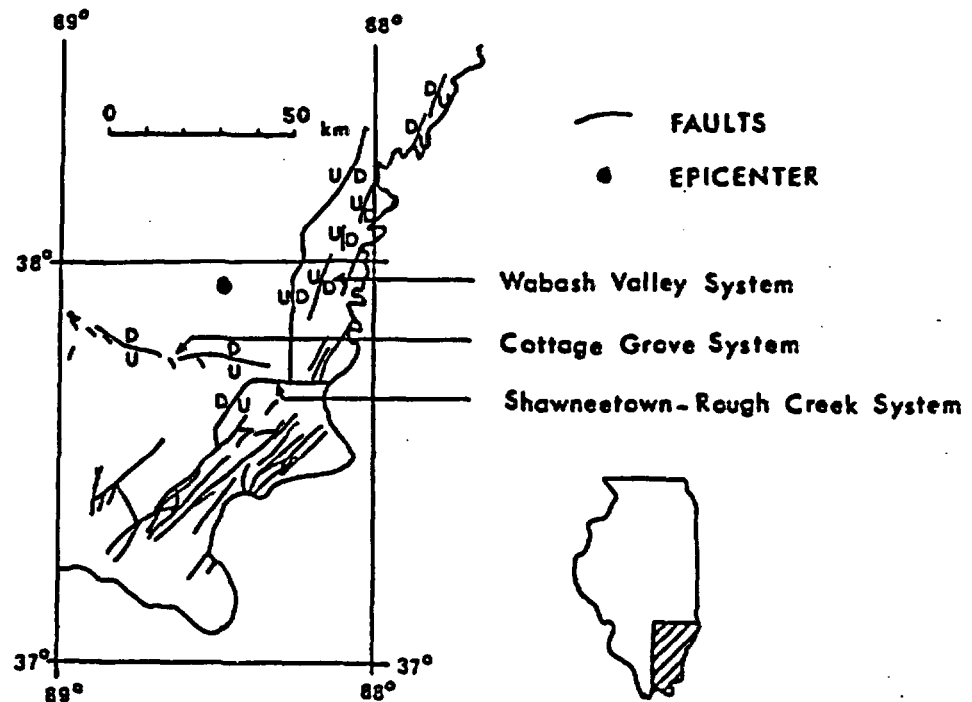


Figure 3.7-12. Relation of the epicenter of the south central Illinois earthquake of November 9, 1968, to faults of that region. After Heigold, 1968.

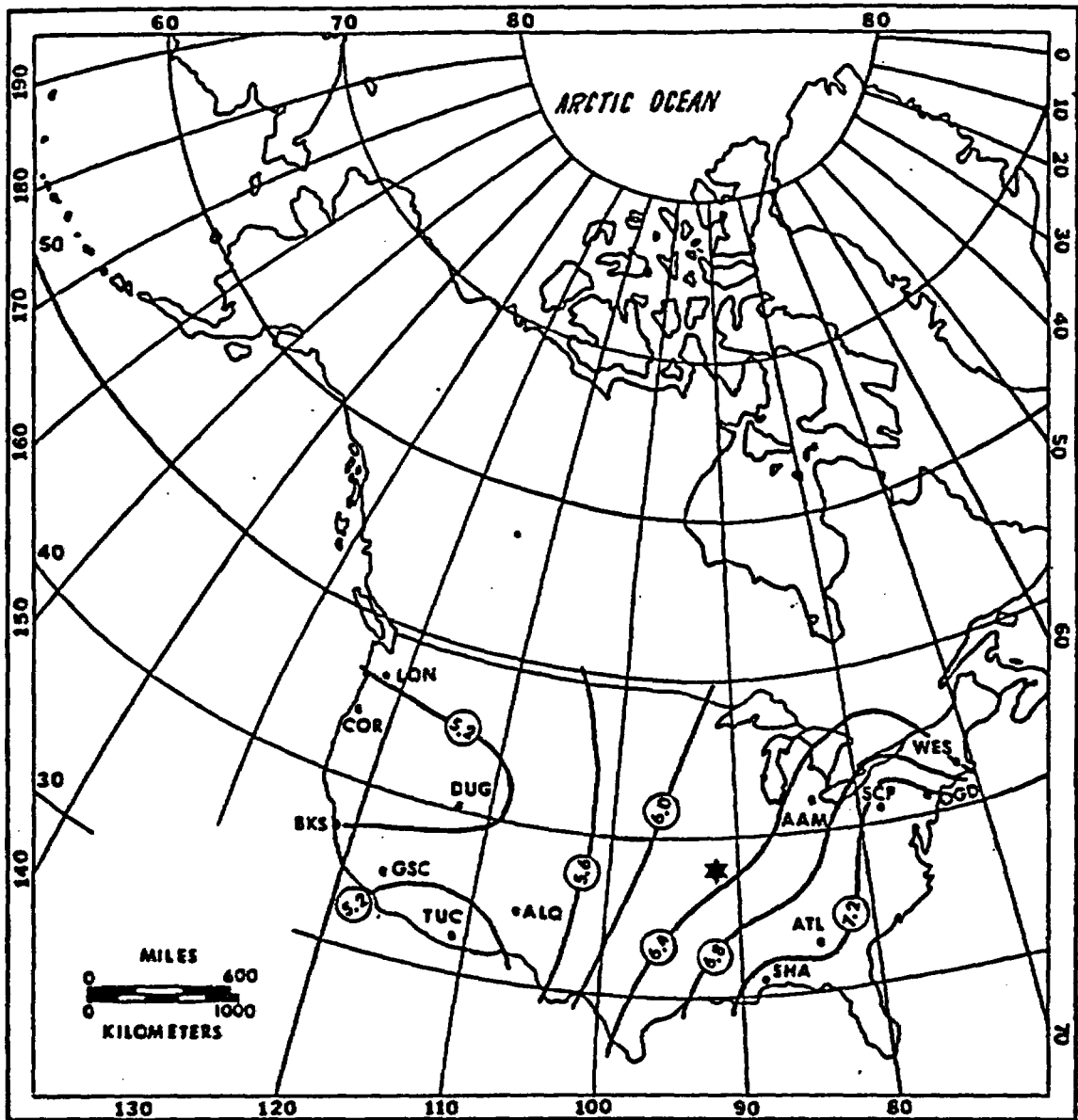


Figure 3.7-13. Iso-magnitude contour map of surface wave magnitudes for the south central Illinois earthquake of November 9, 1968. Contour interval is $.2 M_s$. The star indicates the epicenter and the dots show the distribution of seismograph stations used in magnitude calculations.

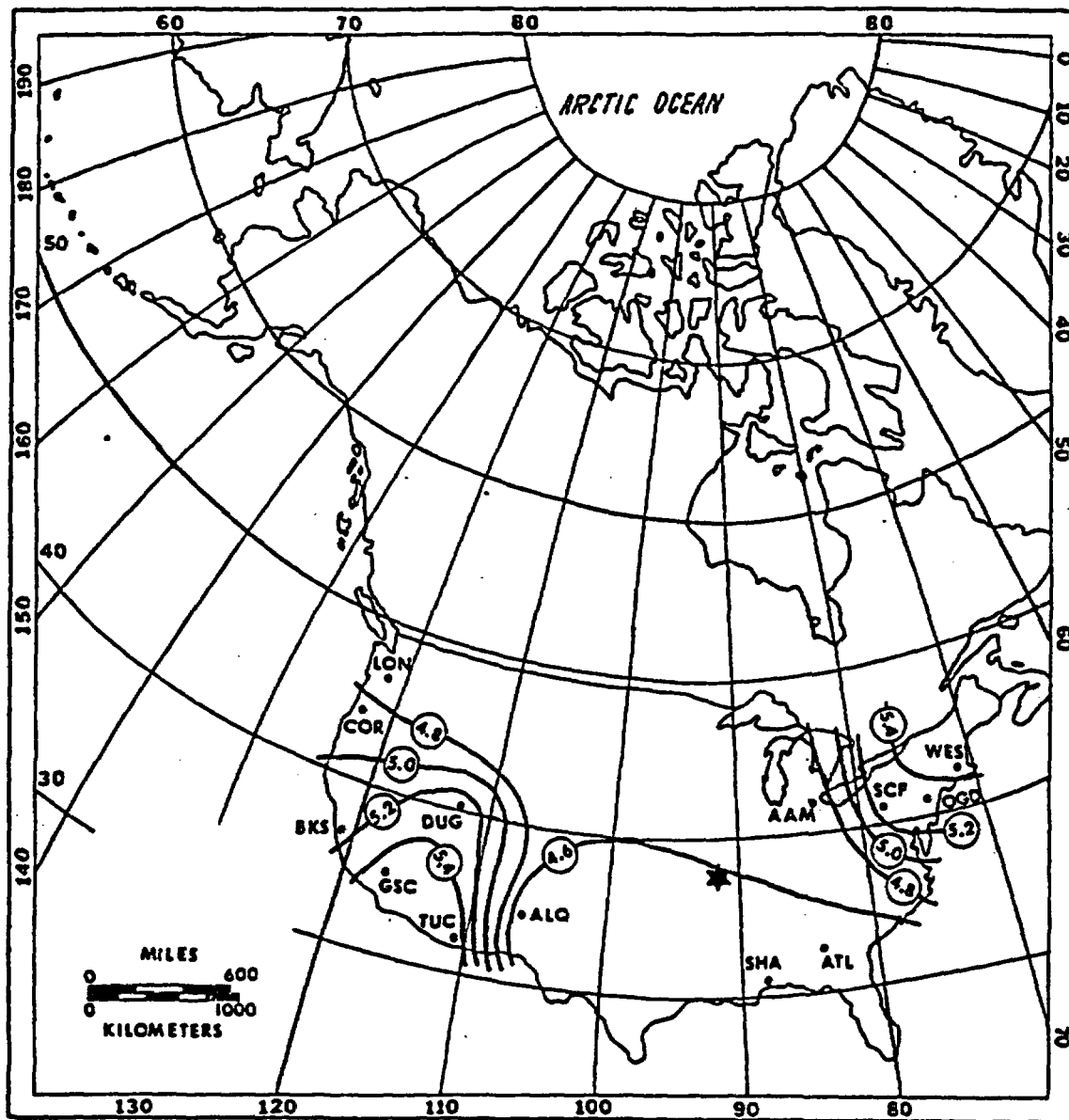


Figure 3.7-14. Iso-magnitude contour map of body wave magnitudes for the south central Illinois earthquake of November 9, 1968. Contour interval is $.4 m_p$. The star indicates the epicenter and the dots show the distribution of seismograph stations used in magnitude calculations.

REFERENCES

- Allen, C. R., 1968, The tectonic environments of seismically active and inactive areas along the San Andreas Fault System: Stanford Univ. Publ., Geological Sciences, v. 11, p. 70-82.
- Allen, J. H. and L. F. Bailey, 1970, Earthquakes and nuclear detonations: Science, v. 167, p. 1012-1013.
- Allen, M. W., 1936, The lunar triggering effect on earthquakes in southern California: Bull. Seismol. Soc. America, v. 26, p. 147-157.
- Anderson, D. L., 1971, The San Andreas Fault: Scientific American, v. 225, p. 52-66.
- Anderson, D. L., C. B. Archambeau, J. N. Brune, C. F. Richter, and S. W. Smith, 1970, Earthquakes and nuclear detonations: Science, v. 167, p. 1011-1012.
- Anderson, J. M., 1972, A study of the possible correlation of strain tilt and earthquakes: M.S. thesis, Univ. of Utah.
- Archambeau, C. B., 1972, The theory of stress wave radiation from explosions in prestressed media: Geophys. Jour. Royal Astr. Soc., v. 29, p. 329-366.
- Archambeau, C. B. and C. Sammis, 1970, Seismic radiation from explosions in prestressed media and the measurement of tectonic stress in the earth: Rev. Geophys., v. 8, p. 473-499.
- Atomic Energy Commission, 1973, Revised nuclear test statistics: Las Vegas, Nevada Operations Office, 13 p.
- Atwater, T., 1970, Implications of plate tectonics for the Cenozoic tectonic evolution of western North America: Bull. Geol. Soc. America, v. 81, p. 3513-3536.
- Atwater, T. and P. Molnar, 1973, Relative motion of the Pacific and North American plates deduced from sea-floor spreading in the Atlantic, Indian and South Pacific Oceans, in Kovach, R. L. and A. Nur, eds., Proceedings of the Conference on Tectonic Problems of the San Andreas Fault System: Stanford, Stanford Univ., p. 136-149.
- Basham, P. W., 1969, Canadian magnitudes of earthquakes and nuclear explosions in southwestern North America: Jour. Geophys. Res., v. 17, p. 1-13.
- Bath, M., 1952, Earthquake magnitude determination from the vertical component of surface waves: Trans. Am. Geophys. Union, v. 31, 81 p.

- Båth, M., 1968, The energies of seismic body waves and surface waves, in Benioff, H., M. Ewing, B. F. Howell, Jr., and F. Press, eds., Contr. in Geophysics (Gutenberg Volume): New York, Pergamon Press, p. 1-16.
- Båth, M., 1969, Handbook on Earthquake Magnitude Determinations, 2nd Revised Edition, Uppsala, Sweden, 158p.
- Bayer, K.C., 1973, Seismic data report, southern Nevada region, December 22, 1971 - December 31, 1972: U.S. Department of Commerce, National Oceanic and Atmospheric Administration, Earth Science Laboratories, 7 p.
- Benioff, H., 1935, A linear strain seismograph: Bull. Seismol. Soc. America, v. 25, p. 283-309.
- Benioff, H., 1949, Seismic evidence for the fault origin of oceanic deeps: Bull. Geol. Soc. America, v. 60, p. 1837-1856.
- Benioff, H., 1951, Global strain accumulation and release as revealed by great earthquakes: Bull. Geol. Soc. America, v. 62, p. 331-338.
- Benioff, H., 1959, A fused-quartz extensometer for secular, tidal, and seismic strains: Geol. Soc. Am. Bull., v. 70, p. 1019-1032.
- Ben-Menahem, A., 1965, Observed attenuation and Q values of seismic surface waves in the upper mantle: Jour. Geophys. Res., v. 70, no. 18, p. 4641-4651.
- Ben-Menahem, A. and D. G. Harkrider, 1964, Radiation patterns of seismic surface waves from buried dipolar point sources in a flat stratified earth: Jour. Geophys. Res., v. 69, no. 12, p. 2605-2620.
- Berger, J., 1972, Strain observations with the laser strainmeter at Pinion Flats geophysical observatory: in Earthquake Research in NOAA 1970-1971: NOAA Tech. Rept. ERL 236-ESL 21, p. 17-18.
- Berger, J. and R. H. Lovberg, 1970, Earth strain measurements with a laser interferometer: Science, v. 170, p. 296.
- Berger, J. and F. Wyatt, 1973, Some observations of earth strain tides in California: Phil. Trans. R. Soc. London A., v. 274, p. 267-277.
- Bolt, B. A. and R. D. Miller, 1971, Seismicity of northern and central California: Bull. Seismol. Soc. America, v. 61, p. 1831-1847.
- Booker, A.H. 1964, Estimation of network capability: AFTAC, AF 33 (657)-12447, VT/2037, January 1964.
- Boucher, G. W., A. Ryall, and A. Jones, 1969, Earthquakes associated with underground nuclear explosions: Jour. Geophys. Res., v. 74, p. 3808-3820.
- Brown, F., 1974, Personal communication: Dept. of Geophysics, Colo. School of Mines, Golden, Colorado.

- Brune, J. N. and P. W. Pomeroy, 1963, Surface wave radiation patterns for underground nuclear explosions and small magnitude earthquakes: *Jour. Geophys. Res.*, v. 68, p. 5005-5028.
- Bufe, C. G., 1972, Strain and tilt observations near an active fault: *Stability of Rock Slopes*, 13th Symposium on Rock Mechanics, ASCE, p. 685-690.
- Carpenter, E. W., R. A. Savill, and J. K. Wright, 1962, The dependence of seismic signal amplitudes on the size of the underground explosions: *Jour. Geophys. Res.*, v. 6, p. 426-440.
- Cloud, W. K. and G. W. Simila, 1973, *Bulletin of the seismograph stations: Berkeley, Univ. of California-Berkeley*, v. 42, p. 1-122.
- Cook, K. L., 1962, The problem of the mantle-crust mix: lateral inhomogeneity in the uppermost part of the earth's mantle: *Advan. Geophys.*, v. 9, p. 295-360.
- Cook, K. L., 1969, Active rift system in the Basin and Range Province: *Tectonophysics*, v. 8, p. 469-511.
- Davis, L. L. and L. R. West, 1973, Observed effects of topography on ground motion: *Bull. Seismol. Soc. America*, v. 63, p. 283-298.
- Dickey, D. D., 1969, Strain associated with the BENHAM underground nuclear explosion: *Bull. Seismol. Soc. America*, v. 59, p. 2221-2230.
- Dickey, D. D., 1971, Strain accompanying the JORUM underground nuclear explosion and its relation to geology: *Bull. Seismol. Soc. America*, v. 61, p. 1571-1582.
- Dix, C. H., 1969, Tidal stresses associated with earthquakes: *EOS, Trans. Amer. Geophys. Union*, v. 50, p. 242.
- Ekren, E. B., 1968, Geologic setting of Nevada Test Site and Nellis Air Force Range: *Geol. Soc. America Memoir* 110.
- Emiliani, C., C. G. A. Harrison, and M. Swanson, 1969, Underground nuclear explosions and the control of earthquakes: *Science*, v. 165, p. 1255-1256.
- Engdahl, E. R., 1972, Seismic effects of the MILROW and CANNIKIN nuclear explosions: *Bull. Seismol. Soc. America*, v. 62, p. 1411-1423.
- Environmental Research Corporation, 1974, Prediction of ground motion characteristics of underground nuclear explosions: *AEC Rept. NVO-1163-239*, 201 p.
- Evernden, J. F., 1967, Magnitude determination at regional and near-regional distances in the United States: *Bull. Seismol. Soc. America*, v. 57, no. 4, p. 591-639.

- Evernden, J.F. and J. Filson, 1971, Regional dependence of surface-wave versus body-wave magnitudes: *Jour. Geophys. Res.*, v. 76, p. 3303-3308.
- Frantti, G. E. , 1965, Investigation of short-period seismic noise in major physiographic environments of continental United States: *Inst. of Sci. and Tech., Univ. of Michigan, Ann Arbor, Michigan.* Project No. 8652, Task No. 865204, AFCRL-65-406, June 1965.
- George, G.D., 1974, Investigation of spatial and temporal migration of seismic activity in the California/Nevada area: M.S. thesis, *Univ. of Wisconsin-Milwaukee*, 125p.
- George, G.D., P.J. Tatar, R.W. Taylor, D.E. Willis, and C.G. Bufe, 1974, Earth strain measurements and strain release in Nevada and adjacent areas: Paper presented at Annual Meeting Seismol. Soc. America, Las Vegas, Nevada.
- Gutenberg, B., 1955, Seismograph stations in California, in *Earthquakes in Kern County, California during 1952: State of California, Department of Natural Resources Bulletin 171, part 2*, p. 153-156.
- Gutenberg, B. and C.F. Richter, 1954, *Seismicity of the Earth and Associated Phenomena: Princeton Univ. Press.*
- Guyton, J.W., 1964, Systematic deviations of magnitude from body waves at seismograph stations in the United States: p. 111-126 in *Proceedings of the VESIAC Conference on Seismic Event Magnitude Determination, VESIAC Staff (ed.), Univ. of Michigan, Ann Arbor, 141 p.*
- Hamilton, R.M. and J.H. Healy, 1969, Aftershocks of the BENHAM nuclear explosion: *Bull. Seismol. Soc. America*, v. 59, p. 2271-2282.
- Hamilton, R.M., F.A. McKeown and J.H. Healy, 1969, "Seismic activity and Faulting associated with a Large Underground Nuclear Explosion", *Science*, vol. 166, p. 601-604.
- Hamilton, R.M., B.E. Smith, F.G. Fisher, and P.J. Paparek, 1972, Earthquakes caused by underground nuclear explosions on Pahute Mesa, Nevada Test Site: *Bull. Seismol. Soc. America*, v. 62, p. 1319-1341.
- Harrison, J.C., N.F. Ness, I.M. Longman, R.F.S. Forbes, E.A. Kraut, and L.B. Slichter, 1963, Earth-tide observations made during the International Geophysical Year: *Jour. Geophys. Res.*, v. 68, p. 1497-1516.
- Healy, J.H. and P.A. Marshall, 1970, Nuclear explosions and distant earthquakes: A search for correlations: *Science*, v. 169, p. 176-177.
- Heigold, P.C., 1968, Note on the earthquake of November 9, 1968, in southern Illinois: *Ill. State Geol. Survey, Environ. Geol. Notes*, no. 24, 16p.
- Herrin, E., 1969, Regional variations of P-wave velocity in the upper mantle beneath North America: p. 242-246 in *The Earth's Crust and Upper Mantle, Amer. Geophys. Union Monograph No. 13, P.J. Hart (ed.): Amer. Geophys. Union, Washington, D.C., 735p.*

- Hileman, J.A., C.R. Allen, and J.M. Nordquist, 1973, Seismicity of the southern California region - 1 January 1932 to 31 January 1972: Pasadena, California Institute of Technology, 83p.
- Hollister, J.C. and R.J. Weimer, Editors, 1968, Geophysical and Geological Studies of the Relationships Between the Denver Earthquakes and the Rocky Mountain Arsenal Well, quarterly of the Colorado School of Mines, vol. 63, no. 1, part A.
- King, G.C.P., and Gerard, V.B., 1969, Earth tides recorded by the 55cm. Cambridge laser interferometer: Geophys. Jour. R. Astr. Soc., v. 18, p. 437-438.
- King, G.C.P., Bilham, R.G., Gerard, V.B., and Davies, D., 1969, New strainmeters for geophysics: Nature, v. 223, p. 818-819.
- King, G.C.P. and R.G. Bilham, 1973, Strain measurement instrumentation and technique: Phil. Trans. R. Soc. London A., v. 274, p. 209-217.
- Knopoff, L., 1964, Earth tides as a triggering mechanism for earthquakes: Bull. Seismol. Soc. America, v. 54, p. 437-438.
- Kumamoto, L.H., 1973, Redundant strain observations in southern Nevada: strain steps from the HANDLEY nuclear test and secular strains: M.S. thesis, Colorado School of Mines, Golden, Colo., 73p.
- Lauderback, G.D., 1942, History of the University of California seismographic stations and related activities: Bull. Seismol. Soc. America, v. 32, p. 206-229
- Lee, M.W. and P. Brown, 1972, Pinion Flats strain measurements: Benioff Instrument, in Earthquake Research in NOAA 1970-1971, NOAA Tech. Rept. ERL 236-ESL 21, p.15-
- Long, L.H., ed., 1968, The world almanac and book of facts, 1969 edition: Doubleday and Co., Inc., New York, 932p.
- Long, L.H., ed., 1969, The world almanac and book of facts, 1970 edition: Doubleday and Co., Inc., New York, 952p.
- Long, L.H., ed., 1970, The world almanac and book of facts, 1971 edition: Doubleday and Co., Inc., New York, 952p.
- Long, L.T. and J.W. Berg, 1969, Transmission and attenuation of the primary seismic wave, 100 to 600 km: Bull. Seismol. Soc. America, v. 59, p. 131-146.
- Longwell, C.R., 1960, Possible explanation of diverse structural patterns in southern Nevada: Am. Jour. Sci., v. 258-A, p. 192-203.
- Mackay School of Mines, 1972, Bulletin of the Seismological Laboratory for the period January 1 to March 31, 1971: Reno, Univ. of Nevada, 36p.
- Major, M.W., 1971, Strain episodes in the Aleutian Islands: ABS. 66th Seismol. Soc. America Mtg., March 25-27, Riverside, California.
- Major, M.W., G. Suttén, J. Oliver, and R. Metsger, 1964, On elastic strain of periods 5 seconds to 100 hours: Bull. Seismol. Soc. America, v. 54, p. 295-346.

- Major, M. W., D. L. Butler, and M. E. Blackford, 1969, Residual strains associated with MILROW: Rept. to Atomic Energy Commission, Las Vegas, Nevada, 26 p.
- Malone, S. D., 1972, Earth strain measurements in Nevada and possible effects on seismicity due to earth tides: Tech. Rept., Seismol. Laboratory, Univ. of Nevada, Reno, 139 p.
- Melchior, P., 1966, The Earth Tides: Pergamon Press, London, 458 p.
- Mickey, W. V., 1963, Equivalent earthquake magnitudes for selected nuclear detonations at the Nevada Test Site: U.S. Dept. of Commerce, Coast and Geodetic Survey, Washington, D. C., 25 p.
- Molnar, P., K. Jacob, and L. R. Sykes, 1969, Microearthquake activity in eastern Nevada and Death Valley, California, before and after the nuclear explosion BENHAM: Bull. Seismol. Soc. America, v. 59, p. 2177-2183.
- Oliver, J., 1964, Propagation of PL waves across the United States: Bull. Seismol. Soc. America, v. 54, no. 1, p. 151-160.
- Olsen, C. W., 1967, Time history of the cavity pressure and temperature following a nuclear detonation in alluvium: Jour. Geophys. Res., v. 72, p. 5037-5041.
- Ozawa, Izuo, 1973, in King, G. C. P. and R. G. Bilham, 1973, Strain measurement instrumentation and technique: Phil. Trans. R. Soc. London A., v. 274.
- Pakiser, L. C. and I. Zietz, 1965, Transcontinental crustal and upper mantle structure: Rev. Geophys., v. 3, no. 4, p. 505-520.
- Press, F., 1960, Crustal structure in the California-Nevada region: Jour. Geophys. Res., v. 65, p. 1039-1052.
- Press, F., 1965, Displacements, strains and tilts at teleseismic distances: Jour. Geophys. Res., v. 70, p. 2395-2412.
- Priestly, K., 1974, Earth strain observations in the Western Great Basin: Tech. Rept. to ARPA, Grant No. AFOSR-71-2041, Seismol. Lab., Univ. of Nevada, p. 185.
- Revock, K. L., 1974, An investigation of nuclear detonations and solid earth tides as possible triggering mechanisms for earthquakes in central California during the time period 1969 through 1970: unpublished M.S. thesis, Univ. of Wisconsin-Milwaukee, 118 p.
- Richter, C. F., 1935, An instrumental earthquake magnitude scale: Bull. Seismol. Soc. America, v. 25, no. 1, p. 1-32.

- Richter, C. F., 1958, Elementary Seismology: San Francisco, W. H. Freeman and Company, 768 p.
- Romig, P. R., M. W. Major, C. J. Wideman, and D. Tocher, 1969a, Residual strain associated with JORUM: Rept. to Atomic Energy Commission, 19 p.
- Romig, P. R., M. W. Major, C. J. Wideman, and D. Tocher, 1969b, Residual strains associated with a nuclear explosion: Bull. Seismol. Soc. America, v. 59, no. 6, p. 2167-2176.
- Romig, P. R. and L. H. Kumamoto, 1972, Interpretation and display of strain data, in Earthquake Research in NOAA, NOAA Tech. Rept. ERL 236-ESL 21, p. 15-16.
- Ryall, A., D. B. Slommons, and L. D. Gedney, 1966, Seismicity, tectonism, and surface faulting in the western United States during historic time: Bull. Seismol. Soc. America, v. 56, p. 1105-1135.
- Ryall, A., J. D. VanWormer, and A. E. Jones, 1968, Triggering of micro-earthquakes by earth tides and other features of the Truckee, California, earthquake sequence of September, 1966: Bull. Seismol. Soc. America, v. 58, p. 215-248.
- Ryall, A. and G. W. Boucher, 1969, Earthquakes and nuclear detonations: Science, v. 167, p. 1013.
- Savage, J. C., W. T. Kinoshita, and W. H. Prescott, 1974, Geodetic determination of strain at the Nevada Test Site following the HANDLEY event: Bull. Seismol. Soc. America, v. 64, p. 115-129.
- Shakal, A. F., 1972, Tectonic strain relief as a function of earthquake magnitude and distance: unpublished M.S. thesis, Univ. of Wisconsin-Milwaukee, 48 p.
- Simon, R. B., 1968, Remarks on a paper by H. Freedman, "Estimating earthquake magnitude": Bull. Seismol. Soc. America, v. 58, no. 2, p. 745-746.
- Smith, S. W., J. McGinley, Jr., C. Scholz, and L. Johnson, 1969a, Effects of large explosions on tectonic strain: Jour. Geophys. Res., v. 74, no. 12, p. 3308-3309.
- Smith, S. W., C. B. Archambeau, and W. Gile, 1969b, Transient and residual strains from large underground explosions: Bull. Seismol. Soc. America, v. 59, no. 6, p. 2185-2196.
- Smith, S. W. and R. Kind, 1972, Observation of regional strain variations: Jour. Geophys. Res., v. 77, p. 4976-4980.
- Solomon, S. C. and M. N. Toksöz, 1970, Lateral variation of attenuation of P and S waves beneath the United States: Bull. Seismol. Soc. America, v. 60, no. 3, p. 819-838.

- Springer, D.L. and R.L. Kinnaman, 1971, Seismic source summary of U.S. underground nuclear explosions, 1961-1970: *Bull. Seismol. Soc. America*, v. 61, p. 1073-1098.
- Suppe, J., C. Powell, and R. Berry, 1974, Regional topography, seismicity, Quaternary volcanism and the present-day tectonics of the western United States: Princeton, Princeton Univ., 52 p. (in press).
- Sydenham, P.H., 1969, A tensional-wire strain seismometer: *Jour. of Sci. Instr.*, Series 2, v. 2, p. 1095-1097.
- Tamrazan, G.P., 1967, Tide-forming forces and earthquakes: *Ecarus*, v. 7, p. 59-65.
- Tamrazan, G.P., 1968, Earthquakes of Nevada (U.S.A.) and tidal forces: *Jour. Geophys. Res.*, v. 78, p. 6013-6019.
- Thompson, G.A. and M. Talwani, 1964, Geology of the crust and mantle, western United States: *Science*, v. 146, p. 1539-1549.
- Thompson, G.A. and D.B. Burke, 1973, Rate and direction of spreading in Dixie Valley, Basin and Range Province, Nevada: *Bull. Geol. Soc. America*, v. 84, p. 627-632.
- Thornbury, W.D., 1965, Regional Geomorphology of the United States: New York, John Wiley and Sons, Inc., 609 p.
- Tocher, D., Pfluke, J.H., and Blackford, M.E., 1971, Strain measurements in the Aleutian Islands: NOAA Tech. Rept. ERL 215-ESL 17, 24 p.
- Toksöz, M.N., D.G. Harkrider, and A. Ben-Menahem, 1965, Determination of source parameters by amplitude equalization of seismic surface waves: *Jour. Geophys. Res.*, v. 70, no. 4, p. 907-922.
- Toksöz, M.N. and H. Kehrler, 1971, Underground nuclear explosions: Tectonic utility and dangers: *Science*, v. 173, p. 230-233.
- Toksöz, M.N., and K.C. Thomson, and T.J. Ahrens, 1971, Generation of seismic waves in prestressed media: *Bull. Seismol. Soc. America*, v. 61, p. 1589-1623.
- van Nostrand, R., 1966, Reverberation effects in signal amplitude, p. 1-10 in *Proceedings of the VESIAC Special Study Conference on Seismic Signal Anomalies, travel times, amplitudes, and pulse shapes*, VESIAC Staff (eds.): Rept. No. 4410-99-X, Univ. of Michigan, Ann Arbor, 173 p.
- van Veen, H.J., Savino, J., and Alsop, L.E., 1966, An optical maser strainmeter, *Jr. Geophys. Res.*, v. 71, no. 22, p. 5478-5479.
- von Seggern, D., 1970, The effects of radiation patterns on magnitude estimates: *Bull. Seismol. Soc. America*, v. 60, no. 2, p. 503-516.
- Wallace, Robert E., 1974, Goals, Strategy, and Tasks of the Earthquake Hazard Reduction Program, U.S. Geological Survey Circular 701.
- Wideman, C.J., 1971, Nuclear explosions: I - Strain steps: Abstracts Cordilleran Section, 67th Annual Meeting of Geol. Soc. America, v. 3.
- Wideman, C.J. and M.W. Major, 1967, Strain steps associated with earthquakes: *Bull. Seismol. Soc. America*, v. 57, p. 1429-1444.

- Willis, D. E., 1968, An investigation of seismic wave propagation in the eastern United States: Univ. of Michigan, Rept. No. 8071-16-T, 86 p.
- Willis, D. E., 1970, Microearthquake studies in connection with the JORUM underground nuclear detonation: presented at the Geol. Soc. America Annual Meeting, Milwaukee, Wisconsin.
- Willis, D. E. and J. M. DeNoyer, 1966, Seismic attenuation and spectral measurements from the Lake Superior experiment: p. 218-226 in The Earth Beneath the Continents, Amer. Geophys. Union Monograph No. 10, J. S. Steinhart and T. J. Smith (eds.): American Geophys. Union, Washington, D. C., 663 p.
- Willis, D. E., G. George, K. G. Poetzi, C. E. Saltzer, A. F. Shakal, R. Torfin, and T. L. Woodzick, 1972, Seismological and related effects of the CANNIKIN underground nuclear explosion: Univ. of Wisconsin-Milwaukee, Tech. Rept. No. COO-2138-9, p. 1-89, A1-A13, B1-B43.
- Willis, D. E., C. G. Bufe, K. G. Poetzi, A. F. Shakal, P. J. Tatar, and R. D. Torfin, 1973, An investigation of explosion-induced ground motion and its relationship to natural seismicity: Univ. of Wisconsin-Milwaukee, Tech. Rept. No. COO-2138-11, 29 p.
- Wilson, J. T., 1972, Mao's almanac - 3000 years of killer earthquakes: Saturday Review, v. 55, Feb. 19, p. 60-64.
- Woollard, G. P., 1969, Tectonic activity in North America as indicated by earthquakes, in Hart, P. J., ed., The Earth's Crust and Upper Mantle: Washington, American Geophys. Union, p. 125-133.
- Yeatts, F. R., 1973, A multipole representation of earthquake source mechanisms: Bull. Seismol. Soc. America, v. 63, p. 211-226.

APPENDIX A

Glossary

A brief glossary has been prepared to define the terms that have been used frequently in this report. More definitions of terms can be found in the other appendices.

Aftershocks - Secondary tremors following the main shock of an earthquake. In the case of nuclear detonations, minor tremors that are sometimes observed in the region of the shot.

Alluvium - A term used to describe detrital or stream deposits such as earth, sand, gravel and conglomerates.

Andesite - A type of volcanic rock.

Body Waves - Compressional (P) or transverse (S) waves which propagate through the interior of the earth. They are not related to a boundary surface.

Block Faulting - A subdivision of the earth's crust into blocks by normal faulting.

Caldera - A large basin-shaped depression that is approximately circular in nature that encompasses a volcanic vent formed by volcanic action.

Clastic - A type of rock formed primarily from detritus that was transported mechanically into its place of deposition.

Detritus - The name given to rock materials such as sand, silt, and mud that were formed by the mechanical disintegration of rock.

Epicenter - The point on the earth's surface directly above the point where an earthquake begins.

Eugeosyncline - A long, narrow geosyncline in which volcanic rocks are abundant.

Fault - A fracture or fracture zone along which there has been displacement of the two sides relative to each other.

Graben - A fault block that has been downthrown along faults relative to the rocks on either side of the block.

Magnitude (of an earthquake) - A logarithmic scale that is used to determine the size of an earthquake and is based on the amplitude of the seismic waves measured on seismograms. The scale can be used to estimate the energy release at the source.

M_b = body wave magnitude
 M_s = surface wave magnitude
 M_L = local magnitude

Microearthquake - An earthquake of small magnitude

Microseism - Low-level ground vibrations, often more or less continuous in nature, caused by wind, waves, etc.

Miogeosyncline - A long, narrow geosyncline in which volcanic rocks are rare.

Normal Fault - A fault in which the displacement of the block lying above the inclined fault plane is downward relative to the lower block.

P_n - The compressional or P wave that is critically refracted at the base of the earth's crust (Mohorovicic discontinuity).

Rhyolite - A type of volcanic rock.

Right-Lateral Faults - A strike-slip fault in which the apparent displacement of the opposite side as one stands on one side of the fault plane looking at the opposite side is to the right.

Seismicity - Refers to the frequency of occurrence of earthquakes in a given region.

Strain - The change in length per unit length in a given direction.

Strike-Slip Faults - A fault in which the displacement is essentially horizontal along the strike of the fault.

Surface Waves - Seismic waves which propagate along the earth's surface with amplitudes that decrease exponentially with depth (Love waves and Rayleigh waves).

Tectonic - Refers to mountain building forces. Earthquakes caused by mountain building forces rather than those caused by volcanic action, landslides or cavern collapses.

Thrust Fault - A fault in which the displacement of the block lying above the inclined fault plane is upward relative to the lower block.

Transcurrent Fault - Strike-slip fault.

Tuff - A type of volcanic rock.

APPENDIX B

Introduction to Analytical Techniques

Correlation studies are used throughout the scientific world in attempts to establish causal relationships and better understand given physical processes. Simply defined, correlation is merely the degree of similarity which exists between observational quantities. In this sense, correlation was employed by very early man when he noted that at the beginning of the four climatic seasons the stars exhibited certain spatial relationships. It could be said that early man established a high correlation between star positions and climatic season. While the reasons for this high correlation are obvious today, they were not at that time and, in fact, provided the initial observations that eventually led to an understanding of the earth's rotational characteristics.

On a more modern level, it is obvious that the data of Figure 1a is more similar to the data of Figure 1b than to the data of Figure 1c. Thus, it is appropriate to say Figure 1a is highly correlated with Figure 1b but poorly correlated with Figure 1c. For scientific work, however, it is necessary that quantitative measures of similarity be used rather than qualitative descriptions such as high and poor. A quantitative measure of similarity between observations X_i and observations Y_i is provided by the correlation coefficient, σ , defined as

$$\sigma = \frac{\sum_{i=1}^N X_i Y_i}{\sqrt{\sum_{i=1}^N X_i^2 \sum_{i=1}^N Y_i^2}}$$

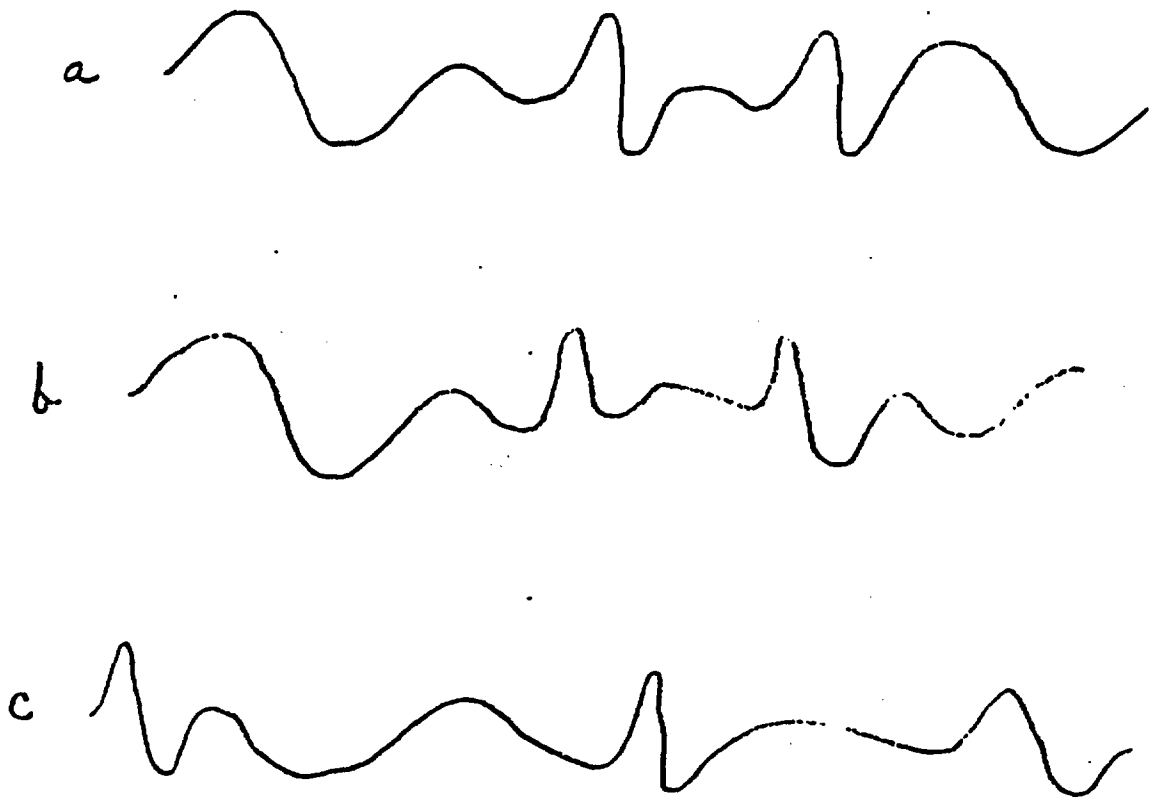


Figure 1. Examples of data with a high correlation coefficient, a and b, and data with a low correlation coefficient, a and c or b and c.

The observations X_i and Y_i are any set of measurements such as educational level (X_i) and income (Y_i) for a group of individuals or the number of sun spots (X_i) and stock market average (Y_i) for some period of time. The correlation coefficient, which measures the degree of similarity between the observations, may be at most 1, which indicates the observations are identical, zero, indicating the observations are in no way similar, or -1, indicating the observations are identical but inverted. In general, the correlation coefficient would fall between these extremes and yield values such as 0.85, 0.32, 0.01, -0.27 or -0.91. While the formula for calculating the correlation coefficient appears complex, it should be remembered that it simply provides a quantitative measure of the descriptive terms employed by all people.

When considering the correlation between two quantities which are themselves a function of a third quantity, it is necessary to consider the correlation coefficient in terms of a variable called the lag. An example of this is provided by the annual birth rate and the total number of students in college. Both of these quantities are a function of time and are shown in Figure 2a and b. It is evident that if the correlation coefficient were calculated using equation 1 for the data of Figure 2, the result would be rather low. If, on the other hand, the correlation coefficient were calculated after the peak in Figure 1a was moved down to the peak in Figure 1b, or the peak in 1b moved back to the peak in 1a, a very high value would result. The very low value of correlation obtained on a one-to-one basis and high value obtained after moving one data set forward or back, simply reflects the fact that the children born in any one year do not enter college until 17 years later. The amount by which one

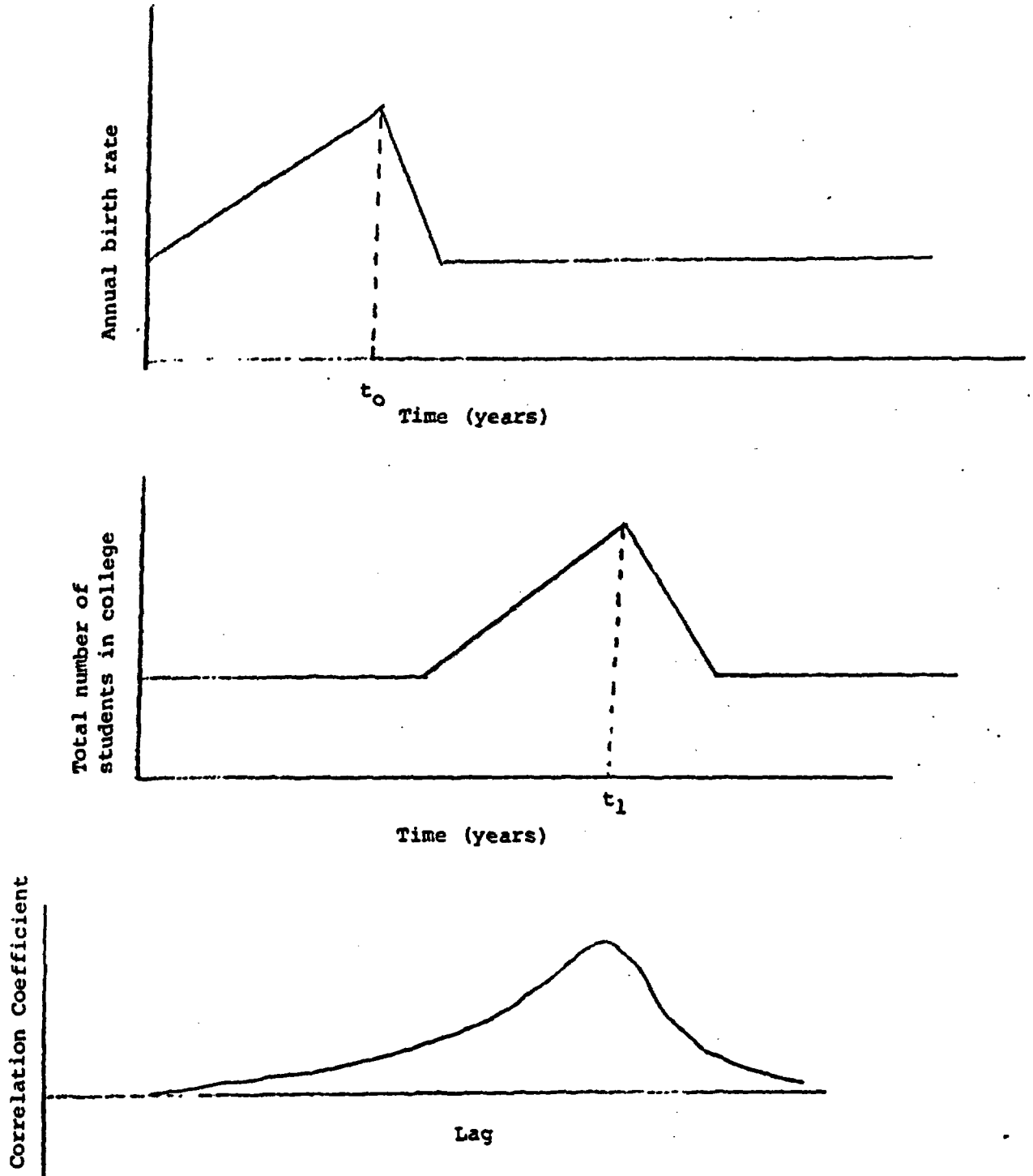


Figure 2. The effect of lag in a data set on the correlation coefficient.

data set is moved prior to calculating the coefficient is called the lag. In scientific work it is usually necessary to calculate the correlation coefficient at as many lags as possible. The resulting correlation coefficients are then plotted versus the lag at which they were calculated. An example of this is shown in Figure 2c for all possible positive lags. Negative lags are also possible and would result from moving Figure 2a to the left. Negative lags are not shown in Figure 2c because in this case they contain no useful information. The lag at which the peak correlation occurs indicates by how much the observations of one data set are behind or ahead of the observations in another data set.

Correlation studies provide a useful tool to determine the degree of similarity which exists between various data sets. Studies of this nature have been highly successful in uncovering the principles which govern observed processes. They cannot, however, be employed to establish a definite causal relationship between all processes which exhibit strong correlation.

APPENDIX C

Celestial Terminology

The daily celestial events included in this investigation relate either to the moon or to the sun. The lunar events are moonrise, moon-noon, moonset, and moon-midnight. At moonrise, the moon is first visible over the eastern horizon to an observer at the locality 35°N Latitude, 120°W Longitude. At moon-noon, the moon is directly over the 120°W Longitude line. At moonset, the moon disappears over the western horizon to an observer at the locality 35°N Latitude, 120°W Longitude. At moon-midnight, the moon is directly over the 120°E longitude line. The lunar day is the time from moon-midnight to moon-midnight and is 24 and 5/6 earth hours in duration.

The daily solar events are sunrise, noon, sunset, and midnight. At sunrise, the sun is first visible over the eastern horizon to an observer at the locality 35°N Latitude, 120°W Longitude. At noon, the sun is directly over the 120°W Longitude line; noon occurred at or near 20:00 hours Co-ordinated Universal Time throughout the study interval. At sunset, the sun starts to disappear over the western horizon to an observer at the locality 35°N Latitude, 120°W Longitude. At midnight, the sun is directly over the 120°E Longitude line; midnight occurred at or near 08:00 hours Co-ordinated Universal Time throughout the study interval. The times of local sunrise and local sunset varied from day to day; the times of local noon and local midnight did not vary more than +6 minutes 20:00 hours and 08:00 hours throughout the study interval. The mean solar day is the time from 00:00 hours to 00:00 hours Co-ordinated Universal Time and is 24 earth hours in duration.

A fortnightly celestial event has a period near a multiple of two weeks. The fortnightly celestial events included in this investigation are either related to the moon, or to the moon and sun together. Apogee and perigee are the lunar fortnightly celestial events. During apogee, the moon is at its maximum distance from the earth and lunar angular acceleration is at its minimum. During perigee, the moon is at its minimum distance from the earth and lunar angular acceleration is at its maximum. When the successive positions of apogee and perigee are joined, the connecting line is the major axis of the lunar orbit. This axis is the lunar apsidal axis and the positions of apogee and perigee are the lunar apsides. The lunar anomalistic month is the time interval from one perigee to the next; this time interval is 27.6 earth days in duration. The time from one perigee to the next apogee, or from one apogee to the next perigee, is approximately 2 weeks, a fortnight, in duration.

The fortnightly events that are related to the moon and sun together are also known as the lunar phases. Lunar phases result from the changing positions of the moon and sun relative to the earth. During syzygy, the sun, the earth, and the moon are all in one straight line. The lunar phases known as new moon and full moon occur during syzygy. During full moon, the moon is behind the earth and sun, during new moon, the earth is behind the moon and sun. During quadrature, the moon is 90° out of phase with the sun relative to the earth. During quadrature, the lunar phase will be either a first quarter or a last quarter. The time interval from new moon, to first quarter, to full moon, to last quarter, and back to new moon again, is the lunar synodic month. The lunar synodic month is 29.6 earth days in duration and the duration from one

syzygy lunar phase to the next syzygy lunar phase is approximately a fortnight. The quadrature lunar phases are approximately a fortnight apart.

The secular celestial events included in this investigation are related to the sun. There are two solar-related secular celestial phenomena included here. The first category includes the earth apsides and the second category includes the events resulting from the tilt in the earth's rotational axis relative to the plane of the earth's orbit. The earth apsides are aphelion and perihelion. During aphelion, the earth is at its maximum distance from the sun and the earth's angular acceleration is at its minimum. During perihelion, the earth is at its minimum distance from the sun and the earth's angular acceleration is at its maximum. During the study interval, aphelion occurred in early July and perihelion occurred in early January. The earth's rotational axis is not normal to the plane of the earth's orbit. This tilt in the axis results in the celestial phenomena known as equinoxes and solstices. During an equinox, the sun is directly over the equator. Day and night are of equal duration in all parts of the world during an equinox. There are two equinoxes per year: the vernal equinox occurs between March 20 and 23 and the autumnal equinox occurs between September 20 and 23. During a solstice, the sun is at its northern or southern extremity. A summer solstice occurs between June 20 and 23 and at that time the northern hemisphere day is at its maximum duration and the sun is at its northern extremity. A winter solstice occurs between December 20 and 23 and at that time the northern hemisphere night is at its maximum duration and the sun is at its southern extremity.

APPENDIX D

Earth Strain Measurement Instrumentation

Measurements of the earth's elastic deformation in response to large scale forces began by Milne in Japan in 1888 and later by Oddone. Milne believed that relative ground movements during an earthquake were the cause of much building damage. To record the relative movements of the ground, he set up a device consisting of two piers separated by an interval of three feet. A rod was connected to one of these piers and extended to within a short distance of the other. A lever system recorded the relative motion of the rock with respect to the pier. While magnification of this crude system was very low, Milne was able to record traces of a few millimeters amplitude in some of the large earthquakes. Oddone's instrument was similar in design to Milne's. Oddone, however, increased the pier separation to three meters and by means of a hydraulic system was able to obtain a magnification of approximately 3600. Due to the lack of a recording mechanism, Oddone was not able to observe the instrument's behavior with respect to earthquakes.

The first properly conceived technique of strain measurement was developed by Benioff in 1935. A 25 meter steel standard was suspended by wire in a jacketed pipe with one end embedded in a concrete pier. The other end of the steel standard was allowed to hang freely with only the jacketed pipe bolted to the second pier. The instrument's location under the laboratory at the California Institute of Technology, helped to provide thermal stability. In addition, asbestos insulation was packed around the steel rod to further reduce short period temperature variations. Benioff's development of an electromagnetic transducer for displacement seismographs

enabled the continuous recording of a greatly magnified ($\times 10^6$) strain signal which in this case was actually a time differential of strain. The strain seismometer developed by Benioff recorded medium period wavelengths from seismic events, but was insensitive to strains of very long seismic or tidal periods. Within the transducer's useful range of frequencies, the strain seismograph was more sensitive to displacements than the Michelson interferometer (Benioff, 1935).

Later, Benioff (1959) detailed a much improved strainmeter which employed a quartz rod as opposed to the previous steel standard. The quartz rod with a lower temperature coefficient reduced temperature noise. New transducers were also installed which output directly in units of strain. The transducers, however, were nonlinear and subject to variation in gain with time. To compensate, continuous calibration was essential and was accomplished with a magnetostrictive element.

Romig (in Romig and others, 1969) developed a modified Benioff capacitive displacement transducer with continuous mechanical calibration. The transducers, constructed by the Colorado School of Mines, were used in strain studies by later researchers (Tocher and others, 1971; Malone, 1972).

Sassa (in Melchior, 1966) constructed an extensometer of a very different design. Simple in construction, the extensometer consisted of an invar wire suspended between two fixed points approximately twenty meters apart. A weight of 350 grams was suspended from the center by a wire 0.2 mm in diameter. Linear deformations of the ground caused variations in the distance between the two fixed points, which in turn produced variation in the tension on the wire. The tensional variation caused the weight to

oscillate vertically and this oscillation was translated into a rotation of a mirror through a bifilar suspension. Displacement resolution of the instrument was on the order of one part in 10^8 .

Sydenham (1969) described a new tension wire extensometer which utilized constant rather than variable wire tension. Experimental results established that creep and secular drift of an Invar 36 wire and measuring system were less than 10^{-7} over several hundred hours with a detection limit of relative displacements on the order of 10^{-10} , which is equivalent to or better than quartz rod systems (Sydenham, 1969). Linear-variable differential transducers measured the movements of the balances which maintained the constant tension. Simplicity of design, rapid installation, and low cost make this system attractive for geophysical use. A major limitation of the system, however, may lie in the excessive tension transients in the wire due to high rotational inertia of the beam balances caused by violent ground movement near earthquake epicenters (Sydenham, 1969). Presently, the University of Cambridge, Department of Geodesy and Geophysics, is marketing these instruments under the name of Cambridge Wire Strainmeters.

Due to the uncertainty of the stability in materials and size limitations of the quartz rod and invar wire extensometers, interest developed in optical systems. The first system using a laser was constructed by Van Veen, Savino and Alsop in 1966. Two mutually perpendicular lasers with end mirrors attached to rock, measured changes in laser cavity length by measuring phase changes between the two lasers. This frequency difference was found by beating the optical outputs in a photomultiplier. The frequency of the electrical output of the photomultiplier provided a

measure of the shear strain in an axis oriented 45° to the laser axes. As it is still not possible to construct a single mode laser over one meter in length, later laser systems have not followed Van Veen's approach in direct coupling of the laser cavity to the rock. Newer systems have adopted the use of a passive interferometer with an external laser.

Vali and Bostrom (in King and Bilham, 1973) developed the first long path laser interferometer strainmeter. The system had a base length of 1020 meters and used a fringe following method for measuring the strain. Several other variations on the laser interferometer have been introduced (King and Gerard, 1969; King and others, 1969; Berger and Lovberg, 1970). While the laser systems have shown to be more than adequate for earth tidal and secular strain studies with a sensitivity of one part in 10^{10} or greater (King and Gerard, 1969), prohibitive costs make their use on an extensive geophysical scale unlikely.

Available Instrumentation

The strain data for this study were collected by the Colorado School of Mines and the Earthquake Mechanisms Laboratory of the National Oceanic and Atmospheric Administration. The instruments are quartz-rod extensometers of Benioff design (1959) with modified Benioff capacitance transducers and integral micrometer calibration. Installed in trenches, the quartz-rod standards are suspended by wire in a five inch jacket pipe with one end imbedded in a concrete pier. The other end of the quartz rod is allowed to hang freely with only the jacket pipe bolted to a second concrete pier.

The capacitance transducers, which are made by the Colorado School of Mines, sense movement of the quartz with respect to the free end pier. The variable capacitance is provided by three square plates shown in Figure D-1. The inner plate is attached to the quartz rod while the other two outer plates are mounted on a translation table driven by a micrometer at a rate of two hundred and fifty micro-inches per revolution. The micrometer is driven by a DC motor which is remotely controlled. Manual override is also possible.

The above described plate assembly forms two capacitors which are parts of two tank circuits driven by a common oscillator. The signals from these circuits are rectified, filtered, and fed into a differential amplifier. The center plate, in response to the quartz to which it is connected, moves in respect to the two plates mounted on the translation table. This causes an increase of capacitance on one side while causing a decrease of capacitance on the other. When the output signal level, which is proportional to the plate movement, exceeds a certain threshold, the micrometer is driven by an automatic recentering circuit. This in turn moves the plate in the proper direction, following the center plate. Output of the amplifier is connected directly to an Esterline-Angus one-milliamp galvanometric chart recorder.

A plywood vault encompasses the free-end of the quartz standards where the above electronics are installed. The trenches, three to five feet deep, are backfilled and compacted. Hatchways which access the vaults are well insulated.

Temperature compensation is accomplished by means of aluminum fold joints between the ten-foot sections of the quartz rods. Romig and Kumamoto

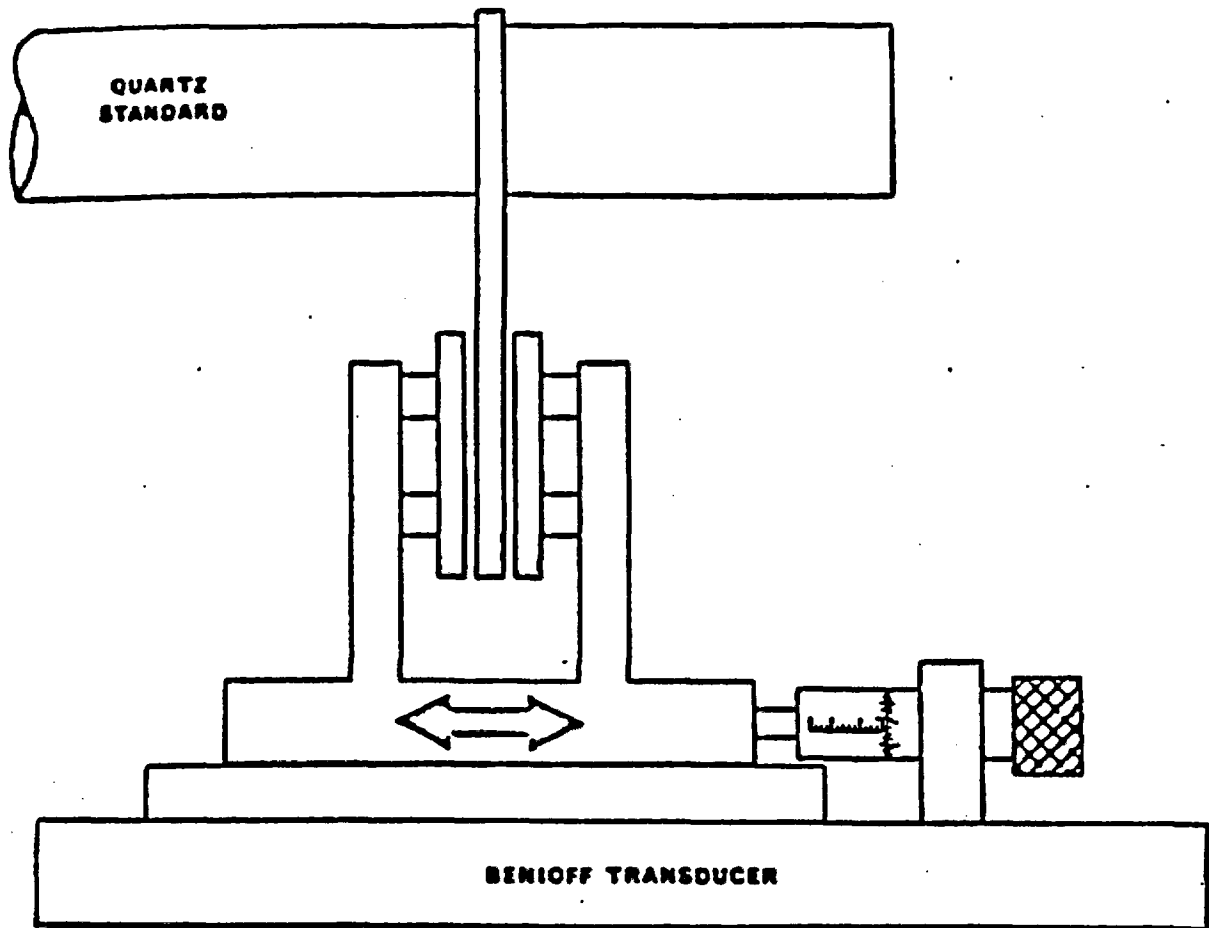


Figure 1. Diagram of the Benioff capacitance strain transducer used in strain measurement in south-central Nevada (from Tocher and others, 1971, page 11).

(1972) have determined that the sensitivity of the quartz-rod extensometers to temperature is less than 1×10^{-7} per degree centigrade, to barometric pressure is 2×10^{-8} per inch mercury, and to relative humidity is less than 1×10^{-10} per percent relative humidity.

Because of the tensor nature of strain, three horizontal components are necessary to unambiguously define the principle axes of strain. The three strainmeter stations in this study have at least three horizontal components which will allow for principle strain axes determination. Scotty's Junction contains four horizontal components which share a common free-end pier and endhouse and a vertical strainmeter. The vertical strainmeter construction differed from the others in that a single length of quartz was grouted to the bottom of a cased hole. The quartz was not thermally compensated so a well insulated endhouse was constructed. Both Twin Springs and Sleeping Mountain have three horizontal components, each of which has a separate free-end pier.

The meteorological data for this study were obtained from the Atomic Energy Commission and were recorded at the Yucca Flats weather observatory.

Distribution List

D. U. Deere, U. of Ill., Urbana, IL
N. M. Newmark, U. of Ill., Urbana, IL
T. F. Thompson, Burlington, CA
L. G. von Lossberg, Baltimore, MD
S. D. Wilson, Seattle, WA
L. S. Jacobsen, Santa Rosa, CA
Carl Kisslinger, CIRES, Boulder, CO
J. T. Wilson, Ann Arbor, MI
W. G. Van Dorn, LaJolla, CA
L. K. Bustad, U. of Calif., Davis, CA
Vincent Schultz, Wash. State U., Pullman, WA
P. A. Witherspoon, U. of Calif., Berkeley, CA
Joseph Lintz, U. of Nev., Reno, NV
C. R. Allen, Calif. Institute of Tech., Pasadena, CA
Perry Byerly, Oakland, CA
J. E. Oliver, Cornell U., Ithaca, NY
W. J. Stauder, St. Louis U., St. Louis, MO
Maj. Gen. Ernest Graves, Asst. Gen. Mgr. for Military Appl., HQ (3)
M. E. Gates, Mgr., NVOO
C. E. Williams, Dep. Mgr., NVOO
R. H. Thalgott, Test Mgr., NVOO (3)
Roger Ray, Asst. Mgr., OPS, NVOO
W. E. Ogle, NVOO
W. S. Twenhofel, USGS, Denver, CO
E. M. Douthett, Dir., OEE/NVOO
R. L. Kinnaman, Dep. Dir., OEE/NVOO
P. B. Dunaway, Sci. Dep., OEE/NVOO
C. P. Broyles, 9100, SLA, Albuquerque, NM
W. D. Weart, 9111, SLA, Albuquerque, NM
J. R. Banister, 9150, SLA, Albuquerque, NM
M. L. Merritt, 9150, SLA, Albuquerque, NM
J. E. Carothers, LLL, Livermore, CA
J. W. Hadley, LLL, Livermore, CA
H. C. Rodean, LLL, Livermore, CA
L. S. Germain, LLL, Livermore, CA
R. W. Newman, LASL, Los Alamos, NM
C. I. Browne - LASL, Los Alamos, NM
K. H. Olsen, Div. J-15, LASL, Los Alamos, NM
T. T. Scolman - LASL, Los Alamos, NM
E. D. Campbell, Chief, Bioenvironmental Br. NVOO
T. M. Humphrey, Chief, Geo/Hydro Br. NVOO
P. N. Halstead, Chief, Seismology Br. NVOO (10)
R. R. Loux, Tech. Info. Br., NVOO (1)
K. W. King, USGS, SRAB, Las Vegas, NV
W. W. Hays, USGS, SRAB, Golden, CO
E. R. Engdahl, CIRES, Boulder, CO
Art Tarr, NOAA/ESL, CIRES, Boulder, CO
M. W. Major, Colo. School of Mines, Golden, CO
Don Tocher, Woodward-Lundgren, Assoc. Oakland CA
R. M. Hamilton, USGS, Reston, VA
Tech. Library, NVOO (2)

TIC 200 2035, TELN. (2)

Distribution List (cont'd)

J. H. Healy, U.S.G.S., Menlo Park, CA
R. Brazee, NOAA/EDS, Boulder, CO
J. F. Lander, NOAA/EDS, Boulder, CO
C. Stover, NOAA/EDS, Boulder, CO
C. B. Archambeau, Cal. Tech., Pasadena, CA
D. L. Anderson, Cal. Tech. Pasadena, CA
S. W. Smith, U. of Wash., Seattle, WA
K. L. Cook, U. of Utah, Salt Lake City, UT
H. N. Pollack, U. of Mich., Ann Arbor, MI
R. M. Turpening, ERIM, Ann Arbor, MI
A. S. Ryall, U. of Nevada, Reno, NV
J. C. Savage, U.S.G.S., Menlo Park, CA
P. R. Romig, Director, Colo. School of Mines, Golden, CO
D. B. Slemmons, U. of Nevada, Reno, NV
J. C. Stepp, AEC, Washington, D.C.
J. F. Evernden, U.S.G.S., Reston, VA
R. B. Keener, Argonne Nat. Lab, Argonne, IL
B. A. Bolt, U. of Calif. - Berkeley, Berkeley, CA
T. V. McEvilly, U. of Calif. - Berkeley, Berkeley, CA
O. W. Nuttli, St. Louis U., St. Louis, MO
L. R. Sykes, Columbia U., Palisades, N.Y.
W. J. Best, AFOSR, Arlington, VA
D. H. Clemments, ARPA, Arlington, VA
J. G. Heacock, ONR, Arlington, VA
P. W. Basham, Dept. Energy Mines & Resources, Ottawa, Ontario
D. Tendall, Sandia Lab, Albuquerque, NM
B. Grote, DNA, Kirtland AFB, NM
J. E. Whitener, R & D Assoc., Santa Monica, CA
M. Nafi Toksoz, MIT, Cambridge, MA

3.7 Magnitude Variations

Earthquake magnitudes which are determined directly from seismic wave amplitudes on seismograph recordings allow a better understanding and interpretation of earthquakes. Richter's (1935) original magnitude scale (M_L - local magnitude) was developed for use in southern California and was limited to earthquakes with epicentral distances of less than 600 kilometers. Magnitude scales (body wave - m_b and surface wave - M_s) were later developed for use at greater distances and other regions. Some inconsistencies arose in the use of these different scales due primarily to the widely fluctuating geologic environments in the earthquake source regions, at the recording stations and along the intervening transmission paths. Richter's equations for the scales have been modified to fit restricted regions in North America by Bath (1969), Evernden (1967), and von Seggern (1970), among others.

Magnitude estimates for any one event (earthquake or underground explosion) commonly vary by one unit between seismograph stations and have been found to vary by as much as three or more units. Magnitude determinations are influenced by several factors including (1) instrument response, (2) nature of the propagation path, (3) the geology in the source region, and (4) the local geology in the vicinity of the seismograph station.

Gutenberg and Richter (1958) used a term, $\log A/T$, in their magnitude equations because of the "considerable variation in prevailing periods determined from instruments of widely different characteristics." A is the amplitude of the seismic signal and T is its period. Instrumentation variability has been minimized in this report by using only data from